

# Advances in Applied Digital Human Modeling & Simulation

# Advances in Applied Digital Human Modeling & Simulation

Edited By

Vincent Duffy

### Published by AHFE International ©

No claim to original U.S. Government works

Published in the United States of America

Version Date: 20200710

ISSN 2771-0718 (Online)

Applied Human Factors and Ergonomics International

International Standard Book Number: 978-1-4951-2094-7 (eBook)

Proceedings of AHFE International Conference (AHFE 2020), 16-20 July, 2020, NY, USA.

This book contains information obtained from highly authentic and regarded sources. Reasonable efforts have been made to publish reliable data and information, but the author and publisher cannot assume responsibility for the validity of all materials or the consequences of their use. The authors and publishers have attempted to trace the copyright holders of all material reproduced in this publication and apologize to copyright holders if permission to publish in this form has not been obtained. If any copyright material has not been acknowledged please write and let us know so we may rectify in any future reprint.

Except as permitted under U.S. Copyright Law, no part of this book may be reprinted, reproduced, transmitted, or utilized in any form by any electronic, mechanical, or other means, now known or hereafter invented, including photocopying, microfilming, and recording, or in any information storage or retrieval system, without written permission from the publishers.

For permission to photocopy or use material electronically from this work, please access (http://www.copyright.com/) or contact the Copyright Clearance Center, Inc. (CCC), 222 Rosewood Drive, Danvers, MA 01923, 978-750-8400. CCC is a not-forthat provides and registration for a variety of users. For profit organization licenses organizations that have been granted a photocopy license by the CCC, a separate system of payment has been arranged.

**Trademark Notice**: Product or corporate names may be trademarks or registered trademarks, and are used only for identification and explanation without intent to infringe.

Visit the AHFE Web site at http://www.ahfe.org

### **Table of Contents**

### Section 1: Digital Human Modeling and Work Design

Using Santos DHM to design the working environment for sonographers in order to minimize the risks of musculoskeletal disorders and to satisfy the clinical recommendations M. Mazzola, L. Forzoni, S. D'Onofrio, C. Standoli and G. Andreoni, Italy	3
Using MRI-derived spinal geometry to compute back compressive stress (BCS): A new measure of low back pain risk R. Sesek, R. Tang, C. Gungor, S. Gallagher, J. Davis and K. Foreman, USA/Turkey	13
The quest to validate human motion for digital ergonomic assessment – Biomechanical studies to improve the human-like behavior of the human model "EMA"  D. Glaser, L. Fritzsche, S. Bauer and W. Leidholdt, Germany	19
Basic method for handling trivariate normal distributions in case definition for design and human simulation D. Hogberg, E. Brolin and L. Hanson, Sweden	27
Section 2: Digital Human Modeling and Human Factors	
Assessing the precision of anthropometric measurements: A Six Sigma approach D. Hale and E. Fallon, Ireland	41
Interactive simulation and ergonomics assessment of manual work with EMA - Applications in product development and production planning L. Fritzsche, R. Schonherr and B. Illmann, Germany	49
Influence of fingertip anthropometry and anatomy on mechanical loads during grasping G. Harih, J. Kaljun, and B. Dolšak, Slovenia	59
Human factors modeling from wearable sensed data for evacuation based simulation scenarios L. Paletta, V. Wagner, W. Kallus, H. Schrom-Feiertag, M. Schwarz, M. Pszeida, S. Ladstatter and T. Matyus, Austria	70
A new representational method of human foot anatomical landmark and its application in foot posture data acquisition  K. Zhao, A. Luximon, B. Ganesan and C. Chan, Hong Kong	79

### **Section 3: Digital Human Modeling Applications**

	The digital evaluation of driver's field of view and its potential impact on cyclist safety R. Marshall, S. Summerskill and S. Cook, UK	89
	Special computational gas flow simulation methods for trunkline network failures S. Pryalov and V. Seleznev, Russian Federation	101
	Digital human model applied to training and education in sports C. Guimaraes, M. Zamberlan, V. Balbio, V. Santos, A. Paranhos, F. Pastura and G. Cid, Brazil	109
	Design and evaluation of a digital human modelling tool for consideration of anthropometric diversity  E. Brolin, D. Hogberg and L. Hanson, Sweden	114
	Investigating the effectiveness of priming in virtual environments C. Butler, Norway	121
Se	ction 4: Ergonomics in Fashion Industry	
	Thermal human modeling: A design tool for functional clothing H. Chao, A. Luximon and KW. Yeung, Hong Kong	129
	A facial mask study for Chinese female Y. Luximon and Y. Cong, Hong Kong	138
	A study of the comfort of the materials for self-grown fashion creation P. Wang and M.C.F. Ng, Hong Kong	143
	Biomechanical model of bare-breasts during running J. Zhou, W. Yu, L. Chen, M. Suh and Y. Cai, Hong Kong	148
	A finite element mechanical contact model of 3D human body and a well-fitting bra Y. Cai, W. Yu and L. Chen, Hong Kong	157

### **Preface**

This book, Advances in Applied Digital Human Modeling, is concerned with human modeling, biomechanics and Simulation. The benefit of this area of research is to aid in the design of systems. Human modeling and simulation can reduce the need for physical prototyping and incorporate ergonomics and human factors earlier in design processes. These models provide a representation of some human aspects that can be inserted into simulations or virtual environments and facilitate prediction of safety, satisfaction, usability, performance and sustainability. These may consider the physiological, cognitive, behavioral, emotional and environmental aspects. The math and science provides a foundation for visualizations that can facilitate decision making by technical experts, management or those responsible for public policy.

Explicitly, the book contains the following subject areas:

- I. Digital Human Modeling and Work Design
- II. Digital Human Modeling and Human Factors
- III. Digital Human Modeling Applications
- IV. Ergonomics in Fashion Industry

Each of the chapters of the book were either reviewed by the members of Scientific Advisory and Editorial Board or germinated by them. Our sincere thanks and appreciation goes to the Board members listed below for their contribution to the highest scientific standards maintained in developing this book:

T. Ahram, USA

T. Alexander, Germany

G. Andreoni, Italy

R. Bhatt, USA

J. Charland, Canada

Z. Cheng, USA

B. Corner, USA

O. Ersoy, USA

R. Goonetilleke, Hong Kong

B. Gore, USA

R. Green, USA

D. Högberg, Sweden

H. Hsiao, USA

J. Lee, USA

Z. Li, China

J. Lockett, III USA

A. Luximon, Hong Kong

C. Moebus, Germany

Y. Motomura, Japan

J. Park, Korea

S. Rajulu, USA

M. Reed, USA

X. Wang, France

J. Yang, USA

W. Zhang, China

Vincent G. Duffy Purdue University West Lafayette, Indiana USA

Editor

### Section 1

Digital Human Modeling and Work Design

## Using Santos DHM to Design the Working Environment for Sonographers in Order to Minimize the Risks of Musculoskeletal Disorders and to Satisfy the Clinical Recommendations

M. Mazzola<sup>a</sup>, L. Forzoni<sup>b</sup>, S. D'Onofrio<sup>b</sup>, C.E. Standoli<sup>a</sup> and G. Andreoni<sup>a</sup>

<sup>a</sup>Politecnico di Milano, Design Department, Milano, Italy

> <sup>b</sup>Esaote S.p.A. Firenze, Italy

### **ABSTRACT**

The percentage of sonographers reporting consequences of pain and discomfort is close to 80% and the Society of Diagnostic Medical Sonography demonstrates that sonographers, on average, experience pain or Musculoskeletal disorders within 5 years of entering the profession. Digital Human Models (DHM) can be an essential tools, supporting the definition of a correct medical environment to perform Sonography in response to the regulatory aspects that standardize the Health Care design and in setting up the ergonomics requirements. The methodology proposed to perform an optimal setting of the workspace considers the different aspects of a diagnostic Ultrasound (US) examination room in a clinical setting: sonographer's seating and examination bed, US system and probe. Vascular and Abdominal applications were considered. The aim of this study is to present an example of how an Advanced DHM can support the design of the working environment for sonographers in order to minimize the risks of muscle-skeletal disorders and to satisfy the clinical recommendations. Results were compared with data presented in previous studies about ergonomics in professional sonography and they demonstrate to be coherent with the plan for an ideal set-up.

Keywords: Digital Human Modeling, Diagnostic Ultrasound Ergonomics, Sonographer, WRMSD

### INTRODUCTION

The Ergonomic evaluation and assessment of sonographers' workspace are very important. The percentage of sonographers reporting consequences of pain and discomfort is close to 80% and the Society of Diagnostic Medical Sonography (SDMS) demonstrates that sonographers, on average, experience pain or Musculoskeletal disorders (MSDs) within 5 years of entering the profession. Higher anatomical sites experienced discomfort reported by sonographers are in the shoulder, neck, low back, wrist and hand/fingers. (Society of Diagnostic Medical Sonography, 2003, Village and Trask, 2007).

Sonographers are exposed to a variety of ergonomics-related risk factors when they perform specific tasks, dealing with the transportation of equipment, the positioning of patients and equipment and the daily use of Ultrasound (US) systems.

Several studies in this research area identified nine major factors of interest (Andreoni et al., 2013, Murpy and Russo, 2000). Among these factors, the transducer design, the US system user interface and control panel design and the sonographer's body posture seem to be relevant for injury and risk prevention. Indeed, a comfortable chair and correct body position protected the sonographer from the onset of neck and back discomfort. These studies contributed to define the best practices for a correct positioning of US equipment, in order to minimize the MSDs risks for professional sonographers.

Nonetheless, the correct observance of these recommendations depends on the sonographer's diligence and this is due to the lack of tools that quantify the distances between the sonographer, the patients and the equipment, but also that can support the design of the clinical environment, in order to verify the correct positioning.

Digital Human Models (DHM) can be important tools that support the definition of a correct medical environment to perform diagnostic US examinations in response to the regulatory aspects that standardize the Health Care design and in setting up the ergonomics requirements.

The aim of this study is to present how an Advanced DHM, i.e. Santos Digital Human, can support the sonographers' working environment design, in order to minimize the risks of muscle-skeletal disorders and to satisfy the clinical recommendations.

Sonography can be performed in different applications. Moreover, thanks to the availability of portable US systems with high level of diagnostic performance, US examinations can be performed in many different settings, ranging from the typical hospital setting examination room, to emergency Departments, patient bedside, patient home, emergency vehicles and so on.

The presented study is mainly focused on Abdominal and Vascular applications to meet differing conditions to simulate a scan and it considers a classic hospital setting environment.

In addition, various probes (Linear probe used for Vascular application and Convex probe used for Abdominal application) are used with different consoles and dissimilar grasps are applied for diverse applications.

### **MATERIAL AND METHODS**

### **Preparation of the Simulation Environment**

In order to design the optimal sonographer's workplace, it is necessary to consider the mutual position of the sonographer and the objects that compose the simulation environment; in particular these objects include: the US console, the patient's bed and the sonographer's sitting chair. In this work, Santos DHM was used to prepare the simulation environment, in accordance with the literature description of the most preferable working conditions (Murphy and Russo, 2000). The workspace was designed considering the possibility to adjust the objects height and their distances from the sonographer's body.

As a consequence, the evaluation of the joint angles were compared, assuming both sitting work posture chair height and bed height as adjustable.

The methodology proposed to perform an optimal setting of the workspace consists of the following steps:

- 1) To design the most comfortable set-up, the seating and bed height are assumed to be adjustable, as well as the console position.
- 2) The Avatar was anthropometrically scaled, representing the 5<sup>th</sup>, 50<sup>th</sup> and 95<sup>th</sup> percentile. In this work, the evaluation was conducted only for the male gender.
- 3) Preparation of the simulation environment. The Height Regulation of the seat was determined to guarantee that the avatar, in neutral sitting position, had the feet resting on the floor.

4) The position of the bed, both for Abdominal and Vascular application and the US console position were determined using the Santos Zone Differentiation (ZD) analysis tool.

### **Anthropometrical Characterization of the Avatar**

The avatars were anthropometrically differentiated by somatotypes and by percentile: 5th, 50th and 95th male percentiles were used to scale the Avatars body sizes. The 5<sup>th</sup> percentile corresponds to the somatotype defined as "Short, Lean and V-shaped", the 50<sup>th</sup> percentile corresponds to the normal Santos somatotype, and the 95<sup>th</sup> percentile corresponds to "Tall, Heavy, H-shaped" somatotype. Avatar's body weight and limb lengths are based on the data of the Standard ISO 3411. Table 1 present body height and weight of the different percentiles.

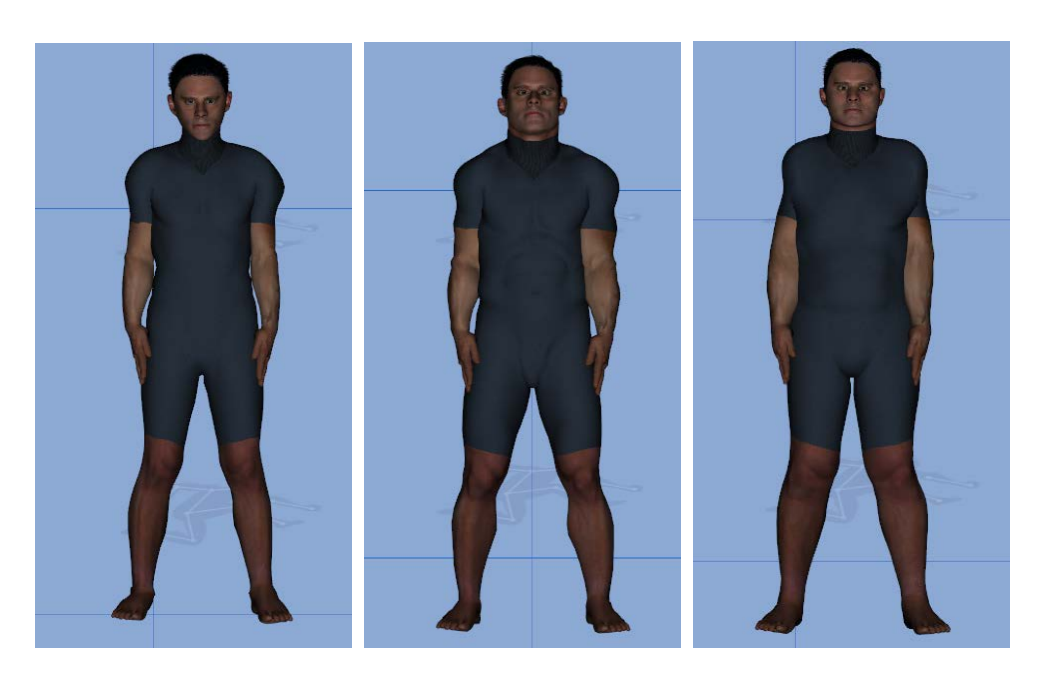


Figure 1: From left to right: frontal picture of Avatar corresponding to the 5th, 50th and 95th percentiles.

Table 1: Anthropometrical measures of the different percentiles, according to the ISO-3411

Percentile	Height (cm)	Weight (Kg)
5 <sup>th</sup>	190.5	94.6
50 <sup>th</sup>	173.07	78.7
95 <sup>th</sup>	156.6	62.8

### **Seat Height Regulation**

To assess the correct height regulation of the sitting work posture on the chair, the Avatar is firstly positioned in the Neutral Sitting posture. Therefore, the seat height has been dimensioned to guarantee that the Avatar's feet rest on the floor.

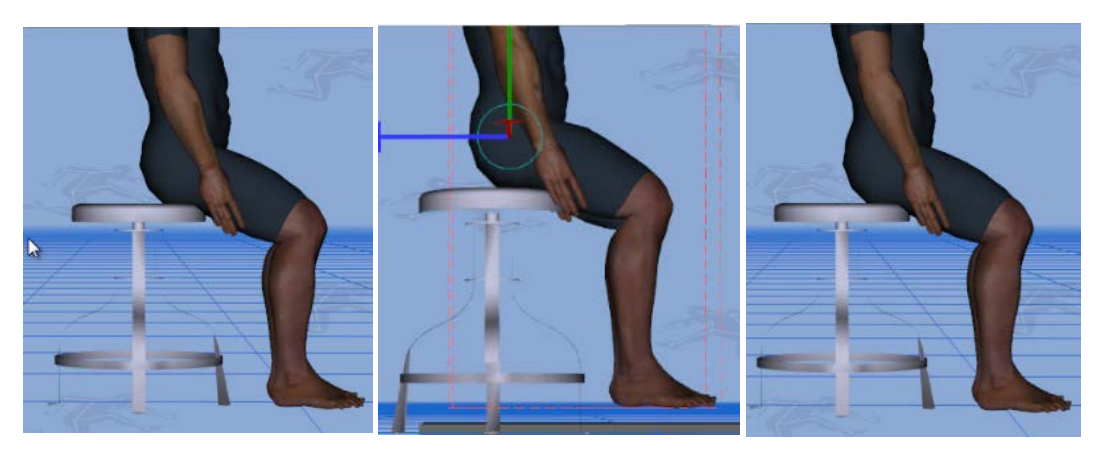


Figure 2: On the left: the avatar is positioned in the neutral sitting posture. In the middle, the seat height is oversized, and the avatar is not able to touch the floor with his feet. On the right, the correct dimension of the seat height, adopted for the simulations.

### Grasps

The orientation of the transducer within the hand, which must be rotated to obtain different images, determined the type of grip used. There are 3 different types of grasp, depending on the analyzed probe application: Longitudinal Pincer Grip, Transversal Pincer Grip and Palmar Grip. An example of each grasp, real and DHM simulated, is presented in Figure 3.

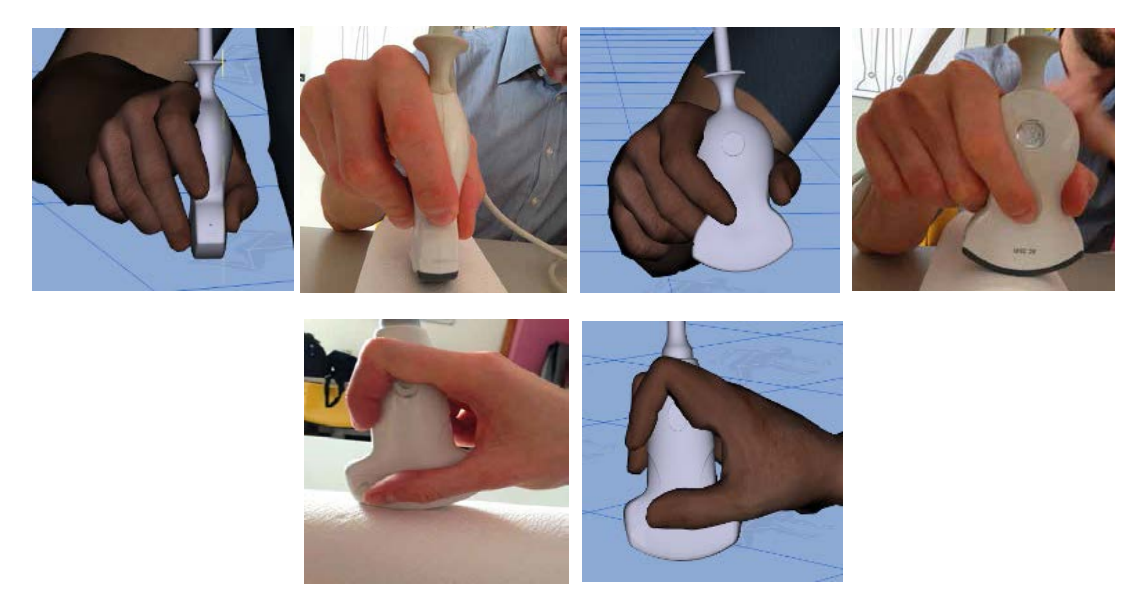


Figure 3: On the top left, the Longitudinal Pincher Grip, DHM simulated and observed. On the top right, the Transversal Pincher Grip and in the second line the Palmar grip.

The aim of the present work is the general assessment of the workspace environment and it considers the posture as the most relevant parameter to be evaluated. As a consequence, each workspace condition can be assumed independently from the specific grasp adopted.

### **Probes**

4 different US probes (Convex array probes CA631 and AC2541; Linear array probes LA523 and SL1543; Esaote S.p.A., Firenze, Italy; see Figure 4) were used for ergonomic analysis; each probe was used with a specific console and with three different grasps, as a consequence of the specific application (Abdominal/Vascular). AC2541 and

SL1543 are ergonomically designed probes, appleprobe Design transducers. Each probe can be grabbed with the three different grasps described above, while each of them is associated with a single application and a specific console. In table 2, for each probe, the related US console and the possible grasps are listed.

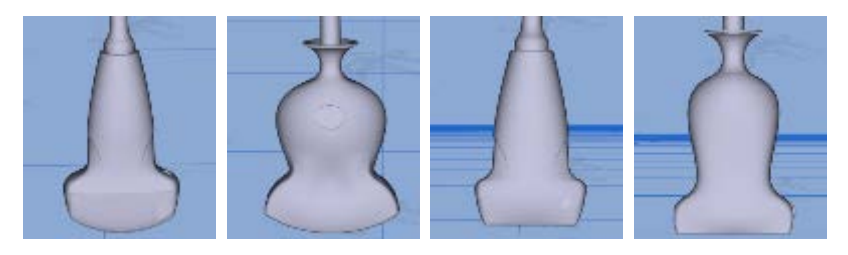


Figure 4. From left to right: probe CA631, AC2541, LA523, SL1543

Table 2: Correspondence of US application, Consoles, Probes and Grasps

	Console + Probe		Grasping	Console + Probe	
VASCULAR	MyLabAlpha	SL1543	Longitudinal	MyLab30CV	LA523
			Transversal		
			Palmar		
ABDOMINAL	MyLabAlpha	AC2541	Longitudinal	MyLab30CV	CA631
			Transversal		
			Palmar		

### **Consoles**

Two different Esaote portable US systems were used for the investigation: MyLab Alpha and MyLab30CV (Esaote S.p.A., Firenze, Italy). They're presented in figure 5 together with the simplified model imported in the DHM and the reaching regions of interest, that correspond to the most used areas of the user interface.



Figure 5: On the left: MyLab30CV Console presented as a simplified .obj model imported in the Santos environment, and a picture of the real interface is presented. In red are showed the different areas of investigations for the simulation conditions of the Left Hand. On the Right: The MyLabAlpha console presented as a simplified .obj model imported in the Santos environment, and a picture of the real interface. In this case, the zones objects of the simulations are showed in blue on the left

In figure 6, the specific target points objects of investigations are showed. In particular, there are 3 markers points (Top Left of the Qwerty Keyboards, Top Left of the Soft Key Menu on the screen and the Trackball) for the MyLab30CV model and two marker points (Top Left of the Touch screen and the Trackball) for the MyLabAlpha model.

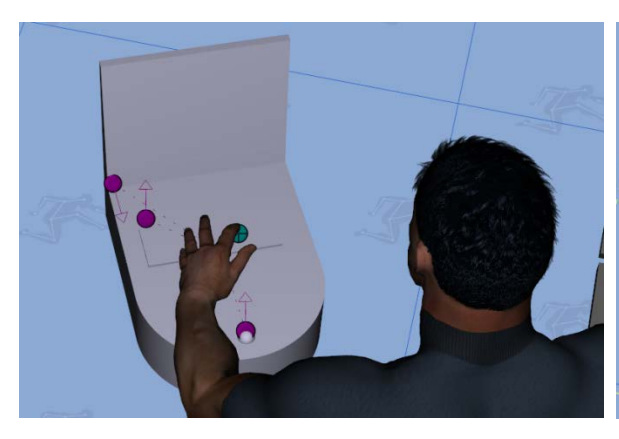




Figure 6: On the Left, the 3 target points of the MyLab30CV US system; on the right, the 2 target points of the MyLabAlpha US system

### **Zone Differentiation for US Probe Reaching Zone**

Santos ZD tool was used to optimize the US probe and the console reaching zones. The ZD system allows the user to analyze information according to posture-based performance measures (Yang et al., 2004, 2006, 2008). In this study, the performance measure adopted to determine the optimal reaching zones was the Effort Performance Measure, in a percentage of 80%, and the Joint Displacement for 20%.

The effort performance measure models the tendency to gravitate towards one's initial position. In sonography, the movement of both left hand (controls adjustment on US system console) and right hand (probes holding, pressing and moving for the exploration of the patient's body) can be described as consecutive small changes respect to the last posture adopted by the avatar. As a consequence, the effort performance measure represents the most convenient performance measure for the ergonomics evaluation of the working environment in sonography. A 20% of Joint Displacement performance measure was set, in order to avoid the possible increase of the distance from the neutral sitting posture of the avatar, that could generate unacceptable postures.

New ZD were generated for both the right and the left hand of the avatar, for each percentile. The computed zone were defined with a volume of  $110 \times 140 \times 110$  cm, with a resolution of 64x64x64.

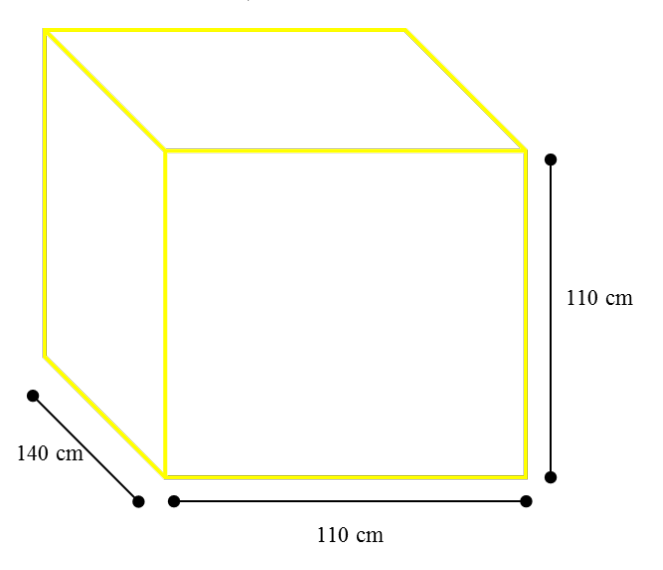


Figure 7. volume of the computed Zone Data

Figure 8 presented the procedure adopted for the optimal positioning of the different workspace objects for the 5<sup>th</sup> percentile avatar somatotype. The optimal position is determined selecting the position that presents the most green colored area for the relative object, that represents the maximum comfort according to the performance measured used for computation (i.e., effort).

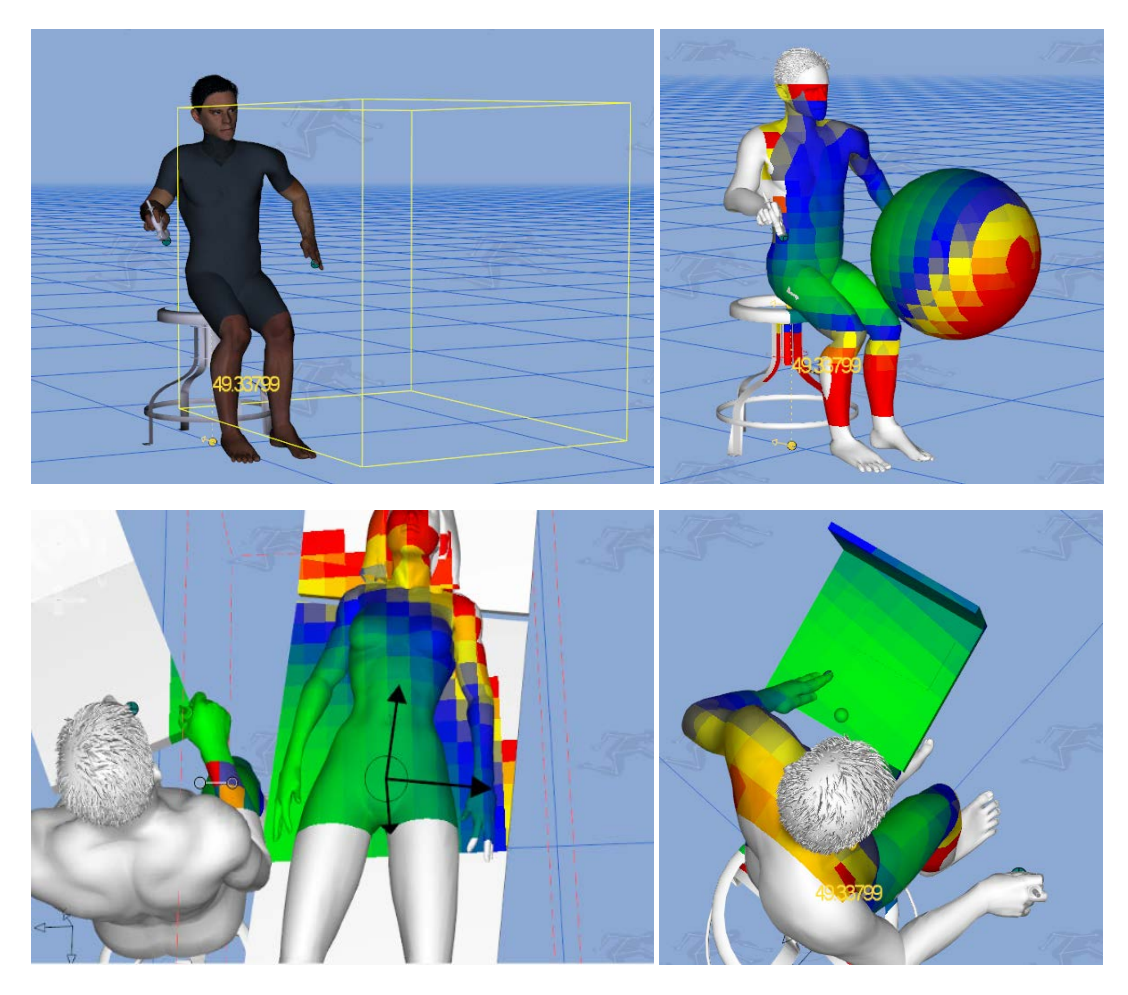


Figure 8. On the top left, the Volume of the computed data for the left end the effector (left hand) is presented in yellow, for the 5th percentile avatar somatotype. On the top right, a sphere has been used to graphically represent the result of the ZD data computed. On the bottom line, the optimal position obtained using the ZD application is presented for the abdominal application.

### **Posture Evaluation**

The posture evaluation was conducted considering the Maximum Holding Time (MHT) Index for the Shoulder, and the Right Shoulder Abduction Angle, considering all the subjects right handed, grasping the probe with the right hand and reaching the US console with the left hand.

### RESULTS AND DISCUSSION

Table 3 presents results of the simulations. In addition to the anthropometrical data of the three avatars, the recommended value of Shoulder Abduction angles, as defined in the Report of Murphy and Russo, is reported. This value represents the reference value and it has been compared with: the Abduction angle of the Right Shoulder, the Left Shoulder in reaching the closest target point (US system trackball) and the Left Shoulder while reaching the touchscreen of the monitor.

Results demonstrate that the 50<sup>th</sup> percentile avatar somatotype presents optimal values, always lower than the reference, for both the right and left shoulder, in all the conditions. Results for the 5<sup>th</sup> percentile avatar are opposite; the abduction angle of the right shoulder is lower than the reference, while the angle of the left shoulder is higher. The 95<sup>th</sup> percentile presents the worst results, being always over the recommended threshold. Results are reported without the differentiation between vascular and abdominal application, due to the fact that, once the operating

volume has been defined and the postural comfort zone determined, the patient should be located there with the specific body part, without modifying the postural asset.

Table 3. Results of the Simulation. Shoulder joints angles are presented and compared with the recommended reference value.

	Shoulder Abduction (Degrees)					
	Height	Weight	Recommended	Right	Left Trackball	Left Screen
95%	190.5	94.6	30	49	52	48
50%	173.07	78.7	30	13	12	26
5%	156.6	62.8	30	27	52	53

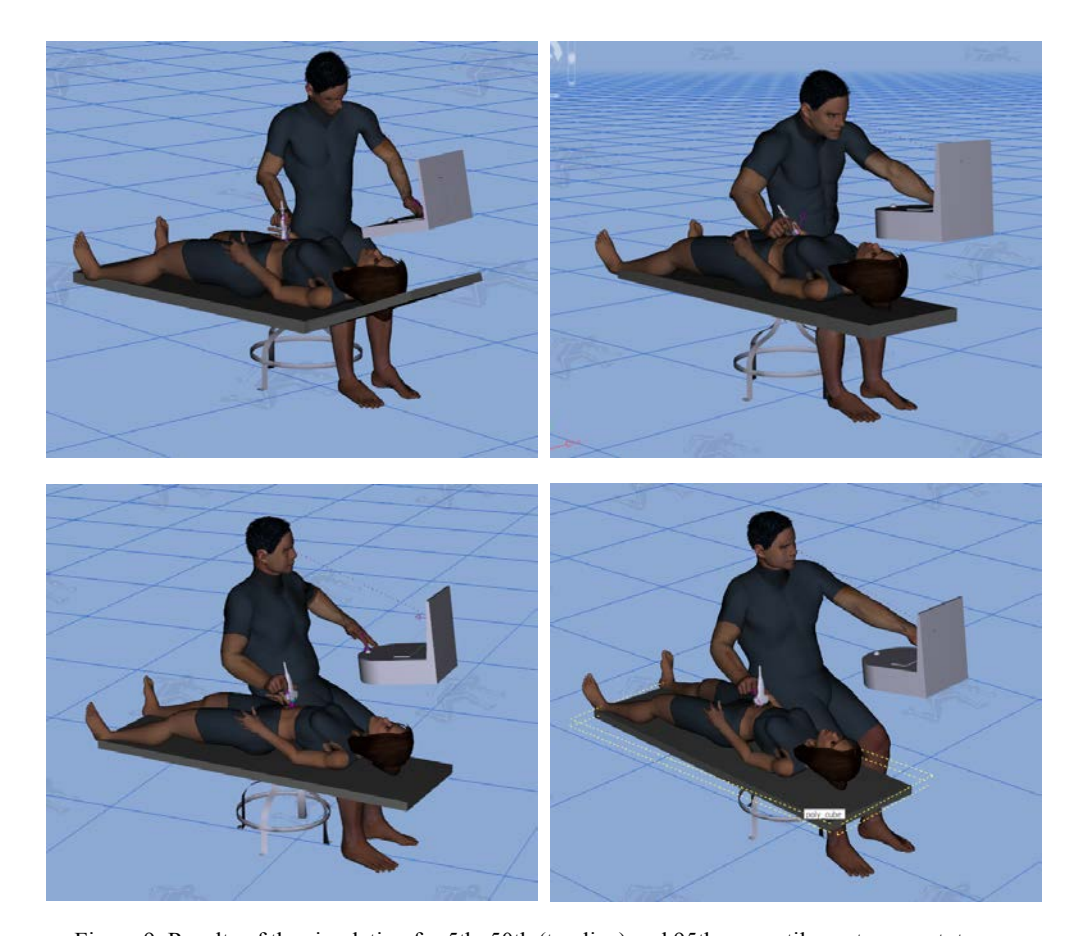


Figure 9. Results of the simulation for 5th, 50th (top line) and 95th percentile avatar somatotypes.

Results of the MHT Analysis are presented in Table 4. Results for the 5<sup>th</sup> percentile avatar somatotypes demonstrates that potential problems and risk of fatigue could arise at the right shoulder level, while the other joints do not present any critical situation, except for a small fatigue for the right wrist. On the contrary, both 50<sup>th</sup> and 95<sup>th</sup> percentiles present possible fatigue at the right and left shoulder level and at the right wrist level. These results could be determined by the mass property of the different percentile and the corresponding force property. Also the limb length can influence the postural evaluation and increasing the level of fatigue of the bigger percentiles. Fatigue at the wrist level is due to the probe grasp. Possible future development could investigate the relation between the MHT, the probe model and the grasp adopted.

Table 4. Maximum Holding Time Index results

МНТ				
	5th	50th	95th	
Clavicle	60 min : 00 sec	60 min : 00 sec	60 min : 00 sec	
R Shoulder	27 min:28 sec	17 min : 46 sec	32 min : 25 sec	
L Shoulder	60 min : 00 sec	15 min: 55 sec	10 min : 25 sec	
L Elbow	60 min : 00 sec	60 min : 00 sec	60 min : 00 sec	
R Elbow	60 min : 00 sec	60 min : 00 sec	60 min : 00 sec	
L Wrist	60 min : 00 sec	60 min : 00 sec	60 min : 00 sec	
R Wrist	42 min : 03 sec	20 min : 18 sec	27 min : 09 sec	

Figure 10 presents the comfort area determines for the two different US consoles. This result is very promising and interesting. On the left it is possible to visualize the MyLab30CV console model, with the three different target points considered and what it can be noticed is that the position of the US console trackball and the touch screen on the monitor are not ergonomically in optimal position and are outside of the preferred comfort zone (green). Also the keyboard presents a decrease in the comfort level, moving the hand from the right to the left.

On the contrary, the position of the controls of the MyLabAlpha US model seems to be optimal, for both the US console trackball and the touchscreen.

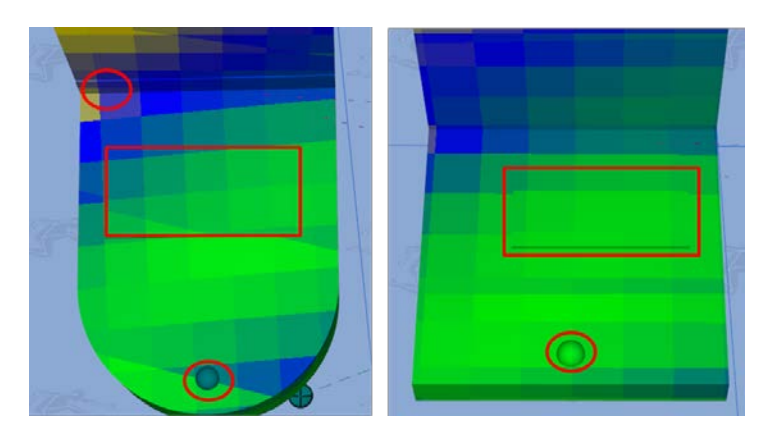


Figure 10. Results of the comfort zone evaluation for MyLab30CV (Left) and MyLabAlpha (Right).

### **CONCLUSIONS**

In this study, a methodology to design the optimal workspace for a diagnostic US examination was suggested. The ergonomic analysis proposed is based on the use of the Santos DHM software, applying its capability in providing a coherent ergonomics design tool, in accordance to referred practical recommendations.

The simulation process studied the optimal positioning of the sonographer's seat, the patient's bed and the US system console, according to the biomechanical characteristic of three different somatotype scaled avatars.

Two US systems were ergonomically evaluated. Results demonstrates that the procedure adopted is coherent with the experimental recommendation for the  $50^{th}$  percentile and the  $5^{th}$  percentile, considering the Shoulder Abduction angles and the MHT Index.

The 95<sup>th</sup> percentile demonstrates to assume, in the optimal position, a posture that can determine fatigue hazard, but its comparison with the reference value could be refined, considering the anthropometrical differences among the

different somatotype.

Results were compared with data presented in previous studies about ergonomics in sonography and they demonstrates to be coherent with the plan for an ideal set-up.

In conclusion, this work demonstrates that DHM can be a promising tool in the early design of the sonographer's working environment, respecting the recommendations and the best practice suggested in literature to minimize the risk of MSDs.

Further developments could propose this DHM approach as an effective tool to design medical workplaces.

### REFERENCES

- Andreoni G., Costa F., Mazzola M., Fusca M., Romero M., Carniglia E., Zambarbieri D., Santambrogio G.C. (2013), "A multifactorial approach and Method for Assessing Ergonomic Characteristics in Biomedical Technologies", Advances in Human Aspects of Healthcare, edited by Duffy V., Chapter 1, 1-12.
- Gregory, V. (1998), "Musculoskeletal Injuries: Occupational Health and Safety Issues in Sonography", Sound Effects 30.
- International Standard ISO 3411 (2007), "Earth-moving machinery Physical dimensions of operators and minimum operator space envelope", Fourth edition.
- Magnavita, N., Bevilacqua, L., Mirk, P., Fileni, A, and Castellino, N. (1999), "Work-related Musculoskeletal Complaints in Sonologists", J Occup Environ Med, Nov; 41(11):981-8.
- Mirk, P., Magnavita, N., Masini., L., Bazzocchi., M., and Fileni., A. (1999), "Frequency of Musculoskeletal Symptoms in Diagnostic Medical Sonographers. Results of a Pilot Survey", Radiol Med, Oct; 98 (4):236-41.
- Murphy, C. and Russo, A. (2000), "Report: An Update on Ergonomic Issues in Sonography", Healthcare Benefit Trust, EHS Employee Health and Safety Services.
- NIOSH Technical Report, HETA 99-0093-2749 Smith, A.C., Wolf, J. G., Xie, G.Y, and Smith, M.D. (1997), "Musculoskeletal Pain in Cardiac Ultrasonographers: Results of a Random Survey", J. Am. Soc Echocardiogr, May; 10(4):357-62.
- Smith and Sainfort (1989) in Kuorinka et al. (1995), "Work-Related Musculoskeletal Disorders: A Reference for Prevention", Philadelphia: Taylor & Francis.
- Society of Diagnostic Medical Sonography (2003), "Industry Standards for the Prevention of Work-Related Musculoskeletal Disorders in Sonography". Village J., Trask C. (2007), "Ergonomic analysis of postural and muscular loads to diagnostic sonographers", Int. Jour. Ind. Ergonomics 37, 781-789.
- Yang, J., Marler, T., Beck, S., Abdel-Malek, K., and Kim, H.-J. (2006), "Real-Time Optimal-Reach Posture Prediction in a New Interactive Virtual Environment", Journal of Computer Science and Technology, 21(2), 189-198.
- Yang, J., Marler, R. T., Kim, H., Arora, J. S., and Abdel-Malek, K. (2004), "Multi-Objective Optimization for Upper Body Posture Prediction", 10th AIAA/ISSMO Multidisciplinary Analysis and Optimization Conference, Albany, NY.
- Yang, J., Verma, U., Penmatsa, R., Marler, T., Beck, S., Rahmatalla, S., Abdel-Malek, K., and Harrison, C. (2008), "Development of a Zone Differentiation Tool for Visualization of Postural Comfort", SAE 2008 World Congress, Detroit, MI.

### Using MRI-Derived Spinal Geometry to Compute Back Compressive Stress (BCS): a New Measure of Low Back Pain Risk

Richard Sesek<sup>1</sup>, Ruoliang Tang<sup>1</sup>, Celal Güngör<sup>2</sup>, Sean Gallagher<sup>1</sup>, Jerry A. Davis<sup>1</sup>, and K. Bo Foreman<sup>3</sup>

<sup>1</sup>Auburn University Department of Industrial and Systems Engineering Auburn, AL, 36849-5346, USA

> <sup>2</sup> Izmir Katip Celebi University Department of Forest Products Engineering Cigli, Izmir, 35620, TURKEY

> > <sup>3</sup>University of Utah Department of Physical Therapy Salt Lake City, UT, 84108, USA

### **ABSTRACT**

Back compressive force (BCF) is a commonly used surrogate for the risk of developing low back pain. Point force estimates of spinal loading have been shown to predict low back pain in epidemiological studies. However, they are an imperfect measure and can over- or under-estimate risk, particularly for very large or small individuals. A logical means to normalize risk over a varied population is to convert these forces to stresses (force/unit area). To achieve this, Magnetic Resonance Imaging (MRI) scans were used to provide area measurements for the intervertebral discs and vertebral bodies of the lumbar region (L3/L4, L4/L5, & L5/S1 segments). Various regression models were explored based on individual subject gross anthropometry. These models allow for the estimation of intervertebral disc (IVD) size using easily measured anthropometric characteristics such as height and gender. Converting the BCF to a back compressive stress (BCS) normalizes and personalizes risk estimates for subjects of varying sizes. Back compressive force data from a previous study was converted to back compressive stress to determine if risk estimates could be improved. Using peak BCF with a cut point of 3400 N (~770 lbs) yielded an odds ratio of 2.76 (1.2-6.6) to predict jobs with injuries and discomfort. Using BCS with a cut point of 280 N/cm², which corresponds to 3400 N load applied to a 50th percentile female L5/S1 IVD area, improved the odds ratio to 5.78 (1.8-18.4). Normalizing for the size of a subject's IVD shows great promise for improving the predictive abilities of biomechanical assessment methods.

**Keywords**: Low Back Pain, Risk, Modeling, Intervertebral Disc (IVD), Back Compressive Force (BCF), Back Compressive Stress (BCS)

### INTRODUCTION

Low back pain (LBP) has been a major socioeconomic burden to modern society, remaining one of the most prevalent health problems in the world for decades (Degenais, Caro, & Haldeman, 2008; Deyo, Mirza, & Martin, 2006; Gore, Sadosky, Stacey, Tai, & Leslie, 2012; Sesek, Gilkey, Drinkaus, Bloswick, & Herron, 2003). A number of studies have suggested that the risk factors for LBP are multifactorial, including personal demographics, physical job factors, psychosocial characteristics, and prior LBP history (Manchikanti, 2000; Rubin, 2007). In addition, it has

been generally accepted in the literature that a majority of LBP complaints have mechanical exposure as the origin (Tang. 2013). The effect of mechanical loading on the lumbar spine can be detrimental (Evans & Lissner, 1959, Nachemson, 1960; Sonoda, 1962; Adams & Hutton, 1983; Brinckmann, Johannleweling, Hilweg, & Biggemann, 1987). Epidemiological evidence suggests that in occupational settings, LBP is prevalent among workers performing manual material handling (MMH) tasks (Andersson, 1998; Marras, 2000) which represents over 20% of total Workers' Compensation (WC) cost (Hashemi, Webster, & Clancy, 1998; Liberty Mutual Research Institute for Safety, 2009). In response to the staggering economic burden facing the industry, a number of studies have sought to develop ergonomic evaluation methods or "tools" to assess the physical demand of MMH jobs and the associated risk of LBP (Chaffin, 1969; National Institute for Occupational Safety and Health, 1981; Waters, Putz-Andersson, Garg, & Fine, 1993; Marras, Lavender, Leurgans, Rajulu, Allread, Fathallah, and Ferguson, 1993; Merryweather, Loertscher, & Bloswick, 2009). For less frequent lifting tasks, biomechanical criteria that focus on the physical limits of the lumbar spine under loading are regarded as the most important (Waters et al., 1993). Using kinetic and kinematic analyses, biomechanical models can estimate the internal response to an external load, which then can be compared with spine tolerance data to evaluate the risk of potential injuries (Chaffin & Park, 1973; Waters et al., 1993). Although biomechanical models vary in capability to analyze complex spinal motions (2D vs. 3D), a back compressive force (BCF) of 3400 N (~770 lbs) has been well accepted in the literature as the cut-off point, above which potential tissue damage may occur (NIOSH, 1981; Waters, 1993; Merryweather et al., 2009).

It should be noted that one fundamental assumption of many biomechanical models and ergonomic tools is a simplified description of spinal geometry with the lumbosacral disc (L5/S1) being the pivot point at which the BCF is applied. However, as mechanical theory states, tolerance of the disc to compressive loading, as measured by force, is also dependent on the size of the disc (Tang, 2013). Evidence has shown a lot of variation in spinal geometry among populations (Tang, Güngör, Sesek, Foreman, Gallagher, and Davis, 2014a). Depending on the individual characteristics, a BCF measure is likely to attribute to over- or under-estimate the LBP risk, particularly for very large or small individuals. A logical means to normalize risk over a varied population is to convert these forces to stresses (force/unit area), namely the back compressive stress (BCS). The purpose of this study was to determine if BCF-based ergonomic risk estimation could be improved by converting to BCS risk estimates that consider the size of a subject's intervertebral disc (IVD).

### **METHOD**

Data used for this investigation were gathered from two previous studies:

- 1) an automotive manufacturing ergonomic field study and
- 2) a morphometric study of low back geometry using MRI technology.

### **Automotive Study**

Data were analyzed from a database consisting of 667 manufacturing jobs from a previous automotive study. The database included historical injury data for the analyzed jobs as well as symptom interviews for 1,022 participants. A subset of 188 subjects with manual material handling tasks was selected for the current study. The subjects ranged in height from 150-203 cm (176.3  $\pm$  9.8), weighed between 52-159 kg (86.3  $\pm$  19.6), and were 22-65 years of age (41.4  $\pm$  11.2). There were 144 male and 44 female subjects. Researchers had no personal information regarding participants beyond height, gender, and self-reported level of discomfort. All data were analyzed in aggregate. The original data were collected at six different automotive plants. Only manufacturing jobs with well-defined activities were included (administrative jobs or jobs that did not have well defined tasks were not analyzed). Subject data used for this study include height and gender (which were used to estimate the lower lumbar spinal geometry) and subject reports of discomfort assessed by ratings of perceived discomfort. In the original study, a peak BCF with a cut point of 3400 N (~770 lbs) was used to predict jobs with injuries. Peak BCF ranged from 441-6424 N (2552  $\pm$  1210). Negative health outcomes were defined as self-reported low back pain (LBP) and LBP- related medical visits reported for the subject's job. Cases included subjects with reported low back pain working on jobs that had not had a reported injury in the previous year. Controls included subjects with no low back pain working on jobs that had not had a reported injury in the previous year. The prevalence of low back pain for this population was 0.14.

### **MRI Study**

Regression models were used to estimate individual spinal geometry, calculating the cross-sectional area (CSA) of

the L5/S1 intervertebral disc (IVD) with subject height and gender. These regression models were developed using geometric measurements on MRI scans and subject anthropometric characteristics (Tang, Güngör, Sesek, Gallagher, Davis, and Foreman, 2014b). MRI scans were performed using a 70cm Open Bore 3T scanner (MAGNETOM Verio, Siemens AG, Erlangen, Germany) at the Auburn University MRI Research Center (Figure 1). MRI scans were analyzed using OsiriX<sup>©</sup> software (version 4.1.1, 32-bit, Pixmeo, Geneva, Switzerland) (Figure 2).



Figure 1. MRI scanning operation at Auburn University MRI Research Center

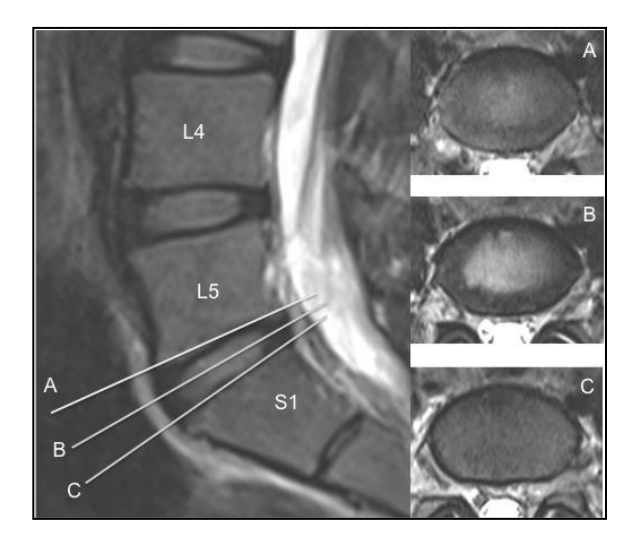


Figure 2. Sample of MRI scan in sagittal and transverse planes

### **Experimental Design**

For each subject, a BCF was calculated as in the original automotive study (at the L5/S1 IVD). Back compressive stress (BCS) was calculated by dividing BCF by an estimate of the L5/S1 IVD CSA through the center of the IVD as shown in Figure 2. The IVD CSAs were estimated using a regression relationship developed in the previous MRI study (Tang et al., 2014b). This relationship is shown in Equation 1 below.

### L5/S1 IVD CSA = -16.959 + 0.179\*HT + 1.7\*GNDR

HT = stature in cm and GNDR = 0 for females and 1 for males

Equation 1: regression relationship of height (HT) and gender (GNDR) to IVD cross-sectional area.

The IVD CSAs ranged from  $9.87-21.11~\text{cm}^2$  ( $15.90\pm2.31$ ). The BCS estimates ranged from  $28.54-422.56~\text{N/cm}^2$  ( $162.66\pm78.14$ ). The cut point for the BCS-based risk classification was selected by determining the BCS for a  $50^{\text{th}}$  percentile female L5/S1 disc loaded to 3400~N (~770 lbs). This corresponds to a  $280~\text{N/cm}^2$  BCS (163~cm stature assumed for a  $50^{\text{th}}$  percentile US woman) (Halls & Hanson, 2014). The BCS risk estimation method presented here is predicated on the concept that for a healthy back the ultimate load (force) that it can safely withstand is a function

of the stress (force/unit area) to which it is subjected, not simply the overall force. In other words, a larger load-bearing surface can handle (distribute) a higher force than a smaller load-bearing surface. Therefore, the BCS model assumes that individuals with larger IVDs can handle higher forces than individuals with smaller IVDs, but the same stress limits (force/unit area) are assumed for each. In practice, BCF-based models tend to overestimate risk for larger (taller) workers (with proportionally larger IVDs) and underestimate risk for smaller (shorter) workers. This BCS model is intended to correct this deficit.

### **Analysis**

Direct comparisons are made between the predictions of a peak BCF model and a peak BCS model computed using area estimates of subject IVDs. Comparisons were made on the basis of predictive ability, sensitivity, specificity, and odds ratios for these tools.

### **RESULTS**

Figure 3 illustrates performance of the traditional BCF model in identifying "risky" jobs (jobs likely to result in the symptoms and injuries for workers) in the previous automotive study. A statistically significant odds ratio of 2.76 (1.2-6.6) was found for this model.

	Outcome			
	Case	Control		
"Risky" Job	11	34		
Predicted	True Positive	False Positive		
"Safe" Job	15	128		
Predicted	False Negative	True Negative		

Figure 3: BCF 2x2 Outcome Matrix (cut point 3400 N)

Figure 4 depicts the performance of the BCS model in identifying "risky" jobs for these same automotive jobs. The odds ratio improved to 5.78 (1.8-18.4) due mainly to decreases in false positives associated with the BCF model.

	Outcome		
	Case	Control	
"Risky" Job	6	8	
Predicted	True Positive	False Positive	
"Safe" Job	20	154	
Predicted	False Negative	True Negative	

Figure 4: BCS 2x2 Outcome Matrix (cut point 280 N/cm<sup>2</sup>)

Table 1 compares the performance of the BCF and BCS models in predicting cases and controls. Agreement (prediction of case/control status) improved from 75% to 85%, positive predictive value (PPV) nearly doubled to 0.43, and specificity rose to 0.95. Sensitivity, however, dropped from 0.42 to 0.23. Negative predictive value (NPV) was relatively unchanged.

### **DISCUSSION**

The concept of back compressive stress (BCS) has great potential for improving the predictive ability of biomechanical models. Accounting for personal characteristics, particularly for persons who differ significantly from the average, can help progress the field of biomechanics. Ideally, as an ergonomic survey tool is perfected, all performance characteristics improve (sensitivity, specificity, PPV, NPV). While overall performance improved significantly with the BCS model, sensitivity dropped significantly (0.42 to 0.23). From a utility perspective, a practicing ergonomist might prioritize improvements to PPV and NPV since these conditional probabilities provide the ergonomist with the most relevant information and conclusions about how to act on the results of survey tool outputs. In this regard, the BCS was a great improvement. However, limitations in this experiment suggest ways

that model output could be further improved, perhaps without compromise to sensitivity.

Table 1: Comparison of BCF and BCS

	BCF	BCS
	3400 N (~770 lb)	280 N/cm <sup>2</sup>
Odds Ratio (95% CI)	2.76	5.78
	(1.2-6.6)	(1.8-18.4)
Agreement	75%	85%
Sensitivity	0.42	0.23
Specificity	0.79	0.95
Positive Pred. Value (PPV)	0.24	0.43
Negative Pred. Value (NPV)	0.90	0.89

### Limitations

There are several limitations associated with this pilot study that should be addressed as the BCS concept is explored further. These limitations can be summarized into two major categories:

- 1. Assumptions regarding personal characteristics: It was assumed that stress capabilities are consistent across individuals. There may be differences based on age, gender, previous injuries, and other personal factors not considered in this research. These should be explored in subsequent research.
- 2. Overly simplistic assessment of risk: Peak compressive and peak compressive stress were the measures of LBP risk. These peak measures do not consider task frequency, duration, and static postures that may greatly impact risk. Subsequent studies should provide a more comprehensive consideration of LBP related risk factors.

Given the limitations described above, the BCS tool performed well and it is anticipated that it can easily be incorporated into new or existing models by simply considering the subject's basic anthropometry (height and gender in this study). There is also the possibility that the risk estimation of other ergonomic tools that do not directly compute BCF can be enhanced. The stress model concept could be used to "scale" risk outputs from other tools based upon the size of the individual subject. For example, the Revised NIOSH Lifting Equation (RNLE) could include an additional multiplier that simply scales risk up or down as compared to reference subject.

### CONCLUSIONS

Based on the findings of this study, the following conclusions are drawn:

- 1. Back Compressive Stress (BCS) shows great promise as a means of improving risk assessments, particularly for relatively large and small subjects and should be explored further.
- 2. The concept of "scaling" risk based on subject size and modifying ergonomic survey tool outputs with this data should be explored.
- 3. Accounting for personal characteristics can help improve ergonomic modeling. Other factors that could be considered include age, obesity, previous injury history, and physical condition.

### Acknowledgements

This research was made possible by a grant from the National Institute for Occupational Safety and Health (NIOSH) Deep South Center for Occupational Health and Safety Education and Research Center [Grant UAB-0002864-019]. The authors would like to acknowledge Dr. Thomas Denney and Dr. Ron Beyers of the Auburn University MRI Center and Dr. James V. Carnahan for their assistance in the conduct of this research.

### **REFERENCES**

- Adams, M. A., & Hutton, W. C. (1983). The effect of fatigue on the lumbar intervertebral disc. J Bone Joint Surg Br, 65 (2), 199-203
- Andersson, G. B. (1998). Epidemiology of low back pain. Acta Orthop Scand Suppl, 281, 28-31.
- Brinckmann, P., Johannleweling, N., Hilweg, D., & Biggemann, M. (1987). Fatigue fracture of human lumbar vertebrae. Clinical Biomechanics, 2 (2), 94-96.
- Chaffin, D. B. (1969). A computerized biomechanical model-development of and use in studying gross body actions. J Biomech, 2 (4), 429-41.
- Chaffin, D. B., & Park, K. S. (1973). A longitudinal study of low-back pain as associated with occupational weight lifting factors. Am Ind Hyg Assoc J, 34 (12), 513-25
- Dagenais, S., Caro, J., & Haldeman, S. (2008). A systematic review of low back pain cost of illness studies in the United States and internationally. The Spine Journal, 8 (1), 8-20.
- Deyo, R. A., Mirza, S. K., & Martin, B. I. (2006). Back pain prevalence and visit rates: estimates from U.S. national surveys, 2002. Spine (Phila Pa 1976), 31 (23), 2724-7.
- Evans, F. G., & Lissner, H. R. (1959). Biomechanical studies on the lumbar spine and pelvis. J Bone Joint Surg Am, 41-A(2), 278-90.
- Gore, M., Sadosky, A., Stacey, B. R., Tai, K.S., & Leslie, D. (2012). The burden of chronic low back pain: clinical comorbidities, treatment patterns, and health care costs in usual care settings. Spine (Phila Pa 1976), 37 (11), E668-77.
- Halls, S. B., & Hanson, J. (2014) Average height and weight charts. Retrieved on February 25, 2014, from: http://www.halls.md/chart/women-height-w.htm
- Hashemi, L., Webster, B. S., & Clancy, E. A. (1998). Trends in disability duration and cost of workers' compensation low back pain claims (1988-1996). J Occup Environ Med, 40 (12), 1110-9.
- Liberty Mutual Research Institute for Safety. (2009). Liberty Mutual workplace safety index. Hopkinton, MA: Liberty Mutual Research Institute for Safety
- Manchikanti, L. (2000). Epidemiology of low back pain. Pain Physician, 3 (2), 167-92.
- Marras, W. S. (2000). Occupational low back disorder causation and control. Ergonomics, 43 (7), 880-902.
- Marras, W. S., Lavender, S. A., Leurgans, S. E., Rajulu, S. L., Allread, W. G., Fathallah, F. A., & Ferguson, S. A. (1993). The role of dynamic three-dimensional trunk motion in occupationally-related low back disorders. the effects of workplace factors, trunk position, and trunk motion characteristics on risk of injury. Spine (Phila Pa 1976), 18 (5), 617-28.
- Merryweather, A. S., Loetscher, M. C., & Bloswick, D. S. (2009). A revised back compressive force estimation model for ergonomic evaluation of lifting tasks. Work, 34 (3), 263-72.
- Nachemson, A. (1960). Lumbar intradiscal pressure. experimental studies on post-mortem material. Acta Orthop Scand Suppl, 43, 1-104.
- National Institute for Occupational Safety and Health. (1981). Work practices guide for manual lifting (Tech. Rep.). Cincinnati, OH: National Institute for Occupational Safety (NIOSH).
- Rubin, D. I. (2007). Epidemiology and risk factors for spine pain. Neurol Clin, 25 (2), 353-71.
- Sesek, R., Gilkey, D., Drinkaus, P., Bloswick, D. S., & Herron, R. (2003). Evaluation and quantification of manual materials handling risk factors. Int J Occup Saf Ergon, 9 (3), 271-87.
- Sonoda, T. (1962). Studies on the strength for compression, tension and torsion of the human vertebral column. Journal of Kyoto Prefectural Medical University, 71 (1), 659-702.
- Tang, R. (2013). Morphometric analysis of the human lower lumbar intervertebral discs and vertebral endplates: experimental approach and regression models (Doctoral dissertation). Auburn University. Auburn, AL.
- Tang, R., Güngör, C., Sesek, R., Foreman, K., Gallagher, S., & Davis, G. (2014). Morphometry of the lower lumbar intervertebral discs and endplates—comparative analyses of new MRI data with previous findings. Manuscript in review, Eur Spine J, November 11, 2013
- Tang, R., Güngör, C., Sesek, R., Gallagher, S., Davis, G. and Foreman, K. (2014). Development of regression models for estimating the geometry of lower lumbar intervertebral discs and endplates using MRI-derived dimensions. Manuscript in review, J Anat, December 6, 2013
- Waters, T. R., Putz-Anderson, V., Garg, A., & Fine, L. J. (1993). Revised NIOSH equation for the design and evaluation of manual lifting tasks. Ergonomics, 36 (7), 749-76.

## The Quest to Validate Human Motion for Digital Ergonomic Assessment – Biomechanical Studies to Improve the Human-Like Behavior of the Human Model "EMA"

Dan Gläser, Lars Fritzsche, Sebastian Bauer and Wolfgang Leidholdt

imk automotive GmbH Annaberger Str. 39 09111, Chemnitz, GERMANY

### **ABSTRACT**

Modern digital human simulation tools try to generate motions over an decreased number of input information to pass the method of step-by-step motion generation as it has been common until now. A key feature of EMA is the self-initiated motion generation, which decreases the effort for users in simulation preparation and increases the validity of simulation results in terms of realistic motion trajectories and biomechanical correctness. EMA has been designed for the simulation of human work activities in industrial production. EMA is already capable of reproducing most of common work-related activities, but there is still a need to improve its performance for some specific tasks. With the advancing number of automatically generated movement, the responsibility of the software to produce valid and reliable movement rises to a new level. Furthermore the necessity of valid motor behavior is based on the requirement of a correct assessment of work time and ergonomics in the simulation. Such assessment functions are already implemented using 'state-of-the-art' methods like MTM (Methods Time Measurement) for time analysis and EAWS (Ergonomic Assessment Worksheet) for ergonomics risk evaluation. In order to improve the quality of the ergonomic, time-related and visual simulation results, several studies have recently been carried out. The results of these studies show a large range in variation and complexity leading to the question, how to transfer information gained with scientific studies into explicit implementations for digital human modeling software.

Keywords: Digital Human Modelling, Biomechanics, Motion Capturing, Process simulation

### INTRODUCTION

Digital human models are established within the field of product development by now. Human models like Ramsis (Human Solutions GmbH) or Santos (SantosHuman Inc.) are indispensable when it comes to designing automotive or aircraft interiors. Another fact about the status quo of digital human models is their very limited capabilities in terms of self-initiated motion generation. Actual models like the Human Builder (Dassault Systemes) have incorporated a human like kinematic structure, but the control of these kinematics is still very complex and time costly. This is due to the current standard process of modelling motions with digital human models in a step-by-step apporach, which includes the manual positioning and alignment of every single body segment or segment groups. One essential characteristic is the manual modeling of human movements based on user input and thus, the user himself is responsible for the validity of the generated movements. Therewith the software only has to ensure, that

the human model comes with a correct kinematic structure and valid ranges of motion. The user is responsible for correct movements in terms of plausibility, ergonomics, time related correctness, and the 'style' or appearance of motion.

New systems for holistic simulation of human work activities provide new approaches for more effective and less time consuming methods of planning human behavior. EMA (Editor for Manual Work Activities) is one of these new tools. EMA follows the idea, that the definition of a process should be reduced to a minimum of parameters to decrease the modeling effort for the software user. To fulfill this requirement, EMA uses a task library consisting of parameterized tasks that are common during typical manual work processes (e.g. pick, place, walk) and which are related to the established planning standard MTM (Methods Time Measurement). After the definition of the work activity of the virtual worker, all movements are generated in an analytical way. Due to this self-initiative approach of planning and motion synthesis the responsibility for valid motion generation shifts from the user to the software itself, and therewith to the software developers. To meet this responsibility, imk automotive GmbH carried out several biomechanical studies during the development of EMA, whose results are used to improve the validity of the motion generation.

The following chapter gives an overview about the EMA method before describing two studies about different challenges in the field of human movement modeling and the implementation of the research findings into EMA. At last there will be a call for a scientific discussion about the necessity of future modeling standards in terms of parameters, which have to be prioritized in human movement modeling.

Input Calculation Output Layout definition Visualization Motion generation Geometry - Walking paths - Video export Interactive 3D Working position Mass Postures Object movement window Body movement Reference objects Productivity Added value Process definition Assessment tools Process times Task mapping Productivity Worker Ergonomic Ergonomics synchronization assessment Spaghetti diagram **EAWS** report **Postures** loads

Figure 1. Overview workflow EMA

### THE EMA APPROACH

EMA is a holistic 3D planning method for manual industrial working activities based on a 3D human model. The basic idea behind the method is a definite process language (Illmann et al., 2013) that is used to describe common work activities. The process language is applied to build activity blocks (hereinafter "tasks") representing common operations like use tool, sit down, walk, but also more specific tasks like ingress car or wipe surface(see "task mapping" in Fig 1.). These tasks are parameterized, which means that a minimum on manual user input is needed (e.g., define location coordinates by mouse-click) in order to reduce the simulation effort. A "pick object" for example requires the selection of an object for right, left, or both hands. Every task also consists of optional parameters, which can be used to adapt the tasks to special circumstances (e.g. block leg movement). For more details about the EMA motion generation please refer to Fritzsche et al., 2011. Before the task definition, there is always a lay out definition (see Fig.1). In ema the lay out definition is comparable with standard CAD/CAE tools. Between the input and the output (ergonomic assessment, time related assessment, spaghetti diagram, etc.) the EMA core calculates the postures and 3D trajectories, which are necessary for a complete representation in the 3D viewer and the assessment tools.

### **Latest developments**

The future success of digital humans depends on the continuous improvement of the current systems. One of the latest developments in EMA is the vertical movement system. The vertical movement system is basically a matrix of fundamental body postures like standing, squatting or lying on the back. Furthermore this system provides the ways to get from one posture to another without returning to a basic posture. At first sight, this seems to be trivial, but if one tries to imagine how to get from lying on the back to one-leg kneeling and which postures in between are necessary, the complexity becomes clear.

Other developments have been made in the computational area. The actual ema version is a fully implemented 64 bit system. Furthermore it is possible to import CAD-data in the .jt format, and an export of complete projects in a csv. File is also possible.

An important feature, which was integrated recently, is the upgrade of 3D scene creation. Objects can now be integrated in hierarchical groups. Above that EMA includes the capability of applying motions on objects, as they occur in real scenarios, like assembly lines.

Due to the request of different user groups, an object library including tools, racks, tables and other often needed objects has been implemented lately. Especially this feature is an advancement in terms of usability, since CAD data of industrial facilities are difficult to gather for end users.

### **Future Challenges**

By now, EMA is able to reproduce most of common work activities as they occur in typical industries like the automotive industry in areas of assembly or body weld. Nevertheless there are many fields of development and challenges in the future of EMA. Future fields of development are for example:

- a complete 3D whole-body collision avoidance
- a detailed hand model
- aging-related performance changes
- simulation of cooperative work
- man-machine-interaction (especially with robots)

### **BIOMECHANICAL STUDIES**

As discussed before, a valid motion generation system is inevitable because the responsibility of creating valid motions shifts to the software with proceeding automation of movement generation. In the development of EMA this responsibility was fulfilled by conducting several biomechanical studies; two of them are described in the following.

### Influences of object mass and geometry on the body posture during carrying (Eske, 2014)

Carrying all kinds of different loads is a typical work activity in almost every industrial sector. Thus, carrying represents a significant part of virtual simulated work activities, what qualifies it as relevant research objective for the EMA development. EMA is currently not capable of considering loads in the automated motion generation. In fact loads are considered in the ergonomic assessment with EAWS, but still they have neither influence on movement speed, time or body postures of any simulated task. To close this gap, the first study investigated the most important parameters of carrying activities in a laboratory study.

The test setup included a VICON motion capture system, several different load carriers (small to medium-sized boxes), as they are commonly used in industry (see Fig. 2) and a test person sample. The boxes were filled with different loads, varying from 1 to 15 kg. Additionally the boxes had different grasping widths of 30, 40 and 60 cm. The task for a test persons consisted of picking up a box from a table, carrying it over approximately 4 m and placing it on a another table. The considered parameters for the measurement and analysis were step length, arm position (upper arm elevation, elbow angle), upper body position (bending) and walking speed.

The clearest result with the strongest correlation was the negative relation between load and step length; the higher the load, the shorter the steps and the more steps are required to walk from one table to another. Other parameters like the bending of the upper body showed almost no change between the test conditions; this indicates that the maximum load of 15 kg (which is a common limit in industrial work design) was still far from the performance limit of the sample. Another interesting result was related to the walking speed, which was neither influenced by the dimension nor by the weight of the carried object. Therewith the constant speed and the decreasing step length lead to an increased step frequency. These study results are now considered for improving the huma-like behavior of the EMA man model when it comes to carrying loads.





Figure 2. Test setup for load carrying study. Left: marker setup. Right: task setup

The second study targeted the field of collision avoidance, which has been researched by a number of different scientific areas. Robotics, human kinetics, psychology and information technology are probably the most advanced, in solving the problems of collision avoidance.

The three scientific fields have a different understanding of collision avoidance and focus on different aspects. The information technology started with path finding of points through in a 2D environment, which is the basis of all further development in the 3D space. Modern robotics found algorithms for path or trajectory planning for manipulators, which are easily comparable with the human arm in their complexity or number of links. So basically there are methods, which could be used to control digital human models up to almost any imaginable complexity. The restriction at this point is, that robots miss some of the human given characteristics. Robots usually neither sense discomfort, nor do they have the specific limitations in the range of motion or other biomechanical parameters. At this point psychology and human kinetics are the expected science to fill the gap of knowledge about the human behavior. But both fields concentrated on either rather concrete and limited aspects of the issue or very broad and general models of movement behavior. There is for example a larger number of studies about movements trajectories of end effectors in the 2D space (Nelson, 1983; Hogan & Neville, 1984). On the other side there are general models of human movement planning. Two concepts in this area are Rosenbaum's (2001) knowledge model and the discomfort model developed through several programs by the Technical University Munich. Rosenbaum's model states, that movement planning is primarily influenced by the aspired end pose, while the path planning itself is a trade of function between internal and external energetic costs. Comfort plays a minor role in his model. In contrast to that, the discomfort model (Zacher & Bubb, 2004) is a posture based model and therewith mostly based on static parameters like joint angles and impacting forces, which are used to calculate discomfort.

Both models seem logical, as a closed theory and applicable in their individual use cases. But both models show weaknesses, when it comes to generalizability of movement planning as a holistic concept. Due to the conflict of the planning parameters comfort and costs, which were displayed through the comparison of the knowledge and discomfort models, this study tried to research the collision avoidance behavior of the upper extremities from a holistic point of view.

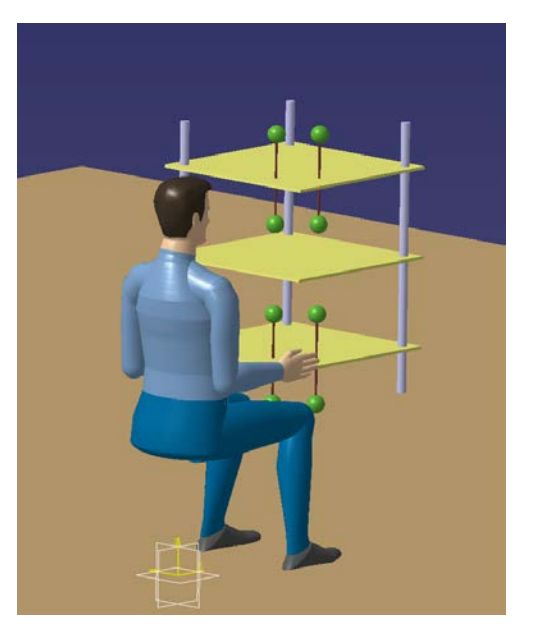
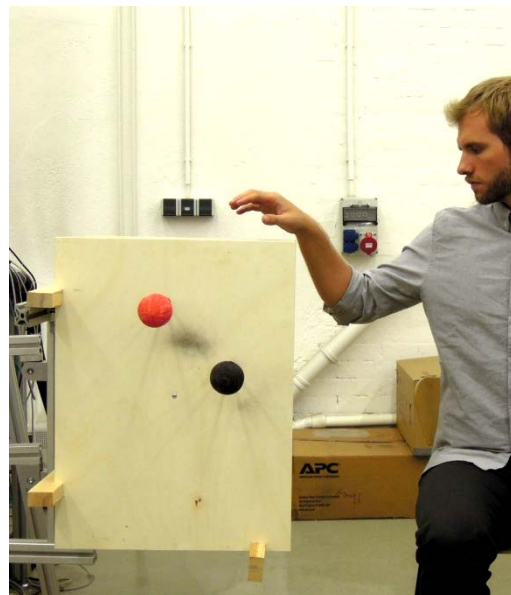


Figure 3. Test setup for collision avoidance study



The study followed a simple collision avoidance setup: Test persons had to move their hand between several targets (see figure 3) and avoid a single collision objects in between. Herein the test persons had to make unconscious or conscious decision about the path they chose. Depending on the task the test person was either faced with a decision between (a.) a short and comfortable versus long and uncomfortable way or (b.) a short but uncomfortable versus a long but comfortable way.

The results showed a variation of avoidance types or characteristics and lead to a classification of four different types:

### a. COMFORT PREFERRING TYPE

Type a. prefers comfortable avoidance strategies, regardless of the potential longer ways.

### b. ADAPTING TYPE

Type c. prefers short distances up to a certain limit of discomfort and switches to a comfort related strategy, when a limit of discomfort is reached.

### c. SHORT DISTANCE PREFERRING TYPE

Type b. prefers shorter distances, regardless of the potential discomfort.

### d. UNDEFINED TYPE

Type d. doesn't show a distinct avoidance strategy.

The four types showed an approximated distribution of 40%(a.), 30%(b.), 10%(c.), 20%(d.), which gives comfort a slight advance as primary planning parameter for collision avoidance. Nevertheless cost related parameters can't be ignored in collision avoidance or motion planning in general. Additionally several avoidance strategies, which are independent from the avoidance type have been identified. These more detailed strategies are for example a tendency for a prevention of elbow movement over shoulder movement or investing in torso movement to save arm movement.

Why these outcomes lead to problems of several layers, will be answered in the next chapter.

### IMPLEMENTATION OF SCIENTIFIC FINDINGS

The gathering of information and knowledge about human behavior is obviously just the first step to an improved digital human modeling. The second and equally challenging part is the implementation of knowledge into the software. The implementation requires the transfer of implicit information into explicit algorithms. To do this, every study requires a different approach for a successful implementation.

The two presented studies represent both ends of a scale, which refer to the grade of complexity and effort for an implementation into planning software like EMA. While the first study gives results with a clear correlation between parameters like mass and step length, the second study produced more questions than it answered, not to mention applicable functions or algorithms. The implementation of the first example requires a function representing the correlation between the parameter mass and step length. Next to that, there is the technical requirement on the software of recognizing loads. In contrary to that the implementation of a holistic automated collision avoidance algorithm for digital human models is very far from being solved. One just has to consider the result of the related study, which not only examined just a minor part of the possible parameters of collision avoidance, but also showed very little correlation between the tested parameters and the observed behavior.

These two studies and earlier findings lead to the conclusion that three particular circumstances result in a higher effort in implementing scientific findings into existing or future software products like EMA (see figure 4). Especially the number of parameters, the variance of the results and the uncertainty of validity have a strong influence on the implementation of findings.

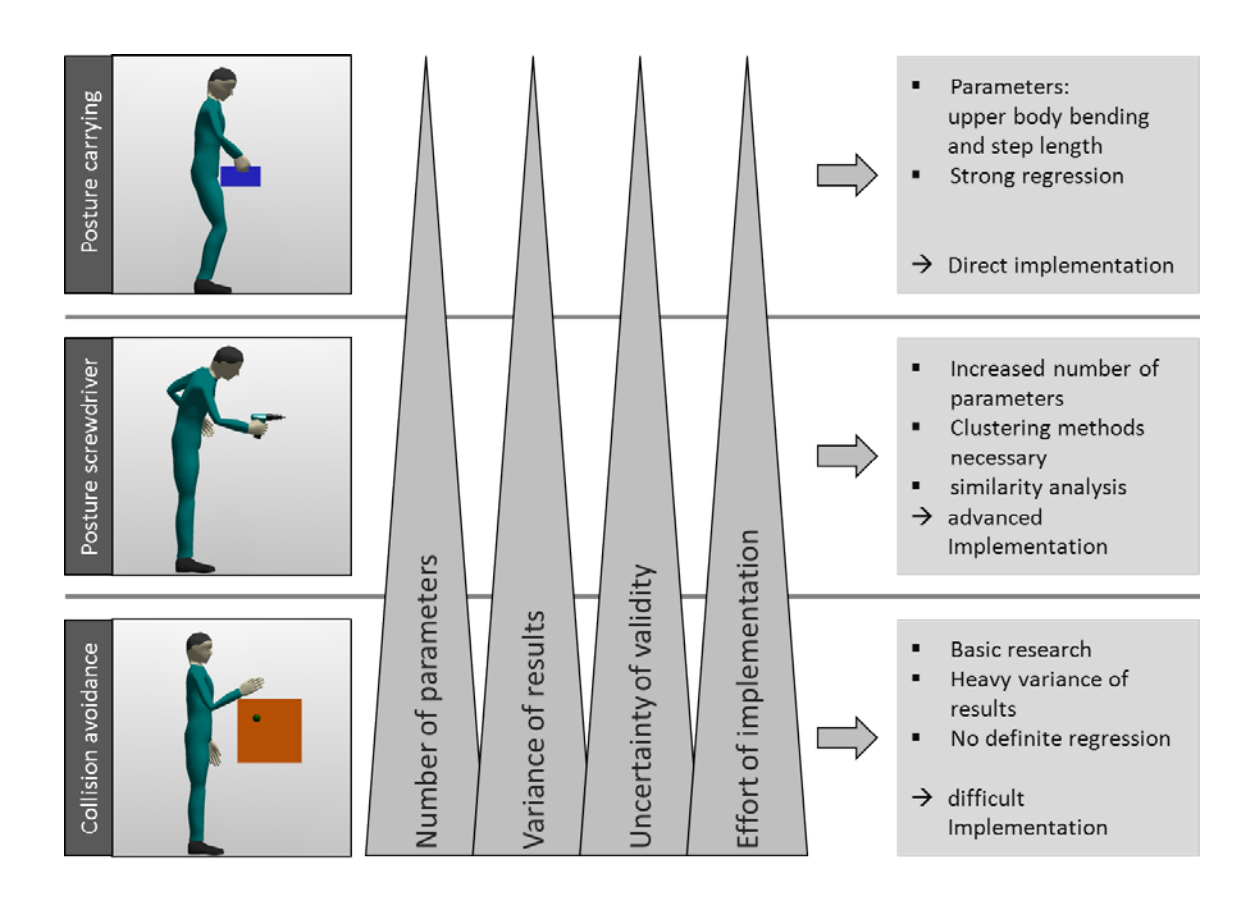


Figure 3. The differences of study outcomes and the consequences for the implementation in EMA

While the number of parameters is a rather obvious influence, the variance of results and the uncertainty of results lead to a new problem. They do not only restrain the implementation in effort, but also have influence on the reliability and validity of the software product. As mentioned in the introduction, there is a shift of responsibility through automated motion generation. If a planning problem, such as collision avoidance, offers more than one possible and likely way of solving a certain movement task, there will always be a conflict of interests in the simulation. This problem grows with the fact, that different solutions of a simulation may lead to different times and different ergonomic assessment, which could add another dimension to the conflict. One reason is the characteristic of today's planning approach in the industrial sector. The planning of a process includes usually only one "optimal" planned process. If there is an ergonomically optimized, a time cost optimized and a best-compromise process, the decision for one solution depends on the user or the philosophy of the company behind. In the case of EMA, the software has to make this decision, until there is the option of parameterized simulation, with parameters for weighting ergonomics, productivity, etc.

For the moment industry standards like MTM and EAWS can be used for the determination of planning times and ergonomic risk assessment. In future software products, with a higher quality and performance of movement generation, it will be necessary to create motion generation standards, which determine the role of possible optimization parameters. This is necessary, because there are possible conflicts of interest in different user groups as described above. User groups as companies or unions may have different priorities and requirements. Since companies usually set a higher value on the productivity and unions might demand optimized ergonomics for working places, software developers depend on a solid base of knowledge and industry standards to fulfill the requirements of possibly all user groups.

### **CONCLUSIONS**

EMA is a modern planning tool that enables the software user to simulate most of the relevant working activities in

manufacturing industries. Nevertheless it is not yet capable of some advanced functions like 3D whole body collision avoidance, which are requested by todays' and tomorrows' users. Due to these requirements and the responsibility that occurs with automated generation of motions, the ongoing process of validating motion generation algorithms is a major topic for digital human modeling research. Since some studies show that human motor behavior isn't explicit in every aspect and the solving of certain tasks as collision avoidance can be done in several legitimate ways, the development of standards for priorities in motion synthesis is essential. Standards are also needed to establish rules for potential conflicts of interest between different user groups and analysis results, such as ergonomic risks and productivity improvements. However, the most sustainable work design considers both aspects simultaneously and equally – EMA provides a basis to this approach.

### REFERENCES

- Eske, S. 2014. "Untersuchungen zum Trageverhalten und unter dem Einfluss von Objektdimension und –gewicht". Bachelor thesis. Technical University Chemnitz
- Fritzsche, L., Jendrusch, R., Leidholdt, W., Bauer, S., Jäckel, T., Pirger, A. (2011). "Introducing ema (Editor for Manual Work Activities) A New Tool for Enhancing Accuracy and Efficiency of Human Simulations in Digital Production Planning." In: V.G. Duffy (Ed.), Digital Human Modeling, HCII 2011, LNCS 6777 (pp. 272–281). Berlin, Heidelberg: Springer.
- Gläser, D. 2013. "Untersuchungen zur Kollisionsvermeidung auf Basis natürlicher Bewegungsmuster". Master Thesis. Technical University Chemnitz.
- Hogan; Neville. 1984. "An organizing principle for a class of voluntary movements." The Journal of Neuroscience 4(11): 2745–2754
- Illmann, B., Fritzsche, L., Leidholdt, W., Bauer, S., Dietrich, M. 2013. "Application and Future Developments of ema in Digital Production Planning and Ergonomics." In: V.G. Duffy (Ed.), DHM/HCII HCII 2013, LNCS 8026 (pp. 66–75). Berlin, Heidelberg: Springer
- Nelson, W.L. 1983. "Physical principles for economies of skilled movements." Biological cybernetics 147: 135–147. http://link.springer.com/article/10.1007/BF00339982 (May 8, 2013).
- Zacher, I.; Bubb, H. 2004. "Strength based discomfort model of posture and movement." SAE transactions 113(1): 87–92.

### Basic Method for Handling Trivariate Normal Distributions in Case Definition for Design and Human Simulation

Dan Högberg<sup>a</sup>, Erik Brolin<sup>a,b</sup> and Lars Hanson<sup>b,c</sup>

<sup>a</sup>School of Engineering Science University of Skövde Skövde, 541 28, Sweden

<sup>b</sup>Department of Product and Production Development Chalmers University of Technology Gothenburg, 412 96, Sweden

> <sup>c</sup>Industrial Development Scania CV, Södertälje, 151 87, Sweden

### **ABSTRACT**

The paper describes a basic approach for the establishment of representative test persons when performing accommodation analyses and wanting to simultaneously consider normal variation in three variables. The main application is for defining a number of different manikins when performing ergonomics simulations for boundary case based accommodation analyses using digital human modelling tools. The method is also applicable when wanting to select representative people to be involved in user trials or to get direct design data. One objective is that the proposed method shall support inclusive design in that it is easy to adopt by non-experts in multivariate accommodation analyses, and accordingly reduce the amount of unsuitable univariate accommodation analyses. The paper introduces the reader to the area of interest, making links to previous research and current problems. The approach for the development of the basic method is explained. The confidence ellipse method is used for defining appropriate boundary manikins according to three selected key variables and desired accommodation level. The paper includes two examples that illustrate the method and compare the method to an alternative method.

Keywords: Anthropometry, Diversity, Digital Human Modelling, Accommodation, Multivariate

### INTRODUCTION

Several methods have been developed for the consideration of anthropometric diversity in design. One example is A-CADRE (Bittner, 2000); a description of 17 body measurement combinations. The collection of such *boundary cases* aims to characterise the anthropometric variation among users in that each case represents an extreme but likely measurement combination (HFES 300 Committee, 2004). The concept behind the boundary case method is that, if the design will fit the boundary cases, people with less extreme body measurement combinations will be catered for by the design as well (Robinette, 2012). Meindl et al. (1993) describe a similar approach for identifying boundary cases using principle component analysis (PCA). PCA can be used to reduce the dimensionality (e.g. from 6 to 2 dimensions) but still represent most of the variance in the data (Jolliffe, 2002). The boundary case methodology procedure is described and evaluated in (Brolin et al., 2012a) and (Brolin et al., 2012b), including a general mathematical description of how to define boundary cases for any number of dimensions.

Design is more and more being performed by the use of computer support, where objects are designed in virtual worlds using computer aided design and engineering (CAD/CAE) tools. In line with this, digital human modelling (DHM) tools have been developed to support designers to consider ergonomic issues in virtual design processes (Duffy, 2009). The DHM tools typically facilitate the creation of human models of almost any sizes, and it becomes a task of the designer to decide the anthropometry of the human models to use in the design task.

Using methods such as the boundary case method for the consideration of anthropometric diversity when using DHM tools is likely to gain the ergonomic qualities of the object being designed, be it products, vehicles or workstations. Still, a study in Swedish vehicle manufacturing companies gave that it was common to use only a few human models as virtual test persons when designing workstations or evaluating manual work (Bertilsson et al., 2010). The study gave that, typically, a small female and a large male, according to stature, were considered as sufficient when performing ergonomics evaluations using DHM tools. This corresponds with findings reported in Robinette (2012). Such an approach mean that one key measurement is used (i.e. *stature*) and that two boundary cases are used (i.e. *small female* and *large male*). The study by Bertilsson et al. (2010) also gave that a common argument for this basic approach was the time needed for each extra virtual test person to be included in a simulation, and that this extra time was not considered worth the possible increase in accuracy in assessing and meeting targeted accommodation levels. Also, the study gave that the comprehension of the complexity of anthropometric diversity in design, and ways to deal with it, was rather scarce, which may also be a reason for the basic approach utilized in the industries studied. However, in essence this is no news and similar concerns have been highlighted for many years (Daniels, 1952; Roebuck et al., 1975; Ziolek and Wawrow, 2004; Robinette, 2012).

There may be many reasons for this gap in best practice, reported in literature by the research society, and observed industry practice, but traditions of how to perform DHM based simulations, and lack of DHM tool functionality and usability, are believed to be important causes. So, the question rises of how to support improved practice when using DHM tools in virtual design processes to consider anthropometric diversity. One way would be "to make it easier to do it right". Indeed, DHM tools' ability to, in theory at least, model any existing anthropometric configuration ought to be utilized when performing simulations of human-product interactions. One step in the direction to aid designers to consider anthropometric diversity is the approach taken when developing the IMMA digital human modelling software (Hanson et al., 2012), where the default manner when performing a simulation includes the definition of a family of anthropometrically representative virtual test persons (a manikin family that represents variance of a number of key measurements) followed by an automatic batch simulation using all these manikins.

Still, as this paper will show, one can consider three human body dimensions simultaneously by doing some basic mathematical treatments of the anthropometric data of the targeted user group. This approach is assumed to be applicable for any DHM tool being used, in the way that the method calculates extreme, but realistic, dimensions of three selected key measurements, in turn acting as input data for regression equations in the DHM tool, used to define the manikin's other measurements. This as a basic but important step from using the univariate (one-dimensional) approach, which in most design purposes is poor in representing anthropometric diversity. In using the trivariate (three-dimensional) approach one can define a number of boundary manikins that concurrently represent variance in three key measurements, for example *stature*, *sitting height* and *waist circumference*, or *shoulder-elbow length*, *forearm-hand length* and *forearm circumference*, *flexed* etc. When selecting key measurements it is recommended to choose measurements that are critical in relation to the design task at hand, and strive for low correlation of these measurements, as not to comprise redundant information (Robinette, 2012). As an example, the selection of manikins in the DHM tool RAMSIS is based on the knowledge that the definition of the characterising property of *length*, *proportion* (ratio of sitting height over body height) and *corpulence* of an individual is sufficient to give an good prognosis of all other body dimensions for this person (Speyer, 1996; Bubb et al., 2006). In RAMSIS these properties are defined by the three key measurements *stature*, *sitting height* and *waist circumference*.

As noted, the approach defines boundary cases, and for some design tasks it might be relevant to define distributed cases instead, or as well. These categories of cases are further described in (HFES 300 Committee, 2004) and (Robinette, 2012). This paper develops the descriptions in (Högberg et al., 2011) and aims here to describe how to calculate boundary cases for trivariate normal distributions. The paper takes a pragmatic standpoint, directing its message towards practitioners and students using DHM tools for design purposes. The method can also be applied when wanting to select representative people to be involved in physical user trials or to get direct design data.

#### **METHOD**

The confidence ellipse method is used for defining appropriate boundary manikins according to three selected key dimensions and a desired accommodation level, here represented by the confidence region. Assuming that all three dimensions are normally distributed, which is appropriate in most cases (Pheasant and Haslegrave, 2006), general statistical methods are applied to analyse the data (e.g. Sokal and Rohlf, 1995; Brandt, 1999). The ANSUR anthropometric data is used in the examples (Gordon et al., 1989). This data is dated and limited in terms of representing "average people" (in that it is based on army personnel measurements), but considered relevant to use for showing principles in that it covers data of a large set of measurements (131) and individuals (1774 men and 2208 women). The presented method is applicable using any well founded anthropometric data though. To illustrate the characteristics of the data, Figure 1 shows a scatter matrix of the ANSUR data for stature and weight for male population. Figure 1 shows two dimensions for easy interpretation, while the following descriptions will cover operations for three dimensions.

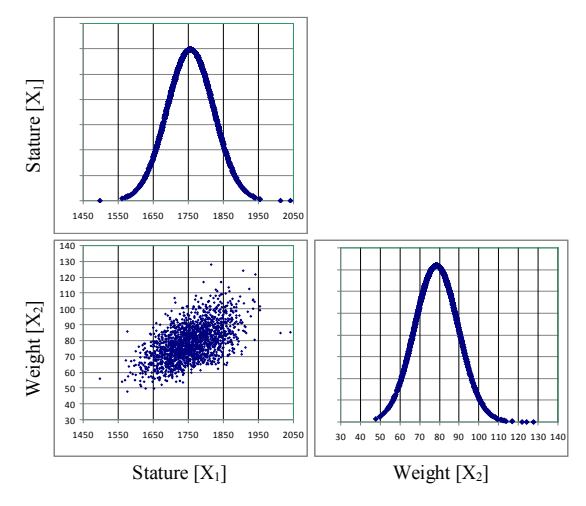


Figure 1: Scatter plot matrix of stature (mm) and weight (kg) for ANSUR data for male population.

The mathematical procedure follows the descriptions in (Brolin et al., 2012a) and (Brolin et al., 2012b), where input data are:

Mean values:  $\mu = [\mu_1 \quad \mu_2 \quad \mu_3]$ , Standard deviations:  $\sigma = [\sigma_1 \quad \sigma_2 \quad \sigma_3]$ ,

Correlation matrix: 
$$\rho = \begin{bmatrix} 1 & \rho_{12} & \rho_{13} \\ \rho_{21} & 1 & \rho_{23} \\ \rho_{31} & \rho_{32} & 1 \end{bmatrix}$$
, and

Desired level of accommodation: P, where: 0 < P < 1, e.g. P = 0.95 for a 95% accommodation objective.

These input data are used to calculate the three dimensional confidence region, based on the definition of eigenvalues, eigenvectors and scaling the ellipsoid, as described in (Brolin et al., 2012a). Axis cases and box cases are then defined on the boundary of the ellipsoid as described in (Brolin et al., 2012a; Brolin et al., 2012b).

The outcomes from the described method is illustrated and compared to an alternative method in two examples.

#### **RESULTS**

A basic demonstrator was built by entering the equations into regular spreadsheet software (Microsoft Excel 2010) without any plugins required; making it easy to calculate and illustrate results, and simple to share. The demonstrator is based on using the female ANSUR anthropometric data (Gordon et al., 1989) and the user just needs to specify which three of the 131 available body measurements to consider and set a desired accommodation level. The spreadsheet draws the associated data from the database, determines the correlation coefficients, solves the calculations algebraically, defines the cases and creates the diagrams automatically. This facilitates easy testing of different measurement combinations and interpretation of outcomes. Output data is presented as *value* (in mm or kg), *z-score* (standard score) and *percentile* for the three selected measurements for 15 boundary cases, representing:

- 1 *centre case* (the average value of the trivariate distribution)
- 6 axis cases (located at the axis end of each eigenvector; where the axis meets the confidence ellipsoid)
- 8 box cases (located at the corners of the cuboid that spans the largest volume inside the ellipsoid)

The output diagrams show, in the three orthogonal 2D-projections, the scatter plot (i.e. data on individuals in the ANSUR database, to show the relation between the artificially drawn cases and real people), the confidence ellipsoid and the location of all 15 cases. The cases are identified, and the diagrams are plotted, in the standardised space. This procedure is appropriate when comparing different normal distributions (Glenberg and Andrzejewski, 2007) and gives each distribution the same significance in the calculations.

#### Example 1

The first case illustrates the functionality of the demonstrator. The three measurements *stature*, *sitting height* and *shoulder-elbow length* are selected and the desired accommodation level is set to 90%. Figure 2 shows the input area of the spreadsheet where the white areas are where the user enters desired values. Each measurement has a unique number which is given when inspecting the anthropometric database within the spreadsheet. In the grey cells data for average values, standard deviations and the correlations matrix are given for the selection of measurements. As seen, in this case the recommendation to select measurements with low correlations is not followed. Some of the correlations are above 0.7 which is considered a high correlation in this context. Hence the result is a rather narrow ellipsoid (Figure 4). This selection of measurements is however made to facilitate comparisons with results in (Brolin et al., 2012a).

Input	Enter measurement numbers and accommodation objective into white cells							
Measurement number	99	93	91					
Name	STATURE	SITTING_HT	SHOULDER_ELBOW_LNTH					
Unit	mm	mm	mm					
Average (μ)	1629	852	336					
Standard deviation $(\sigma)$	63.6	34.9	17.4					
Correlation matrix (ρ)	STATURE	SITTING_HT	SHOULDER_ELBOW_LNTH					
STATURE	1	0.755	0.798					
SITTING_HT	0.755	1	0.420					
SHOULDER_ELBOW_LNTH	0.798	0.420	1					
Accomodation objective	90	%						
	-							

Figure 2: Input area. White cells are entered by the user and grey cells are given automatically.

Figure 3 shows the output area with data for the 14 boundary cases (6 axis and 8 box) and the average case, plus the minimum and maximum value for each measurements among the 15 cases.

ıtput	Case data								
Centre and boundary cases		STATURE		SITTING HT			SHOULDER ELBOW LNTH		
	Value	Z-core	Percentile	Value	Z-core	Percentile	Value	Z-core	Percentile
1 (centre)	1629	0	50.00	852	0	50.00	336	0	50.00
2 (axis)	1784	2.43	99.25	923	2.05	97.98	372	2.11	98.25
3 (axis)	1475	-2.43	0.75	780	-2.05	2.02	299	-2.11	1.75
4 (axis)	1592	-0.58	28.09	863	0.31	62.30	342	0.36	64.22
5 (axis)	1666	0.58	71.91	841	-0.31	37.70	329	-0.36	35.78
6 (axis)	1633	0.06	52.26	803	-1.40	8.11	358	1.29	90.20
7 (axis)	1626	-0.06	47.74	901	1.40	91.89	313	-1.29	9.80
8 (box)	1699	1.10	86.47	871	0.56	71.12	374	2.17	98.52
9 (box)	1521	-1.71	4.40	789	-1.81	3.52	331	-0.26	39.71
10 (box)	1563	-1.04	15.01	776	-2.17	1.50	324	-0.68	24.78
11 (box)	1742	1.77	96.18	859	0.20	57.74	366	1.75	96.03
12 (box)	1695	1.04	84.99	928	2.17	98.50	348	0.68	75.22
13 (box)	1517	-1.77	3.82	845	-0.20	42.26	305	-1.75	3.97
14 (box)	1559	-1.10	13.53	833	-0.56	28.88	298	-2.17	1.48
15 (box)	1738	1.71	95.60	915	1.81	96.48	340	0.26	60.29
Max	1784	2.43	99.25	928	2.17	98.50	374	2.17	98.52
Min	1475	-2.43	0.75	776	-2.17	1.50	298	-2.17	1.48

Figure 3: Output area. Data for the 15 cases and min and max values.

Figure 4 shows the corresponding ellipsoid in standardised space and the 15 cases shown as dots (centre and axis cases in red dots and box cases in grey dots). The spreadsheet gives the three orthogonal projections. The scatter plot illustrates how approximately 10% of the dots (individuals) are located outside the ellipsoid, consistent with the selected accommodation objective of 90%.

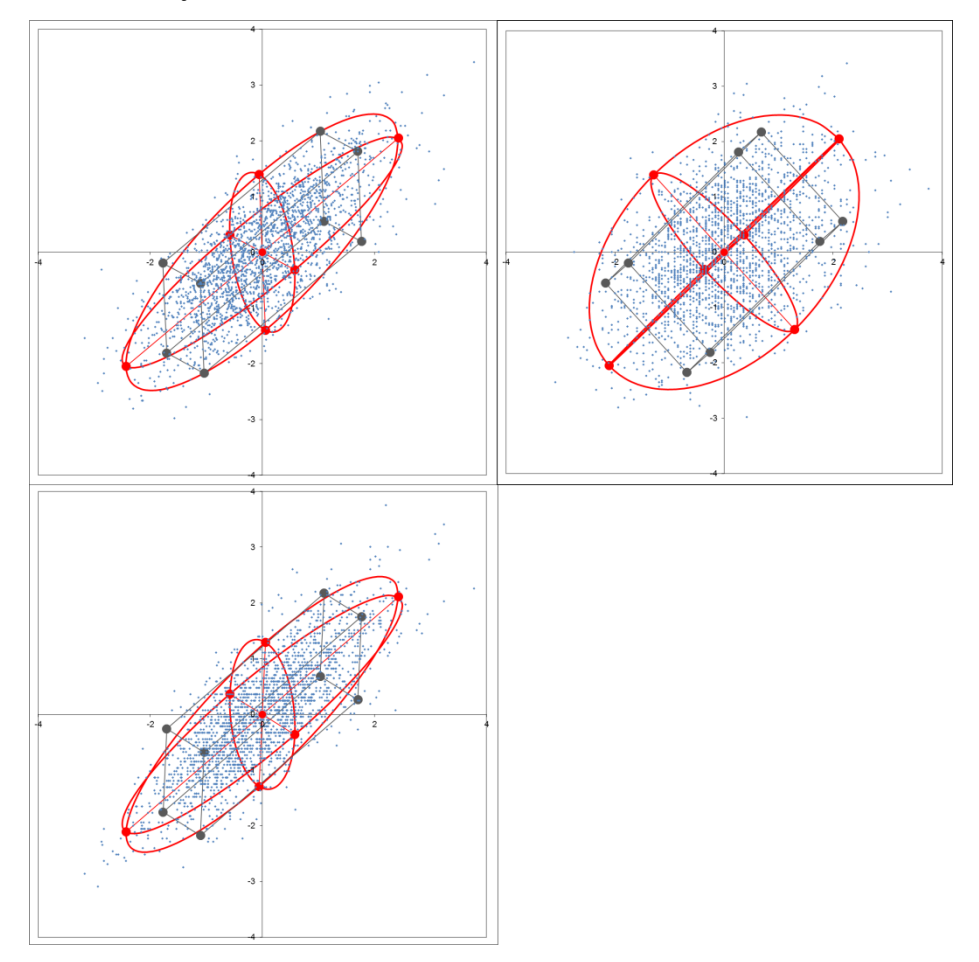


Figure 4: The confidence ellipsoid in the 3 orthogonal projections and the 15 cases (scale in standard scores).

To illustrate, entering the values of stature, sitting height and shoulder-elbow length (Figure 3) in the DHM tool Jack 7.1 (Siemens, 2011) gives manikins as shown in Figure 5, here called a *manikin family*. All other manikin measurements are regressed in Jack from the entered values. Hence, in this case these manikins represent a suggested virtual test group to use for design purposes in ergonomics simulations. The designer may still choose a subset of the manikins if a fewer number of test manikins is wanted, e.g. the 6 axis cases or the 8 box cases.

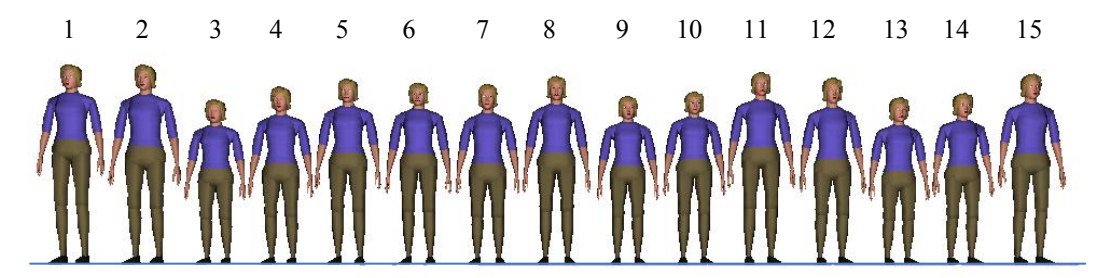


Figure 5: Manikin family of 15 members (1 average, 6 axis and 8 box cases) modelled in Jack.

In Brolin et al. (2012a) the 6 axis cases in the manikin family (Figure 5, manikins 2-7) are applied to a task of extracting values of required adjustment ranges in the design of an office workplace, including a comparison of the outcomes from using four alternative ways to define boundary cases that represent anthropometric diversity. The study in Brolin et al. (2012a) shows that different ways of establishing representative virtual test persons influence the predicted design dimensions related to meeting accommodation objectives.

#### Example 2

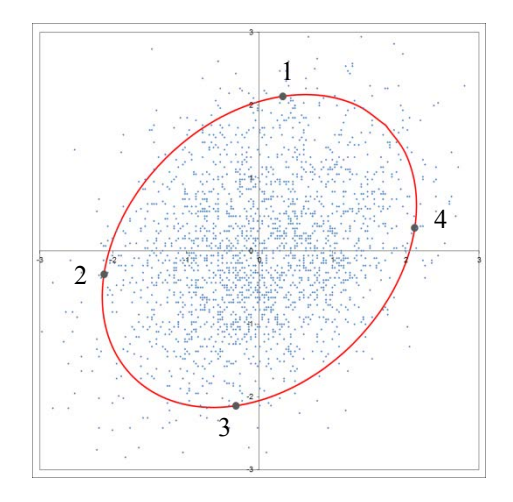
For some design tasks it is possible to conclude that, for certain dimensions, it is enough to use the largest or smallest boundary case for getting data for the design task. An example of this is given in Robinette (2012), in the context of seated workstation design, where the definition of the minimum width of a seat only requires a large case related to *hip-breadth*, *sitting* to get design data. In the example in Robinette (2012), three critical dimensions are identified: *eye-height*, *sitting*, *buttock-knee length* and *hip-breadth*, *sitting*, and the desired accommodation is set to 90%. The method illustrated in Robinette (2012) is based on meeting the 90% accommodation objective by creating four boundary box cases using a bivariate (two dimensional) 90% confidence ellipsoid for *eye-height*, *sitting* and *buttock-knee length* and selecting the maximum value of *hip-breadth*, *sitting*. This is a sensible approach. However, sometimes it may be hard for a designer to know how and when to draw such conclusions of how to handle key dimensions. Of that reason, the method presented in Robinette (2012) (here called Approach 1) is compared with the trivariate approach presented in this paper (here called Approach 2). The objective is to compare the different case dimensions from using the two approaches of meeting the accommodation objective (90% in this case) for three key measurements. Female anthropometric data from ANSUR data is used in this example. Table 1 gives values (in mm and percentile) for dimensions of the 4 box cases using Approach 1 (2D confidence ellipse + max value for third dimension) and Table 2 the values for the 8 box cases using Approach 2 (3D confidence ellipsoid).

	Cases	1	2	3	4	Min	Max
eve-	mm	750	669	728	809	669	809
height,	z-score	0.32	-2.12	-0.32	2.12	-2.12	2.12
sitting	%-ile	62.5	1.7	37.5	98.3	1.7	98.3
buttock-	mm	652	580	526	598	526	652
knee	z-score	2.12	-0.32	-2.12	0.32	-2.12	2.12
length	%-ile	98.3	37.5	1.7	62.5	1.7	98.3
hip- breadth, sitting	mm	493	493	493	493	493	493
	z-score	3.98	3.98	3.98	3.98	3.98	3.98
	%-ile	>99.9	>99.9	>99.9	>99.9	>99.9	>99.9

Table 1: Dimensions for the 4 box cases using Approach 1.

Table 2: Dimensions for the 8 box cases using Approach 2.

	Cases	1	2	3	4	5	6	7	8	Min	Max
eve-	mm	732	666	676	742	801	736	745	811	666	811
height,	z-score	-0.20	-2.17	-1.89	0.09	1.89	-0.09	0.20	2.17	-2.17	2.17
sitting	%-ile	42.1	1.5	3.0	53.5	97.0	46.5	57.9	98.5	1.5	98.5
buttock-	mm	620	552	593	660	585	518	558	625	518	660
knee	z-score	1.03	-1.23	0.13	2.39	-0.13	-2.39	-1.03	1.23	-2.39	2.39
length	%-ile	85.0	10.9	55.1	99.2	44.9	0.8	15.0	89.1	0.8	99.2
hip-	mm	446	382	340	404	429	365	323	387	323	446
breadth, sitting	z-score	2.27	-0.08	-1.64	0.72	1.64	-0.72	-2.27	0.08	-2.27	2.27
	%-ile	98.8	46.7	5.1	76.3	94.9	23.7	1.2	53.3	1.2	98.8



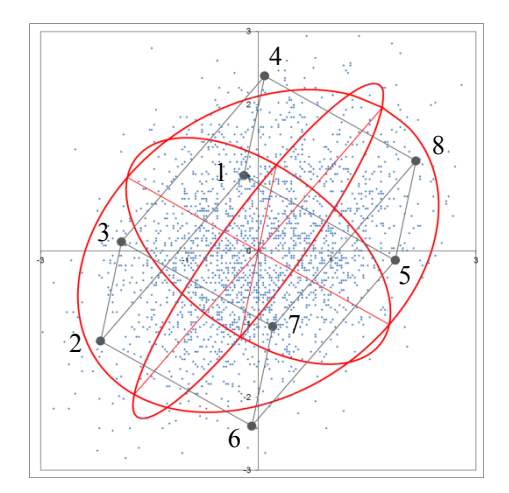


Figure 6: Ellipse and 4 cases (Approach 1, left), Ellipsoid and 8 box cases (Approach 2, right) (scale in standard scores).

By studying the values in Table 1 and the left image in Figure 6 it is possible to see how the equations spread out the cases on the boundary of the ellipse. Correspondingly, by studying the values in Table 2 and the right image in Figure 6 it is possible to see how the equations spread out the cases on the boundary of the ellipsoid. Table 3 shows how the box cases in Table 1 and Table 2 represent types of combinations of *eye-height*, *sitting*, *buttock-knee length* and *hip-breadth*, *sitting* stated in the approximate terms: Extremely large (EL) (seeing z>3 as extremely large), Large (L), Average (A) (seeing -1.2 < z < 1.2 as average) and Small (S).

Table 3: Combinations of approximate types per approach.

	•	Appro	oach 1					Appro	oach 2		•	
Cases	1	2	3	4	1	2	3	4	5	6	7	8
eye- height, sitting	A	S	A	L	A	S	S	A	L	A	A	L
eye- height, sitting	L	A	S	A	A	S	A	L	A	S	A	L
eye- height, sitting	EL	EL	EL	EL	L	A	S	A	L	A	S	A

Table 4 shows difference between maximum and minimum value per dimension for each approach, in order to illustrate in what way the two different approaches represent the range per dimension (assuming Approach 1 accommodates from min to max value in the ANSUR database for *hip-breadth*, *sitting*).

Table 4: Range per dimension per approach.

	Range	Approach 1	Approach 2
1: -1.4	mm	140	145
eye-height,	z-score	4.24	4.34
sitting	%-ile	96.6	97.0
buttock-knee	mm	126	142
	z-score	4.24	4.78
length	%-ile	96.6	98.4
1 : 1 1.1	mm	185	123
hip-breadth,	z-score	6.79	4.54
sitting	%-ile	99.7	97.6
PeopleSize		94	94
BodyBuilder		93	93

The probability levels that the min and max values in Table 1 and 2 answer to, according to two separate anthropometric software, was calculated by using the multidimensional analysis functionality in: 1) PeopleSize 2008 Professional Version 2.02 (PeopleSize, 2009) and 2) RAMSIS BodyBuilder Version 1.4-3.8.31 (Human-Solutions, 2010) (Table 4). For the BodyBuilder calculation *sitting height* was used rather than *eye-height*, *sitting* due to non-availability of the measurement in the software, but since these measurements show high correlation ( $\rho$ =0.997) the value of approximate level of combined accommodation is argued to be legitimate. Correspondingly, *hip-breadth* was used rather than *hip-breadth*, *sitting* ( $\rho$ =0.898). Table 4 shows the same value for Approach 1 and Approach 2 from PeopleSize and BodyBuilder respectively, which indicates that both Approach 1 and Approach 2 offer a similar level of accommodation, which is as expected since both approaches claim to accommodate the same proportion of the population, i.e. 90%. The reasons why both PeopleSize and BodyBuilder indicates a higher level of accommodation (i.e. 94% and 93%) is hard explain since it is not clear how the two software do the calculations and what correlation data they use. However, by the means of a script that counted the percentage of the 2208 subjects that were encapsulated by the 90% ellipsoid gave that 90.53% were encapsulated in the setup in Example 2 (and, to compare, 90.22% in Example 1), indicating that the mathematical methodology works well.

#### CONCLUSIONS AND DISCUSSION

Table 4 shows how the trivariate method (Approach 2) represent a more even range per measurement compared to Approach 1, as expected since Approach 1 is based on assuming the maximum value for one dimension. Using maximum value is sensible since it should mean that all people would be accommodated. Still, as design is a complicated optimisation task of finding the best overall solution that meets many, often conflicting, requirements, the objective to accommodate all users (though in Approach 1 only related to one certain dimension) may be a costly attempt, or causing sub-optimisation since it could lead to drawbacks related to other product qualities. It is argued that the trivariate approach (Approach 2) offers a more controlled way to meet the accommodation objective compared to Approach 1 in this example. Also, the suggested manikin family of Approach 2 is a more design task neutral, hence more general, approach than Approach 1 in that the family better represents the actual variation within the population compared to the cases suggested by Approach 1, which was devised to suit a certain design task. This is obvious by looking at how the two methods differ in representing variation in hip-breadth, sitting. This highlights a fundamental issue of appropriate approach when defining cases and get design data. Should the cases be selected according to the design task, or rather selected to represent the general variation within a population? The latter would resemble a situation when a company has established a well-founded test group that is always recruited to test products being designed, or benchmarked, regardless of type of product or issue to assess. This way of reasoning can also be applied when using DHM tools, where a company may create a manikin family that always will act as their standard virtual test group.

An option would be to mix Approach 1 and 2, i.e. to use a three dimensional confidence ellipsoid and one minimum/maximum value, and thereby consider four dimensions in the design. Another approach would be to use DHM tools to perform large numbers of ergonomics evaluations associated to a specific design task, e.g. related to issues like fit, reach, and comfort, where the software identify which cases within a population (on the boundary and

distributed) that experience the largest problems or draw the most extreme design data. Such an advanced method, called Adaptive Ergonomic Search (AES), is presented in Mårdberg et al. (2012).

This paper describes a more basic approach compared to AES and PCA based methods, but argues that the proposed trivariate method is advantageous compared to approaches based on the use of univariate percentile data in design, and an important step towards enhanced accuracy in meeting desired levels of accommodation, e.g. when using DHM tools for the design of products and workplaces. This paper presents a way to calculate boundary cases on a three dimensional confidence ellipsoid by the means of regular spreadsheet software, providing a basic, low-cost and practical tool. Most computer users have access to regular spreadsheet software (such as MS Excel) making the file easy to distribute, e.g. to practitioners and students that do design where there is a need for the consideration of anthropometric diversity, which indeed is common in design for creating solutions that fit targeted users. An obvious restriction in the demonstrator tool is that only female anthropometrics is considered, and there are plans to add the option to also consider male data. The three dimensional approach is basic compared to more advanced methods, but still an important step forward compared to using the univariate approach for multidimensional design problems. Also, if the three key dimensions are selected thoughtfully, a good prediction of an individual's all other measurements can be drawn (Speyer, 1996; Bubb et al., 2006). Another advantage with the three dimensional approach, where each dimension represent an actual body dimension, is that it is easier to interpret the ellipsoid and the location of the cases, compared to a hyper-ellipsoid of four dimensions of more. Also, having the ellipsoid plotted in the space of real dimensions makes it easier to interpret the ellipsoid and its cases, compared to using PCA which converts and transforms the data to a new coordinate system based on principal components.

Having the ellipsoid plotted together with a scatter plot of real individuals is argued to be important in order to illustrate to the tool user how the ellipsoid encapsulates approximately the percentage of the dots set by the value of the accommodation objective. Also, the scatter plot is argued to be important to highlight that people that are located outside of the ellipsoid by the set accommodation objective are likely to be excluded by the final design. Hopefully this will trigger discussions within the design team, and with managers, of appropriate accommodation levels. Setting an accommodation level of 90% is common, but still that means that 1 of 10 persons is not explicitly considered in the design. Porter and Porter (2001) consider the 90% accommodation objective as somewhat out-ofdate given the concern for quality of life, high productivity and safety. Aiming for higher accommodation levels complies with the concept of *inclusive design*, which has positive implications both on life-quality for more people but also opens opportunities to expand markets by satisfying more users by the design (Waller et al., 2013). The reasoning behind the inclusive design approach is that designers should try to include users rather than exclude users when designing products, systems and environments; it encourages an attitude of "what if we design like this, then we would include these user groups as well, rather than exclude them". The issue of when someone actually is accommodated or not by a design is however often not so precise, but rather a multifaceted "grey area issue" (Clarkson et al., 2013). Hence, accommodation when interacting with a product or workstation is often within a range that can be portrayed: from works well - being frustrated - having difficulty to exclusion (not able to use/perform task/interact). Indeed, the approach presented in this paper does not claim to ensure that someone with anthropometry that would be located within the ellipsoid would be accommodated and that someone outside the ellipsoid would be non-accommodated. Firstly, there may be other measurements than the three measurements, selected on the assumption that they would limit accommodation, which will cause exclusion. Secondly, there may be links between human anthropometry and accommodation of using an object that is not captured when using this method, which would rather be captured by observing digital human models or real people interacting with the object being designed. It may, of course, also be other issues than anthropometry that cause exclusion. Still the presented method is claimed to be a substantial improvement from the common univariate 5 percentile female to 95 percentile male approach, in that the method supports the consideration of multidimensional anthropometry issues in design. Porter et al. (2002) argues that, if user groups are to be excluded of one reason or another, that outcome ought to be the result of a conscious design decision rather than for example an effect of poor information, knowledge or consideration within the design team, and that designers need support, e.g. tools and methods, to enable this. The method presented in this paper is a contribution towards that call.

#### **ACKNOWLEDGEMENTS**

This work has been made possible with the support from VINNOVA in Sweden, within the FFI programme, and by the participating organisations. This support is gratefully acknowledged.

#### REFERENCES

- Bertilsson, E., Svensson, E., Högberg, D., Hanson, L. (2010), "Use of digital human modelling and consideration of anthropometric diversity in Swedish industry". Proceedings of the 42nd annual Nordic Ergonomic Society Conference, Stavanger, Norway, September 6-8, ISBN 9788299574723.
- Bittner, A.C. (2000), "A-CADRE: advanced family of manikins for workstation design". XIVth Congress of IEA and 44th Meeting of HFES, San Diego, pp.774-777.
- Brandt, S. (1999), "Data Analysis Statistical and Computional Methods for Scientists and Engineers, 3rd edition". Springer-Verlag, New York, ISBN 0387984984.
- Brolin, E., Högberg, D., Hanson, L. (2012a), "Description of boundary case methodology for anthropometric diversity consideration". International Journal of Human Factors Modelling and Simulation, 3, pp. 204-223.
- Brolin, E., Högberg, D., Hanson, L. (2012b), "Using experimental design to define boundary manikins". Work, 41(1), pp. 4598-4605.
- Bubb, H., Engstler, F., Fritzsche, F., Mergl, C., Sabbah, O., Schaefer, P., Zacher, I. (2006), "The development of RAMSIS in past and future as an example for the cooperation between industry and university". International Journal of Human Factors Modelling and Simulation, 1, pp. 140-157.
- Clarkson, P.J., Waller, S., Cardoso, C. (2013), "Approaches to estimating user exclusion", Applied Ergonomics, http://dx.doi.org/10.1016/j.apergo.2013.03.001
- Daniels, G.S. (1952), "The average man?" Ohio, Wright Air Development Center, Wright-Patterson Air Force Base. Technical Note WCRD, 53-7.
- Duffy, V.G. (2009), "Handbook of Digital Human Modeling", Taylor & Francis Group, Boca Raton.
- Glenberg, A., Andrzejewski, M. (2007), "Learning from Data: An Introduction to Statistical Reasoning, 3rd ed.". Routledge Academic, New York, ISBN 9780805849219.
- Gordon, C.C., Churchill, T., Clauser, C.E., Bradtmiller, B., McConville, J.T., Tebbetts, I., Walker, R.A. (1989), "1988 Anthropometric Survey of U.S. Army Personnel: Methods and Summary Statistics". Technical Report Natick/TR-89-044. U.S. Army Natick Research, Development and Engineering Center, Natick, MA.
- Hanson, L., Högberg, D., Söderholm, M. (2012), "Digital test assembly of truck parts with the IMMA-tool". Work: A Journal of Prevention, Assessment and Rehabilitation, Vol. 41, Suppl.1, pp. 2248-2252.
- Högberg, D., Bertilsson, E., Hanson, L. (2011), "A basic step towards increased accommodation level accuracy when using DHM tools". Proceedings of: DHM 2011, First International Symposium on Digital Human Modeling, Lyon, France.
- HFES 300 Committee. (2004), "Guidelines for using anthropometric data in product design". Santa Monica: Human Factors and Ergonomics Society. ISBN 0945289235.
- Human-Solutions. (2010), "RAMSIS BodyBuilder Version 1.4-3.8.31". Kaiserslautern, Germany, Human Solutions GmbH.
- Jolliffe, I. (2002), "Principal Component Analysis, 2nd ed.", Springer, New York.
- Meindl, R.S., Hudson, J.A., Zehner, G.F. (1993), "A Multivariate Anthropometric Method for Crew Station Design". Crew Systems Directorate, Human Engineering Division, Armstrong Laboratory, Wright-Patterson Air Force Base, Ohio. Technical Report AL-TR-93-0054.
- Mårdberg, P., Carlson, J.S., Bohlin, R., Hanson, L., Högberg, D. (2012), "Using Ergonomic Criteria to Adaptively Define Test Manikins for Design Problems". Advances in Applied Human Modeling and Simulation. Duffy, V.G. (Ed.). CRC Press. pp. 265-274, ISBN 978-1-4398-7031-0 (print), ISBN 978-1-4398-7032-7 (eBook).
- PeopleSize. (2009), "PeopleSize 2008 Professional". Melton Mowbray, UK, Open Ergonomics Ltd.
- Pheasant, S., Haslegrave, C.M. (2006), "Bodyspace: Anthropometry, Ergonomics and the Design of Work, 3rd ed.", Taylor & Francis, Boca Raton. ISBN 0415285208.
- Porter, J.M., Porter, S.C. (2001), "Occupant accommodation: an ergonomics approach". An Introduction to Modern Vehicle Design. J. Happian-Smith, Ed. London, Butterworth-Heinemann, pp. 233-275.
- Porter, J.M., Case, K., Gyi, D.E., Marshall, R., Oliver, R.E. (2002), "How Can We 'Design for All' If We Do Not Know Who is Designed Out and Why?", XVI Annual International Occupational Ergonomics and Safety Conference, Toronto, Canada, ISOES.
- Robinette, K.M. (2012), "Anthropometry for product design". Handbook of Human Factors and Ergonomics, 4 th ed., G Salvendy (Ed.): John Wiley & Sons, Hoboken, pp.330-346. ISBN 9780470528389.
- Roebuck, J.A., Kroemer, K.H.E., Thomson, W.G. (1975), "Engineering Anthropometry Methods". New York, John Wiley & Sons.
- Siemens. (2011), "Jack Version 7.1", Siemens Product Lifecycle Management Software Inc., California, USA.
- Sokal, R.R., Rohlf, F.J. (1995), "Biometry: the principles and practice of statistics in biological research, 3rd ed.". W. H. Freeman and Co, New York, ISBN 0716724111.
- Speyer, H. (1996), "On the definition and generation of optimal test samples for design problems". Kaiserslautern, Human Solutions GmbH.

- Waller, S., Bradley, M., Hosking, I., Clarkson, P.J. (2013), "Making the case for inclusive design", Applied Ergonomics, http://dx.doi.org/10.1016/j.apergo.2013.03.012
  Ziolek, S.A., Wawrow, P. (2004), "Beyond Percentiles: An Examination of Occupant Anthropometry and Seat Design". Society of Automotive Engineers, SAE Technical Paper 2004-01-0375, Warrendale.

## Section 2

Digital Human Modeling and Human Factors

# Assessing the Precision of Anthropometric Measurements: A Six Sigma Approach

Dermot Hale and Enda F. Fallon

Centre for Occupational Health & Safety Engineering & Ergonomics (COHSEE)

Discipline of Mechanical Engineering

College of Engineering and Informatics

National University of Ireland, Galway

Galway, Ireland

#### **ABSTRACT**

Anthropometrics is the measurement of dimensions of the human body defined between fixed anatomical landmarks (Ulijaszek & Kerr, 1999). The human body however does not generally lend itself to simple measurement as the limits or position of anatomical landmarks can often be open to interpretation. Given that effective anthropometric practices are dependent on the validity of the anthropometric data, it is critical that anthropometrists have confidence in the data they use. This paper discusses existing practices in determining anthropometric measurement error and introduces the Six Sigma technique, Gauge Repeatability & Reproducibility, to the discipline of anthropometry.

Keywords: Anthropometric Measurement, Technical Error of Measurement, Gauge Repeatability & Reproducibility

#### INTRODUCTION

Anthropometrists have long appreciated the need to ensure confidence in the capability of anthropometric measuring instruments (Jamison & Zegura, 1974). Confidence in measurement instruments is based on the accuracy and precision of measurements taken. Accuracy is defined as the ability to measure the true value correctly, whereas, precision is defined as the closeness of the measured readings to each other (Dawson, 2004). In Figure 1, the bull'seye of the target is considered to be the true value of the measured characteristic. The measured values are represented by the plus sign. The top left segment of the figure represents the desired state with regard to the measurement system, where the measurements are both accurate and precise. The top right segment is an indication of precision but inaccurate measurements. The bottom left segment depicts measurements which are accurate but imprecise. In the bottom right segment, the measurements are neither precise nor accurate.

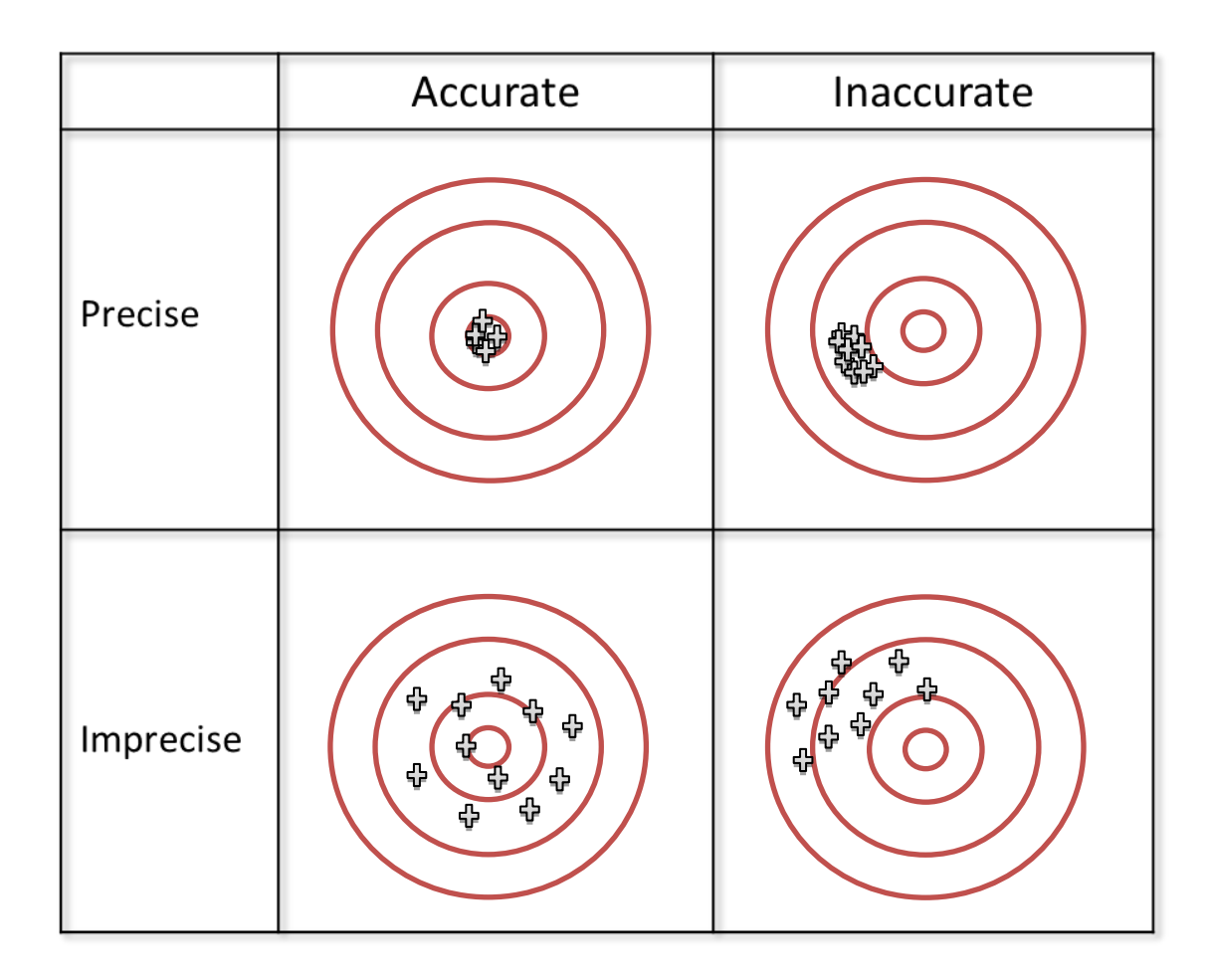


Figure 1: Concepts of Accuracy and Precision

Determining the accuracy of the measuring device through calibration should be the first step in assessing a measurement method. The calibration should be traceable to applicable National and/or International standards. Determining the precision is a function of determining the error when the instrument is used.

The most common method of expressing error in anthropometry is by means of the Technical Error of Measurement (TEM) (Pederson & Gore, 1996). The TEM defines the standard deviation of repeated measurements. The TEM enables anthropometrists to quantify the measurement error when taking and repeating anthropometrical measurements (intra-evaluator) and when comparing their measurement with measurements from other anthropometrists (inter-evaluator). Harris and Smith (2009) contend however, that few studies actually quantify TEM. Furthermore the effectiveness of the TEM has been questioned. Ulijaszek and Kerr (1999) suggest that the lack of reporting of measurement error in anthropometric studies is due to the difficulty in interpreting TEM values in the context of the particular data collected. It is evident therefore, that a more robust and standardised method for evaluating measurement error in anthropometric measuring systems instruments is desirable.

This work reported in this paper seeks to address this issue by introducing the Six Sigma tool of Gauge Repeatability and Reproducibility (Gauge R&R) to the domain of anthropometrics (Breyfogle, 2003). Similar to the TEM, Gauge R&R is a statistical method of determining the variation introduced by the measurement instrument and the anthropometrist. Unlike the TEM however, the output of Gauge R&R provides a standardized acceptance criteria threshold for acceptability of the anthropometric measuring system. In using a standardised approach it is possible to benchmark the effectiveness of a specified instrument against alternative instruments and against specified expected levels of measurement performance.

#### TECHICAL ERROR OF MEASUREMENT

The Technical Error of Measurement (TEM) is described as a representation of 'the typical magnitude of measurement error that one can expect to occur' (Knapp, 1992). TEM is quantified by taking repeated measurements of the same objects as it has been generally assumed that the mean of a series of repeated measurements is the best available estimate of an object's true size (Harris & Smith, 2009). Dahlberg, in 1940, published the following formula for the TEM:

$$S_D = \sqrt{\frac{\sum_{i=1}^n d^2}{2n}}$$

d is the difference between replicate measurements, n is the number of cases, and  $S_D$  is the statistical estimate of the 'true' error. Dahlberg also stated that it was conventional to take just two measurements per specimen (one measurement and a repeated measurement) in conducting anthropometric measurements and calculating the TEM (Dahlberg, 1940). However, Houston (1983) cautioned that Dahlberg's formula would only provide a reliable estimate of the error where no bias (systematic error) exists between the two sets of replicated measurements. Unfortunately, as Houston pointed out, it is very difficult to exclude even quite large biases with certainty particularly where the sample is small. Springate (2012) proposed that unless one can be certain that no bias exists between the replicate measurements, it is preferable to use the following 'method of moments' variance estimator (MME) formula rather than Dahlberg's formula to estimate the random error:

$$S_M = \sqrt{\frac{\sum_{i=1}^{n} (d_i - \bar{d})^2}{2(n-1)}}$$

Springate (2012) also explored the issue of sample size in the context of orthodontic measurement. It was found that as the sample size increases towards 30, the distribution of the estimate of the true random error standard deviation narrows rapidly towards the mean value, see Figure 2 below.

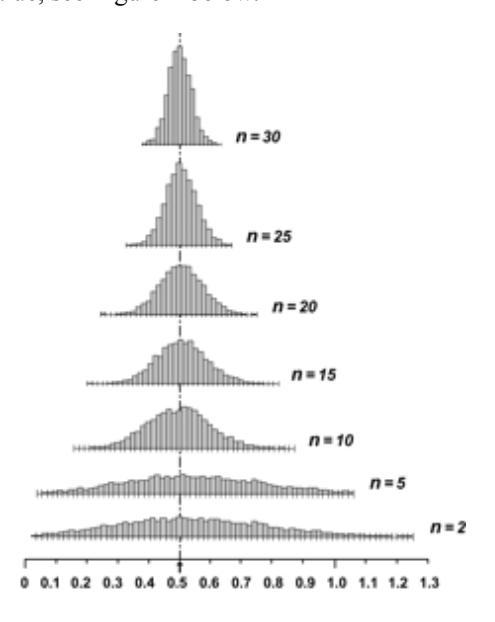


Figure 2: Distribution of the true random error SD as sample size increases

This finding echoes the recommendation of Houston (1983) that a minimum of 25 replicate measurements must be taken to ensure acceptable anthropometric data. Springate (2012) concludes that where the study contains fewer than 20 replicated measurements, the estimate of error will be unreliable, and for less than 25-30 replicated measurements, the resulting estimates of error are potentially unreliable and may under or overestimate the true error.

#### GAUGE REPEATABILITY AND REPRODUCIBILITY

Gauge Repeatability and Reproducibility (Gauge R&R) is a statistical method for determining if a measurement system is suitable for its intended use. Gauge R&R is a key tool of Six Sigma and is well established in medical device, pharmaceutical and automotive manufacturing. Breyfogle III (2003) describes Gauge Repeatability as the variation in measurements considering one part and one operator, and gauge reproducibility as the variation between operators measuring one part. The Gauge R&R test can also be used to compare the measurement uncertainty with the tolerance interval of the process or product characteristic to be measured, which is expressed as a percentage, to determine the acceptability of the measurement instrument (ISO, 2011).

(Burdick, Borror, & Montgomery, 2005) state that the purpose of a Gauge R&R study is to:

- Determine the amount of variability in the collected data that is due to the measurement system.
- Isolate the sources of variability in the measurement.
- Assess whether the measurement system is suitable for broader application.
- Quantify the variability in the measurement process attributed to the operators, parts and operator-part interaction.

In mathematical terms the total variability in measurement data can be expressed as:

$$\sigma^2 Total = \sigma^2 parts + \sigma^2 measurement system$$

The variability of the measurement system ( $\sigma^2$  measurement system) can further be described as the product of  $\sigma^2$  repeatability and  $\sigma^2$  reproducability. Calculations of variance are achieved using ANOVA methods. Once the variation has been calculated the Gage R&R percentage (precision to total variation) can be calculated as follows:

%GageR&R = 
$$\frac{\sigma^2 measurement \ system}{\sigma^2 Total} \ x \ 100 \ (Picard, Page, Kierstead, & Page, 2002)$$

ISO 13053: Quantitative Methods in Process Improvement - Six Sigma advises using the following structured method for conducting a Gauge R&R study (ISO, 2011):

- Select which components need to be measured.
- Have several operators make repeated measurements (for example, 10 components each measured three times by three operators).
- Analyse the results with a spreadsheet or through specialised statistical software (calculation and graphical display).
- Interpret.
- Decide whether the measurement system is acceptable

The standard advises that the usual decision criteria are:

- GRR< 10 %: the measurement system is acceptable;
- 10 %<GRR< 30 %: the measurement system needs improvement.
- GRR> 30 %: the measurement system is unsuitable.

ISO 13053 further recommends that specialised software should be used to run the calculations and format the results (ISO, 2011). While Gauge R&R can be calculated from first principles, the use of statistical software such as Minitab allows for more practical application of the tool.

In the context of anthropometrics, the operator represents the person taking the measurement and the part/component represents the measurement to be taken. The Gauge R&R tool will facilitate the anthropometrist in understanding where measurement error is occurring; whether it is primarily a repeatability difficulty where the anthropometrist cannot achieve consistency in his/her own measurements or a reproducibility issue where the results between two or more anthropometrists is inconsistent. In the following example, the Gauge R&R approach will be applied to the measurement of the anthropometric dimension Bi-deltoid Breadth of a cohort of university students.

#### APPLICATION OF GAUGE R&R TOOL

In applying the Gauge R&R tool, the five step systematic method as described by ISO 13053: Quantitative Methods in Process Improvement - Six Sigma was followed. In the following sections the activities undertaken for each step are described and discussed. The anthropometric measurement system analyzed consisted of students trained in the use of an anthropometric calipers and the identification of Bi-deltoid landmarks. The task to be completed involved the measurement of the anthropometric dimension Bi-deltoid Breadth in a cohort of students. The goal of this demonstrative use of the Gauge R&R tool is to determine if this measurement system is suitable for use in measuring the bi-deltoid breadth of adults (both males and females).

#### Step 1: Select which components need to be measured.

In this study a cohort of university students were selected as the 'components' which needed to be measured. A total of thirteen students volunteered for the study. Prior to its commencement, each student was provided with an information sheet which explained the nature of the study. They were informed that all data collected would be anonymous and confidential and only used for the purposes of the study. Participants signed a consent form and were assured that they could withdraw from the study at any time. For the purpose of confidentiality each student was randomly assigned a number from 1 to 13.

#### **Step 2: Have several operators make repeated measurements**

A total of three operators made repeated measurements in this study. Each 'operator' had previous experience in the use of the anthropometric calipers and the identification of anthropometric landmarks. Graphical aids were used to explain the definition of Bi-deltoid Breadth and its associated landmarks. The international standard ISO 7250-1 Basic Human Body Measurements for Technological Design - Part 1: Body Measurement Definitions and Landmarks were used as the basis of the graphical aids.

ISO 7250-1 defines Bi-deltoid Breadth as the distance across the maximum lateral protrusions of the right and left deltoid muscles (ISO, 2008). Dimension D2 in Figure 3 below shows this dimension graphically:

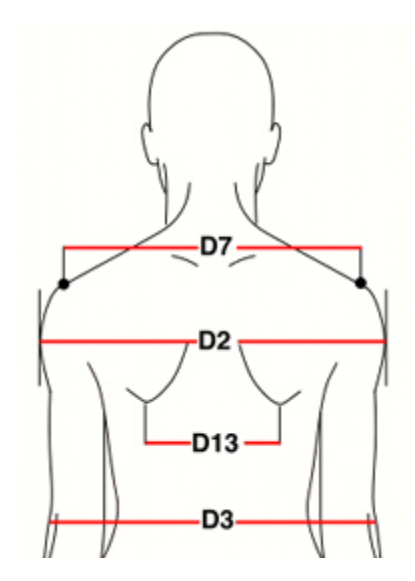


Figure 3: Bi-deltoid breadth (Dimension D2)

ISO 7250-1 states that a large sliding caliper or large spreading caliper should be used and that the subject should sit or stand fully erect with the shoulders relaxed in the standard sitting or standard standing posture.

Measurements were taken in the standard sitting posture. Each 'operator' measured each of the 13 'components' three times in a random order. The measurement data was removed at the end of each of the three trials to prevent bias from feedback. A data collection sheet was utilised to ensure the data was collected systematically and the ambient environment was controlled for the duration of the study.

#### Step 3: Analyse the results with a spreadsheet or through specialized statistical software

As recommended by ISO 13053 (ISO, 2011) specialised software was used to calculate the Gage R&R values and format the results, in this case Minitab Version 16 was used. A Crossed Gage R&R was conducted with a study variation of  $5.15\sigma$  (5.15 is the number of standard deviations needed to capture 99% of the variation (Picard, et al., 2002) and included 95% confidence intervals.

Table 1 below shows the results from the Minitab session window:

Table 1: Minitab Gage R&R Data

#### %Contribution table

			%Contribution	
Source	VarComp	95% CI	(of VarComp)	95% CI
Total Gage R&R	1173.76	( 904.823, 5667.334)	52.36	(25.80, 85.92)
Repeatability	724.58	( 541.787, 1018.955)	32.32	(9.98, 50.00)
Reproducibility	449.18	( 167.844, 4930.646)	20.04	(6.51, 73.28)
Operator	67.86	( 0.000, 4521.069)	3.03	( 0.00, 66.50)
Operator*Part	381.32	( 117.874, 964.342)	17.01	(3.90, 40.43)
Part-To-Part	1068.14	( 420.578, 3264.478)	47.64	(14.08, 74.20)
Total Variation	2241.91	(1588.749, 7228.255)	100.00	

#### %Study Variation

	%Study Var		
Source	(%SV)	95%	CI
Total Gage R&R	72.36	(50.80,	92.69)
Repeatability	56.85	(31.59,	70.71)
Reproducibility	44.76	(25.51,	85.60)
Operator	17.40	( 0.00,	81.55)
Operator*Part	41.24	(19.76,	63.59)
Part-To-Part	69.02	(37.53,	86.14)
Total Variation	100.00		

In Figure 4 below the Minitab Gage R&R graphical output is shown:

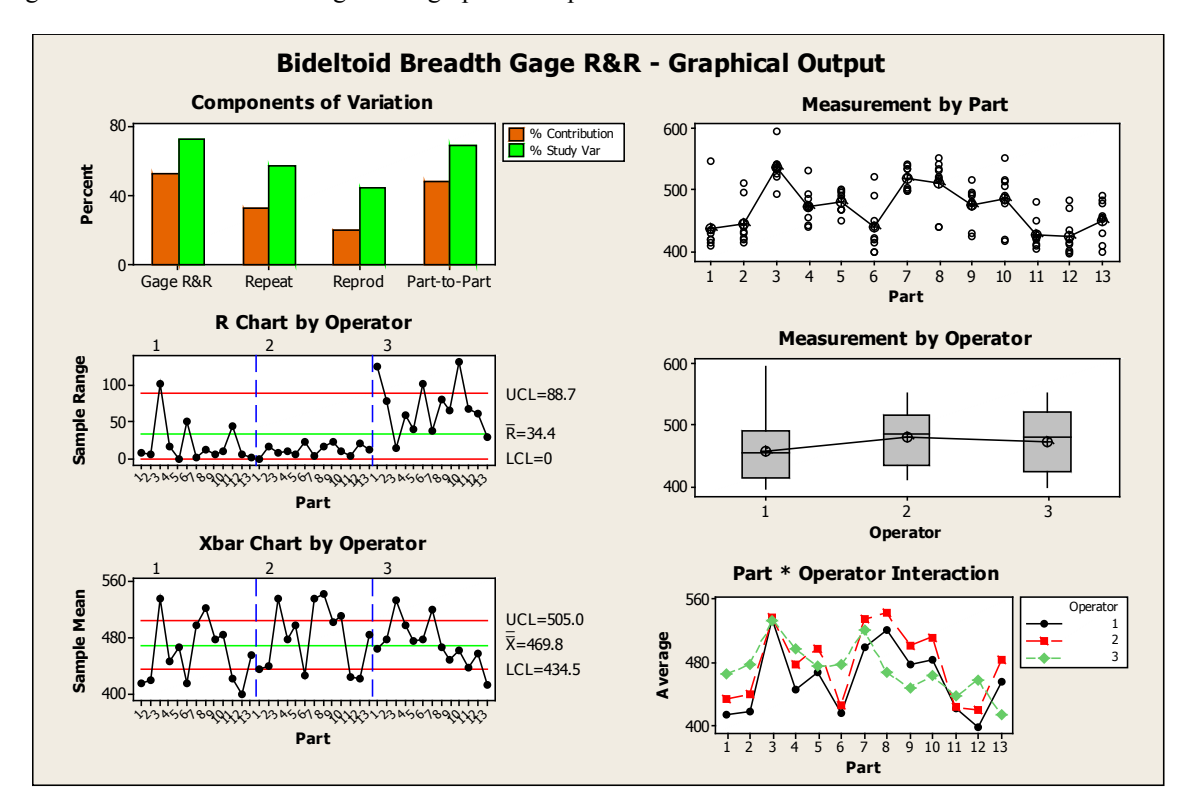


Figure 4: Minitab Gage R&R Graphical Output

#### **Step 4: Interpret**

As can be seen in Table 1, the main output of the Minitab Gage R&R function is a %Study Variation and a %Contribution table. Both tables can be used to determine where variation is occurring. The %Contribution table can be convenient because the Total Gage R&R and Part-to-Part variation sum to 100%. The %Study Variation expresses Standard Deviation in the same units as the process data, and therefore can be used to form other metrics, such as %Tolerance (if you enter in specification limits for your process), and %Process (if you enter in an historical Standard Deviation). Generally the %Study Variation is used to interpret results.

The Total Gage R&R obtained for this study was 72.36%, with a repeatability value of 56.85% and a reproducibility value of 44.76%. It is evident that as the Total Gage R&R is greater than 30%, the measurement system in its current format is unacceptable for use. While the repeatability (operator replicating measurements) aspect of the Gage R&R is a higher contributor (56.85%) to total variation than reproducibility (44.76%) (operators measuring the same part), both are still greater than the 30% threshold. In order to investigate where improvements in the measurement system need to be made it is useful to examine the Minitab graphical output.

In the 'R Chart by Operator' graph there is an evident difference in the range of repeatability measurements taken by each individual operator. Operator 2 achieved the most consistent results when repeating measurements while Operator 3 obtained a range of 132mm when replicating the measurement of 'component' number 10. Despite having similar experience and access to the same measuring equipment and Graphical aids, the effectiveness of each operator in conducting the measurements is not equal. It is worth noting also that no specific issues which could explain the measurement errors were identified during the stud.

The other graphs of interest are the 'Measurement by Part' and 'Part \* Operator Interaction'. In these graphs it can be seen that 'component' numbers 1, 6 and 10 showed the most variation in measurement while 'component number 7 showed consistent measurement.

#### Step 5: Decide whether the measurement system is acceptable

As discussed in Step 4 the measurement system in its current state is unacceptable for use as the Total Gage R&R is greater than 30%. In order to improve the measurement system the following actions could be taken:

- Operators could be provided with advanced training in the use of the calipers and the identification of the relevant anthropometric landmarks
- The calipers could be replaced by a more robust measurement instrument/system such as a laser based one
- The possible effect of fatigue in repeating measurements could be assessed

After any change the measurement system should be re-assessed to determine if the changes have sufficiently improved the repeatability and reproducibility requirements of Gauge R&R to meet the 30% threshold limit.

#### DISCUSSION AND CONCLUSIONS

In the Bi-deltoid Breadth measurements it was shown that the range of replicated measurements of individuals varied considerably. Subsequent Technical Error of Measurement (TEM) values would also vary considerably for the measurements taken for each person due to this variance in range. Therefore a TEM statistic can only be valid for the specific replicated measurements and cannot be used to pre-emptively assess how a measurement system will perform. Furthermore, it has been shown that anthropometrists' must take a minimum of 25 replicate measurements of each anthropometric dimension in order to calculate the TEM. Gage R&R, on the other hand, can be used to establish pre-emptively if a measurement system is suitable for use. This method is of particular benefit where a large number of individuals will be measured, where the replications and calculations required for the TEM would be time consuming.

The demonstration of the application of the Gage R&R tool has also provided an important insight into measurement error in anthropometrics. It has been shown that it cannot be presumed that all anthropometrists will be equally skilled in anthropometric measurement despite having similar experience, and being provided with graphical aids on how to obtain anthropometric measurements according to international standards. While no special causes were

evident during the study, the repeatability variance can be expected to be a result of personal factors such as the appraisers' style of measurement or landmark interpretation and reproducibility variance may be caused by fatigue and/or experience from previous measurements.

While TEM is most suitable for calculating measurement error in studies involving small numbers of anthropometric dimensions, the Gage R&R method has been shown to be a useful tool for preemptively evaluating measurement systems in studies involving large number of anthropometric dimensions guidance on the sources of variation in such studies.

#### REFERENCES

- Breyfogle, F. W. (2003). *Implementing Six Sigma: smarter solutions using statistical methods* (2nd ed.). New York Chichester: Wiley.
- Breyfogle III, F. W. (2003). Implementing Six Sigma: smarter solutions using statistical methods: Wiley. com.
- Burdick, R. K., Borror, C. M., & Montgomery, D. C. (2005). *Design and Analysis of Gauge R and R Studies: Making Decisions with Confidence Intervals in Random and Mixed ANOVA Models* (Vol. 17): SIAM.
- Dahlberg, G. (1940). Statistical methods for medical and biological students. *Statistical Methods for Medical and Biological Students*.
- Dawson, B. (2004). Machine Vision Makes Gaging Easy. Quality Magazine.
- Harris, E. F., & Smith, R. N. (2009). Accounting for measurement error: a critical but often overlooked process. *Archives of Oral Biology*, *54*, S107-S117.
- Houston, W. (1983). The analysis of errors in orthodontic measurements. *American journal of orthodontics*, 83(5), 382-390.
- ISO. (2008). Basic human body measurements for technological design -- Part 1: Body measurement definitions and landmarks. Geneva: ISO/TC 159/SC 3.
- ISO. (2011). ISO 13053-2:2011 Quantitative methods in process improvement -- Six Sigma -- Part 2: Tools and techniques. Geneva: ISO/TC 69/SC 7.
- Jamison, P. L., & Zegura, S. L. (1974). A univariate and multivariate examination of measurement error in anthropometry. *American journal of physical anthropology*, 40(2), 197-203.
- Knapp, T. R. (1992). Technical error of measurement: a methodological critique. *American Journal of Physical Anthropology*, 87(2), 235-236.
- Pederson, D., & Gore, C. (1996). *Anthropometry measurement error*: Sydney: University of New South Wales Press.
- Picard, D., Page, D., Kierstead, M., & Page, B. (2002). The black belt memory jogger: a pocket guide for Six Sigma success. *USA*, *GOAL/QPC*.
- Springate, S. (2012). The effect of sample size and bias on the reliability of estimates of error: a comparative study of Dahlberg's formula. *The European Journal of Orthodontics*, 34(2), 158-163.
- Ulijaszek, S. J., & Kerr, D. A. (1999). Anthropometric measurement error and the assessment of nutritional status. *British Journal of Nutrition*, 82, 165-177.

### Interactive Simulation and Ergonomics Assessment of Manual Work With EMA – Applications in Product Development and Production Planning

Lars Fritzsche<sup>1</sup>, Ricardo Schönherr<sup>2</sup> and Benjamin Illmann<sup>1</sup>

1- imk automotive GmbH, Ergonomics Division Annaberger Str. 73, 09111 Chemnitz, Germany

2 – Volkswagen Sachsen GmbH, Motorenwerk Chemnitz, Industrial Engineering Kauffahrtei 47, 09120 Chemnitz, Germany

#### **ABSTRACT**

The software tool EMA ("Editor for Manual Work Activities") facilitates digital production planning and ergonomics assessment by providing a more efficient and accurate approach to 3D human simulation. EMA uses a modular system for describing human work activities based on a pre-defined library of "complex operations", which allows the generation and simulation of human movements with highly-automated algorithms. Moreover, EMA includes standard tools for the assessment of ergonomic strains (EAWS – "Ergonomic Assessment Worksheet") and production time (MTM – "Methods Time Measurement"). After introducing some basic analysis functions of EMA and their typical use cases, this paper presents an evaluation study that examines the validity of EMA ergonomic evaluations in comparison to paper-pencil-assessments with EAWS. Moreover, this paper shows several use cases of the EMA software application in automotive and aviation industry. These applications illustrate that EMA considerably reduces the effort for preparing human simulations and enables the user to analyze ergonomic conditions (body posture, action forces, manual load handling) and productivity (e.g., walk ways) very thoroughly.

Keywords: Digital Human Modeling, Production Planning, Efficiency, Ergonomics, EAWS

#### INTRODUCTION

It is common sense among scientists and practitioners that ergonomic measures need to be taken as early as possible in the product development process in order to maintain the work-ability of employees and avoid musculoskeletal disorders in manufacturing (Illmarinen, 2006). This will help to reduce absenteeism and improve quality in the final production line, especially considering the aging workforce in most industrial countries (Fritzsche et al., 2014). Digital human models (DHMs) are considered to have a high potential for facilitating proactive ergonomic work and product design (Duffy, 2009). However, most of them are complicated to use and thus, it is very time consuming to prepare and alternate human simulations of entire work cycles. Moreover, most DHMs do not provide comprehensive analysis tools for assessing ergonomic strains and production time based on industrial standards.

Therefore, DHMs may be common in scientific studies but they are far from being a routine tool in "applied

ergonomics" with regard to designing industrial work places. The "Editor for Manual Work Activities" (EMA) is a holistic planning method based on a 3D human model that simplifies the preparation and alternation of digital human work simulations. EMA addresses the need for accurate assessments of expected physical workload in an early phase of production planning by using the EAWS (Ergonomic Assessment Worksheet, Schaub et al., 2012) for ergonomic risk assessment. In addition, EMA uses the MTM-standard (Methods Time Measurement, Maynard et al., 1948) for estimating the expected production time. The following sections provide more details about the functionalities of EMA. An evaluation study examines the accuracy of EMA ergonomic assessments in comparison to paper-pencil evaluations. Finally, some use cases illustrate the application of EMA for industrial work design.

#### **HUMAN WORK SIMULATION WITH EMA**

#### EMA approach to human work simulation

In 2011 EMA was firstly introduced as a software tool "that reduces the effort for preparing simulations of human work" (Fritzsche et al. 2011). Over the past three years, based upon experiences from industrial applications and new software developments, EMA has evolved to a holistic software-based planning method that uses 3D-DHM simulations and a standardized "process language" (Illmann et al., 2013).

The EMA process language is very similar to the MTM process language. It is based on a set of predefined modules, so called "complex operations", containing single motion steps that are needed to complete a more or less simple work task, such as "get and place part". Using a drag-and-drop mechanism, the software user defines the entire work process by arranging these standard operations in a logical sequence (e.g. "get part – get tool – place part – use tool to assemble part – put away tool"). All standard operations contain a number of parameters that need to be specified by the user in an interactive modus. For example, the user needs to define the part, the tool and the location of assembly by mouse-click in the 3D scene. Now, after all relevant parameters are defined, EMA is able to calculate the necessary human movements using highly-automated algorithms that were collected in various motion studies. This basic function is called "self-initiated motion generation". It considerably reduces the effort and time to prepare a complete human work simulation by an estimate of about 50% in comparison to any other DHM software.

Another key to increase the efficiency of human simulations with EMA is the continuous use of object references, which are set while the user defines the location of parts and tools by mouse-click. Using this approach, EMA will always find the referenced object, no matter where it has been moved in the 3D-environment. This enables the user to generate alternative design and planning scenarios in a very short time just by moving the referenced object to another location or by changing certain object preferences, such as shape, size, or weight. Unlike other DHM tools, the user only changes the object parameters while the software automatically re-calculates the necessary human motions in the present simulation instead of having to create a new simulation from scratch. This way, multiple planning options regarding the process sequence, product preferences (weight, dimension, etc.), and human resources (5<sup>th</sup>%ile female vs. 95<sup>th</sup>%ile male) can be tested in a very time- and cost-efficient manner. Altogether, the effort for scenario alternation is being reduced by about 80% in comparison to any other DHM software.

When EMA was firstly introduced in 2011 it was only available as a plug-in for Dassault Systèmes' Delmia V5 software suite that is now called "EMA-V5". Now EMA is also available as a stand-alone software system that includes a digital human model and a 3D graphic engine that is able to handle several common data formats (.jt, dae, etc.). The stand-alone software offers more functions, it is more flexible, easier and quicker to use, and it provides more data interfaces and possibilities for modular expansion. This widens the area of application because it allows more customer-specific adaptations for data exchange and reports. Small and medium-sized companies should be particularly interested in using a lean EMA system without having to purchase a full PLM-system. In summary, there are several advantages that distinguish EMA from other DHM tools:

- Easy to use by drag and drop metaphors
- Self-initiated, parametrical motion generation
- Use of object references enables quick scenario modification
- Use of typical planning language for manufacturing applications
- MTM-based estimation of production time and added value analysis
- EAWS-based ergonomic risk assessment of full-shift physical workload



Figure 1. EMA user interface for scenario set-up.

#### EMA analysis functions for ergonomics and time studies

EMA is specifically designed for production planners because (1) it is easy to use by drag and drop interactions; (2) it uses typical planning language based on MTM standards, for instance "pick & place part, use screwdriver", and (3) it provides a standard screening tool for ergonomic risk assessment, the EAWS. Due to the self-initiated motion generation and the extensive research including motion capturing studies, EMA is able to generate more realistic human motion simulations in regard to task execution and duration independent of the user. This is very important for increasing objectivity and validity of simulation results (for biomechanical studies and future developments see Gläser et al., 2014, in this issue). Based on that, EMA may be used to evaluate some of the most important targets in production planning and compare them by objective figures, in particular with regard to (1) production time and value-added work as well as (2) geometric feasibility and ergonomic risk.

For estimating production time, EMA has included an automatic time calculation that is mainly based on the MTM-UAS standard; for example, placing a part loosely at the table in 20-50 cm reach would be rated as PB2, which equals 30 TMU = 1.08 seconds. However, in some situations MTM-UAS does not provide a proper time code (e.g. for car ingress). In such cases, the more detailed MTM-1 method is used to calculate the standard time for all singular movements that are necessary to carry out the full operation. Using this approach, project experiences have shown that the deviation between EMA production time and MTM-UAS time is less than 5%, which is sufficiently accurate for planning purposes. Furthermore, the development for a data interface between EMA and the MTM standard software system "TiCon" is ongoing and will be available soon. As a result EMA will be able to generate a nearly complete MTM-UAS analysis that can be edited in "MTM-TiCon". Additional analysis functions of EMA can be used to avoid waste; for instance, by examining walk ways in the so-called spaghetti diagram.

For ergonomic risk assessment, EMA has included a semi-automatic evaluation that is based on the EAWS standard method (Ergonomic Assessment Worksheet, Schaub et al., 2012). EAWS is the only commonly used screening tool that allows the evaluation of physical workload based on the production cycle time. The EAWS covers four sections of relevant physical workloads in manufacturing: Section 1 includes symmetric body postures, such as bending, kneeling, arms above shoulder or head level, etc., and asymmetric body postures, such as lateral bending, trunk rotation, and far reach. Section 2 includes action forces of the fingers (e.g. use thumb to press in clips) and armshoulder-forces (e.g. handling of balancers and manipulators). Section 3 includes manual material handling of weights above 3 kg. Section 0 includes specific extra strains (e.g. car ingress/egress, walking during assembly). All four sections are scored based on standard rules in order to calculate a total ergonomic risk score, which indicates areas of low strains ("green"), medium strains with possible long-term risk ("yellow") and areas of high strain with considerable health risks ("red"). EMA is able to automatically calculate EAWS scores based on the human simulation of the work process and some additional user input (forces, weights, extras). This way, the ergonomic score calculation is fully objective and reliable, independent of the software user.

## EVALUATION STUDY OF SEMI-AUTOMATIC ERGONOMIC ASSESSMENT WITH EMA BASED ON EAWS

In order to achieve objective results for ergonomic evaluations, EMA contains an implementation of the Ergonomic Assessment Worksheet (EAWS, Schaub et al., 2012) – a screening tool for physical workload, which covers several ergonomically unfavorable conditions such as awkward postures, manual load handling, and action forces. It is important, that this automated risk assessment leads to correct predictions of later workload, given that investment decisions are made on their basis. Previous studies have shown that DHM process simulations may provide adequate estimations of the prospected workload of real-life situations with the use of comprehensive screening methods like the EAWS (Fritzsche, 2010). However, the objectiveness of such paper-pencil tools was sometimes not satisfying as indicated by deficiencies in the inter-rater reliability. Hence, the full incorporation of the EAWS method into DHM software tools may improve evaluation efficiency, objectivity and validity. Still, it has to be assured, that automatic risk assessment delivers reliable results. Thus, the purpose of this study was to investigate if a DHM software implementation of the EAWS allows an adequate prediction of physical workloads.

#### Method

Twelve planning simulations from a German automobile manufacturer were selected showing assembly operations at vehicles as well as pre-assembly tasks of components. The chosen scenarios were very diverse including different body postures, action forces and manual material handling operations. All scenarios were taken from real planning applications; they had not been prepared especially for this study. The mean duration of a simulation was approximately 90 seconds. The scenes were modeled by different operators, using the software tool EMA. All scenarios contained digital mock-ups of products, resources (tools, fixtures, etc.) and the necessary work environment. The digital manikin used represented the anthropometric model of the 50th percentile of German males according to DIN 33402:2005. As common in real life, weights and estimated forces of parts were given.

Each of the twelve simulations was assessed by three experts with experience on the field of ergonomics risk assessment with EAWS. The scenarios were available to the observers as a video, which allowed them to view the simulation as often as necessary in order to increase the objectivity and inter-rater reliability (Coenen et al., 2013). For the quantitative study of the forecast quality of ergonomic loads, the observers performed a paper-pencil-analysis using the EAWS. Likewise, the EMA software provided an EAWS risk assessment which was exported as an MS-Excel report. This way, the total EAWS scores as well as the detailed scores for each EAWS section were available for each scenario and could be used for comparing risk assessments of real observers vs. simulation results. Thereby, this study focused on the three EAWS sections for postures, action forces and manual material handling. The section for extra scores (e.g., car ingress/egress) was not considered because they are currently defined by manual user input. EWAS-section 4 (highly repetitive tasks for upper limbs) is not yet implemented into EMA and was not considered either.

The agreement of the three experts' EAWS risk assessment was determined with the help of the intra-class correlation (Bartko, 1966) as a characteristic measure for the inter-rater reliability. The observers' scores have been averaged and then compared with the automatically calculated score provided by EMA. Due to the small sample, Kendall's Tau (Arndt et al., 1999) was chosen as indicator for rank correlations. Thereby, every observer worked independently and without comparing with the others. The observers did not know the results of the automatically calculated EAWS-scores beforehand.

#### **Results**

For measuring the inter-rater-reliability of the three ergonomic experts the EAWS scores of the observers were compared (Figure 1). The scores were very close in some scenarios, but also very different in other cases. For observers 1 and 2, the categories green, yellow and red matched in 50% of all cases. Between observers 1 and 3 as well as between 2 and 3, a match occurred in 67% of all cases. Differences such as green vs. red did not appear for any pair of observers. The resulting intra-class correlation value of rk = .869 indicates a good agreement between the three experts regarding the EAWS classification. High agreement was also found for the separate EAWS sections; postures correlated with rk = .833, forces with rk = .862 and manual material handling with rk = .964.

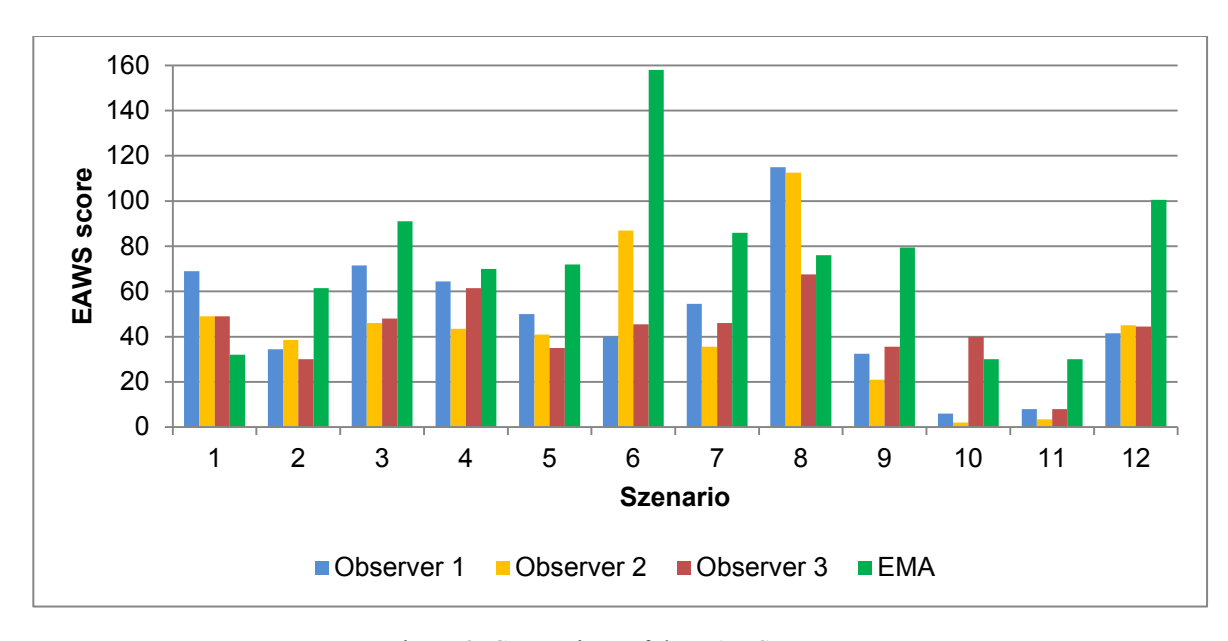


Figure 2. Comparison of the EAWS-scores.

Furthermore, the EAWS total score was compared for each of the twelve scenarios for the three observers and the EMA software assessment. Rarely, there are distinct differences between the observers and EMA; in some cases the EMA-calculated score is considerably higher, whereas other scenarios showed a very good agreement. Kendall's Tau as indicator for the comparison of the observers' scores with the automatically calculated EMA-score is shown in Table 1.

Table 1: Rank correlations of the EAWS-scores (Observers vs. EMA).

Total score	.381 <sup>*</sup>
Postures total	.443 <sup>*</sup>
Symmetrical postures	.515**
Asymmetrical postures	.264
Action forces	.874***
Manual material handling	.789***

<sup>\*</sup> significant with p < .05, \*\* very significant with p < .01, \*\*\* highly significant with p < .001

For the total EAWS scores, an average agreement of  $\tau = .381$  (p < .05) was found. Postures had a stronger accordance with  $\tau = .443$  (p < .05), whereat EMA tends to a higher score, especially for asymmetric postures such as lateral bending, trunk twist and far reach. Thus, symmetrical postures correlated significantly ( $\tau = .515$ , p < .01), whereas asymmetrical postures showed a non-significant correlation of  $\tau = .264$  (p > .05). In contrast to that, both action forces ( $\tau = .874$ ; p < .001) and manual material handling ( $\tau = .789$ ; p < .001) showed very good agreements.

#### **Discussion**

The comparison indicated a good agreement between the three experts in ergonomic risk assessment using the EWAS. In most scenarios scores are at a similar level; where a perfect congruence is very unlikely. In general, the results confirmed the use of the EAWS as an objective screening tool for ergonomics risk assessment.

Significant agreements were found for the total score as well as for the three separate EAWS sections comparing the automatically calculated EMA-score with the observers' assessment. However, EMA tends to reveal higher scores for body postures, which seems to be due to the more correct assessment: EMA registers all body poses automatically and very precisely, whereas the observer needs to "see" critical postures by himself. Especially asymmetric postures, which did not correlate significantly in the study, are sometimes difficult to detect. EAWS scores for lateral bending and twisting already reach their maximum at 30° rotation. Therefore, intermediate twisting of 15° rotation, for example, is hard to detect just by observing a work scenario, no matter if it is a simulation or in

real life. Figure 2 shows a scene of a sample scenario with a twisted trunk. In this case, none of the observers identified any asymmetric posture, while EMA scored 13 points, which is correct based on the EAWS regulations. Thus, the difficulty of detecting asymmetric body postures is the main explanation for deviations in EAWS scores between EMA calculations and observer assessments.

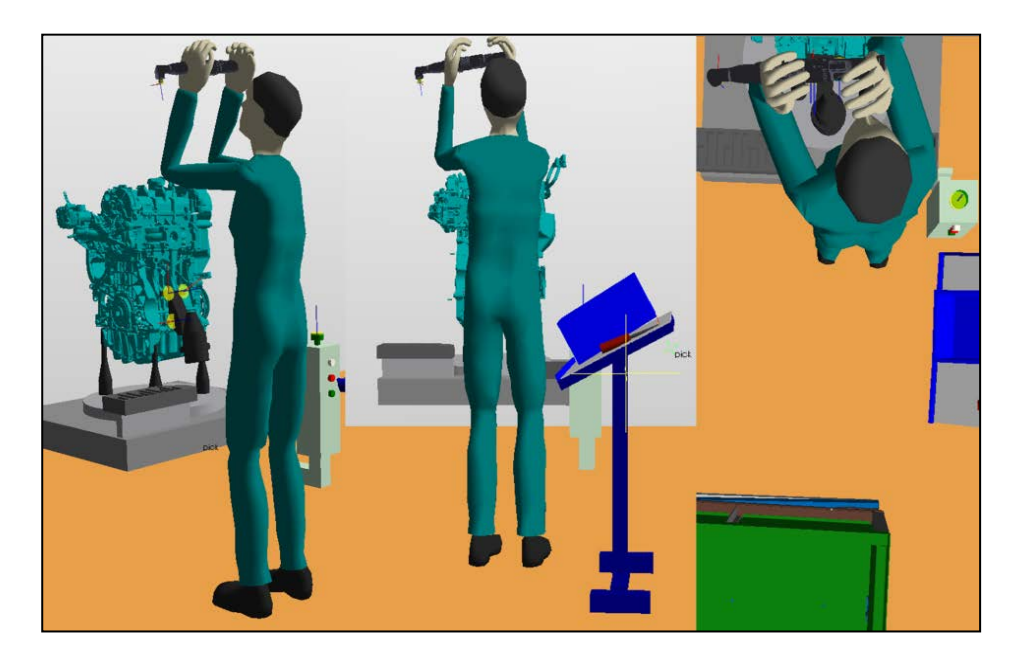


Figure 3. Sample-scenario with marginal asymmetric posture.

A revision of the motion generation algorithms might help to prevent some over-scoring as well, as small correction movements of the feet can help to avoid asymmetric postures. Furthermore, the appearance of the used DHM could be modified in a way that trunk rotation or lateral bending are shown more distinct to the observer. Besides these considerations, future research should address the issue of asymmetric body postures. There might be a discrepancy between the qualitative characterization of the asymmetric postures like "medium" and the quantitative angle specifications, "15°" in the given example. If such a marginal deflection is hardly visible, it also seems questionable whether it should be classified as a significant ergonomic strain. As reported in Takala et al. (2010) the observation and correct assessment of movements of smaller body regions seems to be very particularly challenging for observers. In this study, only one video of each scenario with only one view-perspective was available. Thus, the observers might have overseen some ergonomic strains. Merely the software is able to use the exact joint angles for scoring, which may lead to a higher score in some scenarios.

Scenario 6 revealed a larger disagreement. This can be explained by the fact, that all three observers detected a whole body force (average score = 19.2), while EMA indicated a finger force (score = 69.5). This deviation is an artifact that was due to a modeling error. Furthermore, the observers underestimated the duration of certain unfavorable postures, which again led to a lower score compared to EMA. In scenario 12, the three observers have a good agreement but clearly differ from the EMA-score. Again, the single perspective in view might have biased the appearance, so that actual bending postures were classified as upright. The possibility of manipulating the view individually in the EMA software during the assessment instead of having only a video could have enabled higher agreement between manual and automatic risk assessment in this case.

In general, the results demonstrated that the EAWS software implementation into a human simulation system allows reliable results for an early use of the method. Assessment scores were mainly differing in asymmetric body postures, such as lateral twisting and bending, which are hard to detect even for experts. In this regard digital assessment is more precise because it is based on objective data of joint angles rather than visual judgment. Both the EAWS and the application of DHM simulations illustrated some potential to increase objectivity and reliability of ergonomic risk assessments. In conclusion the study confirmed the suitability of EMA in practical applications for the validation of planning alternatives as well as for the preventive ergonomics risk assessment. Of course, ergonomic experts are still needed to check and verify the ergonomics design at the real workplace during preproduction workshops and after start of serial production because some issues can only be detected in real life.

### APPLICATIONS OF EMA IN PRODUCT DEVELOPMENT AND PRODUCTION PLANNING

In the past three years EMA has been successfully introduced at different German companies. Some of the main customers are AIRBUS, AUDI, BMW, DAIMLER and VOLKSWAGEN. The industrial application of EMA has been a key element to facilitate further improvement. Especially the wide range of industries and tasks has offered significant inputs for improving motion generation, software usability and analysis functions. This section will give an overview about the general approach of using EMA in early phases of product development and production planning in order to evaluate and modify the ergonomic design of products, in terms of feasibility and buildability, as well as entire work processes and shopfloor layout. Figure 4 illustrates how EMA may be used at different stages of the product development process (PDP).

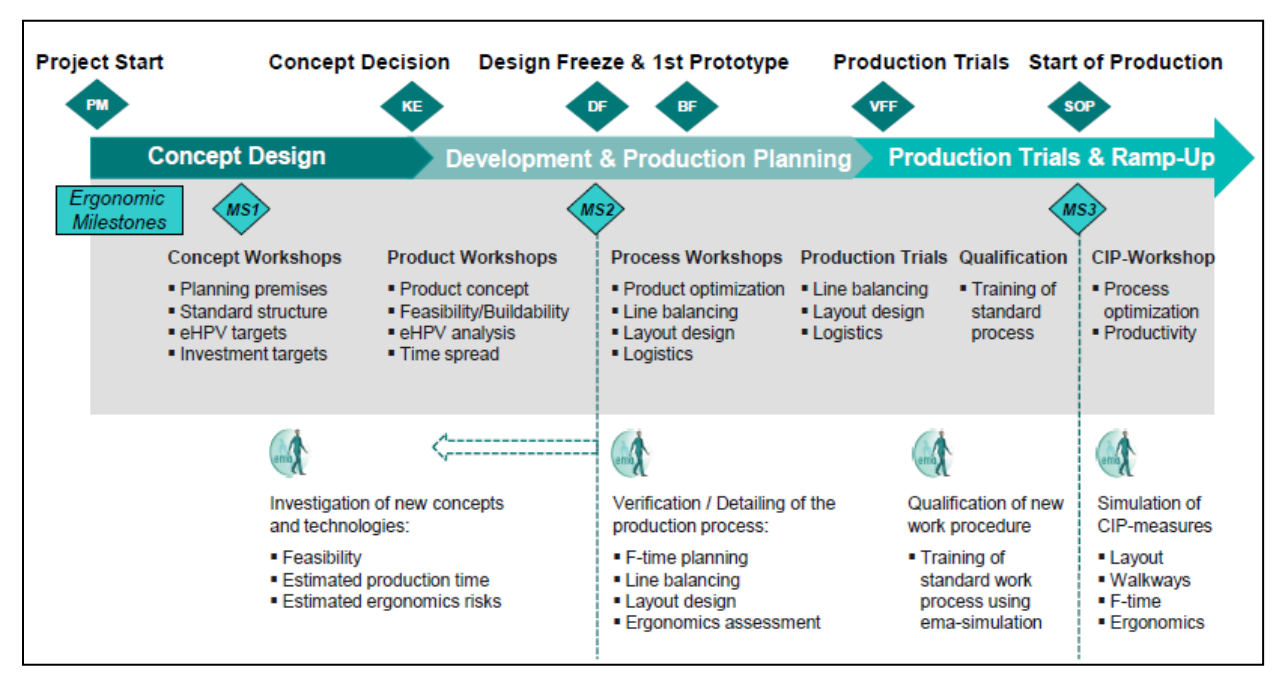


Figure 4. Application of EMA throughout the product development process (PEP).

EMA can be used throughout the entire product development process. Generally, the earlier EMA is used in analyzing product concepts and production layout, the more costs for re-design may be saved. However, EMA may also be used to improve pre-production planning, prepare pilot workshops and support pre-series production trails.

During the concept design the focus of application is on investigating buildability and plausibility checks. At this point, the EMA simulation and analysis functions offer an early estimation of bottle-neck-processes in regard to physical workload and manufacturing time. These early assessments have a strong product-reference; however they could also be used to evaluate concepts for facilities, equipment, and production layout.

In pre-production planning the focus of application is on the definition of standard work sequences. Thereby, EMA can display its full potential in defining and evaluating the entire work process and layout design, particularly by testing various alternatives in the 3D environment. This phase has a strong process focus and lays the foundation for the following pre-series planning. The ergonomic assessment and time analysis now requires greater detail.

Pre-series production trails offer a last chance to optimize product, process and resources before the start of series production (SOP). This requires simulations and analysis to be very detailed and accurate. EMA now offers the possibility to virtually test late design changes without expensive tryouts. In that phase EMA may also be used for qualification matters. Previously prepared simulations may now be used for explaining the new standard work process to management and workers. EMA may also serve to support communication between planning and production by illustrating how the ideal process was intended to run.

After start of production, EMA is particularly useful to investigate layout optimization and the integration of new tools or machinery in running production lines, before they actually exist. This may save costs for redesign to fit new equipment into the existing assembly line. Similarly EMA could be used to support the continuous improvement process to visualize possible process optimizations without interruptions of the running production.

The following examples of application demonstrate how EMA may be used for different tasks throughout the product development process and show how application projects contribute to further EMA improvement.

#### **Application I: Planning Assembly Operations with Hand Tools**

Accurate simulation of tool handling has been a big issue during the development of EMA. In order to be effective in creating the simulation, tools like screwdrivers need to be handled by EMA without further user input. Applications at Daimler (Mercedes-Benz Manufacturing Hungary) and Volkswagen (Kaluga plant in Russia, Zwickau plant in Germany) have offered a variety of scenarios to use specific hand tools. Particularly, the use of welding tongs and different pistol-grip tools have shown the most important determinants for tool handling. Firstly a tool-center point (TCP) needed to be defined, which describes the place and orientation of the application point. Secondly each tool needed a special gripping point to ensure correct hand-wrist-orientation. Thirdly, specific body movements had to be created depending on the tool trajectory; EMA nowadays automatically follows the tool step by step and always finds the optimal posture in reference to the place of application (Figure 5). In the near future the tool-objects will inherit more information about the process, such as involved body forces and necessary movements. This way, manual and automatic tools will cause a different task execution.

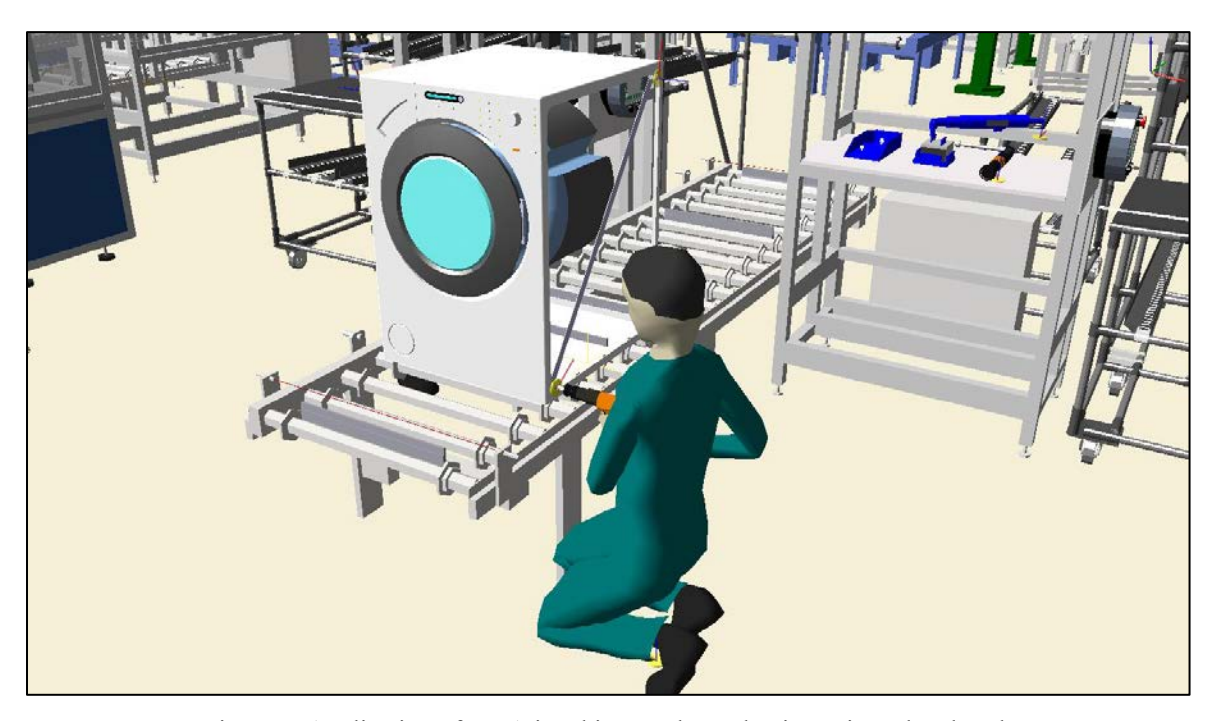


Figure 5. Application of EMA in white-goods production using a hand tool.

#### **Application II: Moving Assembly Line with Analysis of Walkways**

In previous EMA applications all elements of the 3D-environment have been regarded as static which means that no other object except the human model could be animated. A new functionality ("emaDynamics") now allows assigning tasks for nearly all kinds of objects. Therefore, a specific set of complex tasks was designed for planning objects movements and interactions. Moreover, the EMA simulation capabilities needed to be extended by adding dynamic walk path calculation, dynamic collision prevention and advanced synchronization features. Finally, also a new report was created, the so-called "Spaghetti diagram". It shows the walk ways and work positions in the layout as bird view and allows analyzing the exact walk distances. The new dynamic function may be applied, for example, in all situations with moving assembly lines to determine walk ways considering the actual movement of the dynamic assembly line and the relative position change of the static lineside logistics area.

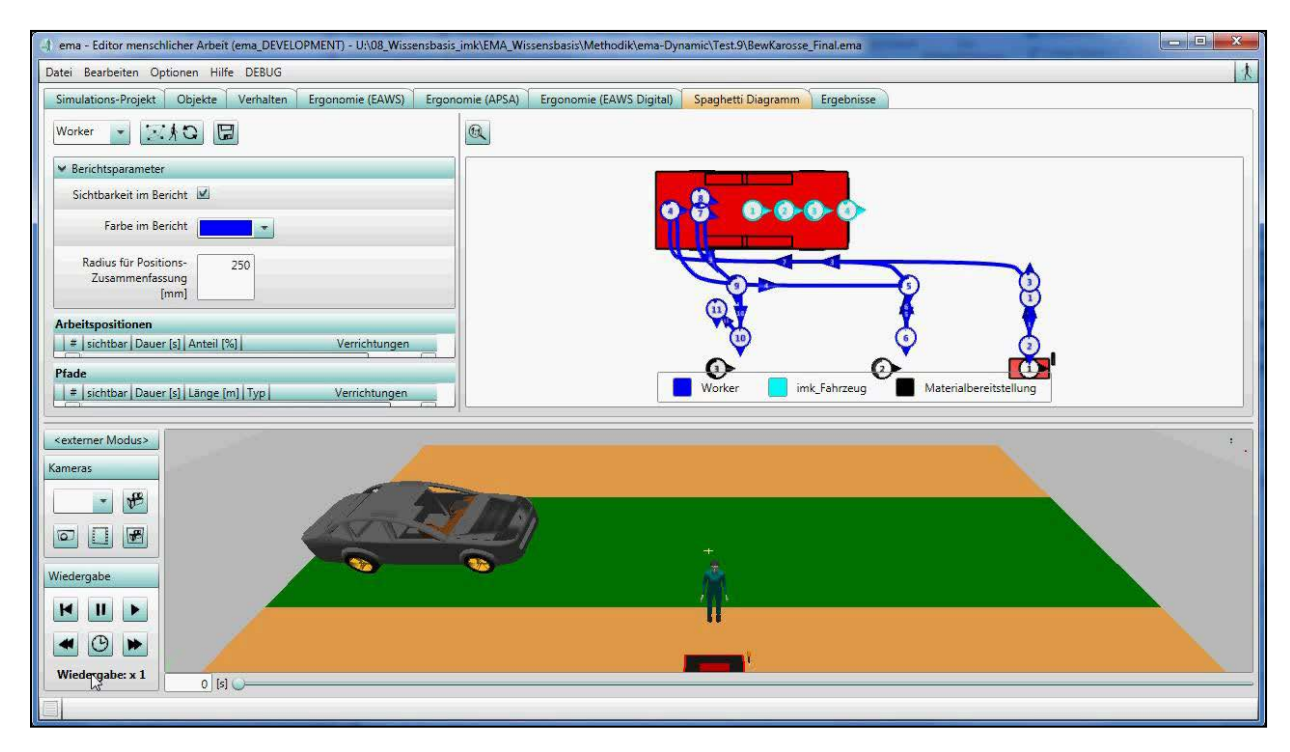


Figure 6. Analyzing walkways on a moving assembly line ("Spaghetti diagram").

#### **Application III: Designing Logistics Areas**

An early application of EMA was the design of a logistics supermarket area for an automobile assembly line (see Figure 7). EMA had several problems simulating material handling tasks, for example with picking and moving multiple parts at the same time. Therefore, the whole operation of material handling needed to be remodeled. Furthermore, the operation for pushing and pulling trolleys and carts needed to be implemented for the purpose of accurate simulation and correct ergonomic assessment using the EAWS.

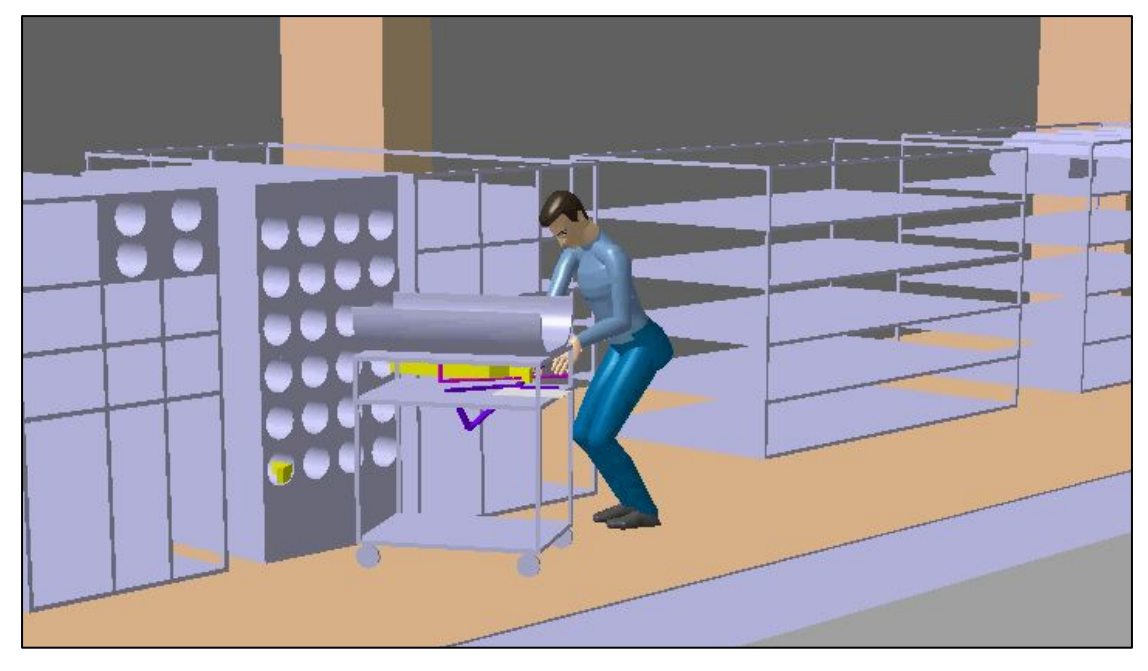


Figure 7. Pushing and pulling during commissioning tasks in a supermarket area.

#### **CONCLUSIONS**

In the past years EMA has evolved from a planning tool that uses an innovative approach for human motion generation to an entirely new planning method. This paper has shown that industrial applications have greatly contributed to the improvement of movement-accuracy and planning-efficiency. A main focus during development was put on motion generation, however also the performance of different assessment methods, such as EAWS for ergonomic assessment and MTM for time analysis, greatly benefited from the requirements that were defined by various EMA customers. Through the use of EMA in the automotive industry, aviation industry, white goods and other industries the range of possible tasks and the system performance vastly increased and created many ideas for future developments. Especially in terms of data exchange of the software and interaction with the surrounding 3D-environment, EMA will soon allow more applications in all phases of the product development process.

#### REFERENCES

- Arndt, S., Turvey, C., Andreasen, N. C. (1999), "Correlating and predicting psychiatric symptom ratings: Spearmans r versus Kendalls tau correlation", JOURNAL OF PSYCHIATRIC RESEARCH, Volume 33 No. 2, pp. 97-104.
- Bartko, J. J. (1966), "The Intraclass Correlation Coefficient as a Measure of Reliability", PSYCHOLOGICAL REPORTS, Volume 19, pp. 3-11.
- Coenen, P., Kingma, I., Boot, C. R. L., Bongers, P. M., van Dieën, J. H. (2013), "Inter-rater reliability of a video-analysis method measuring low-back load in a field situation", APPLIED ERGONOMICS, Volume 44, No. 5, pp. 828-834
- Duffy, V.G. (2009). "Handbook of Digital Human Modeling. Research for Applied Ergonomics and Human Factors Engineering". Boca Raton, Florida, USA: CRC Press, Taylor & Francis Group.
- Fritzsche, L. (2010), "Ergonomics risk assessment with digital human models in car assembly: Simulation versus real life", HUMAN FACTORS AND ERGONOMICS IN MANUFACTURING AND SERVICE INDUSTRIES, Volume 20 No. 4, pp. 287-299.
- Fritzsche, L., Jendrusch, R., Leidholdt, W., Bauer, S., Jäckel, T., Pirger, A. (2011). "Introducing ema (Editor for Manual Work Activities) A New Tool for Enhancing Accuracy and Efficiency of Human Simulations in Digital Production Planning." In: V.G. Duffy (Ed.), Digital Human Modeling, HCII 2011, LNCS 6777 (pp. 272–281). Berlin, Heidelberg: Springer.
- Fritzsche, L., Wegge, J., Schmauder, M., Kliegel, M., Schmidt, K.-H. (2014). "Good ergonomics and team diversity reduce absenteeism and errors in car manufacturing". ERGONOMICS (in press).
- Illmann, B., Fritzsche, L., Leidholdt, W., Bauer, S., Dietrich, M. (2013). "Application and Future Developments of ema in Digital Production Planning and Ergonomics." In: V.G. Duffy (Ed.), DHM/HCII HCII 2013, LNCS 8026 (pp. 66–75). Berlin, Heidelberg: Springer
- Illmarinen, J. (2006). "The ageing workforce—challenges for occupational health". OCCUPATIONAL MEDICINE, Volume 56 No. 6, pp. 362-364.
- Maynard, H. B., Stegemerten, G. J., Schwab, J. L. (1948). "Methods-time measurement". New York: McGraw-Hill.
- Schaub, K., Caragnano, G., Britzke, B., Bruder, R. (2012), "The European Assembly Worksheet", THEORETICAL ISSUES IN ERGONOMICS SCIENCE, doi:10.1080/1463922X.2012.678283
- Takala, E.-P., Pehkonen, I., Forsman, M., Hansson, G.-Å., Mathiassen, S.E., Neumann, W.P., Sjøgaard, G., Veiersted, K.B., Westgaard, R.H., Winkel, J. (2010), "Systematic evaluation of observational methods assessing biomechanical exposures at work", SCANDINAVIAN JOURNAL OF WORK, ENVIRONMENT & HEALTH, Volume 36, No. 1, pp. 3-24.

## Influence of Fingertip Anthropometry and Anatomy on Mechanical Loads During Grasping

Gregor Harih, Jasmin Kaljun and Bojan Dolšak

Laboratory for intelligent CAD systems Faculty of Mechanical Engineering, University of Maribor Smetanova ulica 17, SI-2000 Maribor, Slovenia

#### **ABSTRACT**

Many researchers have investigated the mechanical loads during hand tool use to increase the user performance, satisfaction, and lower the risk of acute and cumulative trauma disorders. While grasping, the mechanical loads are directly transferred to the hand. Rough guidelines of pressure discomfort (PDT) and also pressure-pain threshold (PPT) were provided by previous researchers, where values differ by the subject and the area of the hand. The difference in both limits is between subjects due to the different psychological and physiological factors. In order to understand the physiological aspect of the PDT and PPT difference between subjects, we investigated the influence of the fingertip anthropometry and anatomy on the grasping and the resulting mechanical loads on the fingertip using finite element analysis. Results from the numerical tests have shown significant difference between peak contact pressures as well as the contact pressure distribution between different fingertips. It has been shown that based only on anthropometry the peak contact pressure values and contact pressure distribution cannot be predicted, since geometry of the anatomical structures, especially the bone has significantly higher influence on the peak contact pressure and contact pressure distribution during grasping.

**Keywords**: finger geometry, finite element analysis, contact pressure, pressure discomfort threshold, pressure pain treshold

#### INTRODUCTION

A significant part of manual work is still done using hand-tools, therefore a correct design is crucial for preventing upper extremity acute trauma disorders and cumulative trauma disorders, such as blisters, carpal tunnel syndrome, hand-arm vibration syndrome, tendonitis, etc. (Moore, et al. 1991). Many researchers have paid a lot of attention to hand tools in terms of perceived discomfort. Comfort is strongly correlated to user performance and injury frequency (Kinchington, et al. 2012, Kuijt-Evers, et al. 2007, Mundermann, et al. 2001). Comfort is affected by physical, physiological, and psychological factors, and is subjectively defined by feelings, which differs from subject to subject (De Looze, et al. 2003). Therefore designers have to optimize the human-product interaction in order to reduce the discomfort (Kuijt-Evers, et al. 2004). The feeling of discomfort whilst using a hand-tool can reduce the efficiency of the task, and user's satisfaction. The reduction of discomfort is mainly possible by optimising the functionality of the hand-tool, and the physical interaction between the hand and the handle. It has been also shown that great correlation exists between physical and psychophysical properties of the materials which are in touch by the users (Wongsriruksa, et al. 2012).

The mechanical properties of the skin and subcutaneous tissue is very important during grasping tasks as they are in direct contact and the forces and moments are transferred from the tool to the whole hand-arm system. They have been extensively investigated by many researchers showing that skin and subcutaneous tissue have non-linear viscoelastic properties, where the skin is stiffer than the subcutaneous tissue (Clark, et al. 1996, Edwards and Marks 1995, Pan, et al. 1998, Wan Abas 1994, Wilhelmi, et al. 1998, Wu, John Z., et al. 2007, Zheng and Mak 1996). Both have low stiffness regions at small strains followed by a substantial increase in the stiffness when the strain increases. Brand and Hollisters' (1999) rough guidelines are provided for the maximum suggested pressure versus time application over bony prominences. It has been shown that higher contact pressures than allowed for a specific time can result in discomfort, pain, and ischemia which can lead to ATD and CTD. It has been shown that handtools which require high grip, push, pull or torque exertion on the handle produce high contact pressures, which is known to be one of the primary factors for the development of ATD and also CTD (Eksioglu 2004, Radwin, et al. 1987, Rempel, et al. 1992, Riedel 1995). However some authors have argued that higher contact area can lower the subjective comfort rating, since higher contact area triggers more pressure sensors in the soft tissue (Goonetilleke and Eng 1994, Xiong, et al. 2011). Therefore the designer has to find the optimal contact area which can increase the subjective comfort rating and lower the risk of ATD and CTD which are contact pressure induced.

Aldien et al., (2005) provided rough guidelines of pressure discomfort (PDT) and also pressure-pain threshold (PPT), where PPT is higher than PDT and values differ by the area of the hand. Also different subjects reported different values due to subjective perception of the load on the hand. The PDT limit of 188kPa has been reported by Aldien et al. (2005), however Fransson-Hall and Kilbom (1993) estimated the value as 104kPa. In order to maintain the desired user performance, the designer has to design tool-handles, which distributes contact pressure more evenly and do not exceed the PDT limits (Aldien, et al. 2005).

As comfort ratings when using hand tools are subjectively defined, it is also preferable to use subjective measurement methods such as hand tool testing of targetted populations and questionnaires, when evaluating a hand tool (Kuijt-Evers, et al. 2007). However this method gives only the resulting comfort rating and does not provide any insight into the physiological aspect of comfort and the difference between the subjects. Subjective methods also have clear disadvantages such as time error and context effects (Annett 2002).

Therefore we utilized finite element analysis to investigate the influence of fingertip anthropometry and anatomy on mechanical loads during grasping using three different 3D fingertip models based on reconstructed medical images.

#### **METHODS**

In order to investigate the influence of fingertip anthropometry and anatomy on mechanical loads we used finite element simulation software Abaqus/CAE 6.10 from Dassault Systems (France). Previous authors have shown, that it is a reliable FEA software for simulating human tissue behaviour under mechanical stresses (Wu and Dong 2005, Wu, et al. 2002, Wu, J. Z., et al. 2007).

We modelled three different 3D fingertip models based on reconstructed. Tool-handle was modelled as flat block with corresponding material parameters. Body force was applied on the bones of the fingertip to simulate the finger force while grasping a tool-handle. Numerical tests using predefined forces were performed to produce characteristic contact pressures. For each numerical test we observed the contact pressure distribution at the contact area, continuous peak contact pressure value and vertical fingertip displacement.

#### Finite element model – material parameters

Fingertip bone and nail were assumed to be linear elastic with isotropic material parameters with Young's modulus of 17GPa and 170MPa respectively, with a Poisson ratio of 0.3 (Wu, et al. 2002). The material parameters of skin and subcutaneous tissue were extracted from a uniaxial tensile test, and were fitted to the Ogden hyper-elastic material model (Pan, et al. 1998) (Table 1 and 2). Since skin and subcutaneous tissue are almost incompressible, the Poisson ratio was determined to be 0.4 (Wu, et al. 2002). Steel as a quasi-rigid material was used for the tool handle material with Young's modulus of 210Gpa and a Poisson ratio of 0.3.

Table 1: Material parameters determining hyper elasticity of skin:

	Sk	xin	Subcutaneous tissue		
N	$\mu_i$	$lpha_{ m i}$	$\mu_i$	$\alpha_{\mathrm{i}}$	
1	-0.07594	4.941	-0.04895	5.511	
2	0.01138	6.425	0.00989	6.571	
3	0.06572	4.712	0.03964	5.262	

#### Finite element model – geometrical and boundary conditions

For the FE models we used three different 3D reconstructed models of a human fingertip based on medical imaging (Figure 1) (Yoshida, et al. 2011).

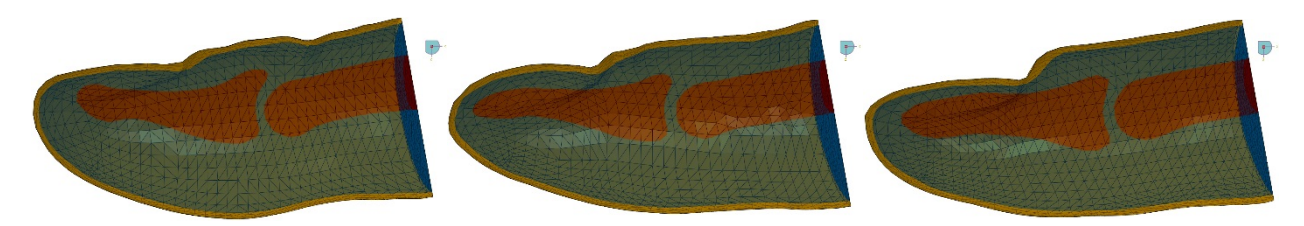


Figure 1. Comparison of anatomy between different fingertips in cut view.

For the grasping simulation a flat block representing a tool handle was modelled and was positioned to be in contact with the fingertip (Figure 2). Displacements and rotations of the block representing the tool-handle were fixed on the lower surface. The displacement and rotations of the fingertip were fixed, except for the displacement along the vertical axis. In the simulations the fingertip and surface were meshed using C3D4 elements (Figure 2).

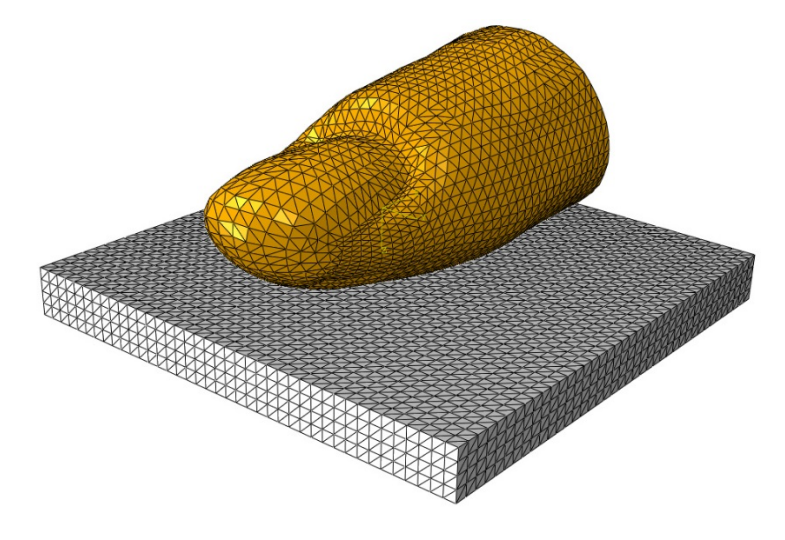


Figure 2. Fingertip and surface meshing.

#### Finite element model – numerical tests

The simulated finger force was set to obtain characteristic contact pressures of 40kPa, 80kPa, 120kPa and 160kPa using the fingertip 003, which was closest to the 50<sup>th</sup> percentile human fingertip geometry. Same finger force was then applied to simulations using other two human fingertips (001 and 002).

#### **RESULTS**

#### Verification

In our previous research we verified and validated our 2D FE model in regard to existing FE models and to experimental data, since it showed great correspondence between both results (Harih and Dolšak 2013).

In order to verify the 3D fingertip model, the closest match according to the anthropometric measurements of the 2D fingertip was chosen. We investigated the continuous peak contact pressure versus vertical displacement of the fingertip. Results show excellent correspondence, since there is only small difference in the contact pressure for the given vertical displacement (Figure 3). The slight difference in the curve shape can be explained by slightly different geometries of the 2D and 3D fingertip models. Thereby it can be assumed, that the 3D fingertip has been verified.

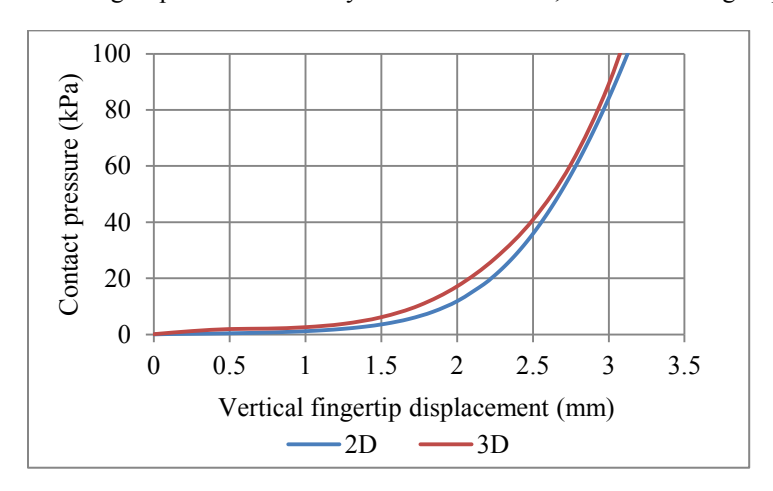


Figure 3. Comparison of continuous peak contact pressure versus vertical deformation of the 2D and 3D fingertip.

#### **Contact pressure distribution**

For each fingertip and load-case we provided contact pressure distribution, which showed the distribution of the contact pressure of the fingertip across the contact area between the fingertip and tool-handle. Thereby direct comparisons and evaluations between different fingertip geometries and load-cases were possible (Figures 4, 5, 6, and 7).

Firstly we observed the load-case where a peak contact pressure of 40kPa was obtained during the contact of the fingertip 003 with the surface (Figure 4), which simulates contact pressure holding a tool in the hands (Aldien, et al. 2005). The finger force, which needed to reach this contact pressure, was then applied to simulations using other two fingertips (001 and 002). The highest contact pressure was obtained with fingertip 001 and was 52kPa, while the contact pressure with fingertip 002 was 41kPa.

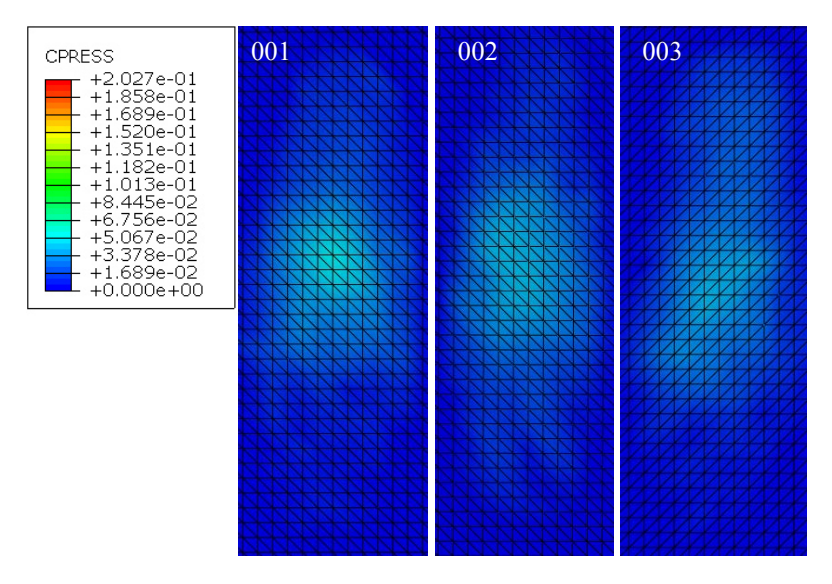


Figure 4. Contact pressure distribution for finger force producing 40kPa with fingertip 003.

For the next load case we set the finger force to produce the maximum contact pressure of 80kPa during the contact of a fingertip 003 with the surface (Figure 5). The resulting maximum contact pressure for the set finger force was with the case of fingertip 001 104kPa and for fingertip 002 84kPa. From the distributions it is also evident, that different fingertip geometries start to show different contact pressure distributions.

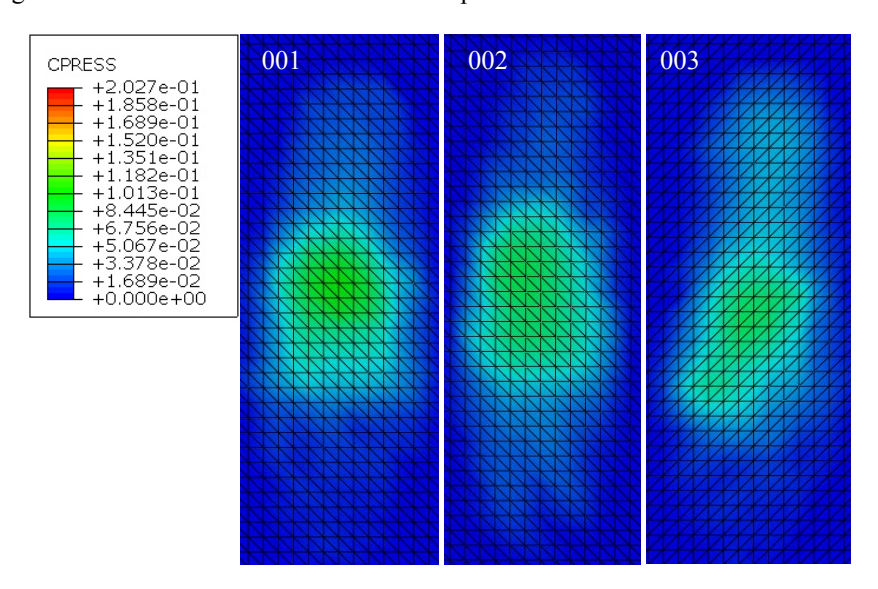


Figure 5. Contact pressure distribution for finger force producing 80kPa with fingertip 003.

In next load case we observed the contact pressure distribution where a maximum contact pressure of 120kPa was obtained during the contact of the fingertip 003 with the surface (Figure 6). The results show the trend that fingertip 001 produces the highest maximum contact pressure (154kPa) followed by fingertip 002 (125kPa). Additionally the difference in contact pressure distributions for each fingertip become more different.

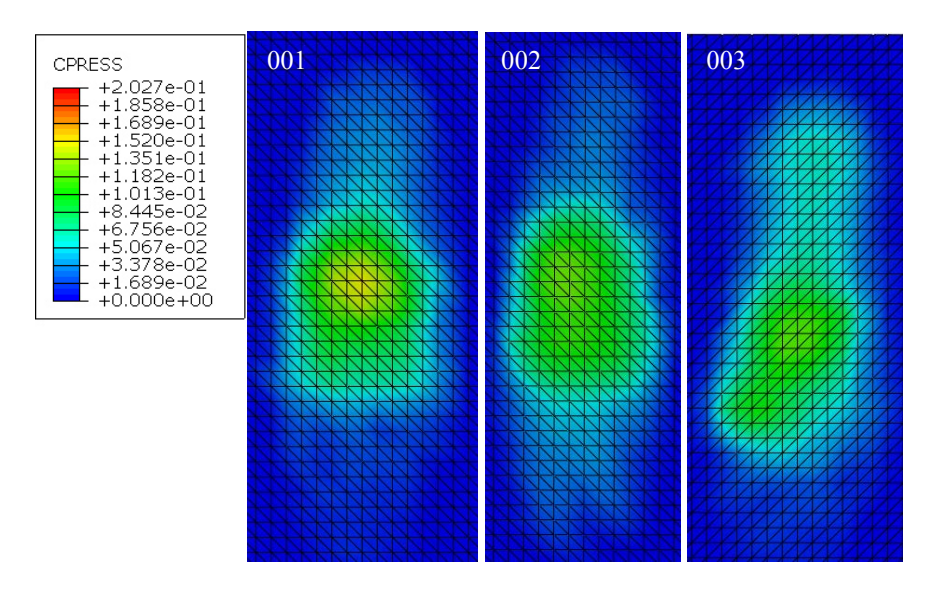


Figure 6. Contact pressure distribution for finger force producing 120kPa with fingertip 003.

The final load case was set to produce 160kPa of maximum contact pressure with the fingertip 003. The finger force needed to obtain this contact pressure was then again applied to other fingertips. The highest contact pressure was again obtained with the fingertip 001 (203kPa) followed by the fingertip 002 (166kPa) (Figure 7).

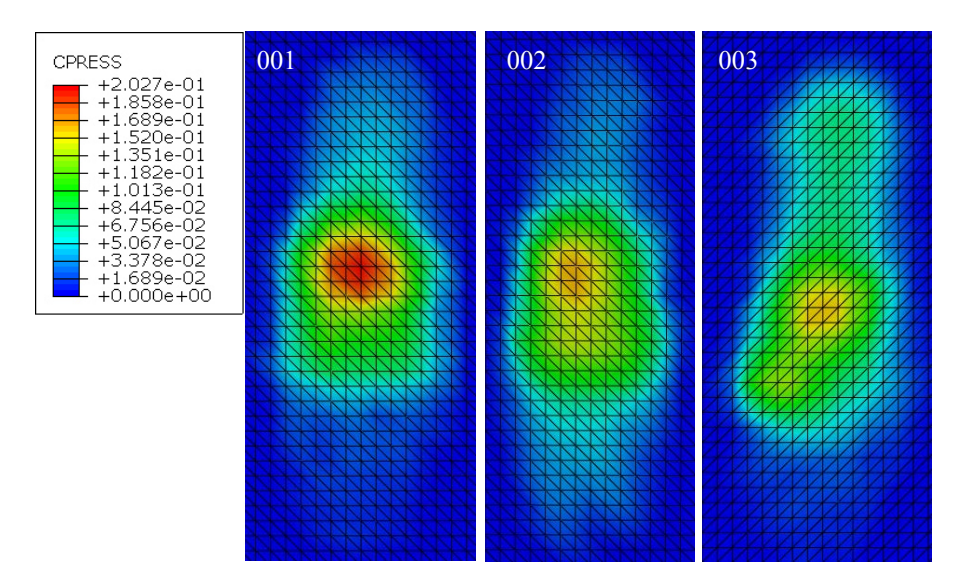


Figure 7. Contact pressure distribution for finger force producing 160kPa with fingertip 003.

#### **Contact pressure – normalized finger force**

We also plotted the maximum continuous contact pressure for each fingertip in comparison to the normalized finger force to observe the difference between the different fingertip geometries (Figure 8). The results show almost linear correlation between the maximum contact pressure and the normalized finger force. It is evident that fingertip 002 and 003 have almost the same behavior, while the fingertip 001 shows significant higher contact pressures for the given normalized finger force.

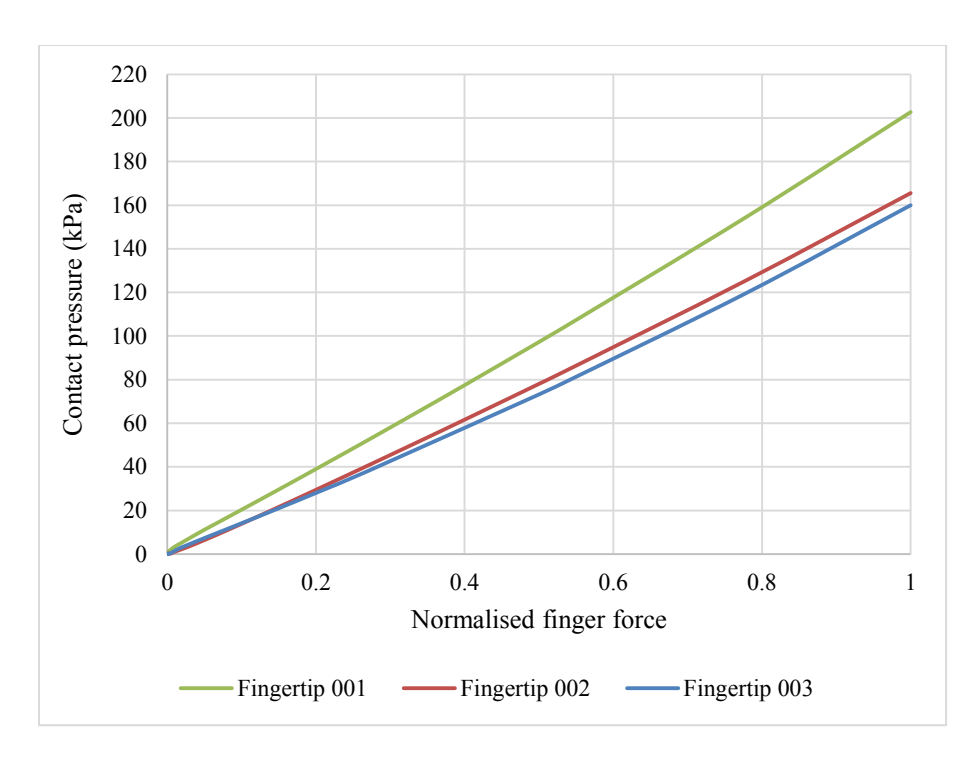


Figure 8. Maximum continuous contact pressure versus normalized finger force.

#### Contact pressure - vertical finger displacement

We also observed the continuous contact pressure in comparison to the vertical finger displacement. Fingertips 002 and 003 show almost the same behavior, where the fingertip 002 shows slightly higher vertical finger displacement for the given contact pressure. The fingertip 001 shows almost the same behavior to a vertical finger displacement of around 3mm. Afterwards the fingertip 001 produces significantly higher vertical finger displacement for the given contact pressure.

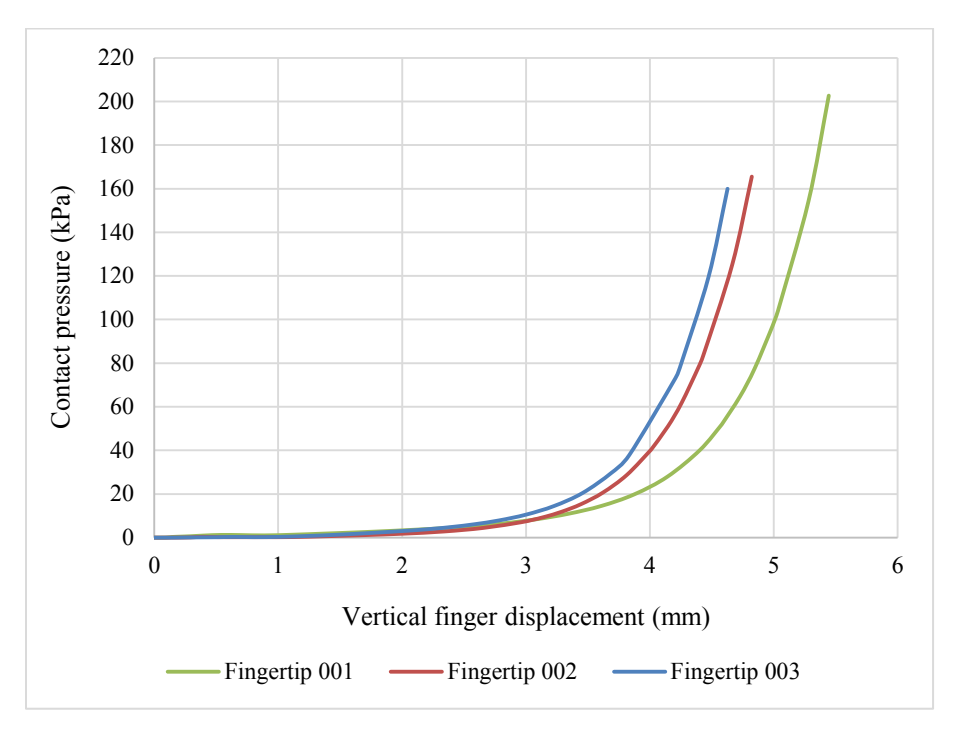


Figure 9. Maximum continuous contact pressure versus vertical finger displacement.

#### **DISCUSSION**

#### **Contact pressure distribution**

It has been shown that power grasps of badly sized and shaped tool-handles can yield in high contact pressures, which can induce many ATD and CTD. Previous research showed different values of PDT and PPT, where values differ by the subject and the area of the hand. In order to investigate the physiological aspect of the difference, we investigated the contact pressure distribution of a three different fingertip geometries with four load cases of 40kPa, 80kPa, 120kPa and 160kPa.

For the first load case, which was set to produce 40kPa with the fingertip 003, the results already show difference between each fingertip (Figure 4). The highest contact pressure was obtained with the fingertip 001. This can be explained by the contact pressure distribution, which shows, that with the fingertip 001 the contact pressure is distributed over smaller area in comparison to the fingertips 002 and 003. The results show that the higher value of contact pressure of the fingertip 001 is due to more concentrated contact pressure, while the contact pressure of the fingertip 002 is more evenly distributed across the contact area. This is even more evident with the fingertip 003, where the contact area is larger especially in the direction towards the end of the finger.

In next load case (80kPa with the fingertip 003) the difference in contact pressure distribution is even more evident (Figure 5). From the maximum contact pressure for each fingertip and contact distribution it can be concluded that the fingertip 001 produces higher maximum contact pressure due to the smaller contact area and strong non-uniform distribution. The fingertip 003 shows completely different contact pressure distribution. This indicates, that higher area of the fingertip is in contact in comparison to the fingertip 001, where contact is established only at the centre. Despite the contact pressure distributions between fingertip 002 and 003 show significant difference, the peak contact pressure is just slightly different. This can be explained by the very even contact distribution of the fingertip 002

In load case, which was set to produce 120kPa with the fingertip 003, the difference in contact pressure distributions by all fingertips continues the trend from the previous load cases. The maximum contact pressure of the fingertip 001 is 154kPa, which is 34kpa over the maximum contact pressure of the fingertip 003 (120kPa). The difference is clearly visible from the contact pressure distribution (Figure 6). While the contact pressure distribution with the fingertip 001 shows smaller contact area and higher differences, the fingertip 003 shows higher contact area and more even contact pressure distribution. Despite the fingertips 002 and 003 produce almost the same contact pressure (125kPa and 120kPa respectively), the contact pressure distributions differ to great extent. Fingertip 002 shows oval like contact area with even contact pressure distribution, while the fingertip 003 shows longer and narrower contact area and contact pressure distribution with higher differences in contact pressure.

Finally we discuss the results from the load case, which was set to produce 160kPa with the fingertip 003. The peak contact pressure was obtained with the fingertip 001 (203kPa), which is 43kPa over the value with the fingertip 003. The peak contact pressure of the fingertip 002 is slightly over the contact pressure of the fingertip 003 (166kPa and 160kPa respectively). The final load case confirms the trend, which showed uneven contact pressure distribution by the fingertip 001. Despite the similarity of the contact area shape of the fingertip 001 and 002, the difference in contact pressure distribution is significant. In case of the fingertip 002, the contact pressure is more evenly distributed. The fingertip 003 shows again significant difference in contact area and pressure distribution. All fingertips have one peak contact area. In fingertip 001 and 002 the location of the peak contact pressure is similar, however the fingertip 003 shows different location.

The differences in peak contact pressures, their locations and contact pressure distributions cannot be discussed without the evaluation of each fingertip geometry and anatomy. Therefore we additionally observed a cut view of each fingertip during contact of the tool-handle with the highest load case (Figure 10). Based on the cut views it is evident that the geometry of the both bones have significant impact on the resulting contact peak pressure as well as the contact pressure distribution. The fingertip 001 distal phalange bone is in comparison to the bone of the fingertip 002 and 003 smaller and shorter. Based on the cut view it is also evident that the angle of the lower contour of the bone in fingertip 001 is slightly tilted upwards in comparison to the fingertip 003. Concave like distal phalange bone

of fingertip 003 with almost no tilt produces uniform contact pressure distribution, which is distributed across the whole length of the finger. This can be explained by the fact that the soft tissue is encapsulated by the bone due to its shape. The shape of the distal phalange bone of fingertip 001 is similar to the shape of the bone of fingertip 002, however it is smaller, which explains the higher peak contact pressure and less uniform contact pressure distribution.

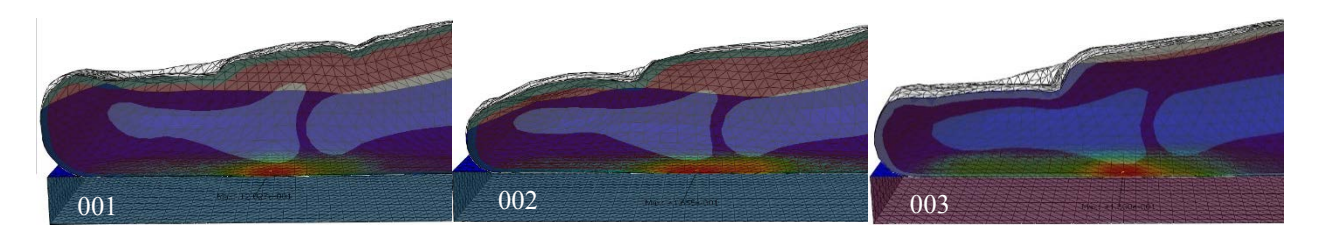


Figure 10. Cut view of each fingertip anatomy during contact of the tool-handle at the highest load case.

#### **Contact pressure – normalized finger force**

We also investigated the continuous peak contact pressure versus normalized finger force (Figure 8). The peak contact pressure point is determined for each fingertip at the highest load case. The results provide continuous values of contact pressure for peak contact pressure point in comparison to the normalised finger force. From the diagram it is evident, that the fingertip 001 shows significantly different curve. For the given normalised finger force fingertip 001 produces higher contact pressure in comparison to the fingertip 002 and 003. Fingertip 002 and 003 show similar behaviour, however it can be observed, that the curves intersect at about normalised finger force of 0.1. This can be explained by the fact that more than one fingertip parameter has influence on the results of peak contact pressure in comparison to the normalised finger force. This suggests that the fingertip amount of soft tissue as well as underlying geometry of anatomical structure of the bone has significant impact on the resulting contact pressure in comparison to the normalised finger force. Based on the results of contact pressure distribution it can be concluded that at lower contact pressure the amount of soft tissue has greater influence on the resulting contact pressure and at higher contact pressures, when the soft tissue is already deformed, the fingertip anatomy and its geometry has higher influence on the resulting contact pressure and distribution.

#### **Contact pressure – vertical finger displacement**

Additionally we also investigated the continuous peak contact pressure in comparison to the vertical deformation of fingertip. All fingertips show the characteristic behavior typical for the hyper-elastic skin and subcutaneous tissue (Figure 9). At the start of the grasping simulation the increase of contact pressure with fingertip vertical displacement is relatively small. However due to the non-linear behavior of the soft tissue, the soft tissue shows substantial increase in stiffness when the contact pressure is increased. Again, the fingertip 002 and 003 show similar curve with similar amount of vertical fingertip displacement and peak contact pressure and fingertip 001 shows significantly different behavior. Since fingertip 001 can be considered as thick finger, it has significantly more soft tissue compared to the fingertip 002 and 003. Therefore also the deformation and vertical displacement is higher than with the fingertip 002 and 003.

#### CONCLUSIONS

We investigated the physiological aspect of the PDT and PPT difference between subjects and the influence of the fingertip anthropometry and anatomy on the grasping and the resulting mechanical loads on the fingertip using finite element analysis. Results have shown there is significant difference in peak contact pressure values as well as contact pressure distributions. It has been shown that based only on anthropometry the peak contact pressure values and contact pressure distribution cannot be predicted. Therefore it is necessary to simulate the whole fingertip using a 3D fingertip model based on medical imaging with correct anatomical structure and geometry. Results suggest that underlying anatomical structure and geometry, especially of the bone, has significant influence on the peak contact pressure as well as contact pressure distribution. Results have shown that the peak contact pressure varies over 20%

between different fingertips, which explains the physiological difference of PDT and PPT.

Future work should investigate more fingertip geometries in order to further investigate influence of fingertip anthropometry and geometry of anatomical structure of the fingertip. Additionally subjective responses could be also evaluated, which would allow the evaluation of the values and their influence on the PDT and PPT.

#### **REFERENCES**

- Aldien, Y., Welcome, D., Rakheja, S., Dong, R., Boileau, P.E. (2005), "Contact pressure distribution at hand-handle interface: role of hand forces and handle size", International Journal of Industrial Ergonomics, 35, pp. 267-286
- Annett, J. (2002), "Subjective rating scales: science or art?", Ergonomics, 45, pp. 966-987.
- Clark, J.A., Cheng, J.C., Leung, K.S. (1996), "Mechanical properties of normal skin and hypertrophic scars", Burns, 22, pp. 443-446.
- De Looze, M., Kuijt-Evers, L., Van Dieën, J. (2003), "Sitting comfort and discomfort and the relationships with objective measures", TERG Ergonomics, 46, pp. 985-997.
- Edwards, C., Marks, R. (1995), "*Evaluation of biomechanical properties of human skin*", Clinics in Dermatology, 13, pp. 375-380.
- Eksioglu, M. (2004), "*Relative optimum grip span as a function of hand anthropometry*", International Journal of Industrial Ergonomics, 34, pp. 1-12.
- Fransson-Hall, C., Kilbom, Å. (1993), "Sensitivity of the hand to surface pressure", Applied Ergonomics, 24, pp. 181-189.
- Goonetilleke, R.S., Eng, T.J. (1994), "*Contact Area Effects on Discomfort*", Proceedings of the Human Factors and Ergonomics Society Annual Meeting Proceedings of the Human Factors and Ergonomics Society Annual Meeting, 38, pp. 688-690.
- Harih, G., Dolšak, B. (2013), "*Recommendations for tool-handle material choice based on finite element analysis*", Applied Ergonomics, 45, pp. 577-585.
- Kinchington, M., Ball, K., Naughton, G. (2012), "Relation between lower limb comfort and performance in elite footballers", Physical Therapy in Sport, 13, pp. 27-34.
- Kuijt-Evers, L.F., Groenesteijn, L., de Looze, M.P., Vink, P. (2004), "*Identifying factors of comfort in using hand tools*", Applied Ergonomics, 35, pp. 453-458.
- Kuijt-Evers, L.F.M., Vink, P., de Looze, M.P. (2007), "*Comfort predictors for different kinds of hand tools: Differences and similarities*", International Journal of Industrial Ergonomics, 37, pp. 73-84.
- Moore, A., Wells, R., Ranney, D. (1991), "Quantifying exposure in occupational manual tasks with cumulative trauma disorder potential", Ergonomics, 34, pp. 1433-1453.
- Mundermann, A., Stefanyshyn, D.J., Nigg, B.M. (2001), "Relationship between footwear comfort of shoe inserts and anthropometric and sensory factors", Medicine and Science in Sports and Exercise, 33, pp. 1939-1945.
- Pan, L., Zan, L., Foster, F.S. (1998), "*Ultrasonic and viscoelastic properties of skin under transverse mechanical stress in vitro*", Ultrasound in Medicine and Biology, 24, pp. 995-1007.
- Radwin, R.G., Armstrong, T.J., Chaffin, D.B. (1987), "Power hand tool vibration effects on grip exertions", Ergonomics, 30, pp. 833-855.
- Rempel, D.M., Harrison, R.J., Barnhart, S. (1992), "Work-related cumulative trauma disorders of the upper extremity", JAMA: the journal of the American Medical Association, 267, pp. 838-842.
- Riedel, S. (1995), "Consideration of grip and push forces for the assessment of vibration exposure", Central European Journal of Public Health, 3, pp. 139-141.
- Wan Abas, W.A. (1994), "*Biaxial tension test of human skin in vivo*", Bio-medical materials and engineering, 4, pp. 473-486.
- Wilhelmi, B.J., Blackwell, S.J., Mancoll, J.S., Phillips, L.G. (1998), "*Creep vs. stretch: a review of the viscoelastic properties of skin*", Annals of plastic surgery, 41, pp. 215-219.
- Wongsriruksa, S., Howes, P., Conreen, M., Miodownik, M. (2012), "*The use of physical property data to predict the touch perception of materials*", Materials & Design, 42, pp. 238-244.
- Wu, J.Z., Cutlip, R.G., Andrew, M.E., Dong, R.G. (2007), "Simultaneous determination of the nonlinear-elastic properties of skin and subcutaneous tissue in unconfined compression tests", Skin Research and Technology, 13, pp. 34-42.

- Wu, J.Z., Dong, R.G. (2005), "Analysis of the contact interactions between fingertips and objects with different surface curvatures", Proceedings of the Institution of Mechanical Engineers, Part H: Journal of Engineering in Medicine Proceedings of the Institution of Mechanical Engineers, Part H: Journal of Engineering in Medicine, 219, pp. 89-103.
- Wu, J.Z., Dong, R.G., Rakheja, S., Schopper, A.W. (2002), "Simulation of mechanical responses of fingertip to dynamic loading", Medical Engineering & Physics, 24, pp. 253-264.
- Wu, J.Z., Welcome, D.E., Krajnak, K., Dong, R.G. (2007), "Finite element analysis of the penetrations of shear and normal vibrations into the soft tissues in a fingertip", Medical Engineering & Physics, 29, pp. 718-727.
- Xiong, S., Goonetilleke, R., Jiang, Z. (2011), "Pressure thresholds of the human foot: measurement reliability and effects of stimulus characteristics", Ergonomics, 54, pp. 282-293.
- Yoshida, H., Tada, M., Mochimaru, M. (2011), "A study of frictional property of the human fingertip using three-dimensional finite element analysis", Molecular & cellular biomechanics: MCB, 8, pp. 61-71.
- Zheng, Y.P., Mak, A.F. (1996), "An ultrasound indentation system for biomechanical properties assessment of soft tissues in-vivo", IEEE transactions on bio-medical engineering, 43, pp. 912-918.

### Human Factors Modeling from Wearable Sensed Data for Evacuation based Simulation Scenarios

Lucas Paletta<sup>a</sup>, Verena Wagner<sup>b</sup>, K. Wolfgang Kallus<sup>b</sup>, Helmut Schrom-Feiertag<sup>c</sup>, Michael Schwarz<sup>a</sup>, Martin Pszeida<sup>a</sup>, Stefan Ladstaetter<sup>a</sup> and Thomas Matyus<sup>c</sup>

<sup>a</sup> DIGITAL – Institute for Information and Communication Technologies JOANNEUM RESEARCH Forschungsgesellschaft mbH Graz, 8010, Austria

> <sup>b</sup> Department of Psychology Karl-Franzens University Graz Graz, Austria

<sup>c</sup> Mobility Department Dynamic Transportation Systems AIT Austrian Institute of Technology GmbH Vienna, Austria

#### **ABSTRACT**

The design and the evaluation of evacuation systems are crucial to guarantee successful responses after an incident. Recent results are presented that target to significantly improve evacuation simulation by parameterizing the human agents' behavior with information on human factors about stress, perception and decision making. In particular, the single person's behavior in its specific situational context is investigated in the frame of its embodied decision making. For this purpose, users were equipped with wearable sensors that capture information about the environment, the psychophysiological status of the user, and its viewing (eye tracking glasses) and motion behavior. The studies take place during regularly performed evacuation exercises of large business buildings. From the correlation between the multisensory perceptual and psychophysiological data on the one hand, and the automatically sensed and interpreted situational context on the other hand, we will extract a rule base with a set of logical "pre-condition – action" pairs that will parameterize the crowd simulation model.

Keywords: Evacuation System, Wearable Sensors, Psychophysiological Status, Eye Tracking, Simulation Model

#### INTRODUCTION

Modelling and evaluation of evacuation systems are pivotal to guarantee efficient reactions in the real system in response to a serious incident. The work described in this paper targets to significantly improve evacuation simulation by introducing parameters of human factors, such as stress, perception and human decision making, into the modeling of human agents' behavior. In particular the single person's behavior in its specific situational context is investigated. The human agent is outlined not only as an abstract information seeking and processing agent but is modelled in the frame of its embodied decision making. The embodiment is characterized in various aspects and fundamentally impacts the agent's information processing behavior. Perception induces orientation from which

specific information sources are selected. Stress as measured from the body worn sensors, i.e., the analysis from the psychophysiological sensing, impacts attention and from this the information processing as well.

In order to consider the embodiment aspect, users were equipped with wearable sensors that capture information about the environment, the psychophysiological status of the user, and its viewing (eye tracking glasses) and motion behavior. The studies took place during regularly performed evacuation exercises of large business buildings. From the correlation between the multisensory perceptual and psychophysiological reactions on the one hand, and the automatically sensed and interpreted situational context on the other hand, we will extract a rule base with a set of logical "pre-condition – action" pairs that will parameterize the crowd simulation model.

In a first stage of the project the wearable multisensory interface was applied to an employee and a visitor of a large company that performed an evacuation exercise. On the basis of the fixation annotated eye tracking videos, the analysis of fixations and saccades as well as the psychophysiological data, events can be classified and associated with typical situational context frames. In particular, the results from the continuously measured gaze patterns of the employee during the evacuation demonstrated that (i) the probability density of gaze on appearances of signage was much smaller than the density on person appearances, (ii) social cues caused the user to change from waiting to acting. Post-event interviews show that the collaborator preferred to follow the guidance of other persons while the visitor followed the guidance from signage.

In summary, the study shows that the data from the wearable multisensory interface provide substantial features to model human factors in evacuation scenarios, this methodology promises better performance of the evacuation simulations

#### EVACUATION SCENARIO AND PSYCHOPHYSIOLOGICAL STUDY

#### **Evacuation Scenario**

Objective of the first human factors study was to evaluate the mechanisms in an evacuation study of a large business building and its industrial environment. The evacuation exercise was applied in a large, eight stories high building, and was performed in the frame of a pre-defined evacuation plan. For the appropriate management of the evacuation, business employees were selected by the evacuation management team and prepared as 'evacuation supporters' with the mission to coordinate the navigation of the test persons in the evacuation exercise. Two evacuation supporters have been advised in each story, with one supporter waiting in the intermediate platform of the staircase, and the second had to do an inspection round through all office rooms to collect all employees and motivate them to progress to the staircase. The purpose to run the study, for the business company, was to make employees familiar with the process in an evacuation exercise, detect deficits in the management and the behavior, and possibly find motivation to update the evacuation concept.

During the evacuation exercise, two employees were equipped with wearable sensors and interviewed before and after the evacuation exercise using a standardized questionnaire (N = 2). The participants were accompanied by two experienced observers who monitored and kept notes during the complete experiment. The employee was equipped in addition with eye tracking glasses and a navigation system (Figure 1). After the end of the experiment, a post-interview was performed with the two test persons, at the final destination.

#### Sample, Material and Study Design

Two participants were tested during an evacuation exercise: One employee of the company where the exercise took place and one visitor who has never been in the company building before. The evacuation exercise consisted of five different parts: (1) Normal working situation before the evacuation ('office'), (2, 3, 4) onset of fire alarm followed by leaving the office, gathering in the stairwell, leaving the stairwell and the building ('alarm, evacuation'), and (5) gathering at the meeting point outside the building ('gathering'). A multidimensional approach (Figure 2) was used to combine subjective assessments of the actual psychological state (BSKE; Janke, Debus, Kallus, Hüppe and Schmidt-Atzert, 1989) before and after the evacuation exercise (part 1 and 5), psychophysiological reactions of the cardiovascular and the electrodermal activity to measure activation/arousal and emotional tone, eye tracking (fixations and saccades), and results of behavioral analysis before, during, and after the evacuation exercise (part 1 to 5) as well as results of post-interviews which were executed after the evacuation exercise at the meeting point (part 5). Due to the limited availability of eye tracking glasses only the employee was equipped with them.

Therefore, the results that combine psychophysiological reactions and eye tracking are only shown for the employee.

The physiological reactions of the cardiovascular and the electrodermal activity were recorded with the portable VARIOPORT system of Becker Meditec. The psychophysiological measures in the statistical analyses were for ECG: heart rate (HR) in beat per minute (bpm) and heart rate variability (HRV) calculated as mean square of successive differences (RMSSD), and for EDA: Skin conductance level (SCL) and count of non-specific skin conductance responses (NS.SCR) of SCR.

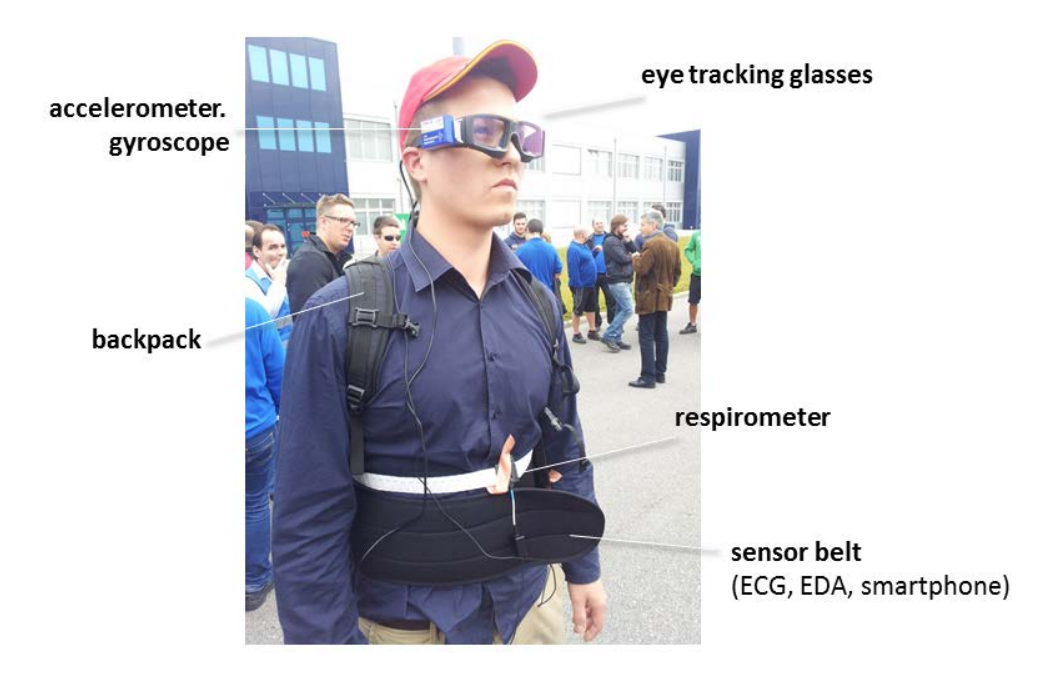


Figure 1. Participant of the user study with wearable sensor interface for human factors analysis.

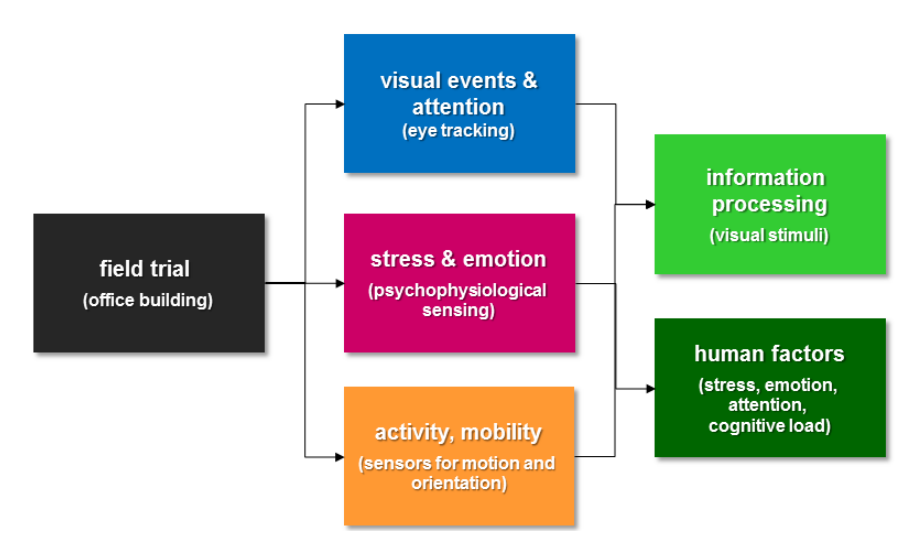


Figure 2. Schematic sketch of the processing of information in the evacuation study and analysis of human factors thereafter.

#### Results

The results of the subjective assessments of the actual psychological state measured before and after the evacuation exercise, showed that after effects of the evacuation exercise are reflected in the actual psychological state only in a lesser extent. The onset of the fire alarm was accompanied by various reactions of the psychophysiological system of the employee (see Figure 3 and Figure 4): An increase of HR, SCL and NS.SCR, which reflect an increase of mental and emotional stress. While waiting in the stairwell and at the meeting place, a decrease of HR, SCL and NS.SCR and an increase of HRV are observable. The psychophysiological reactions of the employee suggest a decrease of mental and emotional stress in these two situations. Therefore, resting points during the evacuation exercise like gathering in the stairwell can be used as "recovery islands" or "safety islands" within an evacuation scenario which could help evacuees to calm down to prevent and avoid panic behavior. Thereby, it is important that these points are clearly signed as points that are "safe". The results of the analyses of the post-interviews show that going outdoors when leaving the building and arriving at the meeting place is experienced as safe by the participants. Generally, fresh air has a positive effect on the well-being of the participants. While the employee, who was familiar with the building, oriented himself to other evacuees, the visitor used the emergency exit signs for path finding. More research is needed to investigate if this behavior is individual for the two participants of this initial study or can be interpreted as general behavior of evacuees.

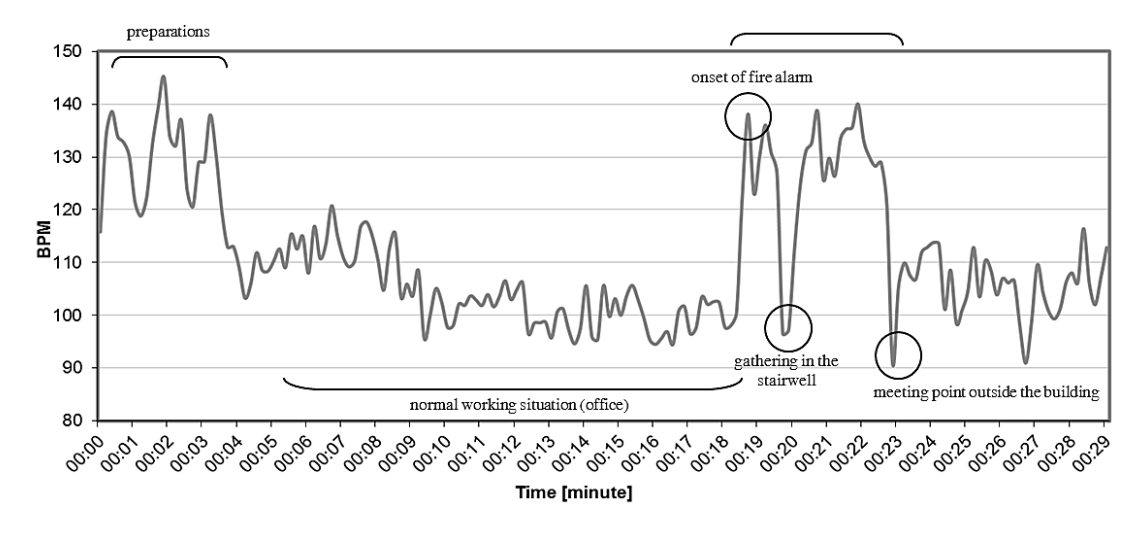


Figure 3. Heart rate (HR) – employee of the large office building.

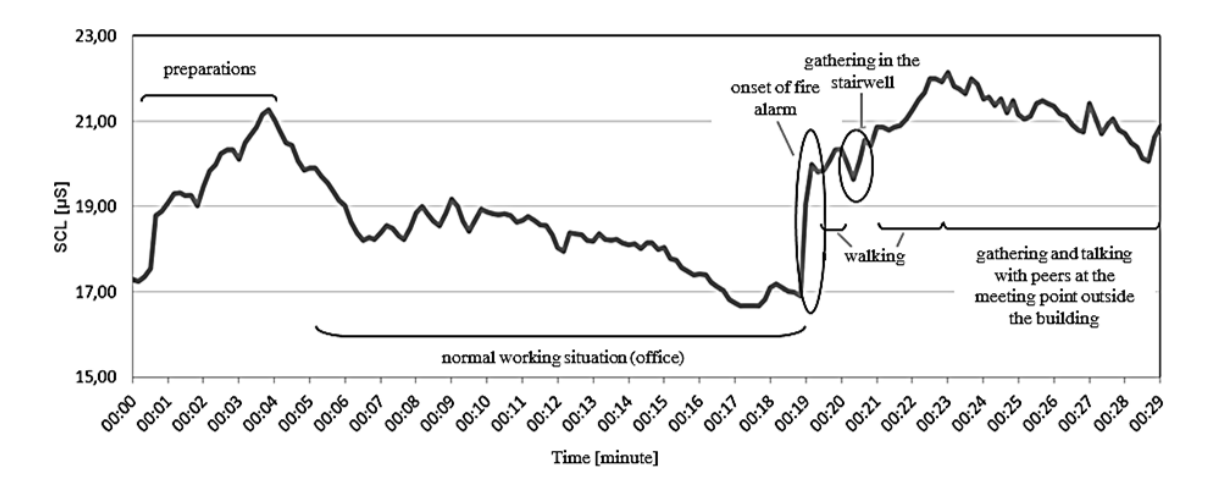


Figure 4. Skin conductance level (SCL) - employee of the large office building.

## FRAMEWORK FOR MOBILE EYE TRACKING AND HUMAN FACTORS MONITORING

For the processing and analysis of visual information we decided to apply eye tracking glasses (ETG) in order to measure the attention process directly during the evacuation task. The mass marketed SMI<sup>TM</sup> eye-tracking glasses - a non-invasive video based binocular eye tracker with automatic parallax compensation - measures the gaze pointer for both eyes with 30 Hz. The gaze pointer accuracy of  $0.5^{\circ}-1.0^{\circ}$  and a tracking range of  $80^{\circ}/60^{\circ}$  horizontal/vertical assure a precise localization of the human's gaze in the HD 1280x960 scene video with 24 fps. An accurate three point calibration (less than  $0.5^{\circ}$  validation error) was performed and the gaze positions within the HD scene video frames were used for further processing.

In marketing and usability engineering, the tracking of human eye movements, i.e. eye-tracking, has been the central technology for capturing visual attention and motivation (e.g. Buswell 1920). For long times the application of eye-tracking technology was limited to stationary settings due to technical restrictions. Only within the last couple of years miniaturized mobile eye-tracking systems have become available and been successfully applied in different areas of research (e.g. Land and Lee, 1994; Land and Furneaux, 1997; Land et al. 1999; Pelz and Canosa, 2001; Hayhoe et al., 2003; Hayhoe and Ballard, 2005) with the major advantage to evaluate attention in the field where the task of interest is performed.

Mobile eye tracking with automated annotation of the eye tracking video by means of computer vision methodology has recently been introduced for the purpose of identifying visual semantics and relate them to the viewing behavior (Fritz and Paletta, 2010). For a calibrated reference to the environment, (Munn et al. 2008; Voßkühler et al., 2009; Pirri et al., 2011) introduced monocular eye-tracking and triangulation of 2D gaze positions of subsequent key frames of the eye-tracking video. Paletta et al. (2013) presented a straight forward solution of mapping distributions of point-of-regard very precisely onto heat maps within a model of indoors environments, a method that will be used in future specified studies on measuring the perception of evacuation signage in detail.

For the segmentation of the eye tracking video record, the experiment was first investigated in terms of cognitive load and alertness (Holmqvist et al., 2011; Figure 5, Figure 6). From the gathered data and by plotting mean trends overlaid to the original data, we deduce the fact that the evacuation task involved the test person into low cognitive load and medium level of alertness.

For the purpose of evaluating the attention of test persons on the basis of information processing on signage along the way, the location of relevant evacuation signs (Figure 8a) and persons (Figure 8b) was extracted by means of computer vision methodology.

For the purpose of monitoring all data channels from the multisensory stream of, the FACTS Monitor (Figure 7) was developed. This framework enables to view in real-time or via post-processing the synchronized data channels, raw sensor signals as well as meta-information resulting from complex processing.

Figure 8a, left, clearly visualizes by means of the position of the POR that the overt attention has not been focused on the signage above (Figure 8a, right). Then from all ETG video frames, where a signage had been detected, the relative distance between the signage and the POR was extracted and overlaid this information in a single image which is depicted in Figure 8c, left. The color coding reveals - in terms of a heat map - the distribution of PORs in the vicinity of the signage which has been positioned above for the purpose of getting a measure on how far the human attention is focused in the frame of signage presence. It can be clearly depicted that signage does not focus attention of the evacuation person.

Figure 8b, left, demonstrates the POR being located on a person, in the hallway of the office building, where persons gathered to wait for an official evacuation guide. (Figure 8b, right) shows the detection of a person by the annotation of a square overlaid on the position of the person, in fact, its head/shoulder based outline in the video frame. We repeated the process described in the paragraph above, this time for the purpose of a POR based heat map in relative distance to person detections. The resulting heat map clearly visualizes that persons are definitely in the focus of attention, with a slight offset that might be due to calibration purposes.

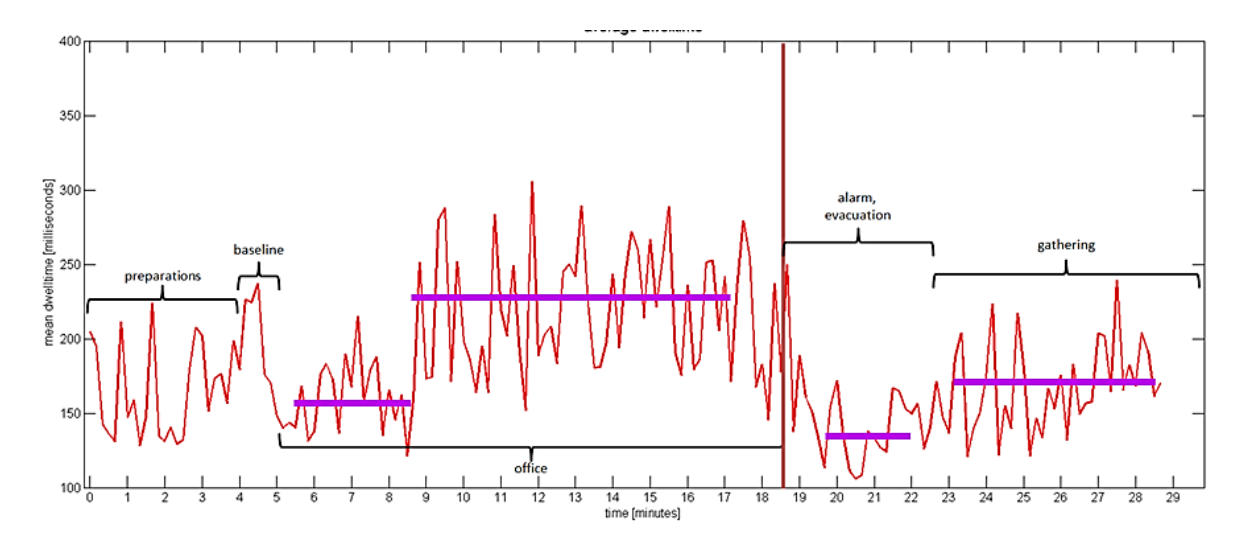


Figure 5. Mean dwell time as a measure of cognitive load.

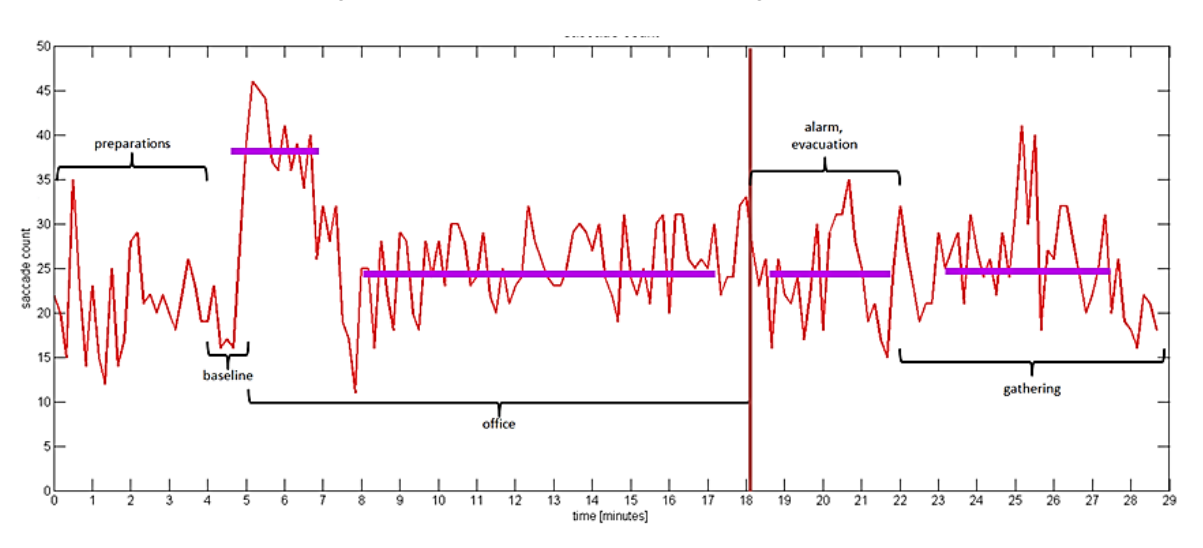
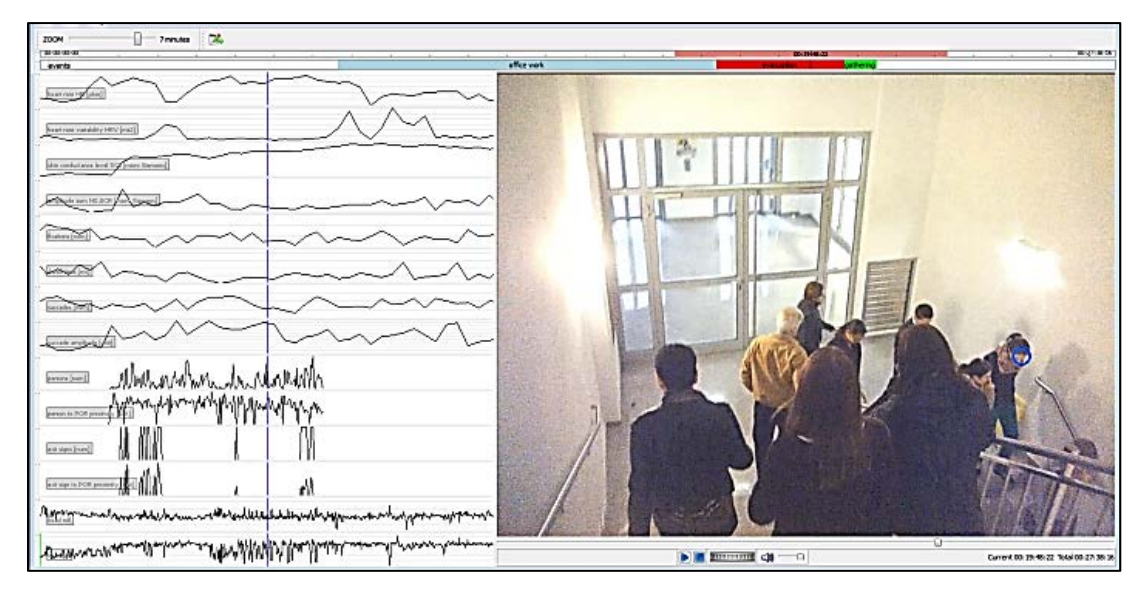


Figure 6. Number of saccades as a measure of alertness.



 $Figure\ 7.\ FACTS\ Monitor\ for\ real-time\ observation\ of\ multiple,\ multimodal\ data\ streams.$ 

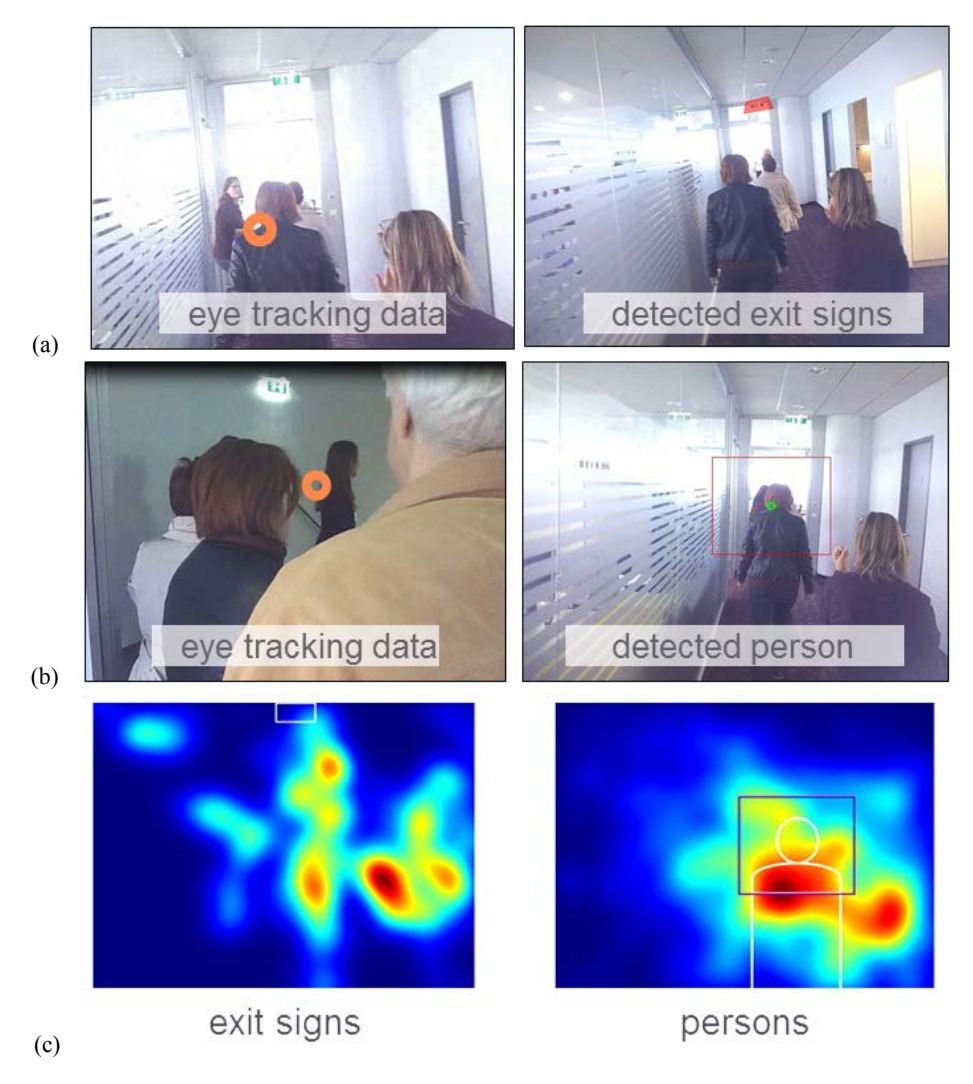


Figure 8. Analysis of eye tracking videos: (a) detected signs, (b) detected person, (c) heat maps relative to scene objects.

#### SIMULATION MODELL AND HUMAN FACTORS

In the case of disastrous accidents (fire, terrorist attacks, etc.) in large public and residential buildings, human factors play an important role in the effective outcome of evacuations (Pu and Zlatanova, 2005). The design and the evaluation of evacuation systems are crucial to guarantee successful responses after an incident. Mathematical models for the simulation of crowd behavior have been investigated as quantitative tool for demonstrating evacuation performance in the case of an emergency (Gwynne, Galea, Owen, Lawrence and Filippidis, 1999; Helbing, Farkas, Molnar and Vicsek, 2001; Sagun, Bouchlaghem and Anumba, 2011; Schadschneider et al., 2009).

Recently, microscopic models have been used for evacuation simulations (Zheng, Zhong and Liu, 2009) where some consider pedestrians as homogeneous and some as heterogeneous individuals (groups) differentiated by characteristics like gender, age and different psychological parameters. Commercially available software for the simulation of pedestrian evacuation (e.g., PedGo, TraffGo, EXODUS) includes several parameterizations, however, with rather limited insight into modeling issues. Attempts to include human factors e.g. by including visibility constraints into the model (Brunnhuber, Schrom-Feiertag, Luksch, Matyus and Hesina, 2012; Veeraswamy, Galea and Lawrence, 2009) or models which enables information sharing during evacuation were made (Okaya, Takahashi and Southern, 2012). In human behavior models (PMFserv; Pelechano and Badler, 2006) are integrated into a crowd simulation that incorporates high level wayfinding to explore unknown environments and also implements roles and communication to realistically spread information about the environment in the crowd.

The combination with human behavior models offers mature models for physiology, stress, perception and emotion and can handle the dysfunctional behavior that emerges in people during disasters, such as trance-like disbelief, milling, grouping and docile "sheep-like" following. Such advanced simulation models can exploit their full potential for emergency planning only if they are linked to empirical investigations of emergency situations that would provide the appropriate parameters to describe social behavior.

The three main factors which influence an emergency evacuation are the building, the environment and the human factors. The most complex and important ones are the human factors and they are the most difficult factors to be described. The presented work targets to significantly improve evacuation simulation by parameterizing the human agents' behavior with information on human factors, such as stress, perception and decision making. In particular, the single person's behavior in its specific situational context is investigated in the frame of its embodied decision making. For this purpose, users were equipped with a wearable sensor equipment that captures information about the environment (localization sensors), the psychophysiological status of the user (e.g. ECG, EDA), and its viewing (eye tracking glasses) and motion behavior.

From the correlation between the multisensory perceptual and psychophysiological data on the one hand, and the automatically sensed and interpreted situational context on the other hand, we will extract a rule base with a set of logical "pre-condition – action" pairs that will parameterize the crowd simulation model. Based on this rule base a behavioral model as described in (Kuligowski and Gwynne, 2010) will be developed were realistic behavior is a result of multiple factors rather than single specific binary if-then conditions. Therefore threshold values for influential factors have to be provided out of the experiments.

This behavioral model will be integrated in an agent based simulation model to allow an egress analysis that is able to reflect the frequently observed human social behaviors, through simulating the cognitive processes of individual agents and interactions among neighboring agents in the simulation environment. This will enable an evacuation simulation with a high degree of reality and a reliable evaluation of alternative evacuation scenarios.

#### CONCLUSIONS

First results that target at a significant improvement of the evacuation simulation were presented in this paper. The parameterization of the human agents' behavior with information on human factors about stress, perception and decision making has been studied thoroughly in an evacuation scenario at a large office building. The combination of visual information from eye tracking and the analysis of information from psychophysiological measures together establish indicators for stress events and reduced information processing by the participant. These events have been identified in the data on the basis of continuous measurements during the evacuation experiment.

The data from the concrete field trial demonstrate that visual orientation as well as social cues are relevant, furthermore, that social gaze is capable to initiate social interactions with consequences on the overall evacuation results, and that orientation is highly focused on the ground during evacuation. We conclude from these cues that it is worth to continue with more focused studies on determining concrete parameters that are intended to be provided to the interface of a cognitive simulation model.

#### **ACKNOWLEDGMENTS**

This work has been partially funded by the Austrian Research Promotion Agency by grant n°836270 (EVES) and by grant n°832045 (FACTS).

#### REFERENCES

- Brunnhuber, M., Schrom-Feiertag, H., Luksch, C., Matyus, T., & Hesina, G. (2012). Bridging the gap between visual exploration and agent-based pedestrian simulation in a virtual environment. In Proceedings of the 18th ACM symposium on Virtual reality software and technology (pp. 9–16). New York, NY, USA: ACM. doi:10.1145/2407336.2407339.
- Fritz, G. and Paletta, L. (2010). Semantic Analysis of Human Visual Attention in Mobile Eye Tracking Applications, Proc. IEEE International Conference on Image Processing, ICIP 2010, Hongkong, China, September 26-29, 2010, pp. 4565 4568.
- Gwynne, S., Galea, E. R., Owen, M., Lawrence, P. J., & Filippidis, L. (1999). A review of the methodologies used in the computer simulation of evacuation from the built environment. Building and Environment, 34(6), pp. 741–749. doi:10.1016/S0360-1323(98)00057-2
- Hayhoe M & Ballard D. (2005) Eye movements in natural behaviour. TRENDS in Cognitive Sciences, Vol. 9, April 2005.
- Hayhoe, M. et al. (2003) Visual memory and motor planning in anatural task. Journal of Vision. 3, pp. 49-63.
- Helbing, D., Farkas, I., Molnar, P., & Vicsek, T. (2001). Simulation of Pedestrian Crowds in Normal and Evacuation Situations, pp. 21–58.
- Holmqvist, K., Nyström, M., Andersson, R., Dewhusrt, R., Jarodzka, H., and van de Weijler, J. (2011). Eye Tracking A Comprehensive Guide to Methods and Measures, Oxford University Press, 2011.
- Janke, W., Debus., G., Kallus, K. W., Hüppe, M., Schmidt-Atzert, L. (1989), "BSKE (EWL)-ak", Univeröffentlichtes Manuskript. Universität Würzburg, Germany.
- Kuligowski, E. D., & Gwynne, S. M. V. (2010). The Need for Behavioral Theory in Evacuation Modeling. In W. W. F. Klingsch, C. Rogsch, A. Schadschneider, & M. Schreckenberg (Eds.), Pedestrian and Evacuation Dynamics 2008 (pp. 721 2008amSpringer Berlin Heidelberg.
- Land, M. and Furneaux, S. (1997) The knowledge base of the oculomotor system. Philos. Trans. R. Soc. Lond. B Biol. Sci. pp. 352, pp.1231–1239
- Land, M.F. and Lee, D.N. (1994). Where we look when we steer. Nature 369, pp. 742–744.
- Land, M.F. et al. (1999) Eye movements and the roles of vision in activities of daily living: making a cup of tea. Perception, Vol. 28, pp. 1311–1328
- Munn, S. M., and Pelz J. B. (2008). 3D POR, position and head orientation from a portable monocular video-based eye tracker. Proc. ETRA, pp. 181-188, 2008.
- Okaya, M., Takahashi, T., & Southern, M. (2012). Effect of Guidance on Evacuation Behavior Simulations Using Agent Communication.
- Paletta, L., Santner, K., Fritz, G., Mayer, H., Schrammel, J. (2013). 3D Attention: Measurement of Visual Saliency Using Eye Tracking Glasses, Proc. ACM SIGCHI Conference on Human Factors in Computing Systems, CHI'13 extended abstracts, p. 199-204, Paris, France.
- Pelechano, N., & Badler, N. I. (2006). Modeling Crowd and Trained Leader Behavior During Building Evacuation. IEEE Computer Graphics and Applications, 26(6), 80–86. doi:10.1109/MCG.2006.133
- Pelz, J.B. and Canosa, R. (2001) Oculomotor behaviour and perceptual strategies in complex tasks. Vision Res. 41, 3587–3596.
- Pirri, F., Pizzoli, M., Rudi, A.: A general method for the POR estimation in 3D space. Proc. CVPR, 2011.
- Sagun, A., Bouchlaghem, D., & Anumba, C. J. (2011). Computer simulations vs. building guidance to enhance evacuation performance of buildings during emergency events. Simulation Modelling Practice and Theory, 19(3), 1007–1019. doi:10.1016/j.simpat.2010.12.001
- Schadschneider, A., Klingsch, W., Klüpfel, H., Kretz, T., Rogsch, C., & Seyfried, A. (2009). Evacuation Dynamics: Empirical Results, Modeling and Applications. In R. A. Meyers (Ed.), Encyclopedia of Complexity and System Science. Berlin Heidelberg New York: Springer.
- Veeraswamy, A., Galea, E.R., & Lawrence, P. (2009). Implementation of Cognitive Mapping, Spatial Representation and Wayfinding Behaviours of People within Evacuation Modelling Tools. In Proceedings of the 4th International Symposium on Human Behaviour in Fire, Robinson College, Cambridge, UK, 13-15 July 2009, (pp. 501–512).
- Voßkühler A., Nordmeier V. and Herholz S. (2009). Gaze3D Measuring gaze movements during experimentation of real physical experiments. Proc. ECEM, 2009.
- Zheng, X., Zhong, T., & Liu, M. (2009). Modeling crowd evacuation of a building based on seven methodological approaches. Building and Environment, 44(3), 437 445. doi:10.1016/j.buildenv.2008.04.002

## A New Representational Method of Human Foot Anatomical Landmark and its Application in Foot Posture Data Acquisition

KaiWei Zhao, Ameersing Luximon, Ganesan Balasankar and CheeKooi Chan

Institute of Textiles and Clothing The Hong Kong Polytechnic University Hung Hom, Kowloon, Hong Kong

#### **ABSTRACT**

Functions like protection and comfort are essential requirements of the footwear or orthosis. Naturally, the status of foot anatomy features, judged from both inside and skin surface, is of great significance to the effectiveness of the product. In this study, a novel method to estimate the foot anatomy structural deformation from the skin surface in three typical postures is proposed, which can effectively reveal the inner anatomy status without using CT or MRI. Technology of scanning with range sensor is adopted, and it considerably promotes the efficiency of acquisition of the foot texture model. Reverse engineering tools are used to precisely catch the anatomical landmark locations, and the relevant data is shown in the way of comparison.

Keywords: Range Sensor, Texture Model, Anatomical Landmark, Structural Deformation

#### INTRODUCTION

Three-dimensional localization of anatomical landmarks of the foot is of great significance in medical use. As (Liu, 2004) related, the malleoli, which is a key landmark in lower extremity examination, plays an important role in leg measurement and defining the axis of the upper ankle joint. As indicated in this paper, in terms of kinetic analysis of the lower limb both in static and dynamic status, the exact position of the ankle joint is also of particular importance in motion capture and key dimension determination. However, there are limitations in traditional methods of anatomical landmark marking. Traditionally, optical markers are attached to the skin close to the malleoli, while this method is not so convincing and doubted of its reliability due to skin movements (Cappozzo, 1994). A different approach to this problem is the idea that an anatomical landmark can be defined by particular shape of the skin. It is widely accepted that the underlying anatomical structure is independent of the skin movements (Besl, 1988). Once a constant representation is figured out for the structural shape, the landmark can be determined. Besides, invariant also means that it is neither dependent on the actual coordinate system nor surface parameterization. Curvature data (key of this method) is chosen as constant shape description (Frobin, 1982). A parameterized representation of the foot surface needs to be produced ahead and coordinates, derivatives and curvature maps are available (Barros RML, 2002). Hence the landmarks are characterized and discriminated. Koenderink shape index (Koenderink, 1992), which is a key tool to separate the convexity from the concavity and shape's color changes according to its deepness and the surface types, is integrated in this method.

(Drerup, 1985) presented a method for the localization of anatomical landmarks on the human body surface. Surface shape with systematic curvature description is analysed in their method. Basic surface coordinates (geometrical

mesh info) are acquired through optical methods such as moiré topography or rasterstereography, which provides the conditions for curvature calculation. Reverse engineering technology is highly needed in pre-processing for geometry feature generation and thus characteristic parameters such as curvature and derivative distribution will be calculated. Localization of vertebra prominens is presented as an example in their works and the results are compared with that of conventional method that the anatomical landmarks are manually palpated and marked, which reveals that the former has higher reliability and accuracy.

As illustrated, two lines are defined by the landmarks: the malleoli, the fibular head, the point anterior to lateral tibial condyle and the medial tibial condyle. These two lines form an angle that is generally regarded as measurement of tibial torsion, the mean of which is 20.58°. This is a typical example of measuring the inner structure by surface anatomy characteristics, which has a promising and broad application prospect.

(Subburaj, 2008) described a computer-aided method used for extracting anatomical landmarks from a three-dimensional digital model generated from multiple CT images. In the experiment, an accurate three-dimensional reconstructed pelvis model was adopted for landmark location. Similar as the method in the literature mentioned above, landmark identification through curvature analysis were used instead of conventional manual palpation way after three-dimensional geometrical feature characterization hence regions like peaks, ridges, pits and ravines on the surface are identified and classified automatically. The result can be applied on significant dimension measurement, pre-operative planning that are essential for the surgeries requiring anatomical landmarks on skin or skeletal tissue, like resecting deceased tissue and positioning custom implants or mega endoprostheses.

Not only is how to identify the anatomical landmarks important but also what to mark must be studied. (Agić, 2006) studied this subject and suggested some geometric descriptors. In terms of the foot functionality, the bone inertial tensor descriptor plays a significant role. Eigenvalue of the inertial tensor can describe the bone shape, thus contributing to the definition of a coordinate system in bone centroid. The medial longitudinal arch also plays an important role among the structural characteristic descriptors in foot shape and kinematics analysis (Razeghi, 2002). Besides, the principal component analysis was applied by to the foot structure and three principal components that respectively reflecting the characteristics of size, shape and comfort were concluded.

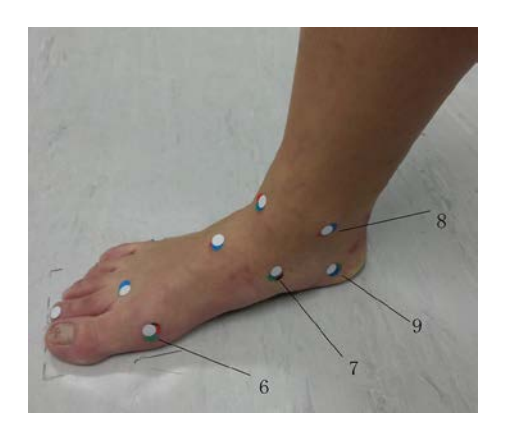
The methods mentioned above have a common serious defect: low efficiency. To calculate the curvature map and then get the convex and concave regions through landmark detecting algorithm is considerably time-consuming and equipment-demanding. With the development of range sensing technology, a novel three dimension scanning tool, Microsoft Kinect, which is characterized by low cost and high efficiency of data acquisition, has come out. It can finish scanning an object together with its color and texture within 1 minute. Basing on Kinect and its supporting suites, a new method of accurately locating the human foot landmarks is presented in this paper, together with its preliminary application in foot posture data acquisition.

## METHOD FOR LOCATING AND DIGITALIZING THE FOOT ANATOMICAL LANDMARKS

#### **Determination of Landmarks for Representation**

The first metatarsal bone is most apt to get fractured among the multiple anatomical structures within human foot, whichever posture he or she is in, e.g. standing under normal pressure, raising the heel to a medium or a higher height and even jumping. The second metatarsal bone follows the first one in this respect. The calcaneous part always bears large quantity of compressive stress and hence is quite inclined to get fatigue fracture. As is known to all, subtalar joint and true ankle joint play an important role in foot and ankle statics, kinetics and kinematics. Hence, the locations of the key functional landmarks, such as the most prominent points on medial and lateral malleolus, can help effectively estimate and evaluate function status of foot anatomy. Accordingly, the locations in terms of the foot surface anatomy were chosen as shown in Figure 1 and Table 1.





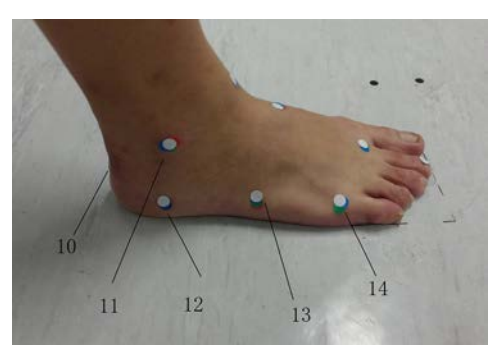


Figure 1. Landmarks (white stickers) for the experiment (for better visual effect, zero-heel posture is taken as the example for landmark show).

Table 1: Landmarks on foot for test

Shin of the Tibia
Anterior border of the lower end of Tibia
Mid dorsal point of the foot
Second metatarso-phalangeal joint
Tip of the second toe
First metatarso-phalangeal joint
Navicular tubercle
Medial malleolus
Medial border of the calcaneous
Calcaneal tuberosity
Lateral malleolus
Lateral border of the calcaneus
Tuberosity of fifth metatarsalis
Fifth metatarsophalangeal joints

#### **Equipment**

Table 2: Experiment equipment

Equipment	Technician (Occupational therapist), Microsoft Kinect Sensor, MSI Laptop, Artec Studio 9 (licensed using the email account: sammymx2008@hotmail.com) for three-dimensional mesh data acquisition and processing, Geomagic Studio (trial version)		
Consent form	Yes		
Foot chosen	Right		
Landmarks for scanning	Described in Table.1		
Distance of camera from people	0.6~0.8m		
Temperature	18°C		

Except for Microsoft Kinect, MSI laptop with a CPU of Intel® Core ™ i7-4700MQ and a graphic card of Nvidia GeForce GTX 765M / GDDR5 2GB, together with a RAM of 16GB DDR3L, was adopted. The performance of the computer can have considerable impact on the efficiency and results. Artec Studio 9 from Artec Ltd. was used in the experiment due to its excellent stability, high efficiency and accurate and powerful function for texture mapping, vertex color assignment and mesh data processing. Geomagic Studio 11 (trial version) was chosen for landmark location measurement and preliminary analysis.

#### **Procedure**

A 25 years old women subject was selected for this study. The basic demographic data was collected including height (156cm) and weight (49 kg). The original anatomical landmarks were identified through touching detection by an experienced occupational therapist, and then marked out with black stickers (with a diameter of 5mm). First of all, three postures were tested: Normal standing, medium heel and high heel position. The marked foot (right foot) of the subject was scanned by Microsoft Kinect, and the textured models with landmarks are output in the format of obj. Secondly, the exported mesh models were imported into Geomagic Studio (trial version), and the landmarks were enhanced. Finally, the key locations and dimensions represented by the markers were measured interactively. Therefore, the correlations between the anatomical structures of the natural standing status and the other two typical postures were measured and identified. Figure 1 shows the experiment procedure.

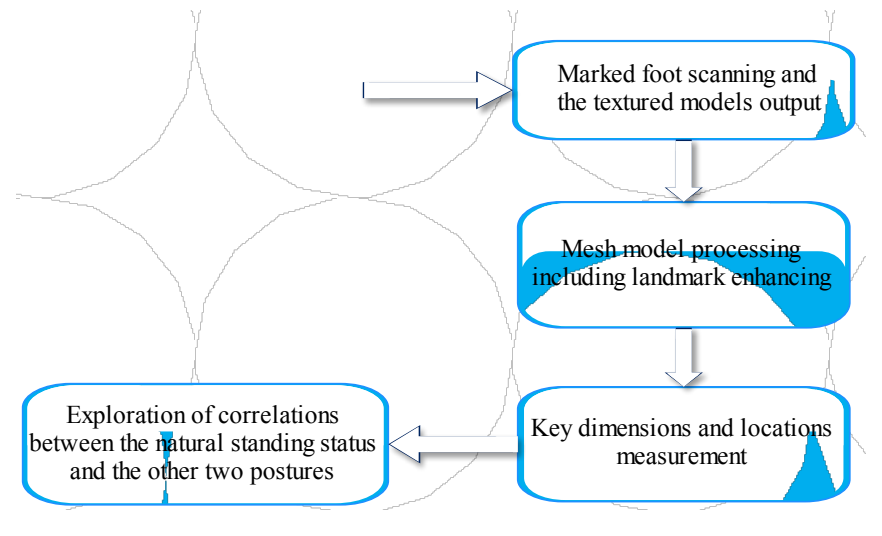


Figure 2. Experiment procedure

#### **RESULTS**

The exported mesh model with texture and color (See Figure 3) were processed through the steps of noise and redundant data removal, smoothing and marker enhancement in Geomagic Studio 11. Meshlab 3.2(64-bit) was used for final check and three-dimensional demonstration. The normal standing, medium heel and high heel postures are the three main categories for measurement. The XY datum plane is determined by 3-point method through randomly picking 3 points far apart to each other and distributed uniformly on the ground mesh data.

Afterwards, the distances from the XY datum plane to each landmark and the linear distances between some of the landmarks in the three postures are measured in Geomagic Studio 11, too. The result can be seen in Table 3.

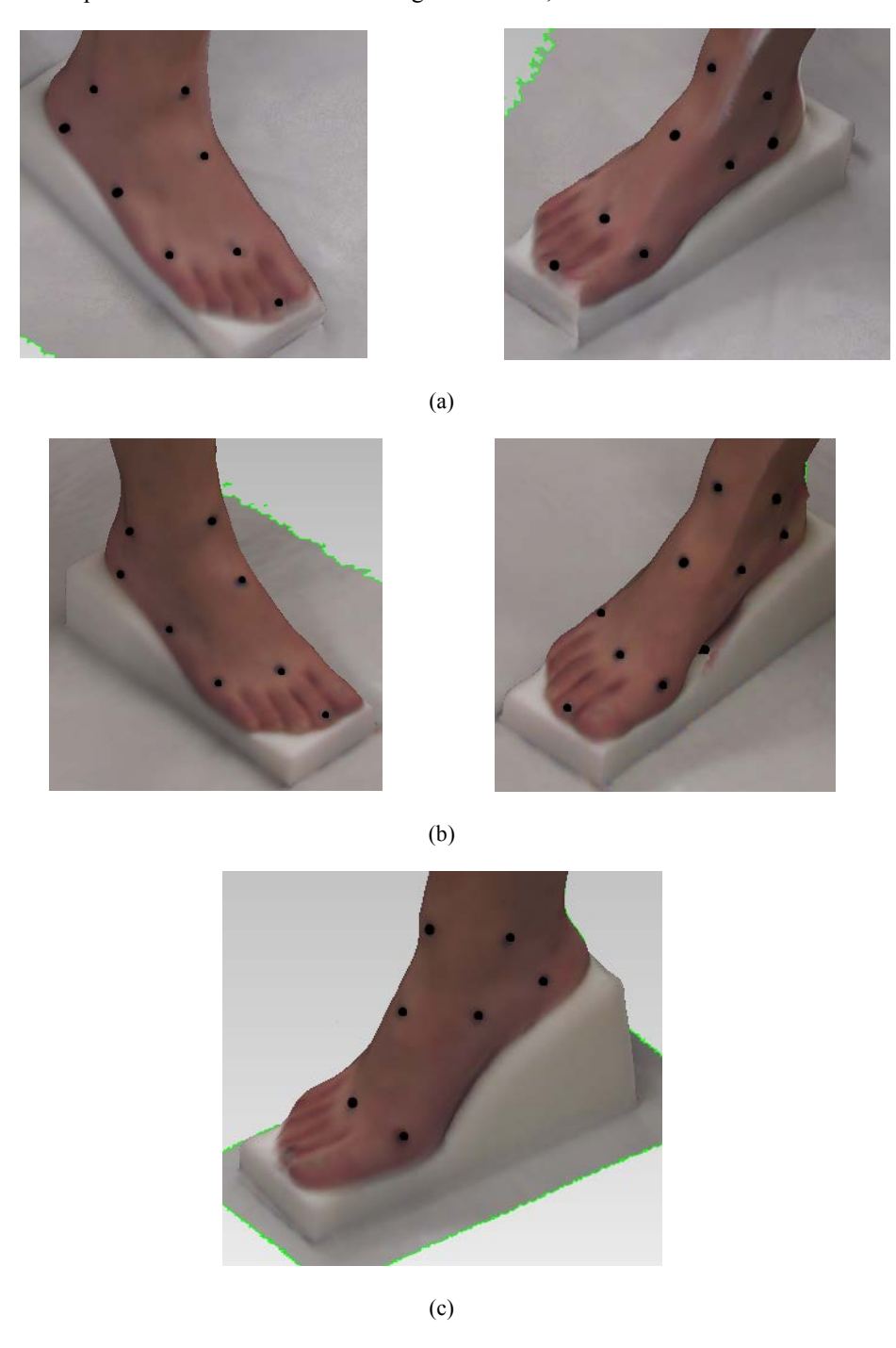


Figure 3. Three-dimensional mesh model, a: low heel (20mm); b: medium heel (40mm); c: high heel (70mm)

Table 3. Distances between the landmarks and the XY datum plane (8 key landmarks of the 14 are chosen)

	Distance to XY datum plane (mm)		
Anatomical landmark	Low(20mm)	Medium (40mm)	High (70mm)
Lateral malleolus	67.519	125.218	136.200
Fifth metatarsophalangeal joints	28.390	42.704	43.610
Tuberosity of fifth metatarsalis	20.653	62.380	69.758
Medial malleolus	78.772	123.758	142.690
Navicular tubercle	43.055	81.426	91.735
First metatarso-phalangeal joint	35.601	47.463	42.783
Second metatarso-phalangeal joint	33.826	49.224	48.286
Calcaneal tuberosity	29.895	86.257	114.373

#### **CONCLUSIONS**

Through measurements on the textured foot mesh model, we can draw the posture features through key landmarks' location. Since it is widely accepted that the anatomical landmarks can reflect the inner structure status during different postures, they can be regarded as descriptions of foot postures in terms of their distinguishing status of different anatomical parts, such as tensioning and compressing. What the new representing method presented in this paper contributes to foot anatomy status analysis most is its qualitative conclusion from the quantitative measurements. For instance, through the measured distances of head of 1st metatarsal bone and the medial cuneiform in Table 3, the angles in terms of the 1st metatarsal bone (regarded as a line segment) between its geometrical status from the normal standing to the medium posture, and from medium to high heel posture, can be calculated. Although due to skin movements and touching errors caused by manual operation by the occupational therapist, the angles may be effectively used for analyzing the stress status of the 1st metatarsal bone and even the whole foot arch.

#### **ACKNOWLEDGEMENTS**

This study was supported by RGC General Research Fund (B-Q26V) and RGC General Research Fund (B-Q31C).

#### REFERENCES

Agić, A. (2006). "Foot structure descriptors". Ergonomia IJE&HF, 28(3), 237–248.

Barros RML, F. P., Paterniani PES, Brenzikofer R, Filho ECL. (2002). "Three-dimensional reconstruction and analysis of human back surface". Paper presented at the Seventh International Symposium on the 3-D Analysis of Human Movement, Newcastle upon Tyne, England.

Besl, P. J. (1988). "Surfaces in range image understanding" (Vol. 27): Springer-Verlag New York.

Cappozzo, A., Catani, F., Leardini, A. (1994). "Skin movement artefacts in human movement photogrammetry". Journal of Biomechanics, 27(6), 755.

Drerup, B., Hierholzer, E. (1985). "Objective determination of anatomical landmarks on the body surface: measurement of the

- vertebra prominens from surface curvature". J Biomech, 18(6), 467-474.
- Frobin, W., Hierholzer, E. (1982). "Analysis of Human Back Shape Using Surface Curvatures". Journal of Biomechanics, 15(5), 379-390. doi: Doi 10.1016/0021-9290(82)90059-8
- Koenderink, J. J., van Doorn, A. J. (1992). "Surface shape and curvature scales". Image and vision computing, 10(8), 557-564. Liu, X., Kim, W., Drerup, B. (2004). "3D characterization and localization of anatomical landmarks of the foot by FastSCAN". Real-Time Imaging, 10(4), 217-228. doi: DOI 10.1016/j.rti.2004.05.009
- Razeghi, M., Batt, M. E. (2002). "Foot type classification: a critical review of current methods". Gait Posture, 15(3), 282-291. Subburaj, K., Ravi, B., Agarwal, M. (2008). "3D shape reasoning for identifying anatomical landmarks". Computer-Aided
  - Design and Applications, 5(1-4), 153-160.

## Section 3

Digital Human Modeling Applications

# The Digital Evaluation of Driver's Field of View and its Potential Impact on Cyclist Safety

Russell Marshall, Steve Summerskill and Sharon Cook

Loughborough Design School Loughborough University Loughborough, Leics, LE11 3TU, UK

#### **ABSTRACT**

Driver vision from vehicles is a long standing issue. One highly topical scenario includes accidents to vulnerable road users and in particular cyclists, from collisions with large goods vehicles (LGVs). In many of these cases driver vision is a potential causal factor in the occurrence of the accident. This paper presents research performed into the evaluation of driver vision, funded by the UK Department for Transport. To support the research, a 3D volumetric assessment technique was developed in the SAMMIE digital human modelling system. This highly visual technique provides an indication of the visible volumes of space around a vehicle and any blind spots. Vision was evaluated for a range of vehicle types from cars through to LGVs. To investigate the potential casual effects of vision in accidents and specifically those involving cyclists, scenarios were identified from UK Police accident data. These scenarios were then modelled and evaluated digitally. The results highlight that blind spots exist on many vehicles and for all driver sizes. Many of these blind spots can be countered by a change in posture of the driver. However, the most significant blind spot was found on Category N3 LGVs to the near-side of the vehicle. The research was also instrumental in a change to the EU Regulation 46 to remove the blind spot from future LGVs.

Keywords: DHM, ergonomics, field of view assessment, cyclist safety, SAMMIE

#### INTRODUCTION

Driver vision from vehicles is a long standing issue and continues to be concern. One highly topical scenario includes injuries and fatalities to vulnerable road users (VRUs) and in particular cyclists, from collisions with large goods vehicles (LGVs) in urban areas. However, accident data show that serious injuries and fatalities continue to occur to VRUs from all types (Categories) of vehicle and from all types of manoeuvre. In many of these cases driver vision is a potential causal factor in the occurrence of the accident. Whilst driver vision is a priority for primary safety, the design of many vehicles ensures that there is likely to be some obstruction due to the solid structure of the vehicle occluding the driver's view.

Regulations exist that specify the need for various field of view requirements for different vehicle Categories. A review of these regulations shows that the complexity of the situation has led to continuous amendment to regulations such as 2003/97/EC (2004) and UN Regulation 46 (2009) that deal with type approval of vehicles and minimum vision requirements. Yet, even with an almost continuous review process in place accidents continue to occur in which driver vision plays a role.

This paper presents research performed into the evaluation of driver vision, funded by the UK Department for Transport and from ongoing research performed with Cemex, a major UK operator of LGVs throughout the UK. To support the research a new 3D volumetric evaluation and assessment technique was developed in the SAMMIE digital human modelling system. This projection technique allows the visible volume that represents driver's direct vision through window apertures, and driver's indirect vision reflected through mirror surfaces to be modelled. This highly visual technique provides a clear indication of the visible volumes of space around a vehicle and conversely, any blind spots.

Road accidents involving cyclists is a highly topical problem. The UK has invested heavily in cycling infrastructure in recent years and has seen an increase in the number of journeys cycled and in the number of cyclists killed or seriously injured (RoSPA, 2012). In particular, issues surround accidents involving LGVs and cyclists have been explored over many years and initiatives by government and by industry have attempted to address the issues. However, accidents to cyclists still occur with a total of 118 fatalities in the UK in 2012. The majority of these accidents also occur in urban areas and London saw six cyclist fatalities within a two week period in November 2013.

To explore these issues, UK Police accident data was used to provide specific scenarios in which the impact of driver vision can be evaluated. These scenarios were modelled within the SAMMIE system and the volumetric projection technique used to explore the impact of blind spots and their potential contribution to accidents with VRUs and specifically cyclists.

#### AN ANALYSIS OF UK ACCIDENT DATA

To evaluate the nature and prevalence of accidents in which driver vision / 'blind spot' was recorded as a contributory factor in UK road accident data an analysis was made of two data sets. Using data available from the UK STATS 19 and 'On the Spot' (Hill and Cuerden, 2005) police accident databases a total of 1906 incidents were identified for the 2008 reporting period (Table 1).

Table 1: Venicle types with	biina spot	as contributing factor if	n UK road accident	t from \$1 A1\$ 19 (2008)

Vehicle type	Vehicle Class	Count
Car	$\mathbf{M}_1$	1009
Goods vehicle: over 7.5 t	N <sub>2</sub> or N <sub>3</sub>	511
Goods vehicle: under 3.5 t	N <sub>1</sub>	157
Goods vehicle: 3.5–7.5 t	$N_2$	65
Bus or coach	$M_2$ or $M_3$	53
Other		111
Total		1906

A cluster analysis (Lenard *et al*, 2011) was applied to the data to explore: accident severity, vehicle type, vehicle movement, first point of contact, drive side and collision partner type (e.g. VRU, Motorcycle, Car etc.). From the cluster analysis a number of scenario types were identified that warranted further exploration. These include:

- 1. Articulated left-hand drive LGVs over 7.5 tonnes (N<sub>2</sub> & N<sub>3</sub> vehicles) changing lane to the right and colliding with cars (25% all casualties, 14% of serious, 6% of fatal)
- 2. Articulated and Rigid right-hand drive LGVs over 7.5 tonnes (N<sub>2</sub> & N<sub>3</sub> vehicles) changing lane to the left and colliding with cars (24% of all casualties, 14% of serious, 6% of fatal)

- 3. Articulated and Rigid right-hand drive LGVs over 7.5 tonnes (N<sub>2</sub> & N<sub>3</sub> vehicles) changing lane to the right and colliding with cars (11% of all casualties, 2% of serious)
- 4. Goods vehicles (mostly small goods vehicles N<sub>1</sub>) reversing into vulnerable road users and motorcycles (16% of all casualties, 29% of serious, 25% of fatal)
- 5. Non-articulated goods vehicles (all N Categories) moving directly forward into other road users, with over-representation of pedestrians, cyclists and motorcyclists (9% of all casualties, 18% of serious, 19% of fatal)
- 6. Articulated goods vehicles over 7.5 tonnes (N<sub>2</sub> & N<sub>3</sub> vehicles) also moving directly forward into other road users (VRUs and cars), (5% of all casualties, 4% of serious, 25% of fatal)
- 7. Goods vehicles (all N Categories) turning left and colliding with vulnerable road users (5% of all casualties, 10% of serious, 19% of fatal)

From the analysis it was clear that accidents in which driver vision was a potential contributory factor occurred in all directions of vehicle movement. This suggests that the visibility of obstacles or other road users could be impaired in any direction. In addition, many of the scenarios involved LGVs and frequently VRUs were over represented in the 'collision partner' field.

#### **ACCIDENT SCENARIOS**

To complement the cluster analysis of the STATS 19 accident data, specific OTS cases were identified that could be used as examples of the scenario types. In total the research identified seven scenarios from the OTS database including a forward moving Category  $M_1$  vehicle colliding with a scooter on roundabout (Marshall at el, 2012), Category  $M_1$  and  $M_2$  vehicles reversing into VRUs (Marshall et al, 2013) and LGV side-swipe accidents with other road vehicles (Summerskill et al, 2012). This paper reports on three of the scenarios that include collisions with VRUs and specifically cyclists.

#### Scenario 1: Category M<sub>1</sub> - Crossroads

This scenario examined the visibility from category  $M_1$  vehicles in a situation where the vehicle is proceeding straight on at a give-way controlled crossroads, crossing the main carriageway. In the OTS case, the driver of the  $M_1$  category vehicle has pulled out of the junction and collided with a cyclist already on the main carriageway.

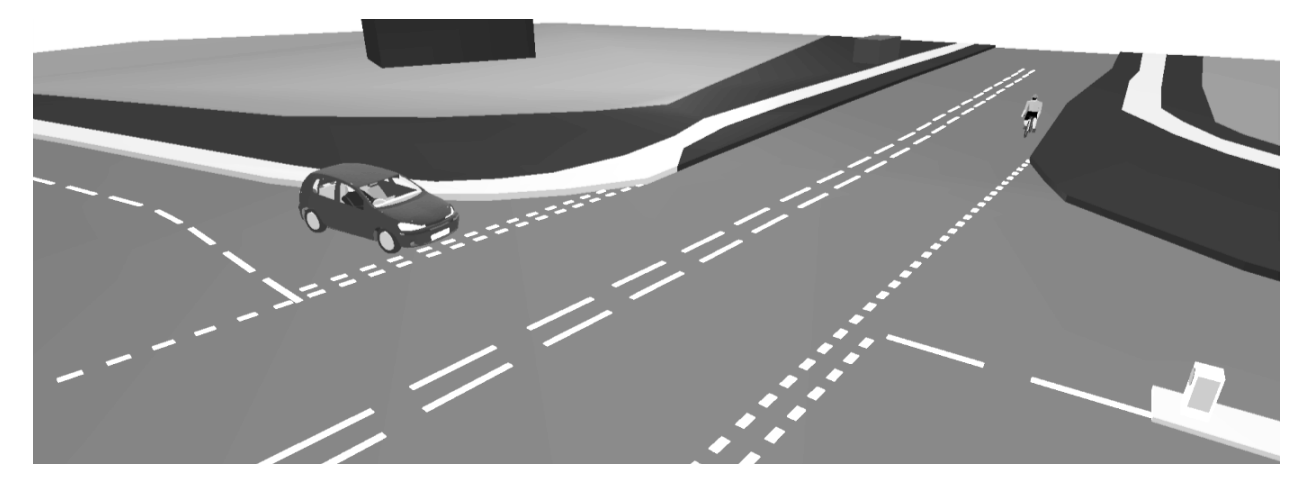


Figure 1. Scenario 1 – Car pulls out at crossroads and collides with cyclist.

#### Scenario 2: Category M<sub>1</sub> - T-Junction

This scenario examined the visibility from category  $M_1$  vehicles in a situation where the vehicle is turning left at a T-junction from a shop car park into a major road. In the OTS case, the driver of the  $M_1$  category vehicle has pulled out of the junction and a cyclist has collided with the side of the vehicle.

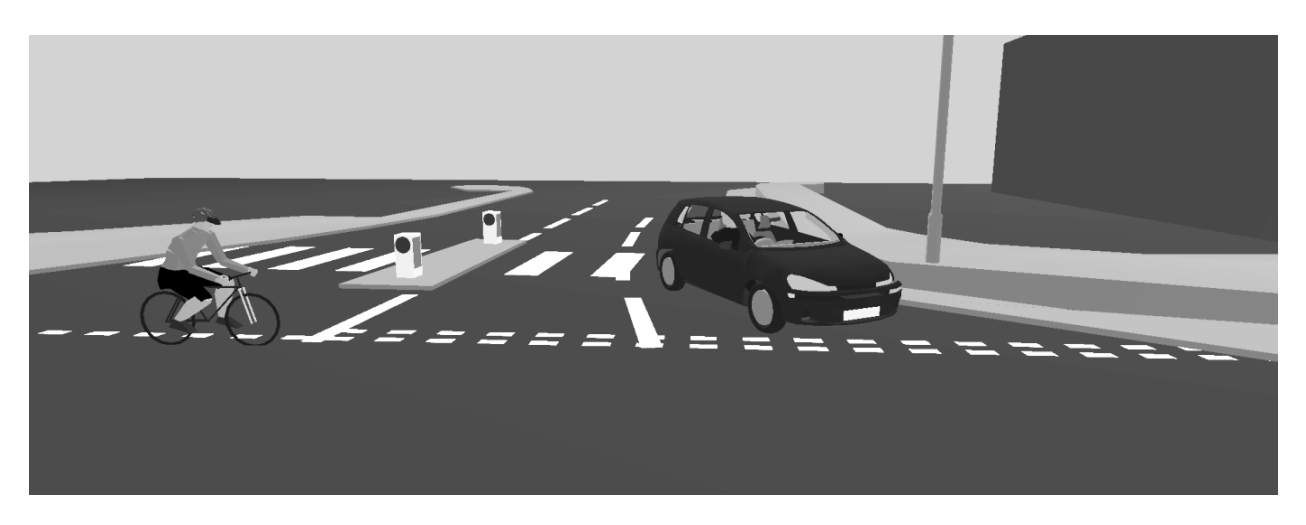


Figure 2. Scenario 2 – Car pulls out of T-junction junction and collides with cyclist.

#### Scenario 3: Category N<sub>3</sub> - Left Turn at Junction

The scenario examined the visibility from category  $N_3$  vehicles in a situation where the vehicle is turning left from the main carriageway into a side-street. In the OTS case, the driver of the  $N_3$  vehicle has pulled away from the traffic lights at the junction and turned left colliding with a cyclist proceeding straight on along the near-side (passenger side) of the vehicle.

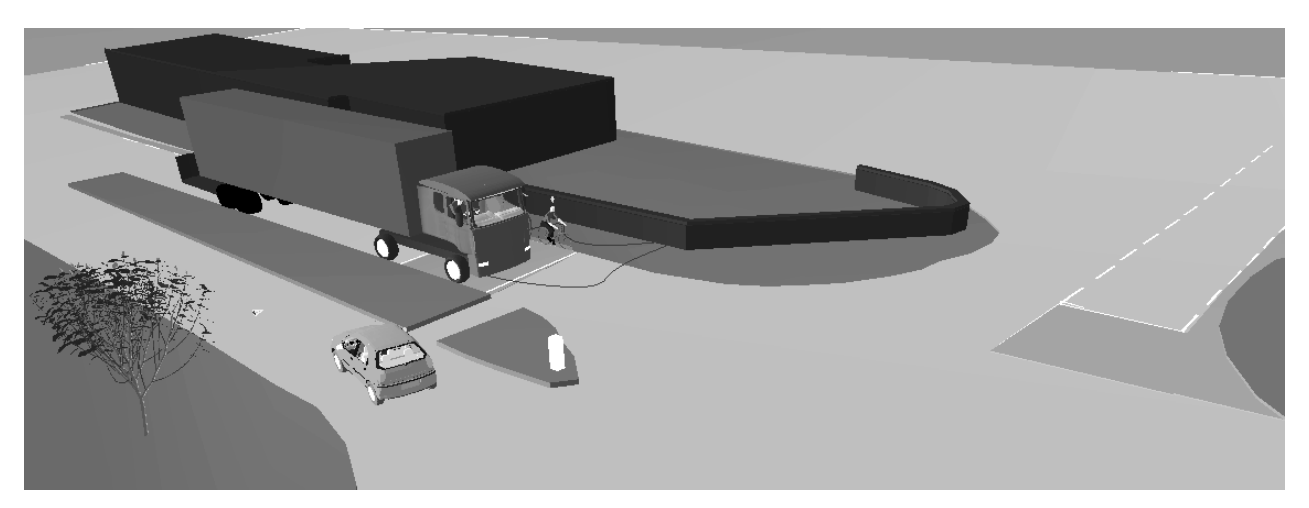


Figure 3. Scenario 3 – LGV turns left at junction and collides with cyclist.

#### FIELD OF VIEW EVALUTION TECHNIQUES

The expected field of view requirements as governed in the regulations such as 2003/97/EC (2004) and UN Regulation 46 (2009) typically describe a 2D area on the ground plane (Figure 4). To evaluate compliance with these areas a range of techniques have been employed in the literature, though many studies rely on real world methods to collect the visual areas, even if they are subsequently then translated into a digital medium. These real world methods rely on light projection techniques or use the driver's vision and ability to see a target marker to identify the field of view (e.g. Reed *et al.*, 2000; Delmonte *et al.*, 2012). In selected cases purely digital projection techniques have been employed to produce virtual evaluations of field of view (Tait and Southall, 1998; Way and Reed, 2003). In both types of approach the projections are typically resolved into a simplification of the field of view as a 2D area.

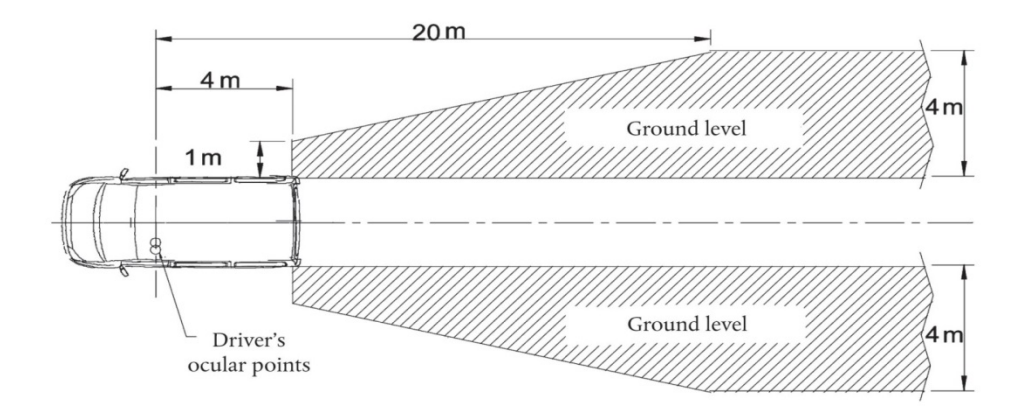


Figure 4. Minimum field of view specified in 2003/97/EC (2004) for Class III (exterior small) mirrors

In reality, the field of view of a driver is a complex 3D volume, projecting from the eyes through window apertures and mirror surfaces. The intersection of this 3D projection with the ground plane is therefore only an approximation of driver vision. The projection of field of view from the eyepoint inherently creates a conical volume (Figure 5) and thus any projected ground plane area is merely a 'slice' through a volume that is not uniform in the vertical axis. The tapering of the volume towards the vehicle aperture or mirror can lead to a situation where a target may be within the visible 'area' but barely within the visible 'volume' and thus potentially not as visible as may be suggested by the type of diagram shown in Figure 4.

To provide a greater understanding of the visible volume afforded the driver a 3D volumetric field of view projection method was developed (Marshall *et al.*, 2013). The projection method was prototyped, validated with real world tests and implemented within the SAMMIE DHM system (Porter et al. 2004). The method allows up to 10 projections of apertures to be combined with 10 projections of mirrors to provide an understanding of the full 360 degree field of view of the driver for any vehicle and conversely allow the identification of any blind spots.

Figure 5 shows the 3D volumetric projection method illustrating the field of view from the Class V close proximity 'look-down' mirror as fitted to a DAF XF Category  $N_3$  LGV. A human is stood within the visible area projected at the ground plane but the visible volume indicates that only their feet and part of their lower leg would be visible to the driver.

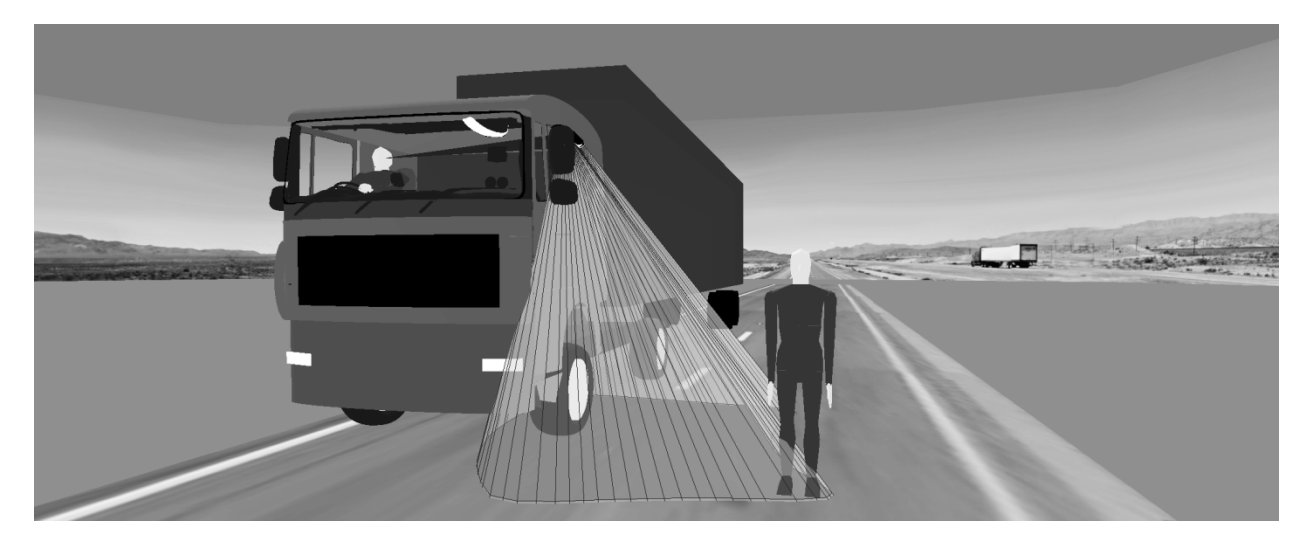


Figure 5. 3D volumetric field of view projection through a Category N<sub>3</sub> LGV Class V mirror and the ability to view a target within the visible 2D area projected on the ground plane.

#### SCENARIO FIELD OF VIEW ANALYSIS

For all of the scenarios the experimental setup included:

- The identification of a range of vehicles (3 x M<sub>1</sub>: Volkswagen Golf, Volkswagen Touran and Hyundai i10, and 3 x N<sub>3</sub>: DAF XF, Volvo 480 and Scania R420) selected from new vehicle registration data to provide vehicles that are highly represented on UK roads and display a variety of configurations
- The 3D contour scanning of the vehicles by FARO arm and subsequent modelling within PTC Creo
- The import into the SAMMIE DHM system and the setup of mirrors and adjustment to the regulations
- The determination of the limits of potential eye point through the modelling of the largest and smallest human models capable of operating the vehicle (e.g. 99<sup>th</sup> %ile Dutch Male and 5<sup>th</sup> %ile UK female)
- The modelling of the road junction and positioning of the vehicles based upon the data available from the OTS database

#### Scenario 1: Category M<sub>1</sub> - Crossroads

The scenario was modelled using the map data provided in the OTS case report (Figure 6). The angle of the junction to the main road has the potential to cause difficulty for the category  $M_1$  driver in terms of positioning for optimum visibility to the left of the vehicle to observe vehicles already on the main road travelling from left to right. The cyclist (circled) is positioned travelling along the main road from left to right across the path of the  $M_1$  vehicle. The  $M_1$  vehicle is positioned to travel across the crossroads bearing slightly left as the junction is offset.

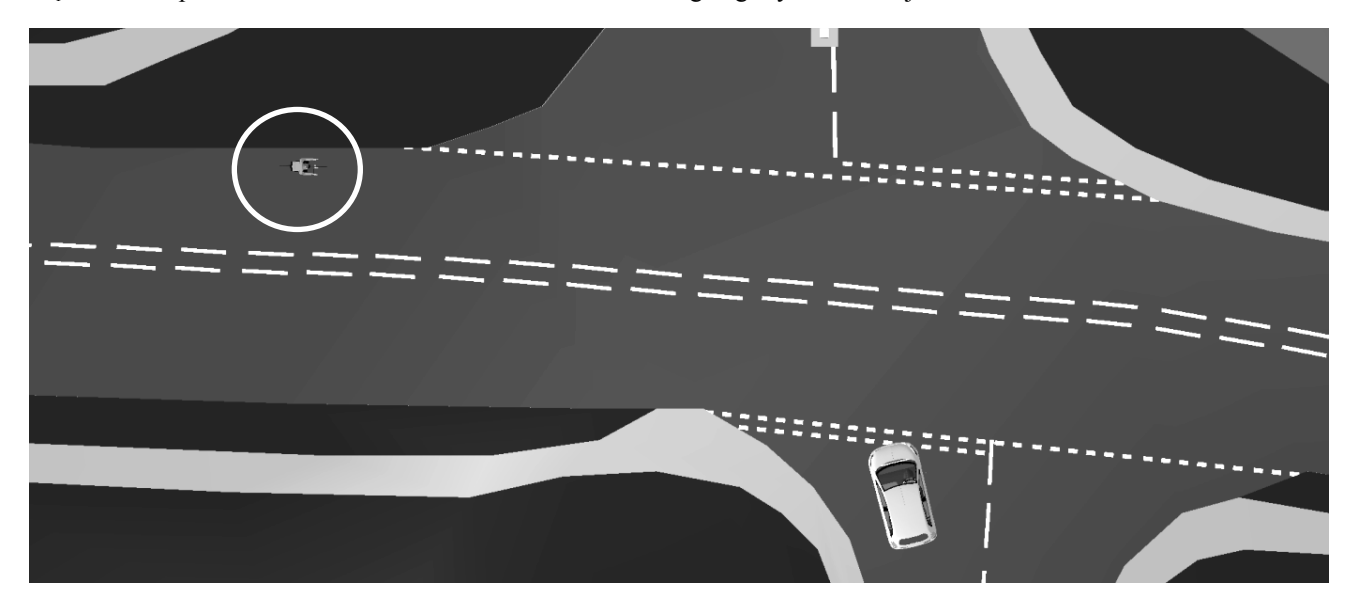


Figure 6. The relative positioning of the vehicles (Hyundai i10 and pedal cycle) at the scenario junction.

Figure 7 shows that in this position the cyclist is completely obscured by the nearside (left) A-pillar of the M<sub>1</sub> vehicle. The driver is looking to the right and left to check the coast is clear prior to pulling off.

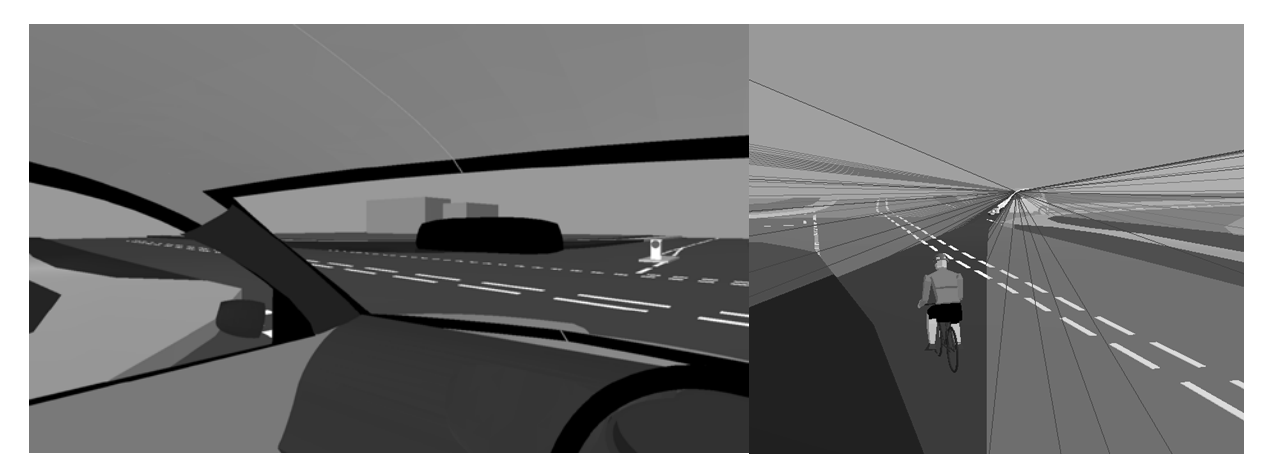


Figure 7. The view of the driver (99<sup>th</sup> %ile Dutch male) of the Hyundai i10 in the direction of the cyclist (direct vision on the left, volume projection on the right).

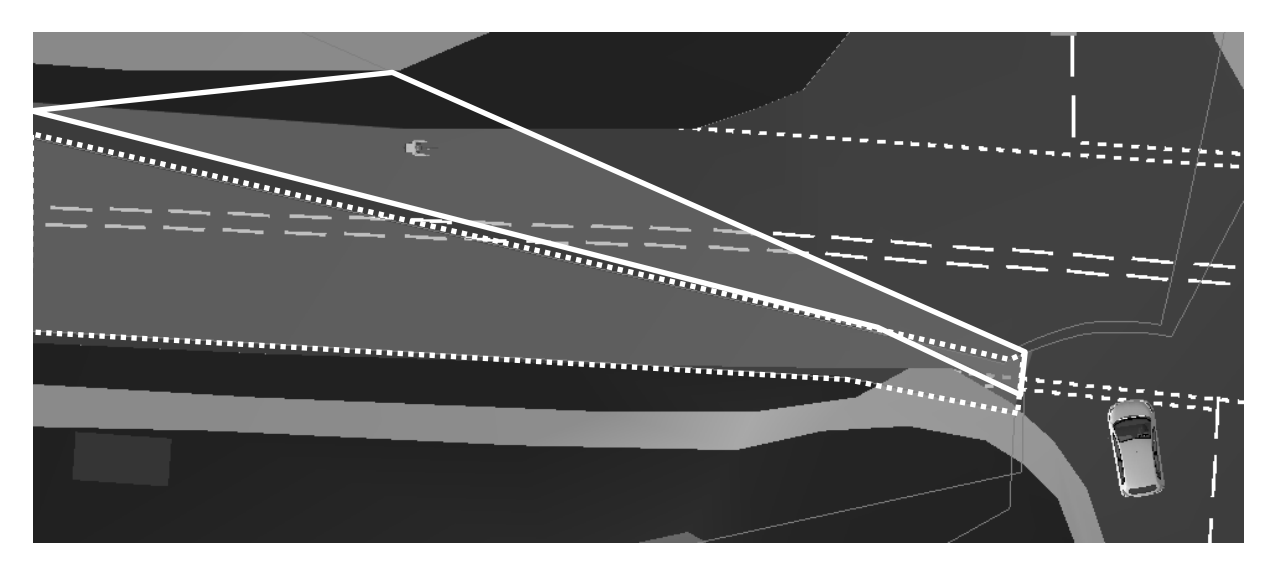


Figure 8. The difference between the blind spot for the 5th%ile UK female (dotted line area) and the 99%ile Dutch male (solid line area).

For all of the assessed  $M_1$  vehicles and drivers there is an effective 'corridor' blind spot caused by the A-pillar. This blind spot's location changes significantly between the two driver size extremes. For the larger drivers of each vehicle the blind spot allows the cyclist to get nearer to the junction and still be obscured. For the smaller driver the blind spot is much further to the left and so the cyclist is visible much sooner. Whilst the  $M_1$  vehicle could pull out in front of the cyclist in either case there is a good chance that the cyclist would see the  $M_1$  vehicle pulling out in front of them and be able to slow and take avoiding action if necessary. The closest the cyclist can get and still be obscured, is approximately 15m from the junction. Travelling at 20mph the cycle would take 1.677s to cover that distance and the cyclist would be able to clearly see the  $M_1$  vehicle pulling out from the junction. The conclusion from this evaluation is that the blind spot from the A-pillar was unlikely to be the only factor contributing to this accident and that the blind spot is relatively easy to overcome by the driver leaning or tilting their head to 'look around' the pillar.

#### Scenario 2: Category M<sub>1</sub> - T-Junction

As with scenario 1, map data provided in the OTS case report was used to model the scenario (Figure 9). The angle of the junction from the road filtering into the main road has the potential to cause difficulty for the category  $M_1$  driver in terms of positioning for optimum visibility to the right of the vehicle to observe vehicles already on the main road travelling from right to left. The cyclist is positioned travelling along the main road from right to left across the path of the  $M_1$  vehicle. The  $M_1$  vehicle is positioned to make the turn to the left as smooth as possible by aligning the front of the vehicle relatively to the left as opposed to perpendicular to the main road.

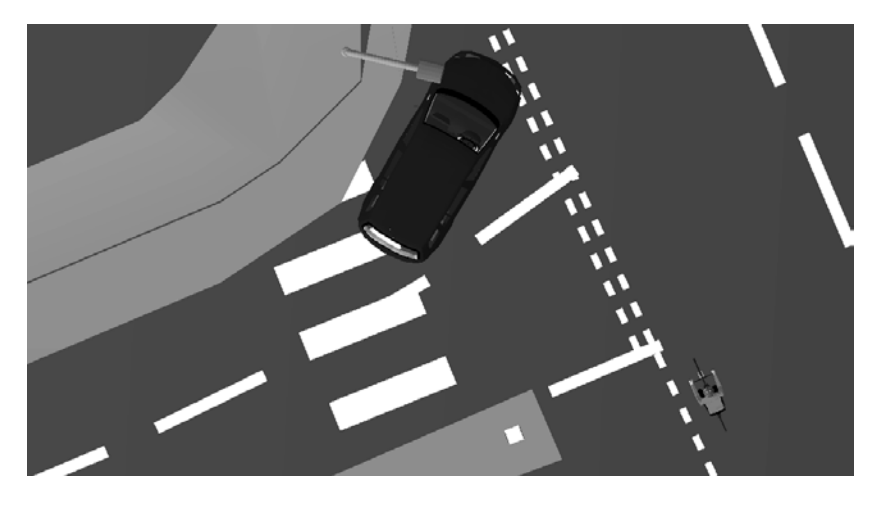


Figure 9. The relative positioning of the vehicles (Volkswagen Touran and pedal cycle) at the scenario junction.

Figure 10 shows that in this position the cyclist is completely obscured by the B-pillar of the M<sub>1</sub> vehicle. The driver is looking to the right to check the coast is clear prior to pulling off.



Figure 10. The view of the driver (99<sup>th</sup> %ile Dutch male) of the Volkswagen Touran in the direction of the cyclist (direct vision on the left, volume projection on the right).

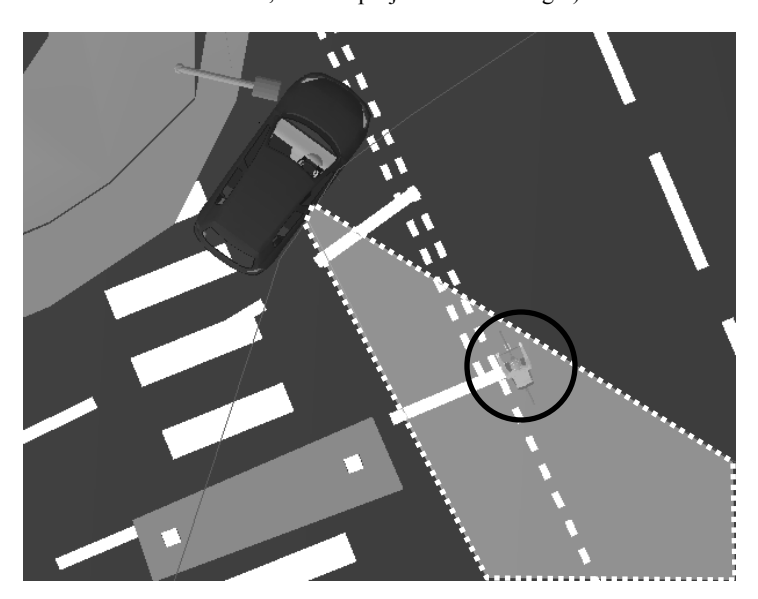


Figure 11. For all vehicles evaluated there is a clear blind spot (dotted line area).

For all of the assessed  $M_1$  vehicles there is a similar blind spot effect from the B-pillar to that observed from the A-pillar in Scenario 1. This blind spot is only in a location likely to obscure the cyclist for the larger drivers of each vehicle as the eye point is further forward for the smaller driver and the field of view is clear through the front right window. It is possible that whilst the  $M_1$  driver is performing their observations prior to setting off that the cyclist could have travelled the length of this corridor to within 4.5m of the vehicle. If after glancing right and not seeing any oncoming traffic the driver would then focus their attention to the direction of turn to the left and set off causing the collision.

#### Scenario 3: Category N<sub>3</sub> - Left Turn at Junction

As before, map data provided in the OTS case report was used to model the scenario (Figure 12). A Category  $N_3$  vehicle is positioned to the right of their lane to provide the largest possible radius for the left turn. The cyclist (circled) is positioned to the left of the lane, against the curb to be as far away from the LGV as possible and potentially to place their foot on the curb whilst they wait at the lights.

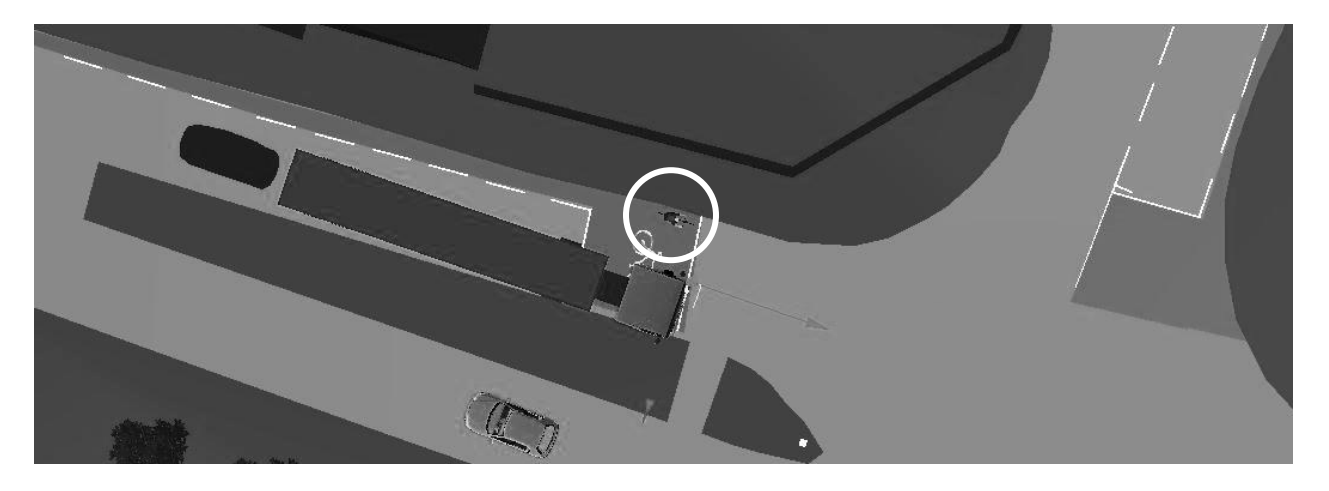


Figure 12. The relative positioning of the vehicles (Scania R420 and pedal cycle) at the scenario junction.

Figure 13 shows that in this position the cyclist is completely obscured by the cab of the N<sub>3</sub> vehicle. The driver is looking to the left to check the coast is clear prior to pulling off.

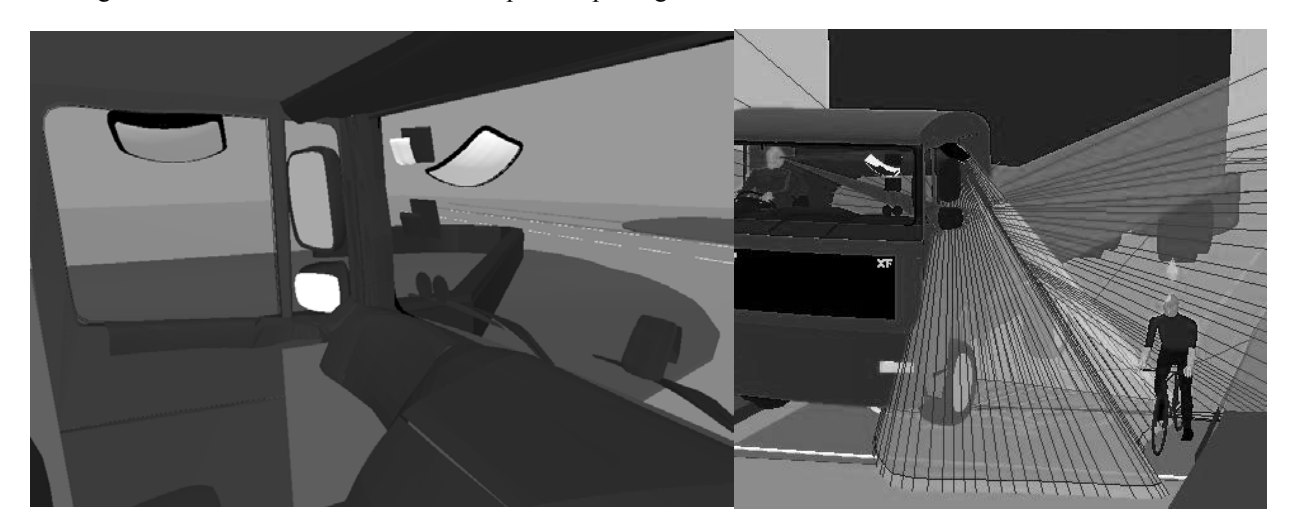


Figure 13. The view of the driver (99<sup>th</sup> %ile Dutch male) of the Scania R420 in the direction of the cyclist (direct vision on the left, volume projection on the right).

For all of the right-hand drive  $N_3$  vehicles assessed there is a similar blind spot to the near-side (passenger side) of the vehicle. The cyclist would be not be visible to the LGV driver either through the passenger window, or in either the Class IV, V or VI mirrors in this position. The difference in eye point of the two drivers has negligible effect on the field of view. If the driver is unaware of the cyclist and the cyclist is unaware of the intention of the LGV to turn left, it is clearly possible for the collision to occur shortly after both vehicles set off.

#### **DISCUSSION**

The evaluations performed in this research identified that blind spots can occur in any direction around all of the vehicle Categories evaluated (M<sub>1</sub>, M<sub>2</sub>, N<sub>3</sub>). In addition these blind spots appear to be a contributory factor in the recreation of accident scenarios taken from UK accident data. These blind spots vary in size and significance and are often influenced by the eye point of the driver, and thus by the size of the driver. For A and B-pillar obscuration an eye point closer to the pillar, combined with a larger pillar can lead to a significant blind spot, capable of obscuring other road users, particularly smaller visual targets such as VRUs. However, A and B-pillar obscuration can easily be countered by the driver moving their eye point by titling their head or leaning the body. However, other contributory factors such as tiredness, the driver being in a hurry, busy road conditions with lots of visual demand, other distractions such as passengers, etc. could all lead to the driver failing to check the blind spot.

For LGVs the near-side blind spot is much more significant, is not affected by driver eye point and regardless of driver behaviour cannot be mitigated. Mirror adjustment is a key factor in minimising the blind spot, but even with mirrors adjusted to the Regulations, the blind spot still exists.

One outcome from the research was a recommendation to the UNECE to amend Regulation 46 to mandate a greater area extending laterally from the near-side of the vehicle. This amendment specified that the area of the ground plane that should be visible to the driver of Category  $N_3$  vehicles should be increased laterally from 2m, to 4.5m. The proposed amendment was presented to the United Nations GRSG committee at the 100th meeting in April of 2011.

In the evaluations performed to: identify blind spots; understanding the nature of blind spots; evaluate the effect of eye point; and in exploring solutions, digital human modelling and the volumetric projection technique offered a range of benefits. The ability to explore the scenarios in 3D with a range of driver size and vehicle was significantly more straightforward utilising a digital approach. It is acknowledged that the lead time in capturing vehicle data and setting up the models is high, but subsequent downstream activities are facilitated. The 3D volumetric projection technique provided a greater understanding of compliance with the 2D mandated areas and provided insight into the true field of view afforded to the driver. Not insignificantly the approach has also been fundamental in the communication of the findings. The ability to show the projections, and to provide fly-throughs of the scenarios has been positively received by drivers, operators, designers, and other professionals involved in road safety.

A further benefit of the digital approach is the ability to rapidly explore potential solutions or proposals for change. Since the completion of the project the Loughborough team have worked with Cemex a major UK operator of LGVs. Cemex have been proactive in road safety and have often implemented beneficial safety systems, and warnings on their vehicles in advance of legislation. An analysis was made of the impact of the fitment of a large coverage aftermarket mirror (SPAFAX VM5) that had the potential to meet the new Regulated area to the Cemex fleet of MAN TGA 26.340 tipper lorries. Due to the lower cab configuration of the MAN vehicles over those evaluated on the project, and the relatively wide coverage of the standard MAN Class V mirror, the potential benefits of the larger SPAFAX VM5 were not clear. After modelling the fitment of the aftermarket mirror to the MAN vehicles (Figure 14) the potential benefits were quickly illustrated and convinced the company to fit the SPAFAX VM5 to their entire fleet.

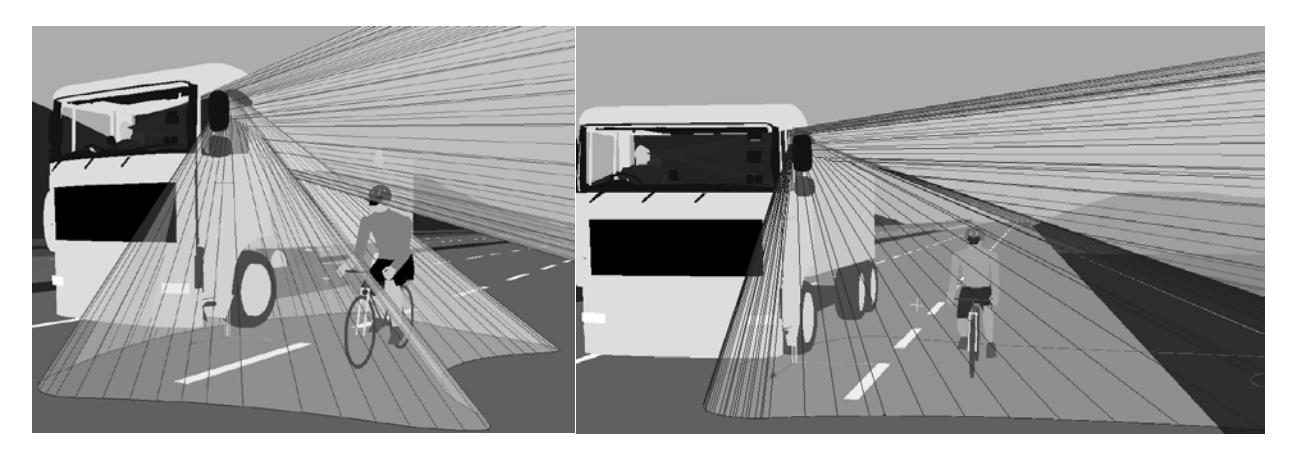


Figure 14. Projection of the standard fit Class V (left) vs. the aftermarket SPAFAX VM5 and the view from the passenger side window as found on the MAN TGA 26.340 tipper

In addition to mirror solutions the projection technique has also been used on preliminary investigations of window panels on the lower portion of the passenger door (Figure 15). The ability to rapidly alter the vehicle configuration in CAD and evaluate the field of view projections clearly highlight the potential benefits of a DHM approach.

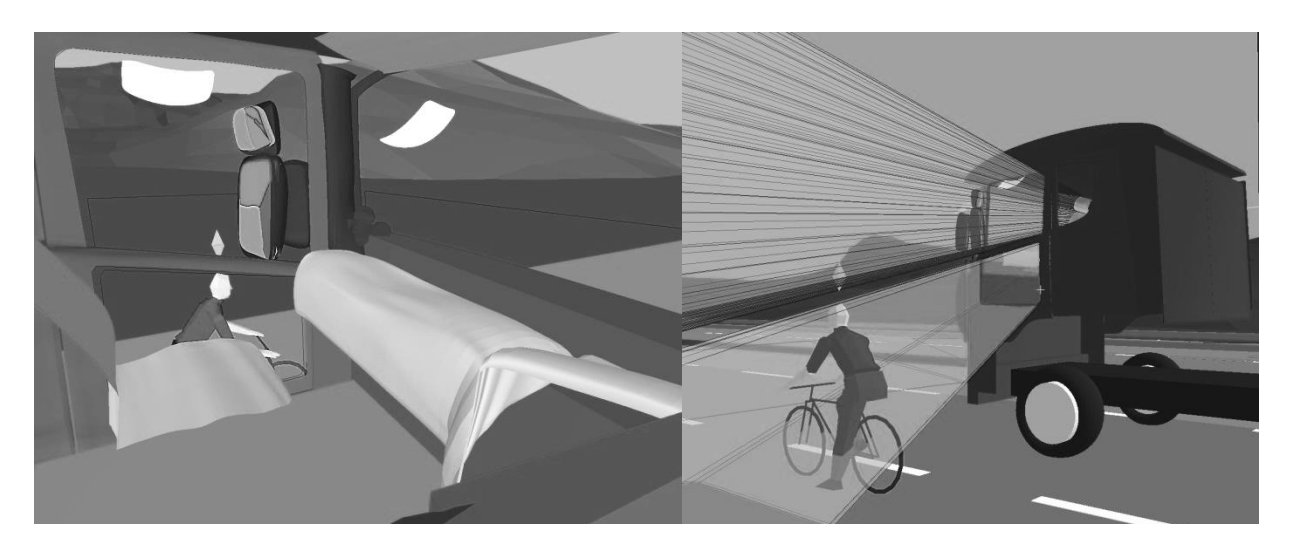


Figure 15. Mock-up of a window aperture in the lower portion of the passenger side door of an LGV. Drivers view on the left, projection to the right.

#### **CONCLUSIONS**

This research reports on the evaluation of driver's field of view and the use of a new 3D volumetric projection technique to investigate its impact on cyclist safety. The UK Department for Transport commissioned an evaluation into the potential of driver vision, and vehicle blind spots to be a causal factor in road traffic accidents. Using UK accident data, scenarios were identified for evaluation. The scenarios were modelled in addition to a range of vehicles and drivers including Category  $M_1$ ,  $M_2$ ,  $N_2$  and  $N_3$  vehicles. Evaluations were performed using a 3D volumetric projection method implemented within the existing DHM system SAMMIE. The evaluations highlighted blind spots in all vehicles resulting from the structure of the vehicle and their potential role in accidents. The most significant finding was a major blind spot to the passenger side of larger Category  $N_3$  LGVs. The blind spot appears between the coverage of the Class V 'look-down' mirror and the view from the passenger door window. The projection technique was instrumental in both locating the blind spot and in the exploration of solutions. The research resulted in a change to EU Regulation 46 to mandate a change to mirrors to remove the blind spot on future vehicles.

#### REFERENCES

2003/97/EC. (2004), "Directive 2003/97/EC of the European Parliament and of the Council on the approximation of the laws of the Member States relating to the type-approval of devices for indirect vision and of vehicles equipped with these devices", Official Journal of the European Union.

Delmonte, E., Manning, J. Helman, S. Basacik, D. Scoons, J. Chappell, J. Stannard, J. Jones, M., Knight, I. (2012), "Construction Logistics and Cyclist Safety Technical Report", Report PPR639, TRL. http://www.tfl.gov.uk/microsites/freight/documents/publications/construction-logistics-and-cyclist-safety-technical-report.pdf

Hill, J.R., Cuerden, R.W. (2005), "Development and Implementation of the UK On the Spot Data Collection Study – Phase 1", Department for Transport Road Safety Research Report No. 59. http://www.dft.gov.uk/pgr/roadsafety/research/rsrr/theme5/Lenard, J. Danton, R. Avery, M. Weekes, A. Zuby, D., Kühn, M. (2011), "Typical pedestrian accident scenarios for the testing of gutenomous emergency broking systems." ESV paper po. 11, 0106

autonomous emergency braking systems", ESV paper no. 11-0196.

Marshall, R. Summerskill, S., Cook, S. (2013), "Development of a volumetric projection technique for the digital evaluation of field of view", Ergonomics, 0, pp.1-14, DOI: 10.1080/00140139.2013.815805.

Marshall, R. Summerskill, S., Cook, S. (2012), "The Use of DHM Based Volumetric View Assessments in the Evaluation of Car A-Pillar Obscuration", in Duffy, VG (ed) Proceedings of the 4th International Conference on Applied Human Factors and Ergonomics, AHFE, Advances in Applied Human Modeling and Simulation. Proceedings of the 4th AHFE Conference, San Francisco, California, USA, pp.255-264.

Reed, M.P. Lehto, M.M., Flannaghan M.J. (2000). "Field of view in passenger car mirrors." The University of Michigan, Transportation Research Institute, Report No. UMTRI-2000-23.

RoSPA, (2012). "Cycling Accidents - Facts and Figures," The Royal Society for the Prevention of Accidents,

- http://www.rospa.com/roadsafety/adviceandinformation/cycling/facts-figures.aspx
- Summerskill, S. Marshall, R., Cook, S. (2012), "The use of volumetric projection in Digital Human Modelling software for the identification of Category N3 vehicle blind spots", in Duffy, VG (ed) Proceedings of the 4th International Conference on Applied Human Factors and Ergonomics, AHFE, Advances in Applied Human Modeling and Simulation. Proceedings of the 4th AHFE Conference, San Francisco, California, USA, pp.245-254.
- Tait, A.R., Southall. D. (1998). "Drivers' field of view from large vehicles Phase 3 Report.", Loughborough University. Report for Department for Transport.
- UN Regulation 46. (2009), "Uniform Provisions for Devices for Indirect Vision and of Motor Vehicles with Regard to the Installation of these Devices", UN ECE Vehicle Regulations.
- Way, M.L., Reed, M.P. (2003). "A Method for Measuring the Field of View in Vehicle Mirrors", Proceedings of the SAE 2003 World Congress, SAE Paper No 2003-01-0297, Detroit, USA, March 2003, 1-8.

### Special Computational Gas Flow Simulation Methods for Trunkline Network Failures

Sergey Pryalov and Vadim Seleznev

Physical & Technical Center, LLC Sarov, 607190, Russian Federation

#### **ABSTRACT**

We consider two new methods for numerical solution of a complete system of partial differential equations describing the flow of a gas mixture in pipeline systems. The first method tracks Lagrangian particles as they move together with the flow of transported fluid. When implementing this method, the flow parameters are found by means of a difference scheme, and the distribution of mass fractions of components and enthalpy of matter along the pipeline, by analyzing the motion of the Lagrangian particles. If we ignore the processes of diffusion, these particles must preserve their composition. The energy equation without diffusion and heat conduction reduces to an ordinary differential equation. The method proposed is free of artificial viscosity, because, for example, when considering the equation of continuity of components, variations in their specific mass fractions at any point in space are related only to physically meaningful processes, namely, to the inflow of "new" particles (with "new" specific mass fractions of the components). The second method includes constructing spline functions along the space and time coordinates of the computational mesh subject to the fulfillment of differential equations at its nodes. The use of splines of high orders of approximation improves the accuracy of modeling.

**Keywords**: Lagrangian Particle Method, Spline Scheme, Computer Gas Dynamics Simulator, Multi-Component Gas Mixture

#### INTRODUCTION

Publications [1–4] propose industry-oriented approaches to numerical modeling of operating conditions of complex trunkline networks that transport process gases, liquids and multiphase fluids. These publications repeatedly pointed at the necessity of improving the accuracy of simulations using the mathematical models proposed, first of all, to enable credible simulation-aided failure analysis. As we know, one of the central accuracy improvement prerequisites is a science-based choice of appropriate techniques for the numerical analysis of the mathematical models developed. The present paper discusses current versions of two efficient techniques of numerical analysis of mathematical gas flow models for trunkline failure analysis. They have demonstrated their efficiency in practice as applied to failure analysis of gas distribution networks of Gazprom's subsidiaries.

## DESCRIPTION OF THE FIRST NUMERICAL ANALYSIS METHOD FOR MATHEMATICAL MODELS OF GAS FLOW IN TRUNKLINE NETWORKS

Let natural gas, which in the first approximation can be treated as a single-component gas with known physical and mechanical properties, be transported through a network of branched pipelines with absolutely stiff rough heat

conducting walls.

To solve the problem, we use the following computational approach: we conventionally assume that each supplier (in our case, "supplier" refers to a dispatching control station) introduces a unique grade of a single-component chemically inert gas, the properties of which are exactly the same as those of natural gas, to the common collector. In this case, as a result of non-isothermal mixing in the common collector and downstream pipelines, a multi-grade homogeneous chemically inert gas mixture will form, possessing physical and mechanical properties of the initially transported natural gas. Its grade (or component) composition will vary with time only due to corresponding variations in the gas supply conditions and parameters of gas consumption from the given pipeline system.

Based on the time variations of the gas mixture composition at the outlet boundary of the downstream pipeline associated with a certain consumer, one can conclude, which particular suppliers influence the volume of gas supply to the given consumer. Constructing the target functions of gas grade shares versus time reduces to numerical modeling of non-steady-state non-isothermal homogeneous multi-component time-variant-composition gas mixture transport through the given gas distribution network of long branched pipelines. Here, considering the natural gas flow velocities in common collectors and downstream pipelines, one can ignore the influence of diffusion and heat conductivity in the gas flow direction without loss of accuracy of simulation results [4].

One of the most promising approaches to credible numerical evaluation of space-time distribution of physical flow parameters in pipeline systems involves using the high-accuracy computer gas dynamic simulator to model the performance of the system of interest (GDS) [1, 4]. The gas dynamics model of non-steady-state non-isothermal turbulent flow (without diffusion and heat conductivity along the gas flow) of a multi-component homogeneous mixture of viscous chemically inert compressible gases through a branched system of long varied round cross-section graded pipelines with absolutely stiff rough heat conducting walls, as implemented in the computational core of GDS, can be represented as follows:

- for each pipe (bend or non-branched segment of the common collector):

$$\frac{\partial(\rho f)}{\partial t} + \frac{\partial}{\partial x}(\rho w f) = 0; \tag{1}$$

$$\frac{\partial}{\partial t}(\rho Y_m f) + \frac{\partial}{\partial x}(\rho Y_m w f) = 0, \quad m = \overline{1, N_S - 1}, Y_{N_S} = 1 - \sum_{m=1}^{N_S - 1} Y_m; \tag{2}$$

$$\frac{\partial \left(\rho w f\right)}{\partial t} + \frac{\partial \left(\rho w^2 f\right)}{\partial x} = -f \left[ \frac{\partial p}{\partial x} + g \rho \frac{\partial z_1}{\partial x} \right] - \frac{\pi}{4} \lambda \rho w |w| R; \tag{3}$$

$$\frac{\partial}{\partial t} \left[ \rho f \left( h + \frac{w^2}{2} \right) \right] + \frac{\partial}{\partial x} \left[ \rho w f \left( h + \frac{w^2}{2} \right) \right] = f \frac{\partial p}{\partial t} - \rho w f g \frac{\partial z_1}{\partial x} + Q f - \Phi \left( T, T_{am} \right); \tag{4}$$

- for each junction (boundary sections of pipelines adjoining the junction):

$$Y_{m, \text{ Joint}} = \sum_{n \in \Upsilon_{\text{IN}}} \left[ {}^{(n)} \rho \Big|^{(n)} w \Big|^{(n)} f^{(n)} Y_m \right] \left\{ \sum_{n \in \Upsilon_{\text{IN}}} \left[ {}^{(n)} \rho \Big|^{(n)} w \Big|^{(n)} f \right] \right\}^{-1}, m = \overline{1, N_S - 1}; Y_{N_S} = 1 - \sum_{m=1}^{N_S - 1} Y_m;$$
(5)

$$h_{\text{Joint}} = \sum_{n \in \Upsilon_{\text{IN}}} \left[ {}^{(n)}\rho \left| {}^{(n)}w \right| {}^{(n)}h^{(n)}f \right] \left\{ \sum_{n \in \Upsilon_{\text{IN}}} \left[ {}^{(n)}\rho \left| {}^{(n)}w \right| {}^{(n)}f \right] \right\}^{-1};$$

$$(6)$$

$$n \in \begin{cases} \Upsilon_{\text{IN}} \in \overline{1, M}, & \text{if } {}^{(n)} w^{(n)} s \ge 0; \\ \Upsilon_{\text{OUT}} \in \overline{1, M}, & \text{if } {}^{(n)} w^{(n)} s < 0; \end{cases}$$

$$(7)$$

$$T_{\text{Joint}} = T\left(p_{\text{Joint}}, h_{\text{Joint}}, \left\{Y_{m,\text{Joint}} \middle| m = \overline{1, N_s}\right\}\right); \tag{8}$$

$$\rho_{\text{Joint}} = \rho \left( p_{\text{Joint}}, T_{\text{Joint}}, \left\{ Y_{m,\text{Joint}} \middle| m = \overline{1, N_S} \right\} \right); \tag{9}$$

$$(n) p = p_{\text{Joint}}, n = \overline{1, M}; \quad (n) \rho = \rho_{\text{Joint}}, n \in \Upsilon_{\text{OUT}}; \quad (n) T = T_{\text{Joint}}, n \in \Upsilon_{\text{OUT}}; \quad (n) h = h_{\text{Joint}}, n \in \Upsilon_{\text{OUT}};$$

$$(n) Y_m = Y_{m, \text{Joint}}, n \in \Upsilon_{\text{OUT}}, m = \overline{1, N_S}; \quad (n) (z_1) = (\xi)(z_1) \ \forall \ n, \xi \in \overline{1, M};$$

$$(10)$$

$$\sum_{n \in Y_{\text{IN}}} {n \choose \rho} |w| f = \sum_{n \in Y_{\text{OUT}}} {n \choose \rho} |w| f ;$$

$$(11)$$

$$s = \begin{cases} 1, & \text{if } n^{th} \text{ pipeline adjoins joining knot the right section;} \\ -1, & \text{if } n^{th} \text{ pipeline adjoins joining knot the left section;} \end{cases}$$

$$(12)$$

- equations of state [5]:

$$p = p\left(\rho, T, \left\{Y_m \middle| m = \overline{1, N_S}\right\}\right); \tag{13}$$

$$h = h\left(p, T, \left\{Y_m \middle| m = \overline{1, N_S}\right\}\right),\tag{14}$$

where  $\rho$  is the gas mixture density; f is the pipeline flow section area; t is the time (marching variable); x is the spatial coordinate along the pipeline axis; w is the projection of the vector of gas velocity averaged over the pipeline cross section to the pipeline axis (on the assumption of developed flow turbulence);  $Y_m = \rho_m/\rho$  is the mass fraction of the m -th component;  $\rho_m$  is the reduced density of the m -th component (mass of the m -th component in unit volume of the mixture);  $N_S$  is the number of mixture components; p is the static gas mixture pressure; gis the gravity acceleration modulus;  $z_1$  is the spatial coordinate of the point in the pipeline axis reckoned from an arbitrary horizontal plane vertically upward (for trunklines, along the Earth radius);  $\pi$  is the Pythagorean number;  $\lambda$  is the hydraulic friction coefficient in the Darcy-Weisbach formula;  $R = \sqrt{f/\pi}$  is the inner pipe radius; h is specific (per unit mass) enthalpy of the mixture; Q is specific (per unit volume) power of heat sources; T is the gas mixture temperature; M is the number of pipes constituting the given junction;  $\Upsilon_{\rm IN}$  is the subset of upstream pipes of the given junction (upstream pipes with respect to the junction are the pipes, through which the gas enters the junction);  $\gamma_{\text{OUT}}$  is the subset of downstream pipes of the given junction (downstream pipes with respect to the junction are the pipes, through which the gas leaves the junction);  $p_{\text{Joint}}$  is the static gas mixture pressure in the given pipeline junction;  $T_{\text{Joint}}$  is the gas mixture temperature in the pipeline junction (i.e. in the inner space of the junction);  $Y_{m, \text{ Joint}}$  is the mass fraction of the m -th gas mixture component in the junction;  $h_{\text{Joint}}$  is the specific (per unit mass) enthalpy of the gas mixture in the junction of interest. The function  $\Phi(T, T_{out})$  characterizes the heat exchange of the gas flow core through the boundary gas layer, pipe wall and insulation with the environment. It expresses the total specific (per unit length) thermal flux along the perimeter  $\chi$  of the cross section having an area of f from the transported gas to the environment ( $\Phi(T, T_{am}) > 0$  means heat removal;  $T_{am}$  is the space-time distribution of ambient temperature at the domain boundary). To indicate that a quantity belongs to the n-th pipe, we use a superscript in parentheses left of the quantity, for example:  ${}^{(n)}\rho$ . The system of equations (1–14) is supplemented with boundary conditions and conjugation conditions. As conjugation conditions we can define boundary conditions simulating a complete rupture of the pipeline and/or its shutoff, operation of valves, etc.

To numerically solve the system of equations (1–14), the computational core of GDS usually employs grid methods. Unfortunately, distribution trunkline networks contain a large number of pipe joints distributed on general collectors extremely nonuniformly. In our case, this results in the necessity of considerable spatial mesh refinement and, consequently, in a much longer runtime. Such an increase in the runtime is intolerable in simulations done to provide computer-aided support of pipeline dipatcher decisions.

To overcome this situation, the computational core of GDS employs a hybrid modification of the known integrointerpolation method developed by A. N. Tikhonov and A.A. Samarsky [6, 7] and S.N. Pryalov's Lagrangian particle method [4]. The Lagrangian particle method is applied only to the equations of component continuity (2, 5, 7) and energy equations (4, 6, 7). Note that this Lagrangian particle method is essentially a dedicated modification of the approach for solving hyperbolic partial differential equations by the well-known method of characteristics [8]. Let us consider the algorithm of applying this method to the component continuity equations.

As we know, in a non-steady-state flow of a gas mixture through a branched network system, regions (moving together with the gas flow) can occur, where concentrations of the mixture components can differ significantly from those in neighbor regions. The use of difference schemes may lead to substantial front "smearing". Given that the difference schemes [6, 7] are conservative, the total mass of the mixture components in the pipeline network will not vary with time. However, the values of component concentrations can decrease (or increase) unreasonably, and as a result, the fluid of these materials will get non-physically "smeared" along the length of the pipeline. The idea of the Lagrangian particle method in this case rests upon the known fact that if we separate a small particle of matter (a small moving volume of matter), the continuity equations of the components will actually describe the motion of this particle (with some set of components) with the gas flow. Accordingly, it is suggested that the component continuity equation be solved by analyzing the motion of some set of particles in the gas flow. Flow parameters in this case can be defined in any manner enabling simulation of a single-component gas flow (for example, by finite differences). Owing to the way of introducing these particles, they are conventionally called Lagrangian.

The general algorithm of flow modeling without multicomponent gas mixture diffusion in branched pipeline systems using the Lagrangian particle method can be described as follows (S.N. Pryalov's algorithm):

- Initially, along the length of every n-th pipeline  $\left(n=\overline{1,M}\right)$  we "place" a set of Lagrangian particles ordered by increasing coordinates (with numbering  $\widehat{p}=\overline{1,\frac{(n)}{Base}N_{Lagr}}$ ) in the amount of  $\frac{(n)}{Base}N_{Lagr}$  at a distance on the order of the length of a spatial mesh cell. A mandatory requirement is that the Lagrangian particles with numbers  $\widehat{p}=1$  and  $\widehat{p}=\frac{(n)}{Base}N_{Lagr}$  lie on the left (coordinate x=0) and on the right (coordinate  $x=\frac{(n)}{Length}$ , where  $\frac{(n)}{Length}$  is the length of the n-th pipeline) pipeline boundaries, respectively. Specific fractions of the components for the particles are defined by approximation of initial conditions. Let  $\frac{(n)}{(\widehat{p})}x^j$  be the coordinate of the  $\widehat{p}$ -th Lagrangian particle belonging to the n-th pipeline for the j-th time step.
- 2. Gas dynamic variables of the gas mixture flow at the next time step  $t_{j+1}$  are calculated (using difference equations approximating the gas dynamics equations (1–14), except for the component continuity equations (2, 5, 7) and energy equations (4, 6, 7)). The values of the specific component fractions at mesh nodes are defined by interpolation between these values for the Lagrangian particles adjacent to the mesh node.
- 3. For each  $\hat{p}$  -th Lagrangian particle of each n -th pipeline, we update the coordinate for the new time step  $t_{i+1}$  using the formula:

$${\binom{n}{(\bar{p})}} x^{j+1} = {\binom{n}{(\bar{p})}} x^j + {\binom{n}{(\bar{p})}} \Delta x^{j+1} = {\binom{n}{(\bar{p})}} x^j + {\binom{n}{(\bar{p})}} x^j, t_j \Delta t_{j+1}.$$

$$(15)$$

- 4. For each pipeline, we delete the Lagrangian particles that leave the pipeline. At the same time, a new particle is generated at the corresponding "outlet" boundary (the boundary, through which the gas leaves the pipe) with specific component fractions  $\{Y_m \mid m = \overline{1, N_s}\}$  equal to the interpolated values of the particles closest to the boundary; inside the pipe and outside the pipe (the latter particle is deleted with respect to the pipe).
- 5. For each pipeline junction, specific component fractions are calculated by the following formula:

where  $_{(L)}(Y_m)^{j+1}$  is the specific mass fraction of the m-th component of the particle located at the outlet boundary of the upstream pipeline;  $\rho_L$ ,  $w_L$  and  $f_L$  are the gas mixture density, velocity and cross section area corresponding to the outlet boundary of the upstream pipeline.

6. For each inlet boundary of each pipeline, a new Lagrangian particle is generated with specific component fractions  $\{Y_m | m = \overline{1, N_s}\}$  corresponding to the boundary conditions (if the boundary is inlet for the given pipeline system) or equal to the specific component fractions in the pipeline junction (if the boundary adjoins the junction).

At the next time step, if the distance between this particle and the following (downstream) particle is smaller than the given distance (on the order of the spatial cell length), this particle is deleted.

7. If  $t_{j+1}$  reaches the limiting value, the simulation is completed. Otherwise, we assume that  $j \leftarrow j+1$  and proceed to step 2.

Since the Lagrangian particle method for the energy equation is not related directly to the finite difference mesh employed for solving the continuity and motion equations, this mesh has almost no effect on the accuracy of the proposed method. Thus, high-accuracy calculated values of gas temperature are obtained without mesh refinement, which speeds up the calculations significantly.

In addition, due to the absence of direct connection between the Lagrangian particle method and the finite difference mesh, this method is free of the so-called artificial viscosity (see above and [6, 7]). As a result, the method makes it possible to obtain solutions without artificial smoothing of temperature fronts, which corresponds to real physical processes. This significantly increases the credibility of simulations compared to the use of difference schemes for the energy equation.

## DESCRIPTION OF THE SECOND NUMERICAL ANALYSIS METHOD FOR MATHEMATICAL MODELS OF GAS FLOW IN TRUNKLINE NETWORKS

To improve the credibility of numerical modeling of trunkline network operation, it is reasonable to use conservative difference schemes.

This section of the paper considers an approach that uses fully conservative spline schemes for solving a complete system of gas dynamics equations for the case of a model describing the flow of a single-component gas in a trunkline. The consequence of (1-14) for an unbranched trunkline, considering the adopted assumptions, is the system of equations [4]:

$$\rho \frac{\partial f}{\partial t} + f \frac{\partial \rho}{\partial t} + wf \frac{\partial \rho}{\partial x} + \rho w \frac{\partial f}{\partial x} + \rho f \frac{\partial w}{\partial x} = 0; \tag{17}$$

$$\rho f \frac{\partial w}{\partial t} + \rho w f \frac{\partial w}{\partial x} = -f \left[ \frac{\partial p}{\partial x} + g \rho \frac{\partial z_1}{\partial x} \right] - \frac{\pi}{4} \lambda \rho w |w| R; \tag{18}$$

$$\rho f \frac{\partial \varepsilon}{\partial t} + \rho w f \frac{\partial \varepsilon}{\partial x} = -p \frac{\partial (wf)}{\partial x} - p \frac{\partial f}{\partial t} + \frac{\pi}{4} \lambda \rho |w|^{3} R + Qf - \Phi(T, T_{am}); \tag{19}$$

$$p = p(\rho, T); \tag{20}$$

$$\varepsilon = \varepsilon (p, T), \tag{21}$$

where  $\varepsilon = h - p/\rho$  is the specific (per unit mass) internal energy.

As we know, for systems of nonlinear partial differential equations (to which the system (17–21) belongs), in the general case, it is impossible to obtain an analytical solution. There exist various methods for constructing difference counterparts of original differential equations that enable obtaining difference equations possessing different properties. To produce a credible solution, the difference counterpart (the difference scheme) should be convergent [6, 7]. This property holds true if the difference scheme possesses approximation and robustness. In addition, the scheme should preferably be conservative and have an increased order of approximation (these properties allow the scheme to produce more accurate numerical solutions).

This section of the paper proposes employing spline schemes for solving a complete system of gas dynamics differential equations [4]. This method involves searching for target values of the gas dynamic parameters at the

nodes of the space-time mesh such that the gas dynamic differential equations at the difference mesh nodes are satisfied, when approximating the distributions of these parameters by splines (along the space and time coordinates).

This method possesses an increased order of approximation; it is proven to be fully conservative, which provides higher credibility of process modeling when analyzing the parameters of gas transport in trunklines. On the other hand, spline schemes are implicit, which makes them more robust compared to explicit and semi-implicit schemes.

Let us begin considering this type of schemes from the simplest case, when splines are used to solve ordinary differential equations (see, e.g., [9]).

Let us discuss application of a spline scheme for solving the system (17–21). Let the spline order be Kt with respect to the time coordinate and Kx with respect to the spatial coordinate. The spline scheme for solving (1) can then be represented in the form proposed by S.N. Pryalov [4]:

$$\rho_{i}^{j+1} \cdot \frac{\{Spline, Kt\}}{t\Delta} (f_{i}^{j+1}) + f_{i}^{j+1} \cdot \frac{\{Spline, Kt\}}{t\Delta} (\rho_{i}^{j+1}) + f_{i}^{j+1} \cdot \frac{\{Spline, Kt\}}{t\Delta} (\rho_{i}^{j+1}) + f_{i}^{j+1} \cdot \frac{\{Spline, Kx\}}{t\Delta} (\rho_{i}^{j+1}) + \rho_{i}^{j+1} \cdot \frac{\{Spline, Kx\}}{t\Delta} (\rho_{i}^{j+1}) + \rho_{i}^{j+1} \cdot \frac{\{Spline, Kx\}}{t\Delta} (\rho_{i}^{j+1}) + \rho_{i}^{j+1} \cdot \frac{\{Spline, Kx\}}{t\Delta} (\rho_{i}^{j+1}) = 0;$$
(22a)

$$\rho_{i}^{j+1} f_{i}^{j+1} \cdot \frac{\{Spline, Kt\}}{t\Delta} \left(w_{i}^{j+1}\right) + \rho_{i}^{j+1} f_{i}^{j+1} w_{i}^{j+1} \cdot \frac{\{Spline, Kx\}}{x\Delta} \left(w_{i}^{j+1}\right) = -f_{i}^{j+1} \cdot \frac{\{Spline, Kx\}}{x\Delta} \left(p_{i}^{j+1}\right) - f_{i}^{j+1} g \rho_{i}^{j+1} \cdot \frac{\{Spline, Kx\}}{x\Delta} \left((z_{1})_{i}^{j+1}\right) - \frac{\pi}{4} \lambda_{i}^{j+1} \rho_{i}^{j+1} w_{i}^{j+1} \left|w_{i}^{j+1}\right| R_{i}^{j+1};$$

$$(22b)$$

$$\rho_{i}^{j+1} f_{i}^{j+1} \cdot \frac{\{Spline, Kt\}}{t\Delta} \left(\mathcal{E}_{i}^{j+1}\right) + \rho_{i}^{j+1} f_{i}^{j+1} w_{i}^{j+1} \cdot \frac{\{Spline, Kx\}}{x\Delta} \left(\mathcal{E}_{i}^{j+1}\right) = -p_{i}^{j+1} \cdot \frac{\{Spline, Kx\}}{x\Delta} \left(w_{i}^{j+1} f_{i}^{j+1}\right) - -p_{i}^{j+1} \cdot \frac{\{Spline, Kt\}}{t\Delta} \left(f_{i}^{j+1}\right) + \frac{\pi}{4} \lambda_{i}^{j+1} \rho_{i}^{j+1} \left|w_{i}^{j+1}\right|^{3} R_{i}^{j+1} + Q_{i}^{j+1} f_{i}^{j+1} - \phi_{i}^{j+1};$$

$$(22c)$$

$$p_i^{j+1} = p(\rho_i^{j+1}, T_i^{j+1}); (22d)$$

$$\varepsilon_i^{j+1} = \varepsilon \left( p_i^{j+1}, T_i^{j+1} \right). \tag{22e}$$

The spline scheme (22) approximates a nondivergent form of mass, momentum and energy conservation laws (17–21). The differential forms of these laws are satisfied at the nodes of the space-time mesh. Accordingly, the divergent forms of the principal conservation laws are also satisfied at the mesh nodes. If the spline order ensures the continuity and differentiability of the functions under the derivative sign in (17–21) (which requires that the conditions  $K_t \ge 2$ ,  $K_t \ge 2$  hold), then there exists a divergent discrete counterpart for each divergent derivative. Consequently, the spline scheme is also conservative for systems of partial differential equations.

As the conservation laws are satisfied in the differential form at the mesh nodes, it follows that all possible representations of a given system are satisfied at these nodes (for example, equations for kinetic energy, total energy, entropy etc.). The existence of divergent discrete counterparts of all the divergent differential derivatives in this case ensures that the spline scheme is not only conservative but completely conservative [6, 7].

This conclusion is extended similarly to the continuum mechanics equations of any dimensionality. Thus, we show that a spline scheme is completely conservative. This enables modeling gas and hydrodynamics processes with higher credibility and accuracy due to the correct modeling of all possible conservation laws. On the other hand, spline schemes are implicit, which makes them more robust compared to explicit and semi-implicit schemes [6, 7]. Increasing the order of the splines used makes it possible to increase the order of approximation of gas- and hydrodynamic equations, which also improves the accuracy of simulations.

#### **EXAMPLES OF PRODUCTION SIMULATIONS**

Efficiency of the method of numerical recovery of gas flows in trunkline systems proposed in the paper was demonstrated in 2010–2014 in production simulations at GAZPROM Mezhregiongaz Moscow LLC within the Alfargus/Mosregiongaz Computer System (Fig. 1).



Figure 1. Example of the Alfargus/Mosregiongaz Computer System application in the control room of GAZPROM Mezhregiongaz Moscow LLC

The method was used for numerical recovery of the flow of natural gas delivered (from a single supplier) to consumers through seven branches of the Moscow Gas Ring (MGR). MGR has a total length of over 200 km and more than 130 consumer branches. The flow was recovered at 106 IPs, which were relatively uniformly distributed over the gas pipeline ring.

The transport flow is transient nonisothermal gas flow. The example of flow diagram (i.e. recovered flow direction and numerical estimates of volumetric flow rate of natural gas [dimension: thousand cubic meters per day] in accordance with color gradation) in the South-East MRG sector (temporal section) was shown on Fig. 2. In table on the right of Fig. 2 one can see quantitative estimates of gas flow rate distribution [column 2, dimension: thousand standard cubic meters per day] and gas pressure [column 3, dimension: gauge atmospheres] for recovered flows in specific branches in the South-East MRG sector (temporal section). In the first column of the table under consideration description of branches are given in topographical map reference.

The example of diagram correlation of time history of calculated and measured estimates of pressure and mass flow rates for one from the IPs, which is used in MGR (gas flow temperature was measured with a poor accuracy and long time intervals and was not suitable for comparative analysis) was shown on Fig. 3. It should be noted that measurement results underwent preliminary verification and smoothing. The recovered gas flow parameters were used to analyze the performance of MGR, and to detect and localize the sources of discrepancy in estimated volumes of gas supply through MGR.

Earlier versions of the flow recovery method were used to investigate trunkline accidents and to train gas pipeline operators in efficient pipeline control under conditions as close as possible to real operation of gas transmission and delivery systems using high-accuracy computer simulators.

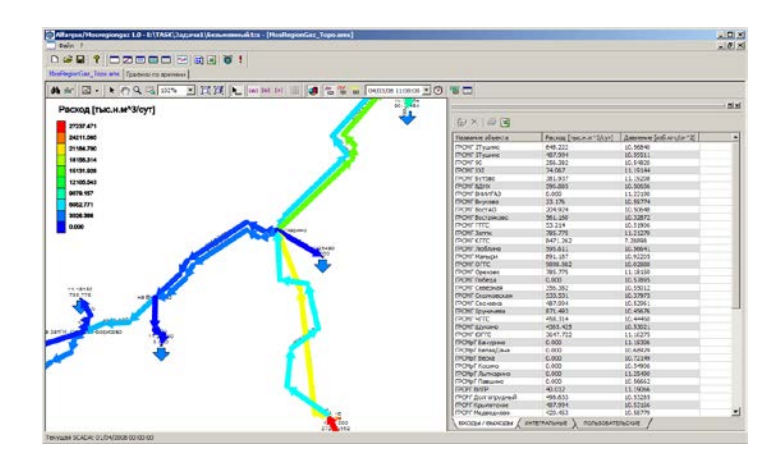


Figure 2. Example of flow diagram in the South-East MRG sector (temporal section)

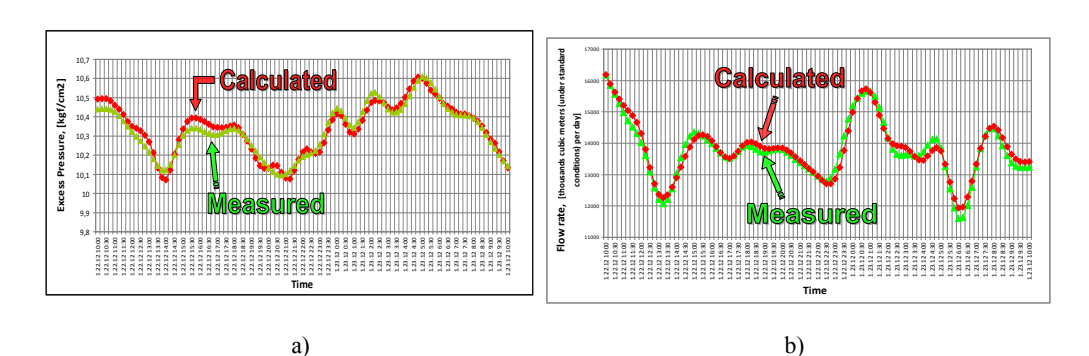


Figure 3: Example of curve correlation of calculated and measured pressure history (a) and mass flow rate (b) for one from the IPs used in MGR

#### **CONCLUSIONS**

In 2008–2014 these methods demonstrated their efficiency as applied to production simulations done to validate discrepancy mechanisms in natural gas supply through the Moscow circular gas trunkline. Application of these methods in practice does not require any special high-performance computers.

#### **REFERENCES**

Ahmed T.H. (2007), "Equations of State and PVT Analysis: Applications for Improved Reservoir Modeling". Gulf Publishing Company, Houston.

Fletcher C.A.J. (1988), "Computational Techniques for Fluid Dynamics: Fundamental and General Techniques". Springer-Verlag, Berlin.

Ortega J.M., Pool W.G. (1981), "An Introduction to Numerical Methods for Differential Equations". Pitman Publishing Inc.

Seleznev V.E. (2007), "Numerical simulation of a gas pipeline network using computational fluid dynamics simulators". Journal of Zhejiang University SCIENCE A. Vol. 8. No. 5. P.755–765.

Seleznev V.E., Pryalov S.N. (2011), "Gas-Liquid Flow Model for Branched Trunklines". Applied Mathematical Sciences. Vol. 5, No. 65. PP. 3233–3261.

Seleznev V.E. (2012), "Numerical Recovery of Gas Flows in Pipeline Systems". Journal of Applied Mathematics. Vol. 2012. Article ID 180645. 25 p.

Seleznev V.E., Pryalov S.N. (2014), "Computational Fluid Dynamics of Trunkline Systems: Methods for Constructing Flow Models in Branched Trunklines and Open Channels". M.: KRASAND.

Samarsky A.A., Popov Yu.P. (1992), "Difference Schemes for Solving Gas Dynamics Problems". Moscow, Nauka.

Tikhonov A.N., Samarsky A.A. (1999), "Equations of Mathematical Physics". Moscow, MSU Publishing Office.

# Digital Human Model Applied to Training and Education in Sports

Carla Guimarães, Maria Cristina Zamberlan, Vitor Balbio, Venetia Santos, Alessandra Paranhos, Flavia Pastura and Gloria Cid

> National Institute of Techynology Ergonomics Laboratory Rio de Janeiro, RJ 20081312, Brazil

#### **ABSTRACT**

The purpose of the study is to present a 3D digital interactive environment that is being developed in a game engine software to work with 3D DHM applied to training and education on Sports. This platform is being developed considering the need to analyze data from the same athletes' movements being repeated in different time or even to compare athletes' movements with different skill levels. The main 3D digital platform advantage is its flexibility to handle motion capture data from different MOCAP systems in order to facilitate kinematic analysis by users of low cost motion capture systems. Another important advantage is its portability that allows it to be used in different hardware platforms, as tablets and cell phones. The 3D platform development followed some specific steps, which make it possible not only to visualize the performed motion but also make the interaction between the user and the 3D character. The first step consists on the automatic reconstruction of the 3D character body segments based on motion capture data. The visual representation has as benefit that reduces noise that may be generated in the process of retargeting the motion capture data to a specific rig and character that differs from the actual bone structure original data. The visual representation is generated based on laser scanning data. This makes the representation to be a precise copy of the original bone position and structure of the athlete' specific movement that is being captured. The second step is to link each bone segment by generating a 3D model with a collision area that is necessary for future interaction with the user. After those steps, the user can select to track and generate data of a specific body segment; to play/pause the athlete movement and to draw graphs of segmental angles, joint angles and angular velocity. This functionality is still under development and test. The first application of the 3D digital platform was the movement analysis of high and low skill level Jiu-Jitsu athletes. This analysis allowed an improvement on the athletes' performance and skills. In the future the integration between the 3D scanned athlete's model and a virtual environment will allow to develop a virtual simulator that can be applied to education, training and entertainment.

Keywords: Digital human modeling, Training, Education, Jiu-jitsu

#### INTRODUCTION

Digital Human Model (DHM) is a digital human representation in the 3D space that can be moved and manipulated to simulate real and accurate movements of people (Guimarães et al., 2013). Digital human modeling is a fast growing area that bridges computer-aided engineering, design, human factors, applied ergonomics and sports coaching and training (Anja Naumann and Matthias Rötting, 2007). The improvement on modeling software and computer technology have allowed digital human modeling to be simulated in a digital environment. Digital human modeling and simulation play an important role in product design, prototyping, manufacturing, sports biomechanics and many other areas (Guimarães et al, 2010).

An example of DHM in sports improvement was a study that had the primary aim to determine the efficacy of three-

dimensional (3D) musculoskeletal modeling in evaluating an resistance-training equipment design (an seated row resistance-training machine). A 3D full-body musculoskeletal model was created using LifeModeler software and incorporated into a multibody dynamics model of the seated row resistance machine generated in MSC ADAMS software (K Nolte, P E Krüger, P S Els, H W Nolte, 2013). With DHM it was possible to simulate musculoskeletal human models interacting with mechanical systems that—allowed many aspects concerning the effects of the resistance-training equipment on the body being studied.

The term "serious games" describes video games designed specifically for training and education (in terms of learning and practice) (Annetta, 2010; Steinmetez and Göbel, 2012). A subset of educational serious gaming focuses on training, where users need to acquire a specific competence or built up a particular set of skills. Serious games provide extensive opportunities for drill and practice and is a very promising tool for sports training. The idea of serious games is to use the motivation inherited in games for other purposes like learning, sports training, rehabilitation exercises, or even advertisement or opinion forming.

Serious games are designed to solve real life problems through environment visualization and simulation (Senerirathne et al., 2011). The integration of technology within educational settings is far from a new concept. Technological innovations have been frequently implemented in attempts to enhance the learning experience. Some technology as inertial sensors, magnetometers, GPS and wireless technologies, or a combination of such devices can improve detailed activity information, sports biomechanics and performance measures data extracted in order to enrich coach and technique evaluation (James et al, 2012).

The purpose of this paper is to present a 3D digital interactive environment that-is being developed in a game engine software to work with 3D DHM applied to sports training and education.

#### 3D INTERATIVE PLATAFORM FRAMEWORK

The Ergonomics Laboratory of the National Institute of Technology and the Ergon Projects Enterprise have developed "serious games" platforms and simulation environments applied to ergonomic work analysis and new ergonomic design. The goal of these simulations has been to help designers and employees to understand and implement ergonomic concepts work environment design. Considering that experience, the Ergonomics Laboratory team and Ergon decided to apply that knowledge to sports training, in special to Combat sports. The efforts are being conducted to the development of an 3D interactive environment system that comprises basic jiu-jitsu movements and its definition based on experts Jiu-jitsu players knowledge and on biomechanics analysis. That system consists of Basic System and modular tools described below (see figure 1):

- Analysis: Allow to get and to record- the "bone" data graph ou diagram or the join movement in 3D
- E-Book consisting of text, images of Jiu-jitsu sport, that can be readable on computers or other electronic devices
- Reports: Return reports with graphs and diagram for printing or saving
- Export Data: Allow to export the RAW data to XML or other exchange data type.



Figure 1: Flow chart

The Analysis stage comprised of two steps before data input in the 3D digital interactive environment:

1° step: athletes scanning and motion capture conducted on the Ergonomics Laboratory. First, the athlete was scanned in a *Cyberware WBX 3D* whole body scanner (Figure 2 and 3), then the scan file was processed to minimize the number of polygons and to close holes – the retopology process (Lerch et al., 2007). For the motion capture session the athlete wore a special suit from *Xsens* with 17 inertial sensors (Figure 4). Then the athlete selected and defined some basic jiu-jitsu movements that were captured (Figure 5)



Figure 2: Scanning process



Figure 3: Saving the scan file for retopology process



Figure 4. Athlete using motion capture sensors

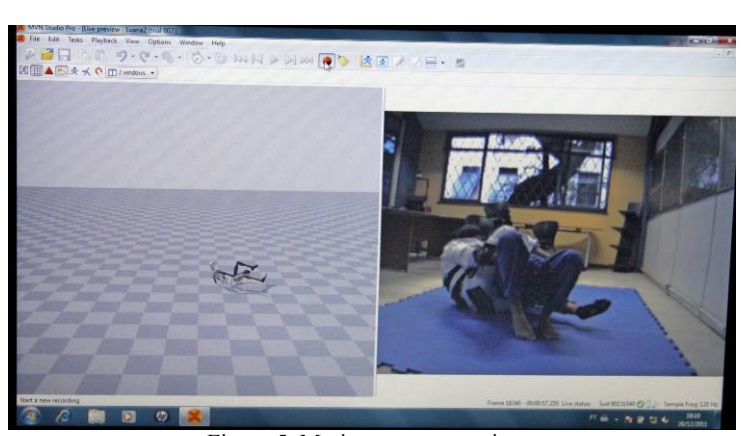


Figure 5. Motion capture session

 $2^{\circ}$  step: 3D Simulation and Modeling – the data captured from XSENS MOCAP and the 3D DHM data from scanning process were incorporated by our virtual platform that was developed as a "serious game" interactive 3D software . The visual representation of the 3DHM at the platform was generated based on XSENS MOCAP data, following position and dimension of bone segments of the virtual body. That makes the visual representation an accurate copy of the original bone position and of the specific actor's movements being captured.

This stage covered the development of an interactive platform using Unity3D game engine. That platform was developed considering the need to analyze data from different athletes movements being repeated in different moments (Kinematics analysis) (Figure 6). The data analysis will allow the kinematic data to be visualized by means of graphics – angular and linear position, angular displacement, and angular velocity. The graphics information can also be visualized with the 3D digital human model. This kind of visualization makes it easy to analyze the data with athletes and coaches.

**E-Book and Reports Stages** complete the interactive platform (Figure 7), The E-book features an entry corresponding to the movement currently under analysis (Figure 6) while the Report Module export the Analisys Results to a exchangable and readable data type as a spreadsheet.

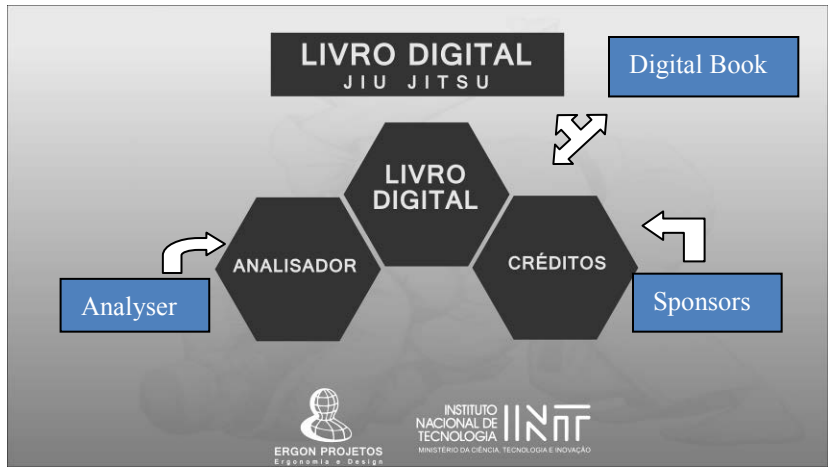


Figure 6. System home screen

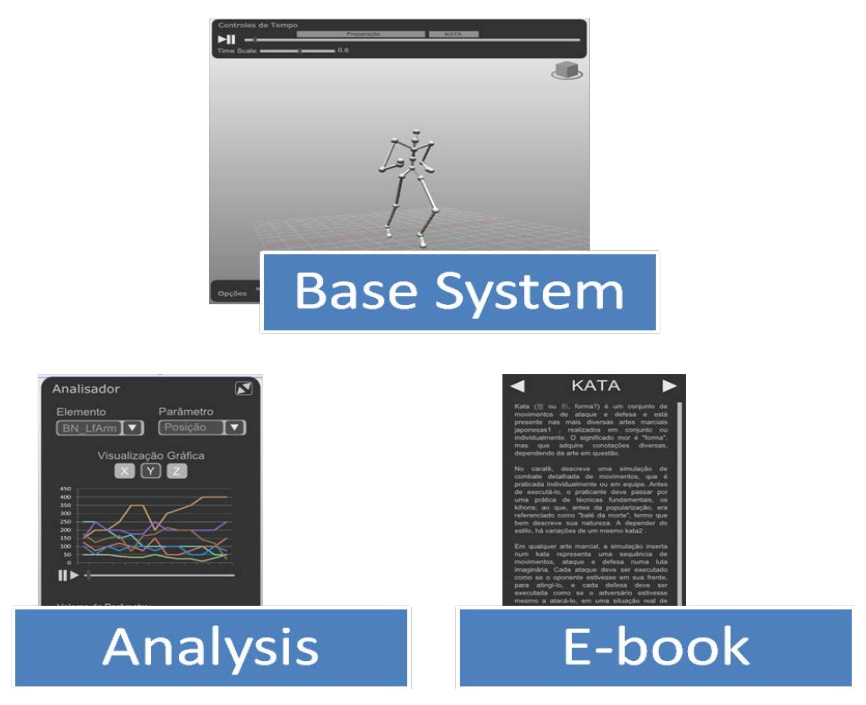


Figure 7. Example of the proposal flow chart applied to a 3D interactive environment

#### CONCLUSIONS

The 3D digital interactive environment is still under development. Its analysis will allow to study and to improve athletes' performance through teaching. In the future the integration between a 3D scanned athlete's model and a virtual environment will enable the development of a virtual simulator that can be applied to education, training and entertainment.

Sponsor by: Ergon Projetos and FAPERJ

The Ergonomic Laboratory researchers would like to thanks Luanna Alzuguir, Jiu-Jitsu European Champions 2014, for taking part and assisting on this research

#### REFERENCES

Annetta, L. A. (2010) A framework for serious educational game design Review of General Psychology, Vol 14(3), Sep, 250 Guimarães C. P; Ribeiro, F; Cid, G.L.; Streit, P.; Oliveira, J., Zamberlan, M.C; Paranhos, A.G. and , Pastura, F. (2013) 3D Digital Platform development to analyze 3D digital human models. A case of study of Jiu Jitsu combat sport. Anais do 2<sup>nd</sup> International Digital Human Modeling Symposium, Ann Habor, Michigan.

Guimarães, C., Pastura, F., Pavard, B., Pallamin. N;. Cid, G., Santos, V., Zamberlan, M.C. (2010) Ergonomics Design Tools Based on Human Work Activities, 3D Human Models and Social Interaction Simulation IHC Congress. Miami.

James, D.A.; Thiel, D.E.; Allen, K.J.; Abell, a.; Kilbreath, S.; Davis, G.M.; Rowlands, D. and Thiel, D.V. (2012) Technology and Health: Physical activity monitoring in the free living environment Procedia Engineering 34, 367-372

Naumann, A. and Rötting, M., (2007). Digital Human Modeling for Design and Evaluation of Human-Machine Systems. In: Israel, J. H. & Naumann, A. (Hrsg.), MMI Interaktiv - Human: Vol. 1, No. 12. (S. 27-35).

Nolte, K.; Krüger, P. E.; Els, P. S. and Nolte, H. (2013) W. Three-dimensional musculoskeletal modeling of the seated row resistance-training exercise South African Journal of Sports Medicine;25(3):67-73

Senevirathne, S. G; Kodagoda, M.; Kadle, V.; Haake, S.; Senior, T. and Heller, B. (2011) Application of serious games to sport health and exercise. In: Proceedings of the 6th SLIIT Research Symposium, Sri Lanka, 27 January

Steinmetz, R. and Göbel, S. (2012) Challenges in Serious Gaming as Emerging Multimedia Technology for Education, Training, Sports and Health, <u>Advances in Multimedia Modeling</u>, <u>Lecture Notes in Computer Science</u> Volume 7131, 2012, p 3

### Design of a Digital Human Modelling Module for Consideration of Anthropometric Diversity

Erik Brolin<sup>a,b</sup>, Dan Högberg<sup>a</sup> and Lars Hanson<sup>b,c</sup>

<sup>a</sup>School of Engineering Science University of Skövde, Skövde, Sweden

<sup>b</sup>Department of Product and Production Development Chalmers University of Technology, Gothenburg, Sweden

> <sup>3</sup>Industrial Development Scania CV, Södertälje, Sweden

#### **ABSTRACT**

Digital human modelling (DHM) tools are useful when evaluating human-machine interaction as they enable consideration of anthropometric diversity by facilitating the creation of human models, so called manikins, of different sizes and proportions. This paper presents the design of a module, as part of a DHM tool, made to enable a more holistic approach when defining manikin characteristics. The module is created based on previous user interviews and literature studies on the use of DHM systems and advanced mathematical methods for anthropometric diversity consideration. The module is aimed to support and guide non-expert users while at the same time support effective use and provide appropriate functionality also for expert users. The module acts as a digital guide and supports standardised working procedures when creating manikins to be used in subsequent ergonomics simulations and analyses, and shows a strong visual connection between user interface choices and their response.

Keywords: Anthropometry, Digital Human Modelling, User Interface, Human Diversity, Manikin

#### INTRODUCTION

Digital human modelling (DHM) tools are useful when evaluating human-machine interaction as they enable consideration of anthropometric diversity by creating human models, so called manikins, of different sizes and proportions (Duffy, 2009). Industry practice has previously been based on the utilization of rough approaches when considering anthropometric diversity (Daniels, 1952; Roebuck et al., 1975; Ziolek and Wawrow, 2004; Robinette, 2012). Even today, ergonomics evaluations and analyses are at times done with few manikins because of the time consuming process of creating and performing analyses for each manikin (Bertilsson et al., 2010b). Because of the fact that humans vary a lot in sizes and shapes, there is considerable uncertainty whether the expected proportion of the target population is covered by the analyses being performed (Robinette, 2012). Hence it is important to support users of DHM tools when they are using these tools and trying to consider human diversity at the same time.

Hanson et al. (2006) suggest a guide and documentation system to support DHM applications by guiding the simulation tool user through an established process which documents, stores and keeps track of ongoing and previous analyses, and facilitates the reuse of studies. Guidelines for the consideration of anthropometric diversity and for how to select relevant test cases, e.g. manikins for virtual simulation and evaluation, have been presented by Dainoff et al. (2004) and Hanson and Högberg (2012) in the form of flowcharts where the type of manikins depends on the design problem at hand. The objective of these approaches is to facilitate guidance through an appropriate process of handling issues related to anthropometric diversity.

Future technological and organizational trends and demands of DHM tools is presented in Wischniewski (2013) through the results of a survey using the Delphi technique. In this survey, 44 experts answered questions and assessed statements regarding upcoming trends in "Digital Ergonomics". Results from the survey show that, among other things, functionality connected to providing sufficient mapping of anthropometric and biomechanical variance, and increased software usability to support software use for novices, was deemed important and state-of-the-art between 2015 and 2020. Software support for virtually designing and evaluating products and processes for different regions of the world was deemed important and state-of-the-art between 2020 and 2025. Important and state-of-the-art after 2025 was considered to be holistic tools that allows for cognitive, anthropometric and biomechanical evaluation of products and work processes. Challenges and deficits using DHM tools was, among other things, considered to be high software complexity, in some cases unknown validity and a lack of standard for models and file formats.

To address these current problems and future challenges the DHM tool IMMA (Intelligently Moving Manikins) was introduced in 2010 as a DHM tool that uses advanced path planning techniques to generate collision free and biomechanically acceptable motions for digital human models (as well as parts) in complex assembly situations. The aim of IMMA is to develop a non-expert tool with high usability, where the tool supports the user to consider human diversity, to easily instruct the manikin to perform tasks and functionality to perform time-dependent ergonomics evaluations to control and assess complete motions (Hanson et al., 2012). This paper presents the design of a module, as part of the IMMA DHM tool, made to enable a more holistic approach when defining manikin characteristics. An aim of the work is to include all necessary functionality but at the same time maintain a high usability of the interface and software tool. The module is aimed to support and guide non-expert users while at the same time support effective use and appropriate functionality also for expert users.

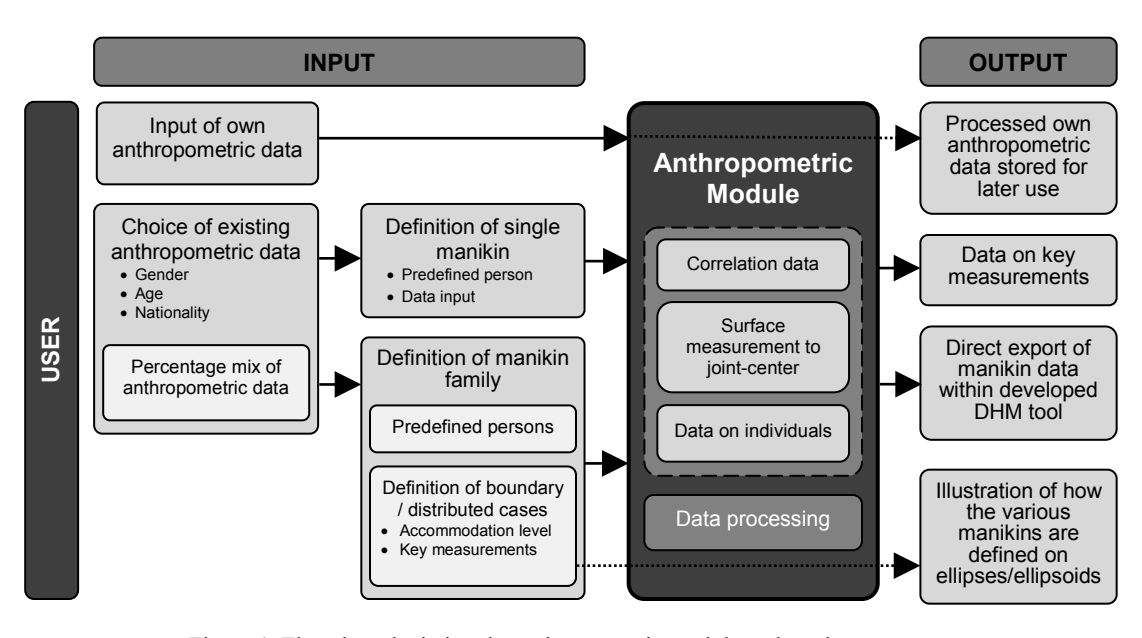


Figure 1. Flowchart depicting the anthropometric module and work process

#### **METHODS**

The module and its user interface is created based on previous user interviews and literature studies of the use of

DHM systems (Bertilsson et al., 2010b) and advanced mathematical methods for anthropometric diversity consideration (Meindl et al., 1993; Speyer, 1996; Brolin et al., 2012). Based on the results from these studies, a module and work process has been described which would facilitate a more supportive way of working with anthropometric diversity in DHM systems (Bertilsson et al., 2010a) (Figure 1). Most of the functionality of the anthropometric module in Figure 1 was implemented in early versions of IMMA, operated by a basic user interface (Bertilsson et al., 2011). Initial evaluations by users, and development of new functionality, confirmed needs for further development of the module and its user interface to achieve intended usability. In addition to added features of the anthropometric module, the structure of the updated interface is based on the five states of the ergonomic design process presented by Dainoff et al. (2004):

State 1: Statement of the design problem

State 2: Defining the target population

State 3: Anthropometric databases

State 4: Representing body size variability using cases

State 5: Transitioning cases to products

The module's user interface is divided into different sections where each section is intended to match a state in the ergonomic design process. To achieve the intended usability the different functions are structured throughout the interface in the same order as they would typically be used in an analysis. Mathematical and statistical methods connected to each state have been developed or adapted from literature. Design of products and workplaces are often aimed at an international target group and therefore functionality for assessing several populations simultaneously is incorporated by combining mean, standard deviation and correlation data from different populations (Dunlap, 1937). To increase flexibility when selecting anthropometric key measurements a conditional regression model (Brolin et al., 2013) is implemented. A conditional linear regression model has the advantage that any measurement can be used as independent key measurement which gives the possibility to only include measurements that have a direct connection to the design problem. To be able to address multi-dimensional design problems, where many body measurements are of interest to include in the analysis, functionality that facilitates the creation of a group of manikins is implemented (Brolin et al., 2012). This functionality creates a confidence region, in the shape of a multidimensional hyper-ellipsoid, based on the selected anthropometric key measurements. Functionality for using principal component analysis (PCA) to reduce the dimensionality of the confidence region and thus limit the number of manikins is also implemented. Functionality for selecting different types of cases on the surface of the confidence region is also added (Bertilsson et al., 2012). The methods have been implemented into the user interface by keeping cognition and usability principles, guidelines and heuristics in mind (Cooper et al., 2012) and by discussing with a usability expert. Ideas and good examples have been adapted from existing software, web sites and literature.

#### **RESULTS**

The resulting user interface is divided into three sections that match state 2, 3 and 4 in the ergonomic design process (Figure 2). State 1 of the ergonomic design process, *statement of the design problem*, is assumed to have been performed at an early stage of the design process before the use of DHM tool is applied and is therefore not included in the user interface. State 5 of the ergonomic design process, *transitioning cases to products*, is considered to be performed during the actual simulation and through following ergonomics analysis. Thus, the main areas of the user interface are:

- Defining target population
- Measurement selection
- Case selection & options

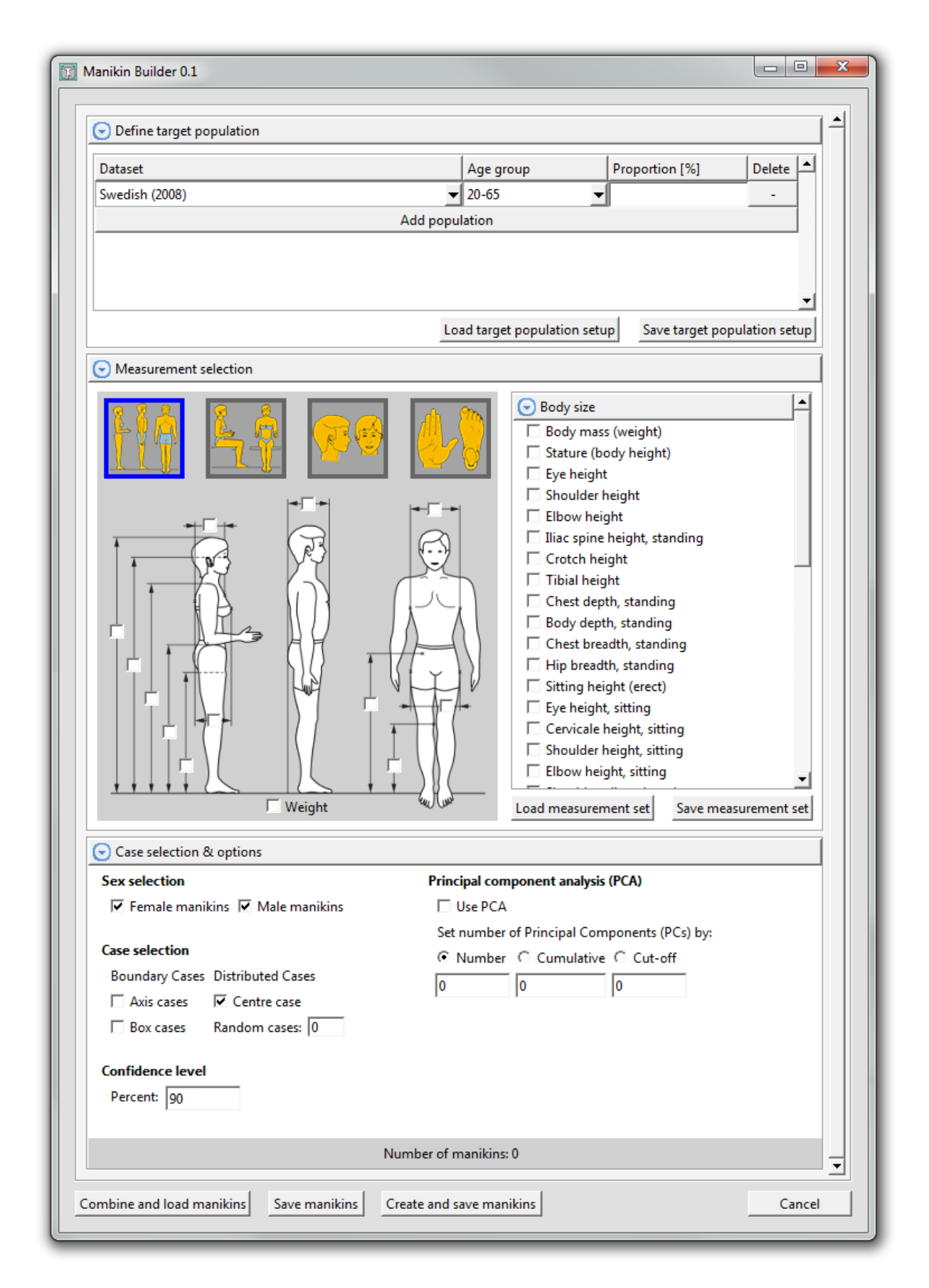


Figure 2. The graphical user interface of the anthropometric module

Defining the target population is done by selecting different population datasets and age groups and proportion of each dataset. Based on the selected datasets and the proportion of each data set, new data for a synthetic population is generated. It is also possible to save and load specific target population setups. Selection of anthropometric key measurements, used to determine the size of each manikin, can be done in two ways, either by selecting check boxes via a graphical interface or directly from a list of measurements. The two check boxes connected to a specific measurement are checked regardless if the graphical interface or the list is clicked. The third section is concerned with additional options such as case selection, size of confidence region and use of principal component analysis (PCA). The user gets immediate feedback on how many manikins that will be created at the bottom of this section, dependent on selected choices. The first choice for the user is to select whether female and/or male manikins should be created. The following case selection is done by specifying which type of cases that should be created. Boundary cases are defined on the surface of the calculated multidimensional confidence region; Axis cases can be found on the ends of the axes of the hyper-ellipsoid and Box cases are found on the edges of a hyper-cuboid that spans the biggest volume inside of the hyper-ellipsoid. It is also possible to select an average centre case with mean values for each selected anthropometric key measurement or to include a selected number of randomised cases based on a normal distribution. The next step is to set the confidence level, which is used to scale the multi-dimensional hyperellipsoid. The hyper-ellipsoid is scaled so that the surface encapsulates a percentage of the data corresponding to the selected confidence level. The number of manikins depends on the dimensionality of the confidence region, i.e. the number of selected anthropometric key measurement, as well as the selected choices in the sex and case selection (Table 1). The number of manikins can quickly become large and difficult to process, even for an automated simulation process as the one used in the IMMA DHM tool. Therefore PCA is useful as it reduces the dimensionality but still explains as much as possible of the variation of the original data based on the number of included principal components (PC). In the interface it is possible to set the number of PCs either by their specific number or the desired cumulative percentage of the variation that the remaining PCs should contribute with. The PCs can also be limited by discarding all PCs that are smaller than a specific cut-off value.

Number of dimensions (p)	1	2	3	4	5	6	7	8	9	10
Axis cases $(n=p\cdot 2)$	2	4	6	8	10	12	14	16	18	20
Box cases $(n=2^p)$	2*	4	8	16	32	64	128	256	512	1024
Centre case (n=1)	1	1	1	1	1	1	1	1	1	1

43

77

143

273

531

1045

Table 1. Number of manikins dependent on the number of dimensions for axis, box and centre cases

25

5

9

15

manikins:

Total number of

#### **DISCUSSION & CONCLUSIONS**

The resulting anthropometric module includes functionality argued to be appropriate for the consideration of anthropometric diversity in a DHM tool, and the user interface supports a structured work process and shows a strong visual connection between interface choices and their response. The user interface is based on anthropometric design guidelines and includes known methods found in literature. In addition, new methods have been developed and implemented that supports the user when creating manikins for ergonomics simulations and evaluation. An aim and a challenge of the work has been to include all necessary functionality but at the same time maintain a high usability of the interface without creating clutter and information overload for the users. One of the main advantages of the interface is the possibility to include necessary factors or measurements that can have an effect on the humanmachine interaction and at the same time limit the number of human models to facilitate time efficient simulation procedures. Some of the trends and demands of DHM tools presented in Wischniewski (2013) are met or regarded by the module, e.g. the module provides sufficient mapping of anthropometric and biomechanical variance as it is possible to create a group of manikins that represents the anthropometric variation within the targeted population. The module should also have an increased software usability to support software use for novices thanks to the clear structure and possibility to explore the user interface by having all necessary functionality visible and possible to select or deselect at any time (Cooper et al., 2012). The importance, presented in Wischniewski (2013), of being able to virtually design and evaluate products and processes for different regions of the world is also regarded through

<sup>\*</sup> For 1 dimension the axis and box cases will coincide

the module as it is possible to mix and combine population data of different groups into a new synthetic population.

Still, added and improved functionality would further increase the usability of the developed module. In the creation of the user interface of the module focus have been to support the creation of a group of manikins used in an automated simulation process. Yet, functionality for creating a single manikin, based on anthropometric measurements from a specific individual, will also be added. Other functionality that could be added in the module is for example the possibility to alter appearance, to add equipment to the manikins and the possibility to preview the manikins that would be created according to the current selection of options. This preview function could be done by displaying what Garneau and Parkinson (2013) call humanoid glyphs that show the size and proportion of each manikin. Existing functionality in the module can also be improved to increase usability. It could, for example, be easier to select anthropometric measurements, which will be important if other types of anthropometric measurements beside body size variables are to be considered, e.g. strength and range-of-motion variables. The somewhat difficult task of selecting principal components to maintain when using PCA could be improved by visualising the options through a chart that shows how much of the variance that each PC describe. Still, additional improvements are necessary before we can have what Wischniewski (2013) describes as a holistic tool that allows for cognitive, anthropometric and biomechanical evaluation of products and work processes. Other demands such as high software complexity, unknown validity and a lack of standards for models and file formats are challenges that need to be addressed. We believe this would be supported by more transparency among companies and researchers involved in the development of DHM systems.

The module and its user interface are not yet completely finished and have not gone through formal user testing. The interface has been designed through analysis of user needs and the utilization of interface design guidelines but will need to go through user testing with different types of users such as simulation experts, industry non-expert users and university students. The results from these tests will show the validity of the design choices and indicate possible improvement areas. The objective of the user test iteration is that the final module and its user interface will offer high usability related to the consideration of anthropometric diversity and contribute to an enhanced accuracy in meeting desired levels of accommodation when using DHM tools for the design of products and workplaces.

#### REFERENCES

- Bertilsson, E., Hanson, L., Högberg, D., Rhén, I.-M. (2011), "Creation of the IMMA manikin with consideration of anthropometric diversity", Proceedings of the 21st International Conference on Production Research (ICPR). Fraunhofer Verlag.
- Bertilsson, E., Högberg, D., Hanson, L. (2010a), "Digital Human Model Module and Work Process for Considering Anthropometric Diversity", In: Karwowski, W., Salvendy, G. (eds.) Proceedings of the 3rd Applied Human Factors and Ergonomics (AHFE) International Conference. Miami, USA.
- Bertilsson, E., Högberg, D., Hanson, L. (2012), "Using experimental design to define boundary manikins", Work: A Journal of Prevention, Assessment and Rehabilitation, 41, 4598-4605.
- Bertilsson, E., Svensson, E., Högberg, D., Hanson, L. (2010b), "Use of digital human modelling and consideration of anthropometric diversity in Swedish industry", Proceedings of the 42nd annual Nordic Ergonomic Society Conference. Stavanger, Norway.
- Brolin, E., Hanson, L., Högberg, D., Örtengren, R. (2013), "Conditional Regression Model for Prediction of Anthropometric Variables", Second International Digital Human Modeling Symposium. Ann Arbor, USA.
- Brolin, E., Högberg, D., Hanson, L. (2012), "Description of boundary case methodology for anthropometric diversity consideration", International Journal of Human Factors Modelling and Simulation, 3, 204-223.
- Cooper, A., Reimann, R., Cronin, D. (2012), "About face 3: The Essentials of Interaction Design". John Wiley & Sons.
- Dainoff, M., Gordon, C., Robinette, K. M., Strauss, M. (2004), "Guidelines for using anthropometric data in product design", HFES Institute Best Practices Series. Santa Monica: Human Factors and Ergonomics Society.
- Daniels, G. S. (1952), "The" Average Man"?". Wright-Patterson Air Force Base, Ohio: Air Force Aerospace Medical Researh Lab.
- Duffy, V. G. (2009), "Handbook of Digital Human Modeling". Boca Raton, CRC Press.
- Dunlap, J. W. (1937), "Combinative properties of correlation coefficients", The Journal of Experimental Education, 5, 286-288.

- Garneau, C., Parkinson, M. (2013), "The use of humanoid glyphs in graphs for representing human variability in the spatial design of products", Second International Digital Human Modeling Symposium. Ann Arbor, USA.
- Hanson, L., Blomé, M., Dukic, T., Högberg, D. (2006), "Guide and documentation system to support digital human modeling applications", International Journal of Industrial Ergonomics, 36, 17-24.
- Hanson, L., Högberg, D. (2012), "Use of Anthropometric Measures and Digital Human Modelling Tools for Product and Workplace Design", In: Preedy, V. R. (ed.) Handbook of Anthropometry: Physical Measures of Human Form in Health and Disease. Springer.
- Hanson, L., Högberg, D., Söderholm, M. (2012), "Digital test assembly of truck parts with the IMMA-tool an illustrative case", Work: A Journal of Prevention, Assessment and Rehabilitation, 41, 2248-2252.
- Meindl, R. S., Hudson, J. A., Zehner, G. F. (1993), "A multivariate anthropometric method for crew station design". Wright-Patterson Air Force Base, Ohio: Crew Systems Directorate, Human Engineering Division, Armstrong Laboratory.
- Robinette, K. M. (2012), "Anthropometry for product design", In: Salvendy, G. (ed.) Handbook of Human Factors and Ergonomics. 4th ed. Hoboken: John Wiley & Sons.
- Roebuck, J. A., Kroemer, K. H. E., Thomson, W. G. (1975), "Engineering anthropometry methods". New York, John Wiley & Sons.
- Speyer, H. (1996), "On the definition and generation of optimal test samples for design problems". Kaiserslautern Human Solutions GmbH.
- Wischniewski, S. (2013), "Delphi Survey: Digital Ergonomics 2025", Second International Digital Human Modeling Symposium. Ann Arbor, USA.
- Ziolek, S., Wawrow, P. (2004), "Beyond Percentiles: An Examination of Occupant Anthropometry and Seat Design". Warrendale: Society of Automotive Engineers, SAE Technical Paper.

## Investigating the Effectiveness of Priming in Virtual Environments

Charles Butler

Norwegian School of Information Technology Oslo, 0185, Norway

#### **ABSTRACT**

This paper considers the usefulness and possibility of using virtual environments for the advancement of priming research. First, the background and foundational research and experiments are considered. Next, the benefits and drawbacks of utilizing virtual environments is examined. Finally, the paper considers the potential of utilizing virtual environments in an attempt to replicate the existing studies to further establish the validity of virtual environments in priming research and then the potential of these methods to push the boundaries of the field.

Keywords: Priming, Virtual Environments, Virtual Worlds

#### INTRODUCTION

Priming can have a considerable, though often unnoticed, effect on our behavior in any number of day-to-day situations. The awareness of this possibility can be useful both to those who seek to influence the behavior of others as well as those who would prefer to resist such influence (or at least be aware that someone may be attempting to influence them). However, as spending time in virtual and augmented environments becomes more common, it becomes ever more important to study the extent to which these environments can exert influence over their users. In the real world, priming attempts can require a great deal of control over the situation in which the attempt takes place. However, in a virtual environment, the developer's control over the experience is only bounded by the expectations of the users, expectations which have often been pre-conditioned to accept unexpected or unusual stimuli in such a setting.

The effectiveness of the concept of priming itself is a primary concern, so the sections that follow outline a number of foundational studies in priming research. A discussion of virtual environments follows, addressing the fundamentals of using such an environment in a research setting in addition to the human factor issues involved. Further complications that warrant mention include issues with the design and implementation of virtual environment as well as the potential effect of varying degrees of experience using virtual environments among research participants. Also included is a discussion of potential virtual world implementations intended to gauge the efficacy of priming within virtual environments by adapting the priming experiments outlined in the Background section to function within a virtual environment.

#### BACKGROUND

#### **Priming**

Priming refers to the incidental activation of knowledge structures, such as trait concepts and stereotypes, by the current situational context (Bargh, Chen, and Burrows, 1996). This activation of certain knowledge structures has the potential to affect our behavior to some extent. It may seem obvious that various details about our environment, or our perception of it, can alter our behavior in various ways, but the intriguing (and potentially disturbing to some) aspect of priming is that both this activation and the potential effect on behavior can happen entirely below our conscious awareness. However, these outcomes can be difficult to engineer and test directly, especially without the awareness of the test subject.

It can be additionally complicated by the various ways in which individuals may perceive and react to a certain situation. As illustrated in Figure 1, Wheeler and DeMaree show the various mechanics of prime-to-behavior effects. A subject first encounters a prime, which activates a knowledge construct. Then the subject's individual perceptions are activated, which can act as potentially encouraging or inhibiting agents before the subject represents some behavior which is then observed. One challenge, then, is selecting a priming mechanism and the surrounding environment that would affect the test subjects both sufficiently and consistently for the results to be measurable and significant.

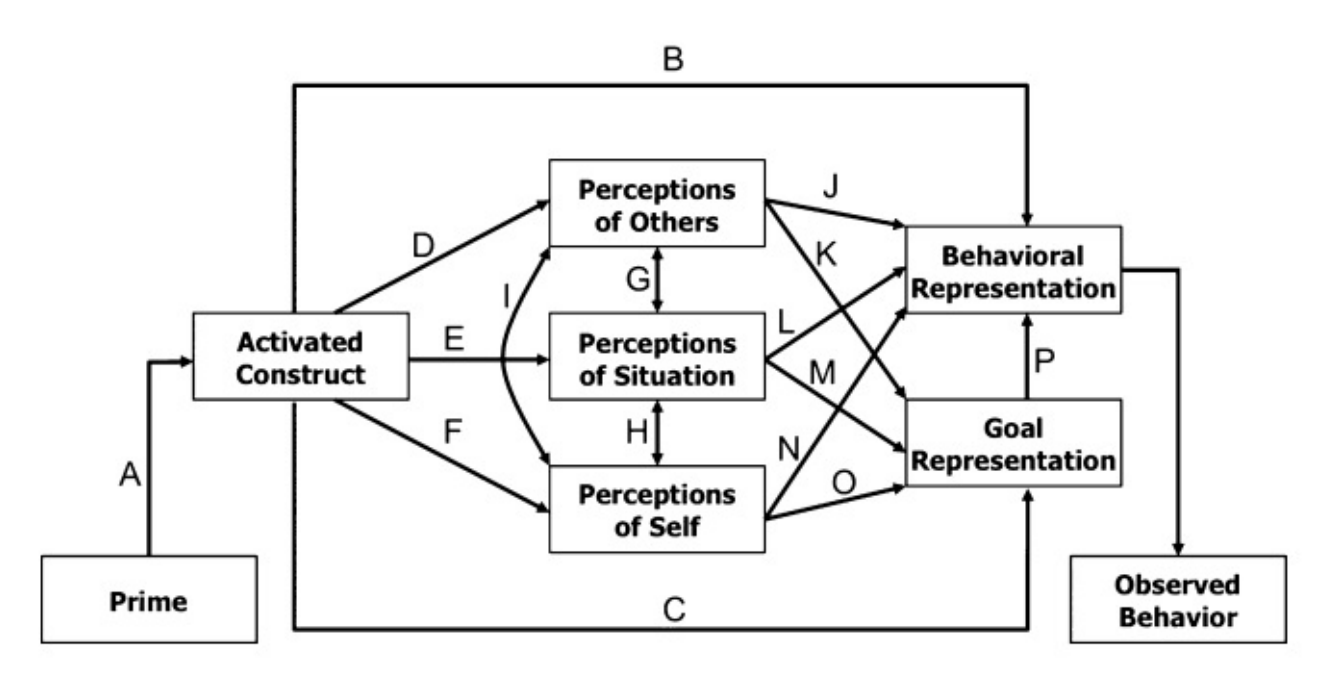


Figure 1. Proposed mechanisms for prime-to-behavior effects. (Wheeler and DeMarree, 2009)

#### **Experiments**

Bargh, Chen, and Burrows conducted a set of foundational priming experiments which seemingly overcame the challenges listed above (Bargh, Chen, and Burrows, 1996). Two of these are especially relevant to the discussion of virtual environments, as they both rely on the physical environment and interaction within the space.

In the first experiment, a group of students at New York University were given a test involving the unscrambling of sentences. However, there were three different versions of the test. One version of the test attempted to prime a *polite* condition in the students by including words such as *patiently* and *courteous*. Another version of the test attempted to prime a *rude* condition by including words such as *intrude* and *interrupt*. A third version of the test was intended to be a neutral control with words considered to be neither *polite* nor *rude*.

After taking the test, the student was instructed to procure the next task from a researcher in a nearby room. When the student approached the room in question, the researcher was deliberately (but non-obviously) appearing busy or otherwise engaged. The true test of the experiment was the amount of time it would take each student to interrupt the researcher. The researcher would ignore the student until either interrupted or a hidden 10 minute time limit had elapsed.

The results were quite striking as shown in the graph below. Of the students primed with the *polite* test, fewer than 20% of them interrupted the researcher before the 10 minute time limit was complete. In contrast, over 60% of the students primed with the *rude* test interrupted before the time limit had expired. In addition, the mean number of seconds elapsed before students of each group would interrupt was considerably different as well, with 326 seconds for the *rude* group and 558 seconds for the *polite* group. Note that the mean for the *polite* group was so close to the 600 second time limit that the difference would likely have been even more stark had there not been a time limit on the experiment.

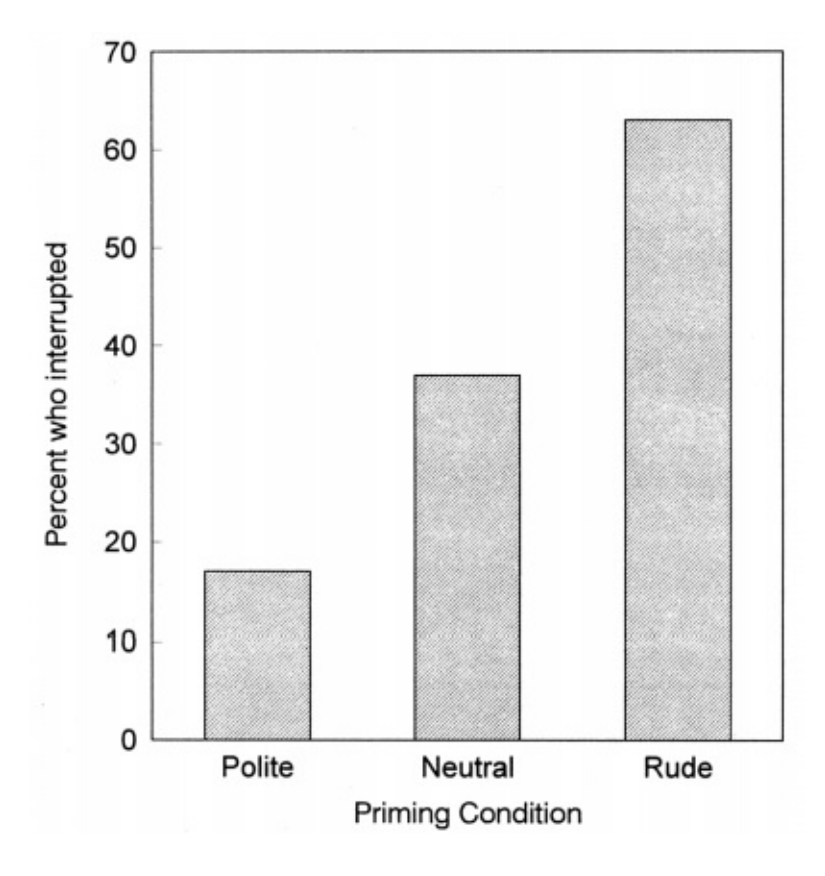


Figure 2. Percentage of participants who interrupted the experimenter. (Bargh, Chen, and Burrows, 1996)

In their second experiment, Bargh, Chen, and Burrows invited students from New York University to participate in a study in which the participants were given a scrambled word sentence test. There were similar to the test from the previously mentioned experiment, though this test only had two versions. One version was a neutral control, and the other attempted to prime the participants for the *elderly* condition by including words such as *old*, *retired*, and *forgetful*. The actual metric in play with this experiment was the amount of time it took the students to walk a fixed distance down the hall after completing the task and exiting the room.

The results of this experiment, though not as obvious as in the previous experiment, show significant differences in the control and primed groups. In addition, this experiment was repeated two times (shown in the graph below as experiment 2a and 2b) with very similar results. The students in both sets of the experiment who were primed with the *elderly* condition covered the specified distance approximately one second more slowly (approximately 12%)

than the students taking the neutral test.

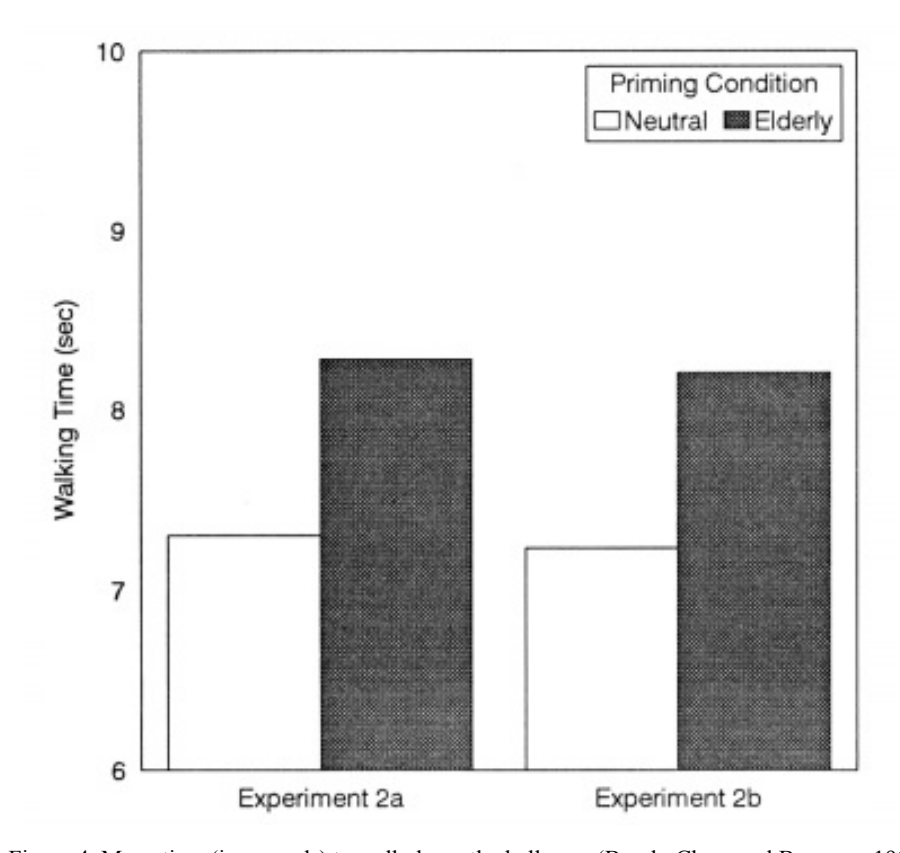


Figure 4. Mean time (in seconds) to walk down the hallway. (Bargh, Chen, and Burrows, 1996)

#### VIRTUAL ENVIRONMENTS

#### **Important Considerations**

Virtual environments present researchers with a number of potential benefits when compared to setting up experiments that require the coordination and control of both people and physical spaces. First, depending on the type of experiment in question, the researcher may need control of a considerable amount of space as well as personnel for an extended period of time. In addition, if the experiment has certain physical requirements for the space, it may be inconvenient or even impossible to gain access to a space that meets the requirements. In the experiment above, the researcher required a room with an exit to a hallway which presented the students with only one option for leaving the area so their traveling time across the distance could be tracked. This is a simple enough requirement, but even that simple requirement might be difficult to fulfill in many buildings.

Consider the suspension bridge experiment intended to test the misattribution of arousal (Dutton and Aron, 1978). This experiment required a researcher to be stationed on two different bridges (an anxiety-inducing suspension bridge and a relatively non-threatening bridge) to interview people as they crossed each bridge. This could be potentially very difficult to set up and control in the real world. However, these environments could be created trivially and at will through the use of virtual environments, and the researchers tasked with interviewing the subjects could potentially be replaced by a scripted non-player character within the virtual environment.

To take the benefits even farther, this could allow a much broader sample of participants (as it wouldn't be limited to the types of people who would be crossing a scary suspension bridge at a time when a researcher happened to be on it asking questions), and it would allow people to engage with the task in any place and at any time. It could even allow the localization of research tasks to take place with relative ease so that researchers could more readily examine cross-cultural effects.

Of course, there are drawbacks to the use of virtual environments as well. First, researchers are likely not experienced developers of virtual worlds, so while certain types of resource savings may be possible, these savings may come at a considerable expense in other areas. Developers and designers may have to be hired or recruited. However, new tools such as Unity 3D or the Unreal Development Kit are now allowing even novices to create impressive 3D virtual environments, there can still be a considerable barrier to entry and time investment involved. To further compound the potential problems, even if a developer is available, eliciting the desired reactions and behaviors from participants in a virtual world can be more difficult than simply implementing the physical area. This approaches the territory of game design, and while many lessons can be learned from popular games, adapting those lessons to a non-game context can be incredibly challenging, even for experienced industry practitioners.

In addition, there are considerable human factor issues to consider, especially if the research may be dealing with participants who may not be very familiar with virtual environments, though this problem will likely lessen as more and more people engage with video games and simulations of various types; however, this does bring up the additional problem of gauging the different perceptions of participants based on the direction and extent of their experience with virtual environments.

#### The Human Factor in Virtual Environments

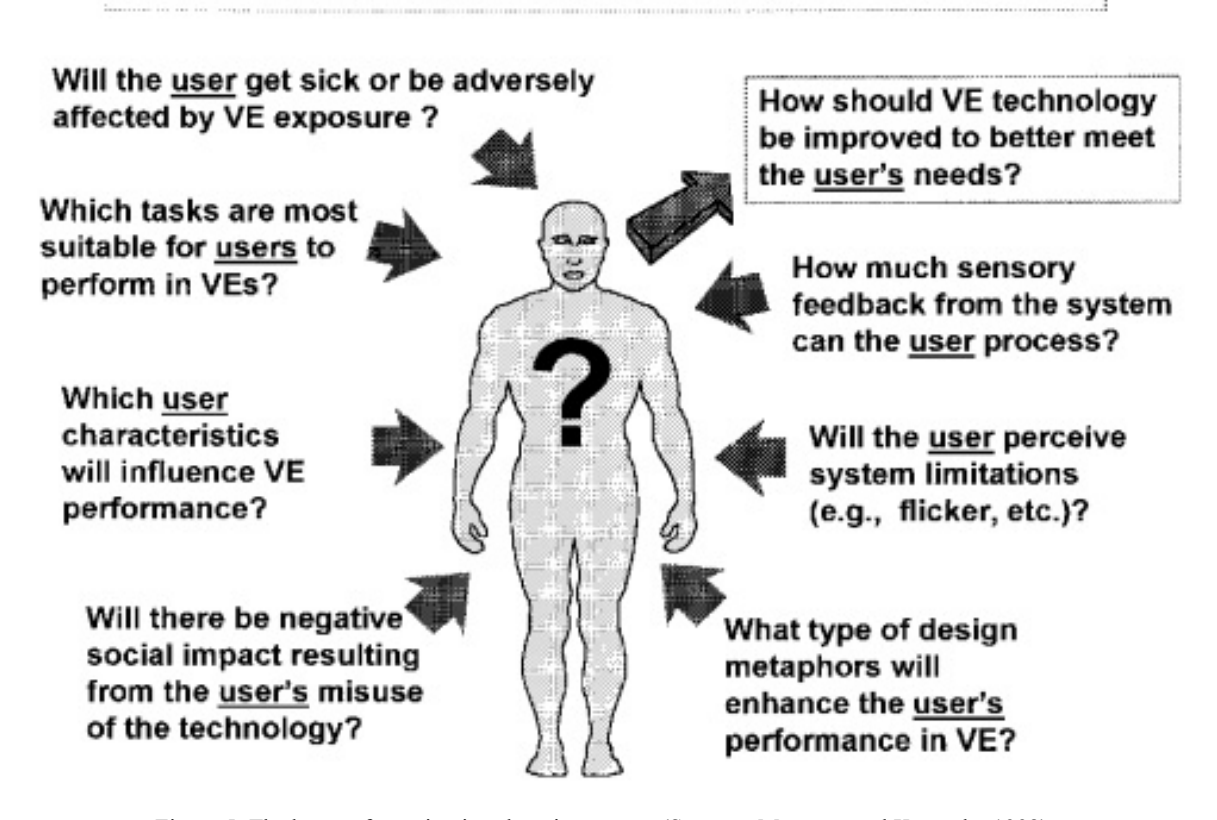


Figure 5. The human factor in virtual environments. (Stanney, Mourant, and Kennedy, 1998)

For example, Stanney, Mourant, and Kennedy list a number of human factor concerns that one should consider when utilizing virtual environments (Stanney, Mourant, and Kennedy, 1998). Some people who are less familiar with technology may find some aspects of virtual environments unsettling or discomforting, even becoming disoriented or nauseous. Screens and the action taking place on them can give certain people headaches or even seizures in extreme cases. Though likely less serious for the users, possibly the most important concern for the researcher is that some tasks just don't lend themselves to being carried out within a virtual environment. Additionally, there could be some tasks which are trivial to design and implement in the real world which would be enormously expensive and time consuming to implement in a virtual environment, and regrettably, it may not always be immediately obvious which tasks are which.

#### **Potential Implications**

The true potential here is to simply do work that would be impossible or prohibitively difficult or expensive in the real world. This encompasses both research tasks and the scale of the testing. In a virtual environment, almost any situation that can be conceived can be created. Depending on the complexity, it may still be expensive to implement, but there are numerous things that just couldn't be done at any price in the real world, if for no other reason than ethical concerns. In addition, the scale at which research could be done in a virtual environment exceeds what could be done otherwise. Web-based environments are now easily creatable and accessible, opening up the potential for literally millions of users to participate in a study.

#### **FUTURE WORK**

#### **Method for Further Establishment of Efficacy**

A key question that will likely remain for some time is the extent to which a virtual environment can replicate the results of a real environment among participants of a study. This can be quite a difficult thing to test, both for the issues with virtual environments listed above, and also simply because we tend to perceive some things in virtual environments in a very similar manner to those in the real world, while others are perceived very differently. To make it more complex, different people likely have very different experiences even within the same environment based on their individual experiences, perceptions, and preferences.

While a considerable barrier, the research could be served by an attempt to replicate a number of the foundational priming studies, such as the two listed previously, in virtual environments, to see if the effects are reproducible. While this may only provide evidence that these specific instances are effective (or ineffective) in virtual environment, it would help provide a base from which other research could be informed.

#### REFERENCES

Bargh, J.A., Chen, M., Burrows, L. (1996), "Human Automaticity of Social Behavior: Direct Effects of Trait Construct and Stereotype Activation on Action", in: Journal of Personality and Social Psychology, Volume 71 No. 2: pp. 230-244

Dutton, D.G., Aron, A.P. (1974), "Some evidence for heightened sexual attraction under conditions of high anxiety", in: Journal of Personality and Social Psychology, Volume 30: pp. 510-317

Stanney, K.M., Mourant, R.R., Kennedy, R.S. (1998), "Human Factor Issues in Virtual Environments: A Review of the Literature", in: Presence, Volume 7 No. 4: pp. 327-351

Wheeler, S.C., DeMarree, K.G. (2009), "Multiple Mechanisms of Prime-to-Behavior Effects", in: Social and Personality Psychology Compass, Volume 3 No. 4: pp. 566-581

### Section 4

Ergonomics in Fashion Industry

# Thermal Human Modeling: A Design Tool for Functional Clothing

Huang Chao a, Ameersing Luximon a and Kwok-Wing Yeung b

<sup>a</sup>Institute of Textiles and Clothing The Hong Kong Polytechnic University Hong Kong, China

<sup>b</sup>Clothing Industry Training Authority Hong Kong, China

#### **ABSTRACT**

Functional and smart clothing has been an up-and-coming products for fashion industry. The human model or mannequin, which is a bridge between customer's physical information and design utilization, has vital importance as primary design tool. The physiological messages of human body may have growing needs for design. The traditional geometric human models (G-model), which convey surface anthropometric data, such as shape, volume and size, may be advanced to functional model. Thermal function is highlighted in this study, based upon an emphasized potential of developing new thermal functional clothing for health enhancement and rehabilitation purpose. After reviewing theoretical basis on thermoregulation and body temperature, as well as the future application in fashion industry, the methodology of developing thermal human model (T-model) is introduced, including experiments, data pre-processing and modeling process. The T-model originated from relatively accurate 3D body scanning data has visualized and quantified skin temperature data obtained from thermographs, which may be adopted to 3D fashion design system, e.g. designing, patternmaking, pattern revision, virtual fitting and grading for functional clothing.

**Keywords**: Thermal human model (T-model), Geometric human model (G-model), functional clothing design, thermography, 3D body scanning

#### INTRODUCTION

In recent years, with the revolutionary changes and remarkable innovations on functional and intelligent materials, a growing trend on functional and smart clothing has been introduced and accepted by designers, producers and consumers (Fan & Hunter, 2009; Mattila, 2006). For some fit or tight fit functional clothing, more design elements on human anatomy, physiology and biomechanics have been undertaken by them to enhance the special functions such as body protection, recovery, rehabilitation, shaping and performance (Jayaraman, Kiekens, & Grančarić, 2006; Wang, 2008) As one of the efficient design tools, mannequins, also known as human model, are frequently-used by fashion designers, patternmakers and manufacturers, which equip them with tangible or virtual 3D model (Stott, 2012; Wang, 2007). Besides, digital 3D human models are increasingly adopted to enhance the efficiency and sustainability in these human centered disciples (Chintala, 2011; Fletcher, 2008; Gray, 1998). In front of these new revolutions on design and technology trends, the traditional geometric human models may not answer the needs of design and manufacturing from the emerging new branch of functional clothing industry. The digital human model applied to fashion and functional design and manufacturing need be endued with more efficient and internal information of human body. There is a necessity toward launching functional human modeling, as an accelerating,

enhancing and inspiring tool for fashionable and functional clothing design.

In this paper, to commence the functional human model design, the study of thermal functional model will be highlighted. Body temperature decides if human being is healthy and comfort. Human body requires to be maintained in a thermoregulatory status (Weller, 2005; Werner, 1980). Clothing is the second skin of human body, which can fulfill the functions to balance the heat and moisture conditions and keep thermal comfort (Hollies & Goldman, 1977). Besides, due to the significant importance of body temperature to human health emphasized by medical researchers, functional clothing with thermal focus like rehabilitation will be a meaningful, practical and innovational functional product to strength human body.

#### THERMAL FUNCTION AND CLOTHING

The structures and functions of human beings are exceedingly complicated. The components construct human body with various body dimension, body shape and coordinating internal functions. As one of the warm-blooded animal, the main function of human body is to keep the body temperature in a constant status (Goyal, 2013). Clothing takes a significant function of the human body protection and keeps it within a thermal comfort, which have been studied more than decades of years (Fourt & Hollies, 1970; Hollies & Goldman, 1977; Newburgh, 1950; Song, 2011). To clarify the relationship between thermal function and clothing is the theoretical basis for this research.

#### **Heat Generation and Loss**

The majority of heat generated from energy metabolism process maintains normal body temperature and excess heat eliminates to the environment by conductivity, convection, radiation, evaporation (Blatteis, 1998; Johnson & Byrne, 2003). Heat exchange between skin surface and the environment can be fulfilled by convention, conductivity, radiation and evaporation. Human body can radiate infrared rays to outside and absorb heat radiation at the same time. By conduction, heat exchange with air or objects close to skin surface but which is often assumed to be negligible. Water vapor evaporated from skin surface and respiratory systems takes away heat. When the air flows, heat also will get lost by convention. To understand thermoregulation of human body, a lot of scholars had set up heat balance equations in different conditions (Cena & Clark, 1981; Jessen, 2001; Parsons, 2002; Wilmore, Costill, & Gleim, 1995). One of the standard heat balance equation in normal rest condition (Marino, 2008; Piantadosi, 2003) is shown below:

$$S=C \pm R \pm C \pm M - E$$

The gain and loss of heat is presented in the equation, where S is heat storage, C is convention and conduction, M is metabolic heat, R is radiation, E is evaporation. When S is positive, the body temperature will rise and negative S result lower body temperature. The balance of heat generation and loss keeps human body in a normal thermoregulation status and retain it in a healthy and comfortable condition (Benzinger, Pratt, & Kitzinger, 1961; Johnson & Byrne, 2003; Parsons, 2002). One of the clothing's functions is to dramatically change the heat exchange relationship by clothing materials. All the parameters in heat balance calculation will directly connect to properties of clothing (Fourt & Hollies, 1970), such as the thermal insulation of clothing.

#### **Features of Human Body Temperature**

Core temperature and skin temperature or shell temperature are used to quantify the body heat status. The normal body temperature of human body is 37°C, which can be measured from rectum, esophagus and tympanic membrane and fluctuate a little bit during exercise and illness (Heymsfield, 2005; McCall, 2010). Body temperature can only be kept in a narrow range from about 97.5°F to 100.4°F (36.4°C to 37.3°C) in core temperature and from about 96.6°F to 99.3°F or 35.8° to 37.4°C in skin temperature (Hall, 2010; Timby, 2009). Big change on body temperature will directly result in human function disorder or even death (Goyal, 2013; Piantadosi, 2003). The hypothalamus is the temperature control centre to protect body from cold and hot conditions by physiological and psychological reaction, such as shivering, increasing activity and metabolism to produce heat and sweating, reduce activity and decreased appetite to lose heat (Bijlani & Manjunatha, 2010; Eysenck, 2004). In fact, the thermoregulation of human being has been studied for more than one hundred years and still under research due to the complicated structure and functions of human body. The physiological role and process of heat production are known but the exact contribution of each heat generating organs may not have a very clear concept (Malan & Canguilhem, 1989).

From present studies, heat generated by metabolism coming from major organs such as brain, heart, liver, kidneys and skeletal muscles (McCall, 2010). Many properties of the organs and tissues, such as the density, heat conductivity, blood flow and metabolic rate are quite different from each other (Juergen Werner & Buse, 1988). Even the relative stable core temperature varies from organs and tissues. Internal heat conductivity, blood circulation and other physiological reaction helps to maintain the core temperature in a dynamic balance. Even these complicated process may not be clearly monitored, the general understanding can be reached is that the thoracic and abdominal organs such as liver and heart, may have higher temperature in rest, as well as the headquarter of human body brain and, and skeletal muscles may make highest contribution to heat production when doing excise (McCall, 2010; Sherwood, 2011).

Skin temperature distribution may vary with each individual's height, weight, age, gender, skin color, and body fat. The seasonal and environmental changes result in skin temperature fluctuation. The internal metabolic rate, human body structure, tissues properties and heat transferring mechanism may affect the skin temperature map (Sherwood, 2011; Wright, 2000). Skin temperature ranking of different body parts and weighting systems of mean skin temperature had been emphasized by many researchers with different protocol and methods (Jones & Plassmann, 2002; Ramanathan, 1964; Young, Hand, Oatridge & Prior, 1994). Skin temperature is a medical diagnose signal for diseases and chronic disorders of human body (Barnes, 1963; Wunderlich, 1871).

Clothes are the covering of human body, like the second skin. On the basis of thermal function previously mentioned, clothing may has vital importance and great potential to have more functions and donations to human health

#### **Thermal Function and Clothing**

These microenvironment bridges human body and out environment. Clothing physiological researchers have been trying to know the theory mechanism and necessarily taking the relationship between thermal function and clothing as first priority for years (Gonzalez & Sawka, 1988; Newburgh, 1950; Renbourn & Rees, 1972). Numerous thermal models and mannequins had been designed based on the heat generation balance principles and tried to predict and simulate human body physiological reaction to clothing and outer environment (Huizenga, Hui, & Arens, 2001; Li, Li, Liu, & Luo, 2004). Functional thermal clothing had been developed to protect human body from unusual environment and occasions (Buijs & Oosten, 1997; Nelson & Henry, 2000; Sheffield, 2013; Shishoo, 2005; Stanton, 1998), for instance fire-protection suit, Arctic clothing, army uniform, space suits, sportswear, etc.

Among the recent developments, new class of materials such as functional and intelligent materials has been introduced. These smart materials together with other technology such as sensors have been used to make smart and intelligent clothing. The garment construction can make use of elements that bringing flexible functional properties to broaden their utility range. Sensors and electronics can be incorporated monitor the user's physiological state, the environment conditions etc (Mattila, 2006).

For normal people and their ordinary life, is it possible to design new thermal function clothing or products, for medical usage such as diseases monitoring and chronic disorders' rehabilitation? What tools may be needed for these kind of functional design? How to provide accurate and fast design tool for functional designs from the viewpoint of customization and mass-production? The questions may not be answered in one word but can rouse the brand new thinking for design concept cultivation and design tools development. Design should be with a view to future. It's necessary to ascertain the prospective design tool for fashion industry. Human models, the linkage of designers and users may be a feasible exploration.

### 3D HUMAN MODEL APPLIED TO COMPUTER-AIDED-DESIGN FASHION DESIGN SYSTEM

#### **CAD** in Fashion Industry

The clothing industry has been changed profoundly in recent years. Globalization, speed of information and communication has stimulated competition. While manufacturers offer unlimited designs, the problem is how to bring products to the market quickly and achieve up-to-date information that is easily obtainable. Fashion CAD systems are now the essential tools required to integrate and achieve success taking the role of the configuration between manufacture and retail. Utilizing a full range of electronic tools, the powerful CAD systems can deliver

clothing at relatively short cycles. Integration and communication utilizing the internet become the new systems designed to achieve this (Beazley & Bond, 2003; Burke, 2006; Pundir, 2007).

Some typical commercial software include Toray-Acs (Japan), Gerber (USA), PGM (USA), Investronica (Spain), Lectra (France), Asahi Kasei (Japan), PAD (Canada), Nac (China), Iecho (China), Arisa (China), Richforever (China), Tupo (China), Docad (China), Syscad (China), ET (China), Right-hand (China), Bili (China), Modasoft (China) are popularly used by the industry and creating efficiency every day. From fashion design, patternmaking to grading, and then to marker, cutting, the fashion CAD system integrated with CAM (Computer Aided Manufacturing) fulfills the whole process of the making of fashion products. Fashion style design, its computer aided design process depends on 3D human model which demonstrating the body shape, dimension and even size messages to designers. These kinds of human models are usually in a geometric format.

Furthermore, 3D CAD is gradually emerging to the fashion design and manufacturing applications. It may be anticipated that 3D design tools will be the next evolving technology for the apparel industry. The ultimate goal is to design and produce customized clothing for individuals, and the 3D approach is the most adaptable approach to make it come into reality (Wang & Yuen, 2005). 3D geometry model developed from 3D body scanner or 3D design software are the main stream to join the 3D design and manufacturing in fashion industry. The trendy and leading techniques in this area include 2D pattern generation from 3D space and 3D draping simulation or called virtual tryon clothing.

#### 2D Pattern Generation from 3D Space

Interactively design can be done to achieve 3D garment with the flattening 3D shape to 2D pattern (3D-2D process) (McCartney, Hinds, Seow, & Gong, 2000). 2D pattern design systems have been used to help designers simplify their work for many years and a looking into 3D features has just been started (Fontana, Rizzi, & Cugini, 2005). Wang's system constructs garments directly in 3D space and then flattens the designed 3D surfaces to obtain 2D patterns (Wang, Wang, & Yuen, 2003). These patterns, however, may not yet directly be adopted for industrial use (Wang, Smith, & Yuen, 2002). Hu et al. employed pattern expert's knowledge to control the process of clothing design with interacting process (Hu, Ding, Zhang, & Yan, 2008). Their system supports collaboration between designers and experiences.

Fuhrmann et al. (2003) proposed another interaction method by geometric pre-positioning of single pieces of clothing patterns with respect to a human body. This approach makes use of developable surfaces such as cylinders or cones, to position clothing patterns around the virtual human. A purely geometrical method was proposed to put clothes on 3D virtual characters by operating clothing on digital human body surfaces (Igarashi & Hughes, 2003). Cho developed a method of individual pattern making method by modifying a traditional draping system with five steps, including defining the surface shape, setting grain lines, fitting the fabric to the surface shape, cutting of the three dimensional surfaces and developing the three dimensionally fitted fabric into 2D patterns. This method was used to make patterns for a tight-fit skirt and could easily create patterns automatically (Cho et al., 2006). To do pattern flattening, material properties had been taken into account which was motivated by the mathematical properties of developable surfaces (Carmo, 1976).

These approach combines the whole process of garment design and display with user interaction, and their work have great contribution to speed up 3D pattern design approach for industrial application. Some commercial software of 3D garment systems had started their industrial trial, such as Assyst-Bullmer (German), Dessingsim (Japan) and LookStailorX (Japan). 3D geometric human model is commonly used in the 2D pattern generation from 3D space process.

#### 3D Draping Simulation/Virtual Try-On Clothing

The research interest of computer graphics had been shown to clothing simulation in the late 1980s and output has bloomed since then. Terzopoulos and his team would be the pioneer to use physical models for cloth simulation (Terzopoulos & Barr, 1987). Zhou et al. had investigated the structure of woven fabrics and simulated its mechanical behavior based on the thin-shell theory (Zhou, Jin, & Wang, 2008a). They also proposed a novel physical model to solve the vibration problem from large rotation (Zhou, Jin, & Wang, 2008b). Their technique can work well with major methods for simulating internal dynamics. Meng and his colleagues brought forward a method by using a geometrical scheme by correction of position to handle collision response, which ensured good stability of simulation without re-computation of dynamic equations (Meng, Mok, & Jin, 2010). Other progress can be reached in (Choi & Ko, 2005), and some textbooks have even been written (House & Breen, 2000; Volino &

Magnenat-Thalmann, 2000). In these 3D draping systems, human models, also called avatars, have been developed and garments can be virtually tried on these model (Kang & Kim, 2000a; Yang, Magnenat Thalmann, & Thalmann, 1992; Zhang, Hou, Zhou, & Yoshio, 2000). The 3D shape of a garment can be estimated by sewing its 2D pattern up on a 3D mannequin (2D-3D process) (Fan, Newton, Au, & Chan, 2001; Kang & Kim, 2000b; Okabe, Imaoka, Tomiha, & Niwaya, 1992).

Commercial fashion CAD software have integrated this function to, such as Gerber, Lectra and PAD. Pad's modular-based software allows 2D patterns to be modified by following sew points. The draping appearance on a digital human model can be created with fabric models and can be linked to measurement data. Gerber's draping system provides the functions to verify fit and ease allowance. The modification results in either 2D or 3D model can be quickly realized and displayed based on 3D human model. The advanced technologies on internet, intranet and virtual reality allow Lectra to incorporate pattern design module with E-Design, E-Manufacturing, E-Sales and Lectra on-line, which may help the users fast react from market need and design. The system makes it become possible to watch garment collection on a virtual reality catwalk.

3D geometric human model is a key component to support the computer-aided 3D fashion design and manufacturing, which is becoming the trendy efficient tool. For thermal functional clothing development, a thermal human model is essential to be created serving as an effective design tool. In the following part, the thermal modeling process will be introduced and illustrated by steps.

#### THERMAL HUMAN MODELLING

#### **Experiment and Data Pre-Processing**

The developments of medical imaging and anthropometry technology, an in-depth and specific foundation have been taken to further understanding human body in physical and medical aspects. This has enabled the development of thermal human models for function clothing design. In this study, under thermoneutral condition (temperature:  $24\pm1^{\circ}$ C, relative humidity:  $60\pm5\%$ ), male and female subjects at rest had been scanned by a 3D body scanner system in a naturally standing gesture. Surface data of human body have been collected in a digital format, which will help to set up the basic geometric model (G-model) from cloud point data of scanned human body. The noninvasive thermography technique have been adopted by an infrared camera to capture thermal imaging which can record the skin temperature distribution of subjects in real time.

To put all the 3D human body in the same coordinate system and run modeling function synchronously, the original G-model after scanning need to be alignment by mathematical and statistical methods, such as principle component methods (Luximon & Chao, 2013). Most of the 3D body scanned data may possibly be noised by the environment and should be cleaned and smoothed by 3D software such as Rapidform and Meshlab or using algorithm methods such as Adaptive Moving Least Squares method (Dey & Sun, 2005). The aligned and cleaned human body will enhance the quality of thermal modeling, which is shown in Figure 1.





Thermal imaging records real skin temperature distribution of human body. These kind of invisible information may be captured by IR camera and presented in images. In thermal human modeling process, the IR data pre-processing assists to understand temperature's distribution and features of subjects by mathematical plotting methods such as Matlab software. Different temperature range and color palettes can be set to display the temperature information. In Figure 2, the subject's IR images have been pre-processed in a 'Jet' palette with a temperature range of 29°C to 36°C, from front and back side. Red and yellow is the relatively high temperature, blue and green represents the low temperature. The data plotting technology is necessary to interpret the biological messages with various functions.

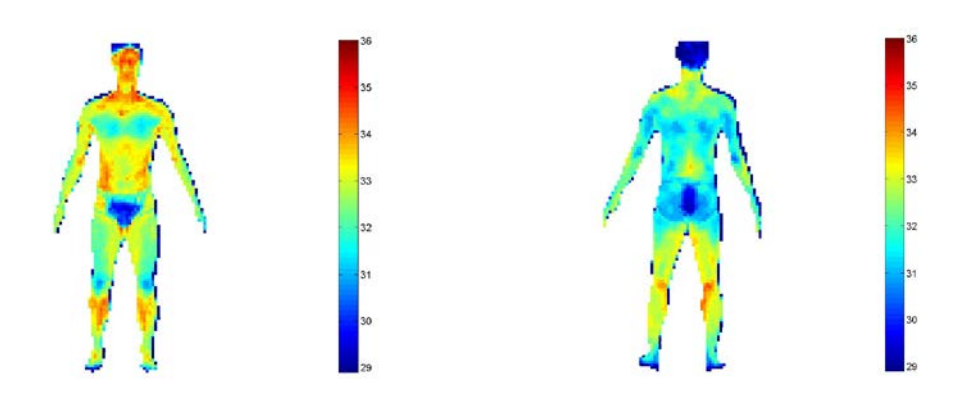


Figure 2. Pre-processed IR data: front and back

#### **Modeling Process**

Corresponding points should be sorted out between IR image and G-model. In this study, 28 sets of points were selected for both front and back view. As human body has unique and symmetrical shape, characteristic points should be selected to make sure the exact mapping from 2D IR picture and 3D human model. The distribution of these points may cover all the featured position in the profile of human body. For example, anatomical points in forehead, chin, acromion, arm pit, crotch, knee cap, back of knee, ankle, cubital fossa, elbow, wrist would be chosen. The only body covering underwear has obvious lines to be observed, which also should be highlighted. In the mapping process, the closer corresponding relationship is set, the better matching would be.

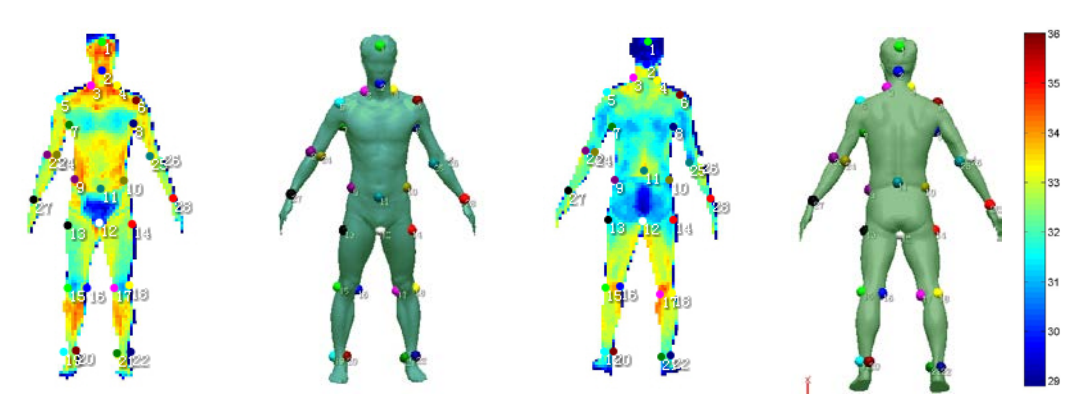


Figure 3. Corresponding points of IR picture and 3D geometric model: front and back

#### **Results and Discussions**

Utilizing 3D design software, such as Rapidform, or mathematical programming with Matlab software, the thermal human model (T-model) can be achieved, see Figure 4. The skin temperature data of subjects were transferred to exact 3D human body, the temperature distribution and features can be clarified easily for design and manufacturing process. The T-model has been created, including both accurate human body's dimensional data and real subjects'

skin temperature distribution. It may be optimistically conclude that the thermal functional model can be constructed and realized by means of effective experiment design and latest thermal imaging technologies. Due to human body's complicated shape, as well as the accuracy limitation with current facilities, some minor parts of the mapping may not be perfect which would be polished in further research.

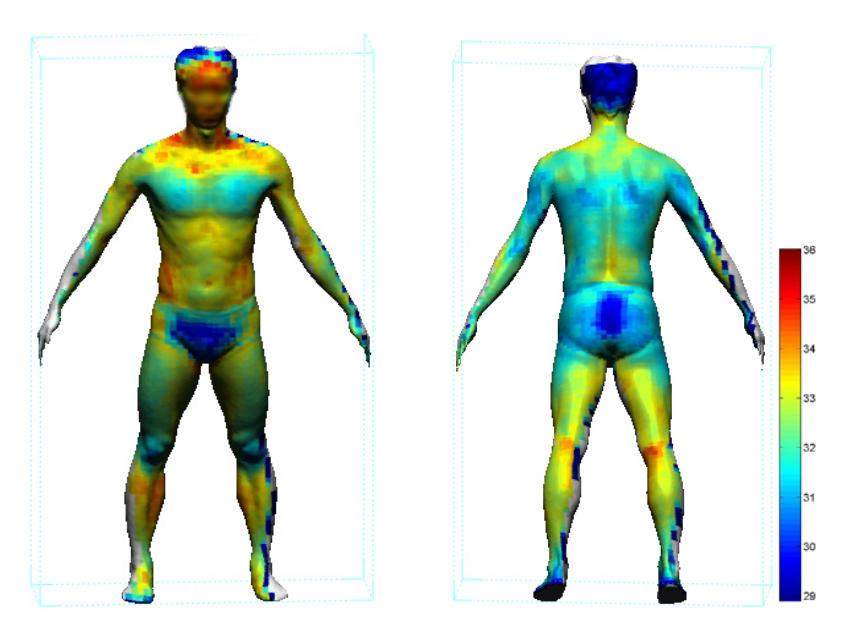


Figure 4. T-model: front and back

#### **CONCLUSIONS**

Multidisciplinary studies lead innovations and revolutions. Comparing to single, isolated dimensional information presented by traditional geometric models, T-model reproduce both spatial information and real thermal characters of human body, which is groundbreaking to understand skin temperature of human body from a visualized, quantitative and practical aspect. That means, when the fashion insiders use T-model for functional clothing development, they will easily find out the precise position of high skin temperature or low skin temperature areas and the accurate size of the skin temperature areas, which will greatly upgrade the accuracy and efficiency of functional thermal design and implement using 2D and 3D software for patternmaking, pattern revision, virtual fitting and grading. Furthermore, as an potential useful design tool, a digital T-model can be further developed into an estimative mannequin by means of 3D printing or other mannequins making techniques. Functional human model is a new thinking for fashion and functional product development. The method to create T-model is a concept display. More details should be considered to improve this model and more ideas would be actualized in further research work.

#### **REFERENCES**

Barnes, R. B. (1963). Thermography of the Human Body Infrared-radiant energy provides new concepts and instrumentation for medical diagnosis. Science, 140(3569), 870-877.

Beazley, A., & Bond, T. (2003). Computer-aided pattern design and product development: Blackwell Pub.

Benzinger, T., Pratt, A., & Kitzinger, C. (1961). The thermostatic control of human metabolic heat production. Proceedings of the National Academy of Sciences of the United States of America, 47(5), 730.

Bijlani, R. L., & Manjunatha, S. (2010). Understanding Medical Physiology: A Textbook for Medical Students: Jaypee Bros. Medical Publishers.

Blatteis, C. M. (1998). Physiology and Pathophysiology of Temperature Regulation: World Scientific.

Buijs, C., & Oosten, J. G. (1997). Braving the Cold: Continuity and Change in Arctic Clothing: Research School

CNWS, School of Asian, African, and Amerindian Studies.

Burke, S. (2006). Fashion Computing: Design Techniques and CAD: Burke Publications.

Carmo, M. P. D. (1976). Differential Geometry of Curves and Surfaces. Englewood Cliffs, NJ: Prentice-Hall,.

Cena, K., & Clark, J. A. (1981). Bioengineering, Thermal Physiology and Comfort: Elsevier Science.

Chintala, G. (2011). Trends in CAD/CAM: To Capture Global Markets: Lambert Academic Publishing.

Cho, Y., Komatsu, T., Inui, S., Takatera, M., Shimizu, Y., & Park, H. (2006). Individual pattern making using computerized draping method for clothing. Textile Research Journal, 76(8), 646-654.

Choi, K.-J., & Ko, H.-S. (2005). Research problems in clothing simulation. Computer-Aided Design, 37(6), 585-592.

Dey, T. K., & Sun, J. (2005). An Adaptive MLS Surface for Reconstruction with Guarantees. Paper presented at the Symposium on Geometry Processing.

Eysenck, M. W. (2004). Psychology: An International Perspective: Psychology Press.

Fan, J., & Hunter, L. (2009). Engineering Apparel Fabrics and Garments: Elsevier Science.

Fan, J., Newton, E., Au, R., & Chan, S. C. F. (2001). Predicting Garment Drape with a Fuzzy-neural Network. Textile Research Journal, 71(7), 605-608.

Fletcher, K. (2008). Sustainable Fashion and Textiles: Design Journeys: Earthscan.

Fontana, M., Rizzi, C., & Cugini, U. (2005). 3D virtual apparel design for industrial applications. Computer-Aided Design, 37(6), 609-622.

Fourt, L. E., & Hollies, N. R. S. (1970). Clothing; Comfort and Function: M. Dekker.

Fuhrmann, A., Groß, C., Luckas, V., & Weber, A. (2003). Interaction-free dressing of virtual humans. Computers & Graphics, 27(1), 71-82.

Gonzalez, R. R., & Sawka, M. (1988). Biophysics of heat transfer and clothing considerations. Human performance physiology and environmental medicine at terrestrial extremes, 45-95.

Goyal, M. R. (2013). Biofluid Dynamics of Human Body Systems: Apple Academic Press.

Gray, S. N. (1998). Cad/Cam in Clothing and Textiles: Design Council.

Hall, J. E. (2010). Guyton and Hall Textbook of Medical Physiology: Enhanced E-book: Elsevier Health Sciences.

Heymsfield, S. (2005). Human Body Composition: Human Kinetics.

Hollies, N. R. S., & Goldman, R. F. (1977). Clothing comfort: interaction of thermal, ventilation, construction, and assessment factors: the Fiber Society, Inc. Comfort Symposium proceedings: Ann Arbor Science Publishers.

House, D., & Breen, D. E. (2000). Cloth modeling and animation: A K Peters.

Hu, Z.-H., Ding, Y.-S., Zhang, W.-B., & Yan, Q. (2008). An interactive co-evolutionary CAD system for garment pattern design. Computer-Aided Design, 40(12), 1094-1104.

Huizenga, C., Hui, Z., & Arens, E. (2001). A model of human physiology and comfort for assessing complex thermal environments. Building and Environment, 36(6), 691-699.

Igarashi, T., & Hughes, J. (2003). Clothing manipulation. Paper presented at the Proceedings of the 15th ACM symposium on user interface software and technology.

Jayaraman, S., Kiekens, P., & Grančarić, A. M. (2006). Intelligent textiles for personal protection and safety: IOS Press.

Jessen, C. (2001). Heat Production and Heat Balance of the Body Temperature Regulation in Humans and Other Mammals (pp. 27-36): Springer.

Johnson, L. R., & Byrne, J. H. (2003). Essential Medical Physiology: Academic Press.

Jones, B., & Plassmann, P. (2002). Digital infrared thermal imaging of human skin. Engineering in Medicine and Biology Magazine, IEEE, 21(6), 41-48.

Kang, T. J., & Kim, S. M. (2000a). Development of three-dimensional apparel CAD system Part 1: Flat garment pattern drafting system. International Journal of Clothing Science and Technology, 12(1), 26-38.

Kang, T. J., & Kim, S. M. (2000b). Development of three-dimensional apparel CAD system Part II: Prediction of garment drape shape. International Journal of Clothing Science and Technology, 12(1), 39-49.

Li, Y., Li, F., Liu, Y., & Luo, Z. (2004). An integrated model for simulating interactive thermal processes in human–clothing system. Journal of Thermal Biology, 29(7), 567-575.

Luximon, A., & Chao, H. (2013). Shape Modeling: From Linear Anthropometry to Surface Model. Paper presented at the ACHI 2013, The Sixth International Conference on Advances in Computer-Human Interactions

Malan, A., & Canguilhem, B. (1989). Living in the Cold: 2nd International Symposium: Proceedings of the Second Symposium on Living in the Cold, Held in Le Hohwald (France), April 23-29, 1989: John Libbey.

Marino, F. E. (2008). Thermoregulation and Human Performance: Physiological and Biological Aspects: Karger.

Mattila, H. R. (2006). Intelligent Textiles And Clothing: Woodhead Publishing Limited.

McCall, R. P. (2010). Physics of the Human Body: Johns Hopkins University Press.

McCartney, J., Hinds, B. K., Seow, B. L., & Gong, D. (2000). Dedicated 3D CAD for garment modelling. Journal of Materials Processing Technology, 107(1-3), 31-36.

Meng, Y., Mok, P. Y., & Jin, X. (2010). Interactive virtual try-on clothing design systems. Computer-Aided Design,

- 42(4), 310-321.
- Nelson, C. N., & Henry, N. W. (2000). Performance of Protective Clothing: Issues and Priorities for the 21st Century. Seventh volume: ASTM.
- Newburgh, L. (1950). Physiology of heat regulation and the science of clothing. Academic Medicine, 25(2), 158.
- Okabe, H., Imaoka, H., Tomiha, T., & Niwaya, H. (1992). Three dimensional apparel CAD system. Computer Graphics (ACM), 26(2), 105-110.
- Volino, P., & Magnenat-Thalmann, N. (2000). Virtual Clothing: Theory and Practice: Springer.
- Parsons, K. (2002). Human Thermal Environments: The Effects of Hot, Moderate, and Cold Environments on Human Health, Comfort and Performance, Second Edition: Taylor & Francis.
- Piantadosi, C. A. (2003). The Biology of Human Survival: Life and Death in Extreme Environments: Life and Death in Extreme Environments: Oxford University Press, USA.
- Pundir, N. (2007). Fashion Technology: Today and Tomorrow: Mittal Publications.
- Ramanathan, N. (1964). A new weighting system for mean surface temperature of the human body. Journal of applied physiology, 19(3), 531-533.
- Renbourn, E. T., & Rees, W. H. (1972). Materials and clothing in health and disease: history, physiology and hygiene: medical and psychological aspects: HK Lewis.
- Sheffield, C. (2013). Space Suits: Being the Selected Legal Papers of Waldo Burmeister and Henry Carver, Attorneys-At-Law: Orion.
- Sherwood, L. (2011). Fundamentals of Human Physiology: Cengage Learning.
- Shishoo, R. (2005). Textiles in Sport: Elsevier Science.
- Song, G. (2011). Improving Comfort in Clothing: Elsevier Science.
- Stanton, S. L. (1998). U.S. Army Uniforms of the Cold War, 1948-1973: Stackpole Books.
- Stott, M. (2012). Pattern Cutting for Clothing Using CAD: How to Use Lectra Modaris Pattern Cutting Software: Elsevier Science.
- Terzopoulos, J. C. P., & H. Barr. (1987). Elastically deformable models. ACM SIGGRAPH 1987, 205-214.
- Timby, B. K. (2009). Fundamental Nursing Skills and Concepts: Wolters Kluwer Health/Lippincott Williams & Wilkins.
- Wang, C. C. L., Smith, S. S. F., & Yuen, M. M. F. (2002). Surface flattening based on energy model. CAD Computer Aided Design, 34(11), 823-833.
- Wang, C. C. L., Wang, Y., & Yuen, M. M. F. (2003). Feature based 3D garment design through 2D sketches. Computer-Aided Design, 35(7), 659-672.
- Wang, C. C. L., & Yuen, M. M. F. (2005). CAD methods in garment design. Computer-Aided Design, 37(6), 583-584.
- Wang, R. (2007). CAD Technology for Clothing Biomechanical Engineering Design: Hong Kong Polytechnic University (Hong Kong).
- Wang, S. (2008). Intelligent Thermal Protective Clothing: Hong Kong Polytechnic University (Hong Kong).
- Weller, A. S. (2005). Body temperature and its regulation. Anaesthesia & Intensive Care Medicine, 6(6), 206-209.
- Werner, J. (1980). The concept of regulation for human body temperature. Journal of Thermal Biology, 5(2), 75-82.
- Werner, J., & Buse, M. (1988). Temperature profiles with respect to inhomogeneity and geometry of the human body. Journal of applied physiology, 65(3), 1110-1118.
- Wilmore, J. H., Costill, D. L., & Gleim, G. W. (1995). Physiology of sport and exercise. Medicine & Science in Sports & Exercise, 27(5), 792.
- Wright, D. B. (2000). Human Physiology and Health: Pearson Education.
- Wunderlich, C. A. (1871). On the Temperature in diseases: The New Sydenham society.
- Yang, Y., Magnenat Thalmann, N., & Thalmann, D. (1992). Three-dimensional garment design and animation: A new design tool for the garment industry. Computers in Industry, 19(2), 185-200.
- Young, I. R., Hand, J. W., Oatridge, A., & Prior, M. V. (1994). Modeling and observation of temperature changes in vivo using MRI. Magnetic resonance in medicine, 32(3), 358-369.
- Zhang, M., Hou, D., Zhou, A., & Yoshio, S. (2000). Three Dimensional Simulation and Pattern Making of Collar Using Geometric Model. Journal of DongHua University, 18(3), 53-57.
- Zhou, C., Jin, X. G., & Wang, C. L. (2008a). Efficient and stable simulation of cloth undergoing large rotations. Computing in Science & Engineering, 10(4), 30-40.
- Zhou, C., Jin, X. G., & Wang, C. L. (2008b). Shear buckling and dynamic bending in cloth simulation. Computer Animation and Virtual Worlds 19(3), 493-503.

# A Facial Mask Study for Chinese Female

Yan Luximon a and Yan Cong b

<sup>a</sup> School of Design The Hong Kong Polytechnic University Hung Hom, Kowloon, Hong Kong

<sup>b</sup> Institute of Textiles & Clothing The Hong Kong Polytechnic University Hung Hom, Kowloon, Hong Kong

# **ABSTRACT**

Facial mask, an essential product for skincare, has become a part of daily life for female population. Existing facial mask design has a lot of misfits including missing regions, corrugation and misplacement. There is a need to build a relationship between a 3D face shape and a 2D mask template. An accurate 3D face model and anthropometric measurements are initial steps to design of masks. 3D surface flattening is a method to generate 2D patterns and is widely used to trim materials in garment and footwear industry. In this study, a manual generation of 2D flat pattern from a set of 3D Chinese female face models was described. Facial mask templates with different sizes and cuts were produced and evaluated. The results revealed that sizing dimensions mainly differed in the width for different face models. In addition, the location and area for eye and mouth regions had a relatively large deviation and therefore it should be paid more attention in the mask design. This study provided more insights into the relationship between 2D flat pattern and 3D face shape. The results were expected as a reference for facial mask design and improve its quality to fit.

Keywords: 3D Surface Flattening, Facial Mask, Anthropometric Measurement, Head and Face

#### INTRODUCTION

Healthy skin is an important fight sign of aging and has the ability to enhance people's physical appearance and esthetic appeal. As skincare craze is sweeping the world, markets of facial masks are exuberant. The shapes for existing facial mask products have large variations within and among brands (Figure 1). Manufacturers design the mask shapes without uniform standards or scientific statistical information of the human face. Poor fitting seems to be a common problem for most of facial mask products. Such masks will be unable to be attached firmly onto the face and will inhibit the absorption of the essence by the skin. Therefore the efficiency of masks will be reduced.

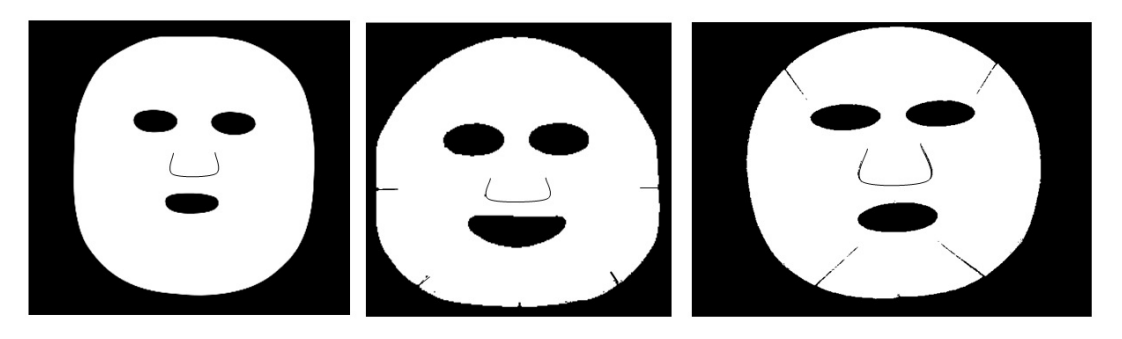


Figure 1. Examples of various facial masks

Accurate anthropometric measurement for head and face is the first step to design a high quality of fit mask. Traditional head and face anthropometric measurements are conducted directly on living subjects. More than 200 measurements, including distance, circumference and angles, were indentified based on the landmarks visually on people's faces (Farkas, 1994; Kolar and Salter, 1997; Du et al., 2008). However, these 1D measurements were time-consuming and lack of 3D information. With the advance of 3D scanning techniques, the individualized 3D surface contours of human body shape can be easily captured in a fast, non-invasive and accurate way (Robinette et al., 2002; Azouz et al., 2006; Luximon et al., 2009; Xi and Shu, 2009). A set of software and CAD design tools were further developed to automatically analyze the dimensional data and assist the product design (Luximon et al., 2011). The method based on 3D scanning and CAD techniques provides more information on the 3D shape of human head and was used to develop the head and face product designs such as helmet shells (Liu et al., 2008) and spectacle frames (Kouchi and Mochimaru, 2004). This method therefore provides an opportunity to develop the facial mask design.

While the accurate 3D model of head and face provides an important reference to develop the mask shape, it does not work well to create the texture atlas for the designer and manufacturer. 3D surface flattening is to map a 3D surface onto a 2D plane. This method is critical to create a texture atlas and is widely used to trim the materials in shoe and garment industry (Jing et al., 2005; Liu et al., 2010). The 3D surface flattening will determine the shape, accurate boundaries, and the positions of cutting lines of mask materials in order to fit the contour of the face well. However, this method has not been well documented in facial mask design. The relationship between 2D flattened fabric and 3D face contour has not been understood in detail.

This study aimed to develop a flattening method to improve facial mask design based on 3D Chinese face model. Proper facial mask templates for Chinese female were expected to guide mask manufacture with accurate dimensions and locations of eyes, mouth and nose.

#### **METHODS**

#### **3D** Chinese female face models

In order to improve the fit of facial mask design for Chinese female, an accurate anthropometric model is needed. SizeChina database has more than 2000 3D head scans collected in China (Ball et al., 2012). A set of FACEFORMs of Chinese female with different sizes have been created using SizeChina database (Luximon and Ball, 2012). A parameterized modeling method was used to create those face models (Luximon et al., 2012). The measure of face breadth was used as a main reference when calculating the face models. All selected scans were set for three categories (5%tile, 50%tile and 95%tile) in terms of face breadth for model creation. Figure 2 shows the models in 5%tile and 95%tile which represent the small and the large sizes of Chinese female's face. Two physical models were printed by the rapid prototyping machine and were used as the bases to create 2D flattened face templates in this study.







(b) Large size

Figure 2. Faceforms for Chinese female

# Template design

The traditional process to generate 2D flat patterns in footwear industry was followed to create the 2D patterns from two 3D face models. The paper tape was first attached on the printed face models. The locations of eyes, mouth and nose were marked down carefully. Then, the tapes were manually cut and flatten on the board to get the 2D patterns. The flattened patterns were further corrected to symmetric design considering manufacturing requirements. Several facial masks materials with different thicknesses were also tested for minor correction of templates.

In order to identify the boundaries of the facial mask and the locations of eyes, mouth and nose, dimensions representing these characteristics were defined on the patterns as Figure 3. These dimensions were proposed based on designer's suggestions and user's feedbacks. To remove the fabric distortion and obtain a fitting template, different cut patterns were tried including different positions, directions, amounts and lengths of cutting lines.

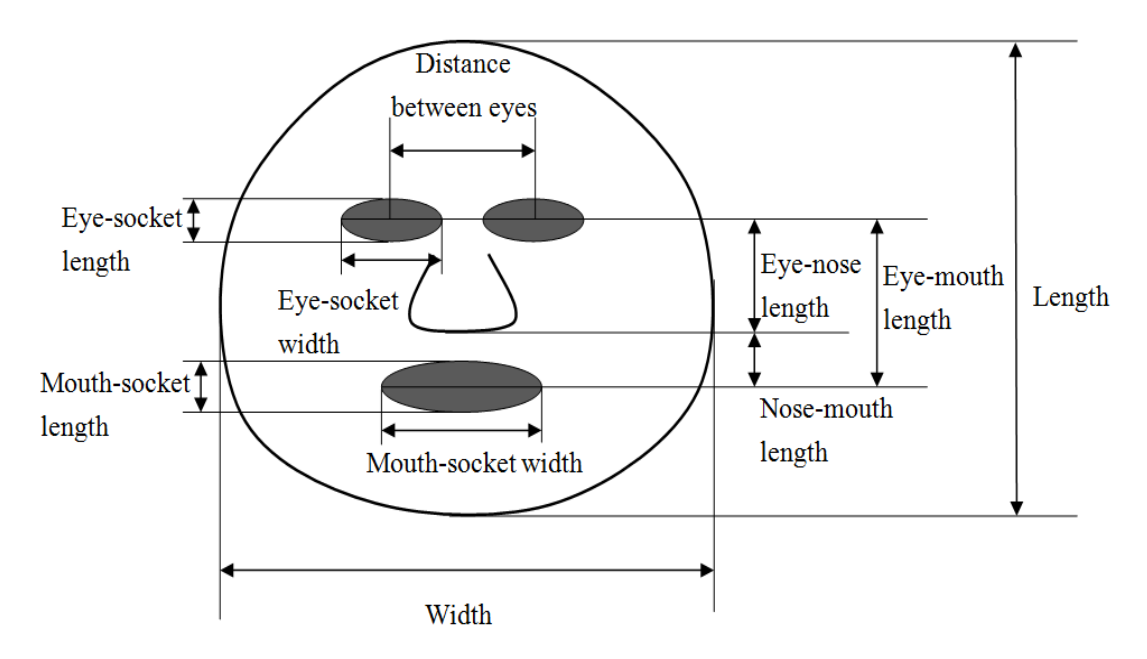


Figure 3. Dimensions of facial mask

#### RESULTS

Figure 4 shows preliminary facial mask templates with appropriate cut patterns and dimensions. There are few special features for the new templates. New templates had shorter length especially at chin region, but wider at jaw region. New templates had less cutting lines than the current products in the market, especially at the forehead region. The cutting lines were almost vertical and located at the lower face region. Another difference was of the two small cutting lines which were located at the bottom of ala of nose. This cut pattern can efficiently remove the fabric distortion and make the mask more fit to the face contour. In addition, the nose cutting line was much wider and the distances between eyes were much larger comparing to normal masks. The cutting lines were closely related to the face shapes. The flattened facial masks were corresponding to previous results which found that Chinese female had wider face and interpupillary distance, bigger jaw and smaller chin than Western female (Luximon et al., 2010).

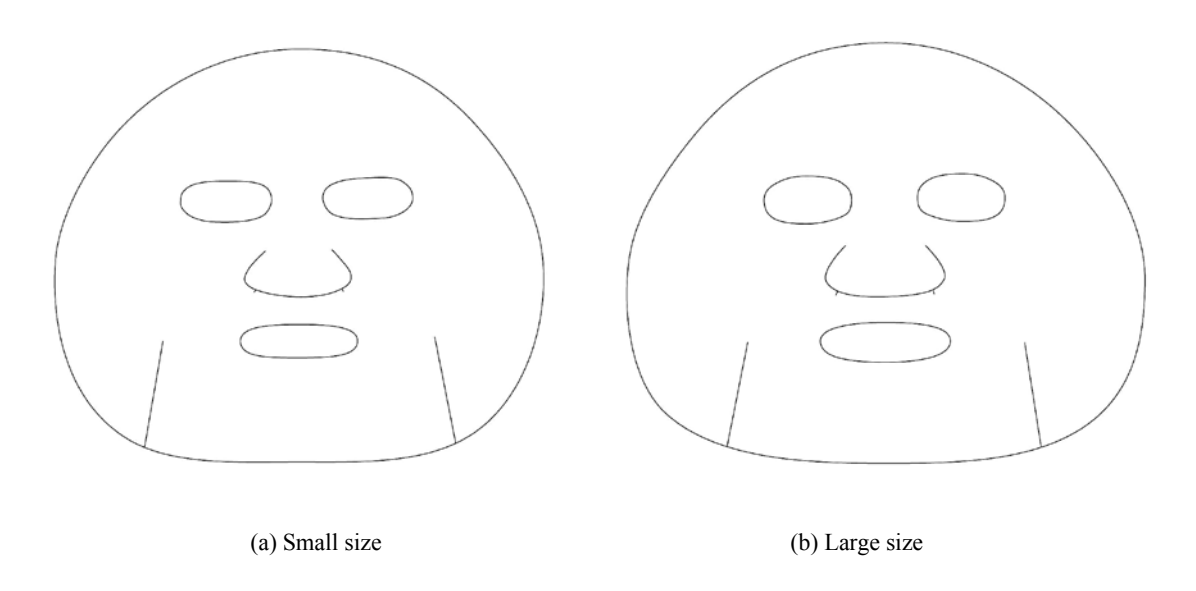


Figure 4. Facial mask templates for different sizes

Mask dimensions and locations of eyes, nose and mouth in the template were measured as the definitions in Figure 3. It was found that the dimensions were mainly different in the width measures for different face sizes. The template width of the large size was 14.6mm (5.9%) greater than that of the small size. The distance between eyes had a large variation among different face sizes and the distance increased by 5.8mm (8.1%) for the large face template. The variance of eye sockets was also large, especially for its length, which increased by 3.1mm (14.8%) compared with the small face template. Although the designs for eye sockets had a significant difference among different face sizes, the differences of locations and shapes for nose region were small. The difference for eye-nose length was only 0.8%. Another large difference was found at the mouth region. The nose-mouth length of the large face template increased by 0.7mm (3.1%) compared to the small size template. The mouth socket also had a larger area for the large face template. The differences for the mouth socket width and length were 6.3mm (10.7%) and 3.1mm (18.5%), respectively.

#### **CONCLUSIONS**

In this study, a manual generation of 2D flat pattern from 3D face model has been described. Based on this method, a set of facial mask templates with different cutting patterns were developed. These templates provided the important references such as the dimensions and cutting line designs for mask manufactories to improve the quality of mask fit, especially for Chinese female. The results can be not only used for facial mask designs, but also further used for medical purpose such as scald treatment. Minor adjustment might be needed for different types of non-woven materials or other materials. Future study could be conducted to find out the allowance when considering material properties.

Although manually designing a 2D pattern can provide more insight into the development of the mask fit, the method is complicated and time-consuming, requiring a specialized craft. Therefore, the method is not suitable for individual design in a faster and more experience-independent way. With the development of computer technology, flattening simulation using CAD allows releasing the heavy dependencies on experience in manual design and is thought as an alternative solution to non-expert users. An automatic generation of 2D flat pattern from 3D human head and face model based on CAD method could be developed in the future work.

#### **ACKNOWLEGEMENT**

This work was supported by the Departmental General Research Fund (DGRF) from the Hong Kong Polytechnic University (G-UB41).

#### REFERENCES

- Azouz, Z.B., Rioux, M., Shu, C., Lepage, R. (2006), "Characterizing human shape variation using 3D anthropometric data", THE VISUAL COMPUTER Volume 22 No. 5. pp. 302-314.
- Ball, R.M., Luximon, Y., Chow, H.C.E. (2012), "Anthropometric Study on Chinese Head", PROCEEDING OF ASIAN WORKSHOP ON 3D BODY SCANNING TECHNOLOGIES, April 17-18, Tokyo, Japan.
- Du, L., Zhuang, Z., Guan, H., Xing, J., Tang, X., Wang, L., Wang, Z., Wang, H., Liu, Y., Su, W., Benson, S., Gallagher, S., Viscusi, D., Chen, W. (2008), "Head-and-Face Anthropometric Survey of Chinese Workers", ANNALS OF OCCUPATIONAL HYGIENE Volume 52 No. 8. pp. 773-782.
- Farkas, L.G. (1994), "Anthropometry of the head and face", 2nd edition. New York: Raven Press.
- Jing, F., Joneja, A., Tang, K. (2005), "Modeling wrinkles on smooth surfaces for footwear design", COMPUTER-AIDED DESIGN Volume 37, pp. 815-823.
- Kouchi, M., Mochimaru, M. (2004), "Analysis of 3D face forms for proper sizing and CAD of spectacle frames", ERGONOMICS Volume 47 No. 14. pp. 1499-1516.
- Kolar, J.C., Salter, E.M. (1997), "Craniofacial anthropometry: practical measurement of the head and face for clinical, surgical and research use", Springfield, Illinois, USA: Charles C Thomas.
- Liu, H., Li, Z., Zheng, L. (2008), "Rapid preliminary helmet shell design based on three-dimensional anthropometric head data", JOURNAL OF ENGINEERING DESIGN Volume 19 No. 1. pp. 45-54.
- Liu, Y., Zhang, D., Yuen M.M. (2010), "A survey on CAD methods in 3D garment design", COMPUTERS IN INDUSTRY Volume 61. pp. 576-593.
- Luximon, Y., Ball, R.M., Justice, L. (2010), "The Chinese face: a 3D anthropometric analysis", PROCEEDING OF TMCE2010, April 12-16, Ancona, Italy.
- Luximon, Y., Ball, R.M., Chow, H.C.E. (2011), "Facefinder: An online anthropometric tool for Chinese design". PROCEEDING OF THE 8<sup>TH</sup> INTERNATIONAL SHIBORI SYMPOSIUM TECHNOLOGY SHAPED BY CREATIVITY, December 28-31, Hong Kong.
- Luximon, Y., Ball, R.M., Justice, L. (2012), "The 3D Chinese head and face modeling", COMPUTER-AIDED DESIGN Volume 44 No. 1. pp. 40-47.
- Luximon, Y., Ball, R.M. (2012), "Faceforms: A 3D design tool for Chinese", PROCEEDING OF THE INTERNATIONAL TEXTILE & APPAREL SUSTAINABILITY CONFERENCE (ITASC2012), July 16-21, Mauritius.
- Robinette, K., Blackwell, S., Daanen, H., Fleming, S., Boehmer, M., Brill, T., Hoeferlin, D., Burnsides, D. (2002), "Civilian American and European Surface Anthropometry Resource (CAESAR)". Final Report. In: SUMMARY, AFRL-HE-WPTR-2002-0169 vol. I. Air Force Research Laboratory, Human Effectiveness Directorate, Bioscience and Protection Division, 2800 Q Street, Wright-Patterson, AFB OH 45433-7947.
- Xi, P., Shu, C. (2009), "Consistent parameterization and statistical analysis of human head scans", THE VISUAL COMPUTER Volume 25 No. 9. pp. 863-871.

# A Study of the Comfort of the Materials for Self-Grown Fashion Creation

Phoebe W. Wang and M.C.F. Ng

Institute of Textiles and Clothing The Hong Kong Polytechnic University Hung Hom, Kowloon, Hong Kong

# **ABSTRACT**

There have been increasing attempts for fashion material production to be re-defined towards cost effective, low environmental impact, labour friendly and biodegradable. Among them, biotechnology is believed to be one fine substitute for fashion creation in future. A study is being carried out with an aim to explore futuristic development of fashion design and applications where and when the materials can be grown from natural renewable resources and degradable rather than being designed and produced in the traditional tedious way. This paper reports the investigation of the bacterial cellulose formation process in different concentrations of tea broth and different incubation times. Through the comparison and evaluation of the comfort factors of the materials, the optimal favourable material towards self-grown fashion creation was presented.

Keywords: Self-grown, Nature, Bacterial Cellulose, Comfort, Fashion Creation

#### INTRODUCTION

Bacterial cellulose can be grown directly from the fermentation of sweetened tea by a symbiotic relationship between acetic acid bacteria and yeasts (Durfresne and Farnworth, 2000; Teoh *et al.*, 2004; Malbasa *et al.*, 2011). It has shown tremendous potential as an effective biopolymer in various fields (Ul-Islam, Khan and Park, 2012a; Ul-Islam, Khan and Park, 2012b). The mechanical strength of the cellulose is higher than those of plant cellulose, which has increased its utilisation in biomedical and other related fields. It has been applied for wound dressings, tissue regeneration and skin substitutes materials (Bae and Shoda, 2004; Czaja, Krystynowicz, Bielecki and Brown, 2006; Czaja, Young, Kawechi and Brown, 2007). However, seldom has the idea been conceived for artistic purposes, and in particular, in the fashion fields. This study is being carried out to investigate the bacterial cellulose formation process in different concentrations of tea broth and different incubation times. Through the comparison of the comfort factors of the materials which were grown out from different cultivated conditions, the favourability of the self-grown material towards fashion creation was identified and presented.

#### MATERIALS AND METHODS

#### **Materials**

Green tea was the substrate for the fermentation whereas sucrose was the carbon source. Tea fungus was obtained from a microbiology institute in Mainland China.

#### **Culture Media and Cultivation**

Substrate for cellulose fermentation was prepared by adding 60g/L of commercial sucrose to tap water and after boiling 5g/L of dry green tea was added. The tea leaves were steeped for 15 minutes and removed by filtration, after cooling to about 30°C and it incubated under aerobic conditions at 28°C.

#### Effect of Various Concentrations of Tea Broth on the Bacterial Cellulose Formation

Different amounts of dry green tea was added into boiled water with the same amount of sucrose as sweetened tea broth for bacterial cellulose pellicle formation, these amounts were 10, 15, 20 g/L respectively.

#### **Effect of Different Incubation Time on the Bacterial Cellulose Formation**

The effects of different incubation times (every other day) for the bacterial cellulose pellicle formation were examined.

## **RESULTS**

The bacterial cellulose pellicle grew well in sweetened green tea broth after 8 days of cultivation. With the increase of the amount of tea, the colour of tea broth changed from light yellow to yellow. In the first three days of fermentation, only bubbles appeared but with no pellicle. The cellulose pellicle was yielded on the fourth day of fermentation and grew thicker gradually. Table 1 shows the effect of different tea concentrations and against incubation times of bacterial cellulose formation. The symbols '+' and '-' stand for 'exist' and 'nil' respectively.

Table 1 Effect of different tea concentrations and incubation times on the bacterial cellulose formation

Concentration	2 days 4 days		6 days	8 days	
	F B P	F B P	F B P	F B P	
10g	- + (-)	+ - (+)	+ - (+)	+ - (++)	
15g	- + (-)	+ - (+)	+ - (++)	+ - (++)	
20g	- + (-)	+ - (+)	+ - (++)	+ - (+++)	

F=floc, B=bubble, P=pellicle; -: nil; +: exist

#### APPRAISAL AND EVALUATION

After cultivation, bacterial cellulose was formed at the interface of air in fermentation vessel. Six specimens of the biofilm (i.e., C1T4, C1T6, C1T8, C2T4, C2T6 and C2T8) were selected from two different broths by 10g/L and 20g/L of tea concentration in different cultivation times of 4 days, 6 days and 8 days respectively. These cellulose specimens were further evaluated for the comfort performance when they dried out.

Tactile sensations like smoothness, roughness, stickiness, scratchiness, softness and stiffness were obtained by touching the material (Kaplan and Okur, 2009; Liu and Little, 2009). The sensation of comfort was directly recognised by the person experiencing it (Slater, 1977). In this study, five professional fashion designers were invited to participate in the evaluation of these specimens by scaling and rating their objective perceptions (Ng, 2013). The factors of evaluation are hand comfort, flexibility comfort and breathability comfort (Sztandera, Cardello, Winterhalter and Schutz, 2013). For hand comfort, specimen being rotated between the thumb and one or two other fingers of the same hand to feel the texture, structure, and friction; for flexibility comfort, specimen were stretched and manipulated by two hands to assess how flexible or stiff the material were; for breathability comfort, the materials were laid on the arm skin to assess whether people feel sweating or uncomfortable after five minutes. The sample size of the material was 20cm x 20cm. Subjects assessed the samples using a 5-point scales, with 1 being uncomfortable

and 5 being comfortable. Table 2 shows the appraisal result. According to the result, the average scores of the attributes are graded and presented in Table 3.

Table 2 Appraisal result of comfort performance for the selected Self-grown materials

Subject	Specimen	НС	FC	BC
A	C1T4	2	1	4
	C1T6	3	2	3
	C1T8	3	3	3
	C2T4	2	2	4
	C2T6	4	5	4
	C2T8	4	4	2
В	C1T4	2	1	3
	C1T6	3	2	4
	C1T8	4	4	2
	C2T4	2	1	4
	C2T6	4	5	3
	C2T8	5	4	2
С	C1T4	2	1	4
	C1T6	3	2	3
	C1T8	3	3	3
	C2T4	2	3	4
	C2T6	4	5	3
	C2T8	4	4	2
D	C1T4	3	1	4
	C1T6	4	3	3
	C1T8	4	4	3
	C2T4	3	1	4
	C2T6	4	5	4
	C2T8	5	4	3
Е	C1T4	2	1	4
	C1T6	3	2	3
	C1T8	4	3	2
	C2T4	2	1	4
	C2T6	4	5	3
	C2T8	5	3	2

HC=Hand Comfort, FC=Flexibility Comfort, BC=Breathability Comfort

C1= 10g/L tea concentration broth, C2= 20g/L tea concentration broth

T4=4 days, T6=6 days, T8=8 days

Table 3 Average scores of the evaluation factors among the selected self-grown materials

Specimen	НС	FC	BC
C1T4	2.2	1.0	3.8
C1T6	3.2	2.2	3.2
C1T8	3.6	3.4	2.6
C2T4	2.2	1.6	4
C2T6	4	5.0	3.4
C2T8	4.6	3.8	2.2

#### **RANKING AND WEIGHTING**

The three factors that are most critical to the comfort performance were ranked for their relative importance towards self-grown fashion creation. A weighting from 1 to 3 was assigned to each factor, with 3 being the most important and 1 being the least. Table 4 shows the result of the ranking. The six specimens with average scores of comfort performance evaluation were then multiplied by the weighting of the factors to obtain the average weighting of the specimens for each factor. Table 5 shows the results.

Table 4 Ranking of the three factors most critical to the comfort performance of self-grown fashion creation.

Ranking in Order of Importance	Weighting	Factors
1st	3	FC
2nd	2	BC
3rd	1	HC

Table 5 Results of the ranking of the factors among the selected self-grown materials.

Specimen	HC(1)	FC(3)	BC(2)	Total
C1T4	2.2(2.2)	1.0(3.0)	3.8(7.6)	12.8
C1T6	3.2(3.2)	2.2(6.6)	3.2(6.4)	16.2
C1T8	3.6(3.6)	3.4(10.2)	2.6(5.2)	19.0
C2T4	2.2(2.2)	1.6(4.8)	4.0(8.0)	15.0
C2T6	4.0(4.0)	5.0(15.0)	3.4(6.8)	25.8
C2T8	4.6(4.6)	3.8(11.4)	2.2(4.4)	20.4

The sums of the average weightings of the six selected materials were obtained. The results suggested the overall favourability of comfort performance towards self-grown fashion creation. Table 6 shows the results.

Table 6 Results of the ranking of the overall comfort performance of the six specimens towards self-grown fashion creation.

Ranking in Order	Sum of the Average Weighting	Specimen
1st	25.8	C2T6
2nd	20.4	C2T8
3rd	19.0	C1T8
4th	16.2	C1T6
5th	15.0	C2T4
6th	12.8	C1T4

#### **CONCLUSION**

This study has been carried out to investigate the bacterial cellulose formation process in different concentrations of tea broth and different incubation times. Through comparison and evaluation of the comfort factors of the materials which were grown out from different cultivated conditions, the favourability of the materials towards self-grown fashion creation were evaluated and presented. As the result, the material was grown from 20g/L of tea concentration broth on 6-day cultivation has the most comfortable for fashion creation.

## REFERENCES

- Bae, S. Shoda, M. (2004). Bacterial Cellulose Production by Fed Batch Fermentation in Molasses Medium. *Biotechnology progress*, 20(5), 1366-1371.
- Ciechańska, D. (2004). Multifunctional Bacterial Cellulose/Chitosan Composite Materials for Medical Applications. *Fibres & Textiles in Eastern Europe*, 12(4), 48.
- Czaja, W. Krystynowicz, A. Bielecki, S. Brown Jr, R. M. (2006). Microbial cellulose—the natural power to heal wounds. *Biomaterials*, 27(2), 145-151.
- Czaja, W. K. Young, D. J. Kawecki, M. Brown, R. M. (2007). The future prospects of microbial cellulose in biomedical applications. *Biomacromolecules*, 8(1), 1-12.
- Dufresne, C. Farnworth, E. (2000): Tea, Kombucha, & health: a review, food research international 33: 409-421.
- Kaplan, S. Okur, A. (2009). Determination of coolness and dampness sensations created by fabrics by forearm test and fabric measurements. J. Sensory Studies 24, 479–497.
- Liu, R. Little, T. (2009). The 5ps model to optimize compression athletic wear comfort in sports. JFBI 2, 41-52.
- Malbasa, R. Loncar, E.S. Vitas, J.S. Canadanovic- Brunet, J. M. (2011): Influence of starter cultures on the anti-oxidant activity of kombucha beverage. Food chemistry 127: 1727-1731.
- Ng, F. (2013). Mapping the Way Ahead by Double-Rank Appraisal Method (DRAM) against Subjective and Objective Constraints in Design Research. *DesignEd Conference* 2013. Hong Kong.
- Slater, K. (1977). Comfort properties of textiles. Textile progress, 9(4), 1-70.
- Sztandera, L. M. Cardello, A. V. Winterhalter, C. Schutz, H. (2013). Identification of the most significant comfort factors for textiles from processing mechanical, handfeel, fabric construction, and perceived tactile comfort data. *Textile Research Journal*, 83(1), 34-43.
- Slater, K. (1977). Comfort properties of textiles. Textile progress, 9(4), 1-70.
- Teoh, A.L. Heard, G. Cox, J. (2004) Yeastecology of kombucha fermentation. International Journal of food Microbiology 95: 119-126.
- Ul-Islam, M. Khan, T. Park, J. K. (2012a). Water holding and release properties of bacterial cellulose obtained by in situ and ex situ modification. CarbohydratePolymers, 88(2), 596–603.
- Ul-Islam, M. Khan, T. Park, J. K. (2012b). Nanoreinforced bacterial cellulose—montmorillonite composites for biomedical applications. Car-bohydrate Polymers, 89(4), 1189–1197.

# Biomechanical Model of Bare-Breasts During Running

Jie Zhou<sup>a</sup>, Winnie Yu<sup>b</sup>, Lihua Chen<sup>c</sup>, MinyoungSuh<sup>d</sup> and YiqingCai<sup>a</sup>

<sup>a</sup> Apparel and Art Design College Xi'an Polytechnic University Xi'an, PRC

<sup>b</sup> Institute of Textiles and Clothing The Hong Kong Polytechnic University Hong Kong, PRC

<sup>c</sup> College of Mechanical Engineering Beijing University of Technology Beijing, PRC

> <sup>d</sup> College of Human Ecology Kansas State University Manhattan KS, USA

#### **ABSTRACT**

Sports bras are designed to reduce mammary glands or breast movement during exercises, but there is no standardized, valid and reliable method to evaluate relative three-dimensional (3D) breast movement; and there is no literature to predict the 3D force acting on the breasts during activities. A reliable method is essential to evaluate 3D breast movement and to determine the effective design features of supportive sports bras. This study derived and validated a new Breast Coordinate System (BCS) for investigating 3D breast movement, so as to identify the most effective bra features and to analyze the effects of breast volume and bra strap properties on breast movement, then to develop theoretical models of breast force generated during bare-breasted running. In the light of this, 3D mechanical models have been developed based on a system comprising a mass, springs and dampers. The orthogonal force exerted on the breasts during running was derived. The predicted results of maximum breast force were verified with previous literature. The new methods will contribute to future research on human locomotion and the design of close-fitting garments.

Keywords: Breast, Biomechanical Model, Movement, Mass-Spring-Damper, Running

#### INTRODUCTION

Breast tissue moves along with the thorax, but also presents inherent movement since it does not contain any skeletal structure. A bra works as external supports relieving breast movement. Especially, a sport bra is designed to minimize the movement of the breasts during the exercise (McGhee & Steele, 2010). The breast displacement is governed by the force associated with exercising motions and the force is the most critical factor to consider when the sport bra is designed. Apparent from Newton's second law, F=ma, the breast mass and acceleration play important roles in calculation of breast force.

Historically, breast size was measured in volume rather than in mass. Conventional bra sizing is not reliable and cannot measure the breast volume or mass (Pechter, 1998). Previous researchers estimated that the breast mass was in a wide range of 150g to 2000g (Turner &Dujon, 2005). The vertical displacement of the breasts increased by 70% when the breast mass increased from 100g to 700g (Haake& Scurr, 2010), so the exercise-associated force can greatly affect the large-breasted women. Factors affecting the breast movement included the types of breast support (Scurr et al., 2011), levels of activities (Mason et al., 1999) and breast mass. However, previous research on breast movement and bra design has predominantly been limited to empirical studies (Lawson &Lorentzen, 1990; Mason, Page, & Fallon, 1999; Scurr, White, & Hedger, 2011; White, Scurr, & Hedger, 2011). To investigate the internal forces in the breast tissues, Gefen& Dilmoney (2007) have considered the structural support from Cooper's ligaments, the fascia of the pectoralis muscle, and the ribs. Haake& Scurr (2010) used a mass-spring-damper system to introduce a theoretical mechanical breast model.

This research aims to develop the breast mechanical model to estimate the breast displacement and force during exercise. The breast is considered as an object of mass-spring-damper system. Through the free-falling breast tests with a female subject, spring constant and damping coefficient was calculated. An equation to calculate net force affecting the breast discomfort during running was established. The breast mechanical model is expected to provide a theoretical foundation to understand optimum support and comfort in sport bra design.

#### **METHODOLOGY**

#### **Mass-Spring-Damper System**

In this study, the mass-spring-damper system is based on the Kelvin-Voigt model (Yang &Qiang, 2009). The breast movement was assumed to be represented by a point mass at the nipple (Gefen& Dilmoney, 2007; Haake& Scurr, 2010) in an ideal mass-spring-damper system in which mass (m), spring constant (k) and damping coefficient (c) are to be determined. It is assumed that the breast is a homogeneous object with elastic and viscous properties; both breasts are identical in perfect symmetry; and orthogonal forces acing on the breasts are considered.

A typical damped spring movement of a visco-elastic object is shown in Figure 1. The elastic movement is governed by spring constant (k) that is related to the oscillation frequencies  $(\omega)$ , as shown in Equation 1. Viscous movement is governed by the damping ratio  $(\zeta)$  that can be calculated from the Logarithmic decrement  $(\delta)$  of the breast in the time domain, which refers to the natural logarithm of the ratio of amplitudes of two adjacent peaks  $x_n$  and  $x_{n+1}$  in displacement (Equation 2). Then, damping ratio (c) and damping coefficient  $(\zeta)$  are defined by Equation 3 and Equation 4 respectively.

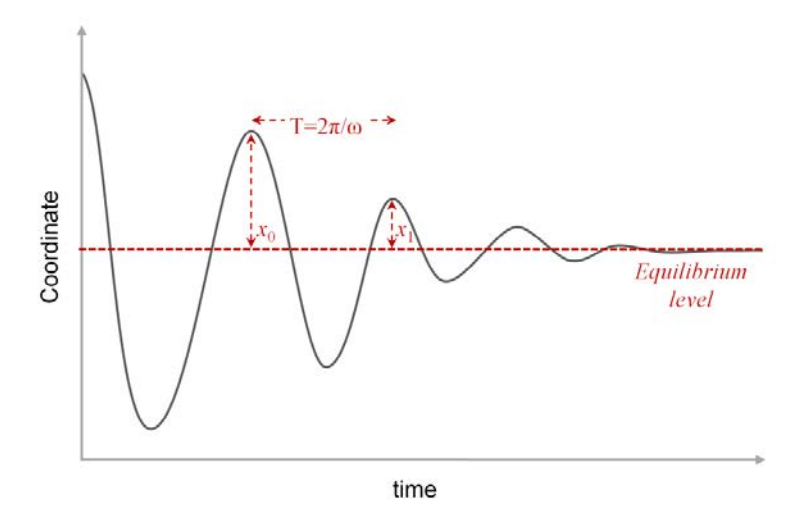


Figure 1.Damped spring movement

$$k = \omega^2 m \tag{1}$$

$$\delta_n = \frac{1}{n} \ln \frac{x_0}{x_n} \tag{2}$$

$$\zeta = \frac{c}{2m\omega} = \frac{1}{\sqrt{1 + \left(\frac{2\pi}{\delta}\right)^2}} = \frac{1}{\sqrt{1 + \left(\frac{2\pi}{\ln(x_0/x_1)}\right)^2}}$$
 [3]

$$c = 2\zeta m\omega$$
 [4]

During running, the nude breasts have a range of oscillating displacement (x) in the time domain, from which velocity  $(\dot{x})$  and acceleration  $(\ddot{x})$  can be derived. The net force  $(F_N)$  applied to the breast is a sum of spring force  $(F_S)$ , damping force  $(F_D)$ , and total force  $(F_T)$  acting on the breasts, as shown in Equations 5, 6, and 7 respectively. The net force can be written in a function of time with given mass, spring constant, and damping coefficient (Equation 8).

$$F_S = -kx = -kf(t)$$
 [5]

$$F_D = -c\dot{x} = -cf'(t) \tag{6}$$

$$F_T = mg [7]$$

$$F_N = mg + c\dot{x} + kx = mg + cf_x'(t) + kf_x(t)$$
 [8]

The methods to determine the constants of breast mass (m), spring constant (k) and damping coefficient (c) will be presented in the following sections.

# 3D Body Scanning for Estimation of Breast Mass

Breast mass (m) was calculated by multiplying breast volume (v) by breast density  $(\rho)$ . Breast volume was measured by image analysis of the 3D scanned breast surface. The image was captured by  $TC^2$  body scanner (NX-16, Textile/Clothing Technology Corporation, USA), and the data cloud was import into the Rapidform XOR software for meshing, filling holes, trimming the breast shell, building the curvy breast base (Figure 2). Then the breast shell and base were connected together to make the breast solid for the automatic calculation of breast volume. The breast root was determined manually based on the change of surface curvature.

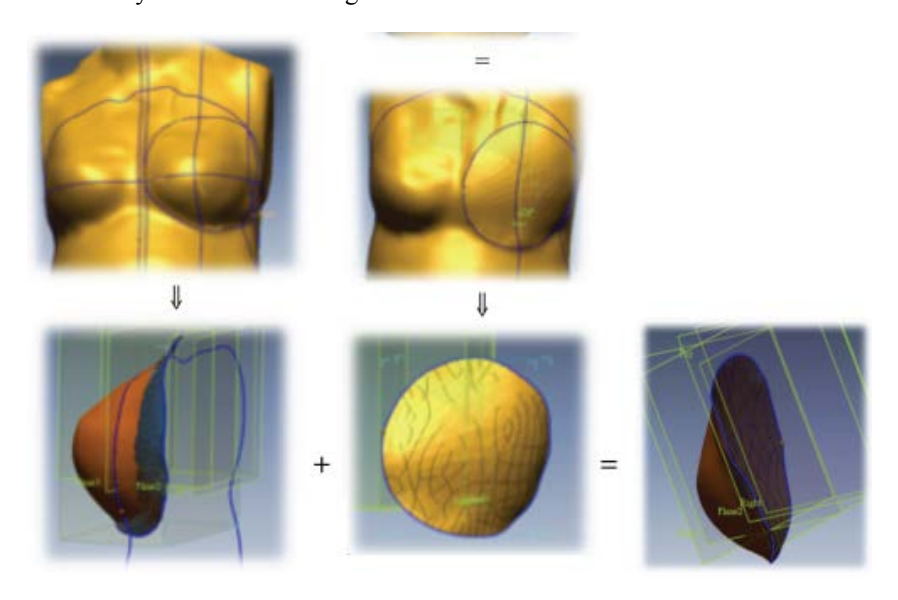


Figure 2.Extracting breast volume from a 3D body image

Breast density could be estimated from the breast fat and glandular tissue, whose densities are approximately 500 kg/m³ and 1,060 kg/m³, respectively (Vandeweyer & Hertens, 2002). Breast density changes in the percentage of fat and glandular tissue, depending on age, nutritive condition, and ethnic group. According to Katch et al. (1980), a breast density of 1,017 kg/m³ was adopted. This paper presents the methods tested on a Chinese woman with her informed consents. She is aged 40, married and has one child. Her breast size was 80B in a ptotic drooping tear shape. Her breast volume was 311.5 cm³ and therefore by multiplying the density, the breast mass was computed to be 0.3168 kg.

# Breast Free Falling Experiment For Determining Spring Constant And Damping Coefficient

To estimate the damping ratio of human breast, the same subject participated in a breast free-falling experiment. She lifted up her left breast to the highest position, and then released it to fall freely. The breast vibration was captured using the Vicon motion analysis system (Vicon, 612, Oxford Metrics, Oxford, UK). Markers were attached to the nipple and sternal notch. Six cameras on the ceiling recorded 3D coordinates of passive retro-reflective markers on the breast at the frequency of 120 Hz in order to track the breast movement. Each marker was 9.5mm in diameter and 1.81g in weight. The measurement was repeated for three times. The vertical movement of the nipple (Figure 3) against time was used to obtain her inherent spring constant and the damping coefficient.

# **Motion Capture of Breast Displacement and Acceleration During Running**

The subject was asked to run with bare breasts at a constant speed of 6 km/h on a treadmill, for at least 100 seconds. To remove the background noise signals during motion capturing, the motion data was first smoothed out by using a low pass filter with a cut off frequency of 8 Hz. MATLAB version 7 (The MathWorks, Inc.) was used to plot the breast coordinates against time. The breast displacement was defined as the change of the coordinates from a static condition to a dynamic condition. Three running strides were taken for analysis.

# **RESULTS**

## **Spring Constant and Damping Coefficient**

The waveforms of the vertical breast movement in Figure 3 show the damped and oscillating behavior of the nude breast. The breast fell from a high position and entered into the equilibrium within a second. The first and second peaks were recorded to be approximately 1.2 cm and 0.3 cm respectively.

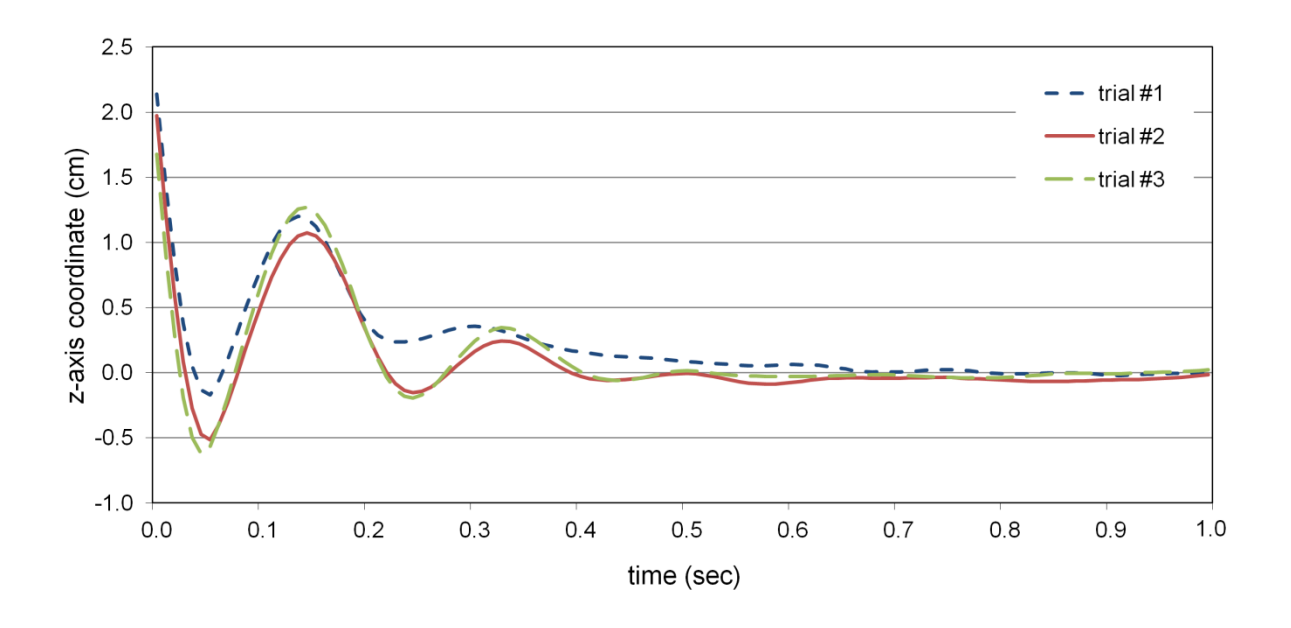


Figure 3. Vertical movement of a free-falling breast

The similar behavior was observed for repeated experiments. Detailed measurements are extracted and given in Table 1.

Table 1. Free-falling breast observation in a braless condition

Trial #	z <sub>0</sub> (cm)	z <sub>1</sub> (cm)	T (sec)	f (Hz)	ω (rad/sec)	$\delta_1$	ζ	$k_0$	$c_0$
1	1.17	0.32	0.2	5	31.42	1.2657	0.1976	312.36	3.9606
2	1.15	0.32	0.2	5	31.42	1.2792	0.1996	312.36	3.9710
3	1.29	0.36	0.2	5	31.42	1.2763	0.1991	312.36	3.9623

Based on these measurements, spring constant and damping coefficients of the nude breast were calculated as below.

$$k_0 = 312.36 \ (\pm 0.00) \ (N/m)$$

$$c_0 = 3.9546 \; (\pm 0.21) \; (Ns/m)$$

These values were slightly different from the findings in previous research (Haake & Scurr, 2010). Higher spring constant and lower damping coefficient was observed in this investigation due to the different age, race, and personal history e.g. breast-feeding. Future studies on the damped spring movement of human breasts should recruit a larger sample size to obtain the statistical result for more generic biomechanical modelling.

## **Breast Force During Bare-Breasted Running**

When the subject was running on the treadmill, her breast movement was captured in real time. Figure 4 shows the breast movement in a form of continuous waveforms. Two cycles of the waveform were used to show a full single running stride. There was a small vibration when the breast moved upwards, which was consistent with the findings from Haake & Scurr (2011).

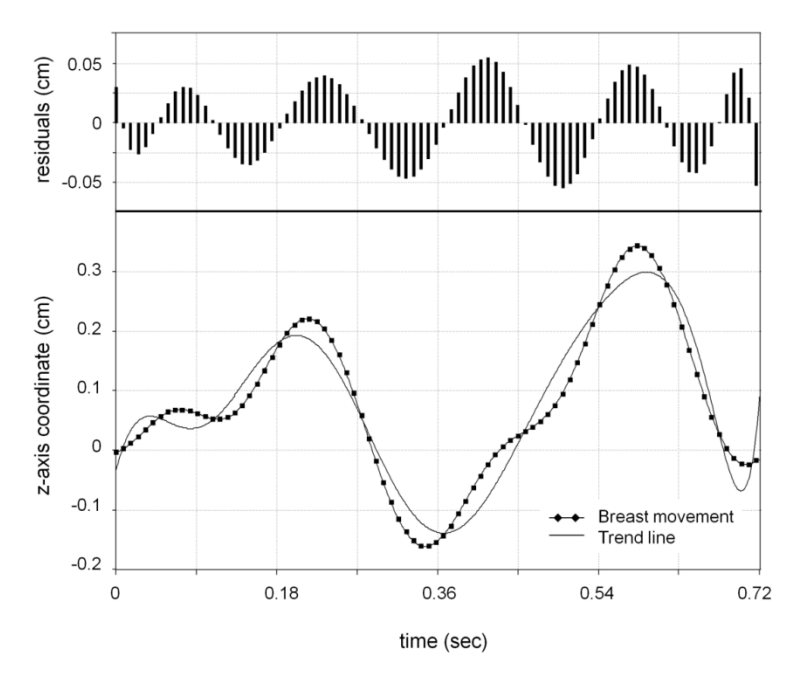
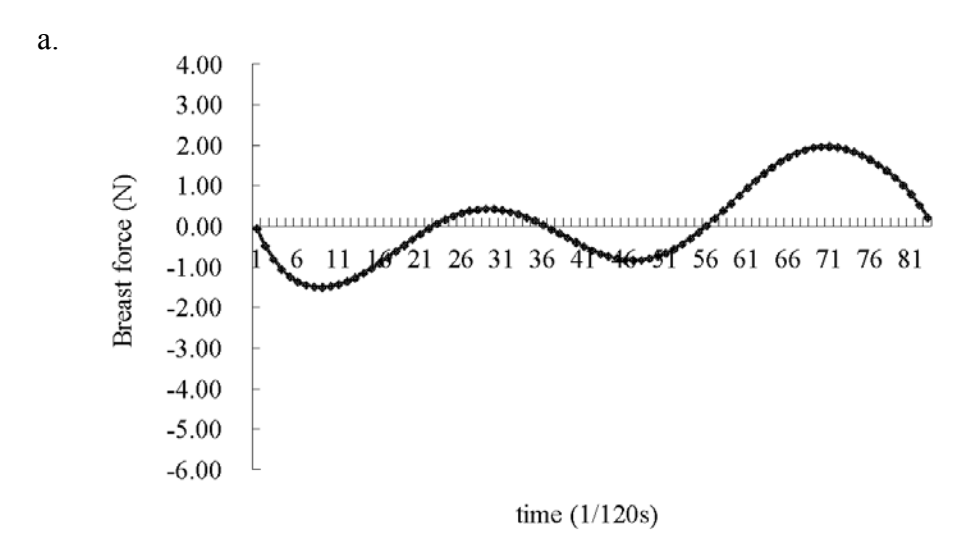
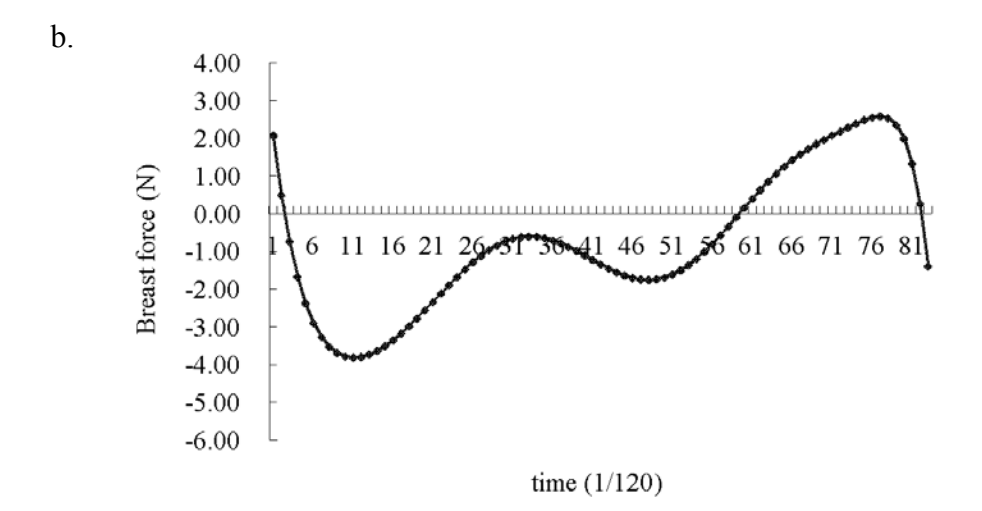


Figure 4. Vertical movement during breast jogging

A trendline of the vertical breast displacement (z) can be presented in a function of time (t). Then the first and second differential functions derived from it becomes the velocity  $(\dot{z})$  and acceleration  $(\ddot{z})$  of the breast movement, respectively.

Using Equations 5 to 7, the spring force  $(F_S)$ , damping force  $(F_D)$ , and total force  $(F_T)$  during bare breast running can be calculated respectively with a given mass, spring constant, and damping coefficient. Then, the net force  $(F_N)$  was estimated in a function of time by adding up these forces using Equations8, **Error! Reference source not found.** The net force shown in Figure is considered the excessive force that causes breast discomfort during the exercise.





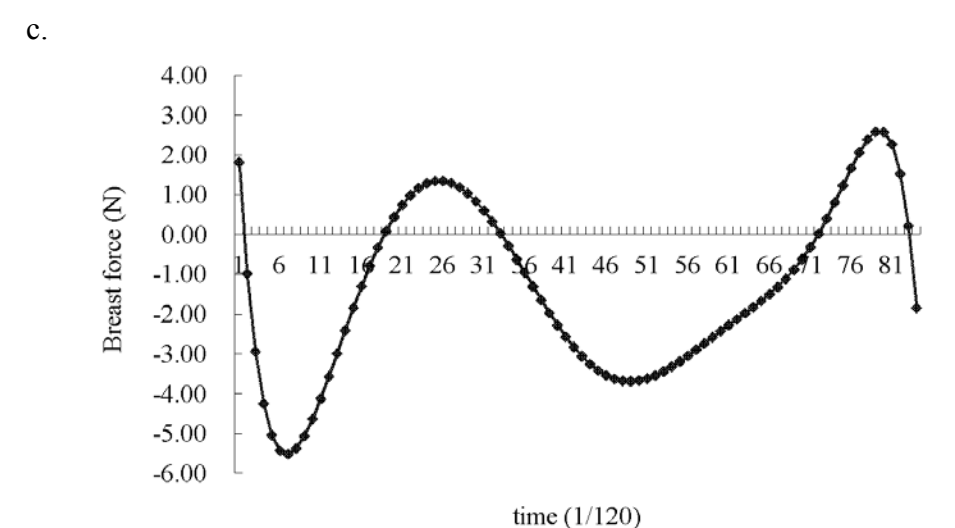


Figure 5. Net force during bare-breasted running(a: x-direction; b: y-direction; c: z-direction)

As shown in Figure 5, the net force was the biggest in superior-inferior (z) direction. The downward force was about twice bigger than the upward force. Therefore, the upward breast support is critical in bra design. The net force in medial-lateral (x) direction is much smaller, but the considerable amount of net force was observed along the anterior-posterior (y) direction. Specifically, the net force was more dominant in posterior direction. This implies that the control on breast movement is important in anterior-posterior direction as well. Elastic modulus of underband and shoulder strap should be carefully decided to provide optimum control along the downward and posterior directions.

#### CONCLUSIONS

Movement of breasts can be explained with a mass-spring-damper system. The spring constant and damping coefficient were computed based on the waveform of breast vibration during free-falling. The breast mass was calculated from the breast volume extracted from a 3D scan body image. Considering the spring and damping forces during running in the breast mechanical model, the net force can be computed. This new knowledge will be useful to reduce the exercise-associated discomfort on the breasts by providing the necessary amount of support by a sports bra. An effective sports bra should be designed in a way to minimize the net force in all directions. However, excessive control in posterior direction may let the wearer feel constrained too much in bras. Compromise between support and comfort is inevitable.

#### REFERENCES

Bowles, K. A., Steele, J. R., & Munro, B. (2008). What are the breast support choices of Australian women during physical activity? *British Journal of Sports Medicine*, 42(8), 670-673.

Gefen, A., & Dilmoney, B. (2007). Mechanics of the normal woman's breast. *Technology and Health Care Electronic Resource*, 15(4), 259.

Haake, S., & Scurr, J. (2010). A dynamic model of the breast during exercise Sports Engineering, 12(4), 189-197.

Haake, S., & Scurr, J. (2011). A method to estimate strain in the breast during exercise. Sports Engineering, 14(1), 49-56.

Katch, V. L., Campaigne, B., Freedson, P., Sady, S., Katch, F. I., & Behnke, A. R. (1980). Contribution of breast volume and weight to body fat distribution in females. *American Journal of Physical Anthropology*, 53(1), 93-100.

Lawson, L., & Lorentzen, D. (1990). Selected sports bras: Comparisons of comfort and support. *Clothing and Textiles Research Journal*, 8(4), 55-60.

- Mason, B. R., Page, K., & Fallon, K. (1999). An analysis of movement and discomfort of the female breast during exercise and the effects of breast support in three cases. *Journal of Science and Medicine in Sport Formerly Australian Journal of Science and Medicine in Sport Electronic Resource Electronic Resource*, 2(2), 134.
- McGhee, D. E., & Steele, J. R. (2010). Breast elevation and compression decrease exercise-induced breast discomfort. *Medicine & Science in Sports & Exercise*, 42(7), 1333-1338. doi:10.1249/MSS.0b013e3181ca7fd8
- Page, K. A., & Steele, J. R. (1999). Breast motion and sports brassiere design: Implications for future research. Sports Medicine Electronic Resource, 27(4), 205.
- Pechter, E. A. (1998). A new method for determining bra size and predicting postaugmentation breast size. *Plastic & Reconstructive Surgery*, 102(4), 1259-1265.
- Scurr, J. C., White, J. L., & Hedger, W. (2011). Supported and unsupported breast displacement in three dimensions across treadmill activity levels. *Journal of Sports Sciences*, 29(1), 55-61. doi:10.1080/02640414.2010.521944
- Turner, A. J., & Dujon, D. G. (2005). Predicting cup size after reduction mammaplasty. *British Journal of Plastic Surgery*, 58(3), 290-298.
- Vandeweyer, E., & Hertens, D. (2002). Quantification of glands and fat in breast tissue: An experimental determination. *Annals of Anatomy Anatomischer Anzeiger*, 184(2), 181-184. doi:10.1016/S0940-9602(02)80016-4
- White, J., Scurr, J., & Hedger, W. (2011). A comparison of three-dimensional breast displacement and breast comfort during overground and treadmill running. *Journal of Applied Biomechanics*, 27(1), 47-53.
- Yang, W. Y., & Qiang, W. (2009). Mechanical behavior of materials. Beijing Shi: Hua xue gong ye chu ban she.
- Zhou, J. (2011). New methods to evaluate breast motion in braless and sports bra conditions. (Unpublished Doctoral dissertation). Hong Kong Polytechnic University, Hong Kong.

# A Finite Element Mechanical Contact Model of 3D Human Body and a Well-Fitting Bra

Yiqing Cai<sup>a</sup>, Winnie Yu<sup>a</sup> and Lihua Chen<sup>b</sup>

<sup>a</sup> Institute of Textiles and Clothing The Hong Kong Polytechnic University Hong Kong, PRC

<sup>b</sup> College of Mechanical Engineering Beijing University of Technology Beijing, PRC

# **ABSTRACT**

This paper presents the methods of developing a finite-element (FE) mechanical contact model to simulate the interaction between human breasts and a well-fitting bra. In the FE model, the human breasts are modelled as hyperelastic material, and the bra is meshed as elastic beam and shell. The FE contact model between the breasts and the bra is defined as a contact pair. The mathematical formulation describes the strain–stress contact mechanics of the 3D human body and the bra under pre-tension. The simulation results provide a fundamental guideline for the calculation of the force mechanics of any body–garment interaction.

Keywords: Finite Element, Contact Model, Simulation, Breasts, Bra, Fit

#### INTRODUCTION

Clothing physiologists have found that excessive bra pressure not only cause discomfort but also various types of health problems (Lee et al., 2000; Miyatsuji et al., 2002). Bra pressure is affected by the bra size, the style of bra, the elastic modulus of fabrics, the 3D geometric shape and the synthesized elastic modulus of the human body (You et al., 2002). In the past, many research works have conducted wear experiments with sensing elements (inserted between the human body and clothes) to measure garment pressure and the relevant subjective sensations (Kawabata et al., 1988; Makabe et al., 1993; Nakahashi, et al., 2000). However, there are still limitations in practical pressure measurements due to restrictive pressure sensing range and discrete measuring points on a human body. Therefore, a more efficient technique to obtain information about the interaction between a bra and human body is necessary.

Finite elements (FE) methods have been proposed to simulate the biomechanical interactions between human body and garment. Finite elements analysis has been applied to yarn mechanics and fibrous assemblies for decades (Wang, et al., 2011), but the FE research of the contact mechanics between a garment and a human body is still in its infancy. Previous studies (Balaniuk et al., 2007; Perez et al., 2008; Rajagopal et al., 2010; Rajagopal et al., 2008; Samani, 2001; Sinkus et al., 2005) tended to use 3D body surface scanned images, magnetic resonance images (MRI), or Computed Tomography (CT) in prone configurations for constructing geometric model of breast. However, it is

so hard to derive the mechanical properties of breast tissues (fat, grand, skin) from in vivo breast indentation tests that most research used ex vivo data (Lu et al., 2009). The breast tissues were overall assumed to be incompressible Krouskop et al., 1998), homogenous (Sarvazyan et al., 1995; Skovoroda et al., 1995) and isotropic (Fung et al., 1993; Krouskop et al., 1998), with uniform density (Jonathan et al., 2007; Wang et al., 2011). Imaoka and Atkinson (1996) built a mathematical model to simulate the interaction between a body and garment, based on an assumption that the body is rigid. Yu et al. (2008) developed a FE model of the female foot for high-heeled shoe design to investigate the plantar contact pressure and internal loading responses of the bony and soft tissue. For the body-bra relationship, Li et al. (2003) developed a computer-generated body model to theoretically calculate the skin pressure distributions, breast deformation and inner stress in the skin based on arbitrary skin, breast tissue and bone. However, the tissue properties were based on the ex-vivo data, the breast boundary was not clearly determined, only single-layer skin was considered, and the single-material bra model was over-simplified.

Knowledge about the interaction between the viscoelastic breasts and multi-layer multi-component bra structure is hitherto unavailable. In this study, a finite-element mechanical contact model for a 3D human body and bra is used to treat the bra as a flexible shell based on elasticity theory. In this model, the human body and garment are meshed as basic cells, the contact cells between body and garment are defined to describe the contact relationship, and the material coefficients are initially assigned based on ex vivo data at specified parts that potentially will contact with the bra, and then by iterative procedure of mixed formulation, the material coefficients are optimized when the predicting results matched with the experimental data. This paper shows the methods and results of the FE simulation of contact mechanics of human body and bra wearing.

#### FINITE-ELEMENT CONTACT MODEL DEVELOPMENT

An overview of the development procedures of the finite-element mechanical contact model between a 3D human body and a well-fitted bra is shown in Figure 1, based on the theories of hyper-elastic contact mechanics.

#### **3D Geometry Model Generation**

Geometry models of the breast and bra were generated from the acquired 3D surface scans of a female subject in standing position after she found the best-fit bra in the fitting trials. The images were saved in ASCII format and loaded into the Rapidform XOR software. As the breast is a visco-elastic deformable body composed of skin, fat and gland (Gefen and Dilmoney, 2007) and the thorax is elastic rigid body, Boolean operations were used to define the breast boundary and intersection surfaces between the breast and thoracic regions.

#### **Breast Sub FE Model Generation**

The FE models of the breast were generated from the IGS file acquired in Rapidform software. The thorax wall was modelled as a continuous volume and was assumed to completely restrain displacements as the posterior demarcation of the deformable model. Fat and glandular tissues were summarized as one component, and the skin was attached over the breasts as shell elements. The thorax and muscles are considered as one component with uniform mechanical properties. Eder (2013) summarized the mechanical properties of fibro glandular and fat tissues used in previous FE simulations of breasts with cancer cells, but the data for the normal breasts are very limited. Data reported in the literature was not validated because the mechanical properties of individual tissue types were derived from ex-vivo experiments on small specimens, which cannot be measured in-vivo. To solve this problem, the authors in a previous work (Chen et al., 2013) have validated the material parameters of breast tissue and skin by using a bared-breast running experiment. A less than 1% root-mean-square error RMS (Equation 1) of the predicted breast displacement was considered acceptable. Then the optimal values of body material parameters are determined.

$$RMS = \frac{{}_{100}}{{}_{N_t \cdot N_d}} \sqrt{\sum_{i=1}^{N_d} \sum_{j=1}^{N_t} \left(\frac{D_{ij}^E - D_{ij}^F}{D_{ij}^E}\right)^2}$$
 (1)

where  $N_t$  is the number of sample data points,  $N_d$  is the number of markers,  $D^E$ ,  $D^F$  are the displacement obtained from Experiment and FE simulation.

For simulating the breast soft tissues, different material models such as linear elastic, piecewise-linear elastic, exponential elastic, and different hyper-elastic constitutive models were tried out. Eder (2013) concluded that hyper-elastic model is most suitable for modelling the breasts.

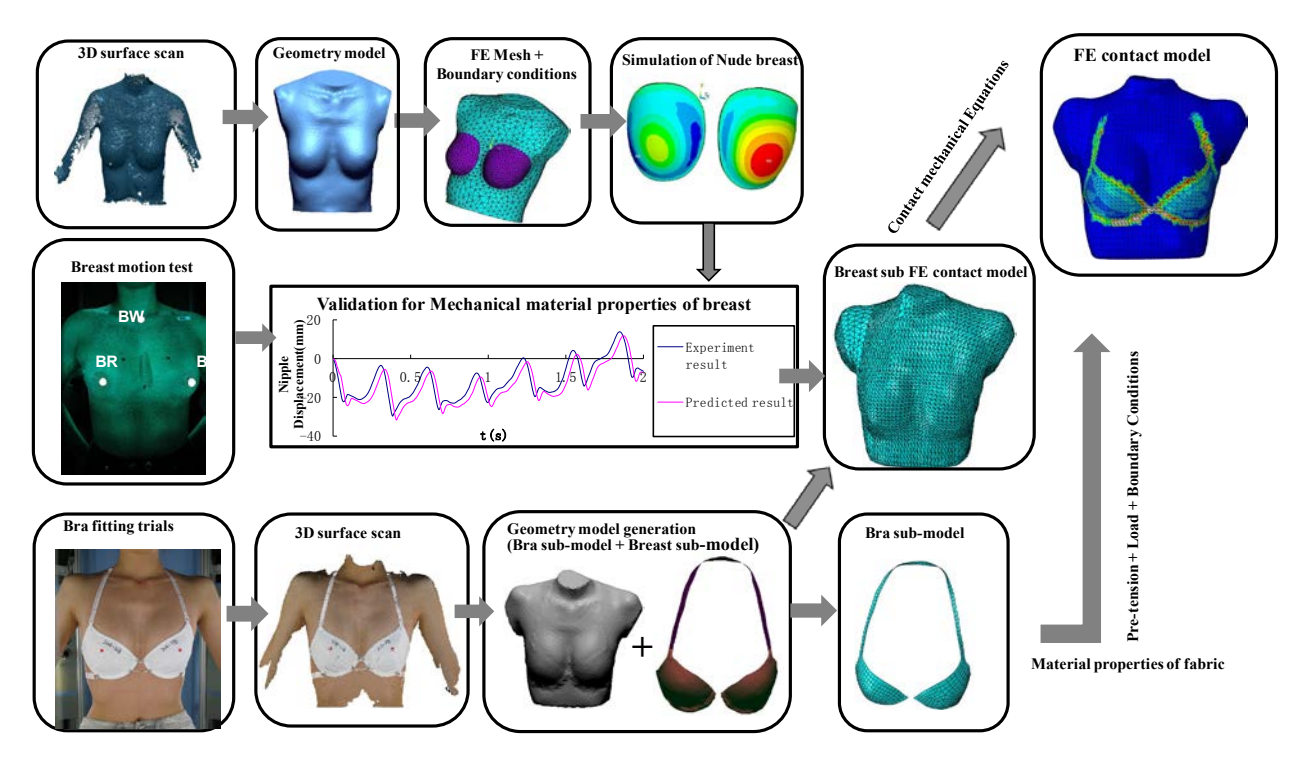


Figure 1. Development of finite-element mechanical contact model

#### **Bra Sub FE Model Generation**

FE model of the bra was also generated from the IGS file acquired in Rapidform software. The bra cups, straps and bands are modelled as shells, while the gore is modelled as a beam. Table 1 shows the mechanical parameters and geometric parameters of the bra components.

Table 1. The mechanical			

Components	Width(mm)	Thickness(mm)	Modulus E (kPa)	Poisson's ratio v	
Strap	15	0.75	1318	0.34	
Band	15	0.75	1318	0.34	
L cup	72.5	1.05	3500	0.32	
R cup	72.5	1.05	3500	0.32	
Wire	null	3.0	200000000	0.3	
Gore up	6	null	200000000	0.3	
Gore lower	16	null	200000000	0.3	

#### **FE Contact Model Generation**

The relationship between breast and bra during wear is complex. In this study, the model is based on the following assumptions:

- (a) The human body is an elastic rigid volume and the breast is a flexible body with hyper-elastic properties.
- (b) The bra is an elastic and continuous shell with material linearity and geometric nonlinearity.
- (c) The contact between the breast and the bra is in a standing position, considering pre-tension of bra.

In finite-element modelling, the contact forces must be applied to each nodal point of each finite-element mesh. Based on the assumptions above, different contact elements are applied including surface-to-surface contact, node-to-surface contact, line-to-surface contact, and line-to-line contact, for tracking the contact position, transferring the contact stress and preventing the contact surface from mutual penetration. With the software Abaqus 6.12 (3D Experience Company, France), a combined algorithm of the Lagrange Multiplier, the Penalty Method and Solver Constraints is used to treat the frictional sliding contact problems.

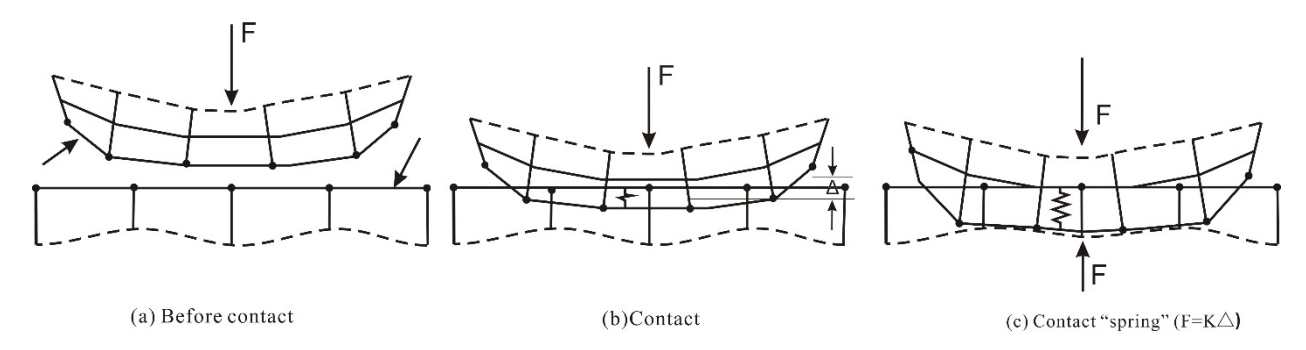


Figure 3. Illustration of contact algorithm

At initial, there is pre-tension (20% tension) and gravity in the FE contact model. The boundary displacement is regarded as the displacement of rigid thorax. As the breasts are attached to the Pectoralis major muscle on the ribcage, the displacement boundary conditions were applied at the posterior surface of the breast.

Based on the Virtual Work Theory (Tan, 2007), the equation for this contact model is

$$\int_{\Omega^{e}} \{\sigma^{e}\}^{T} \{\delta \varepsilon^{e}\} dU = \int_{\Omega^{e}} \{P_{V}^{e}\}^{T} \{\delta \overline{u}^{e}\} d\Omega + \int_{\Gamma^{e}} \{P_{S}^{e}\}^{T} \{\delta \overline{u}^{e}\} d\Gamma + \int_{\Gamma^{e}} \{r(u)^{e}\}^{T} \{\delta \overline{u}^{e}\} dC$$
(Equation 1)

where

 $\{P_{\nu}^{e}\}$  =body force vector of element

 $\{P_s^e\}$  = face force vector of element

 $\{r(u)^e\}$  = force vector of contact interface

 $\{\delta \overline{u}^e\}$  = virtual displacement vector in element

 $\{\delta u^e\}$  = virtual displacement vector of node

 $\{\sigma^e\}$  = virtual stress vector in element.

 $\{\delta \varepsilon^e\}$  = virtual strain vector in element

 $\Omega^e$  = region of element

 $\Gamma^e$  = load boundary on element

 $C^e$  = contact boundary on element

while

$${\overline{u}^e \brace u^e} = [N^e] \lbrace u^e \rbrace$$
 (Equation 1-a)

$$\{\delta \overline{u}^e\} = [N^e]\{\delta u^e\}$$
 (Equation 1-b)

$$\{\delta \varepsilon^e\} = [B^e] \{\delta u^e\}$$
 (Equation 1-c)

$$\{\sigma^e\} = [B^e][D_{ep}]\{u^e\}$$
 (Equation 1-d)

where

 $[N^e]$  = Element shape function matrix

 $[B^e]$  = Element strain matrix

 $[D_{ep}]$  = Elastic-plastic matrix

So Equation 1 becomes

$$\{\psi(u)\}^e = -\int_{\Omega^e} [B^e]^T \{\sigma\} d\Omega + \{R(u)^e\} + \{P^e\} = 0$$
 (Equation 2)

where:

$$\{R(u)^e\} = \int_{C^e} [N^e]^{\mathrm{T}} \{r(u)^e\} dC$$

$$\{P^e\} = \int_{\Omega^e} [N^e]^{\mathsf{T}} \{P_V^e\} d\Omega + \int_{\Gamma^e} [N^e]^{\mathsf{T}} \{P_S^e\} d\Gamma$$

The whole contact model as an integration of all elements in Equation 2, is presented in Equation 3

$$\{\psi(u)\} = -\int_{\Omega} [B]^{T} \{\sigma\} d\Omega + \{R(u)\} + \{P\} = 0$$
 (Equation 3)

# **RESULTS**

The material parameters of breast tissue and skin were first obtained from the literature for the initial FE modeling of the thorax, two breasts and a skin layer. Then the parameters were iteratively changed until the predicted results are similar to the experimental results of the nipple displacement in orthogonal directions during bared-breast running as shown in Figures 4a to 4c. It is found that the predicted results matched well with the experimental results in both superior-inferior (z) and anterior-posterior (y) directions, with RMS <1%. In the medial-lateral (x) direction, the RMS is 3.83%, probably due to the large arm swung during the running experiment.

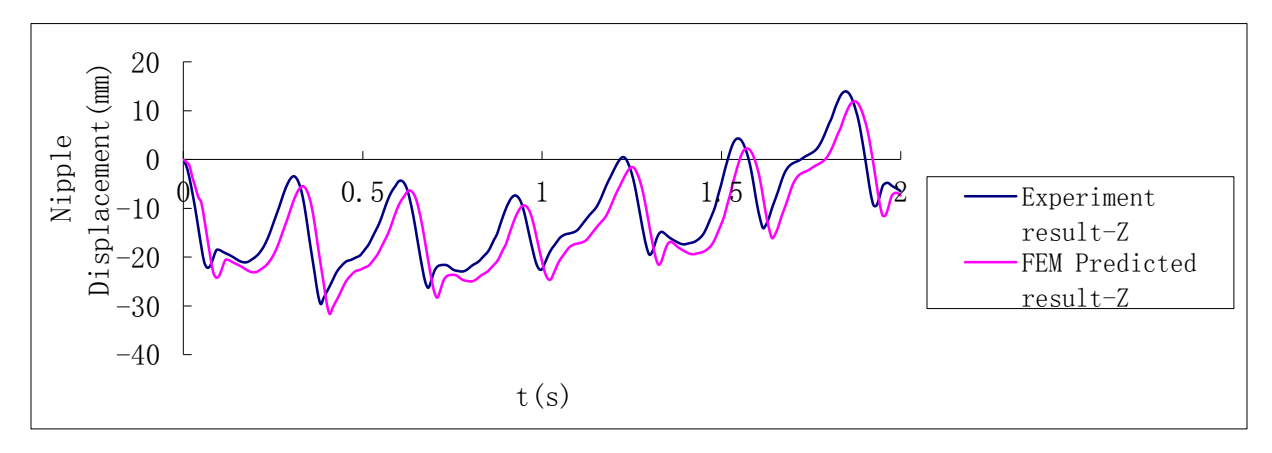


Figure 4a. Predicted result and experimental result of nipple displacement in z-direction

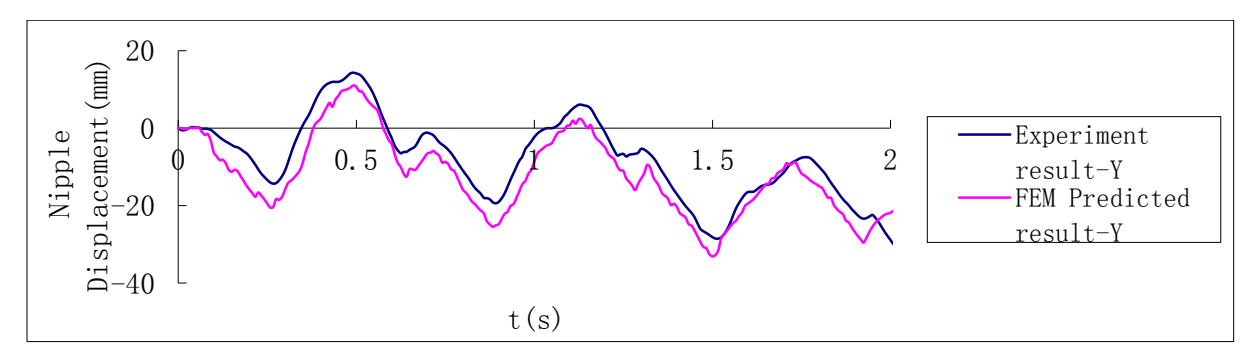


Figure 4b. Predicted result and experimental result of nipple displacement in y-direction

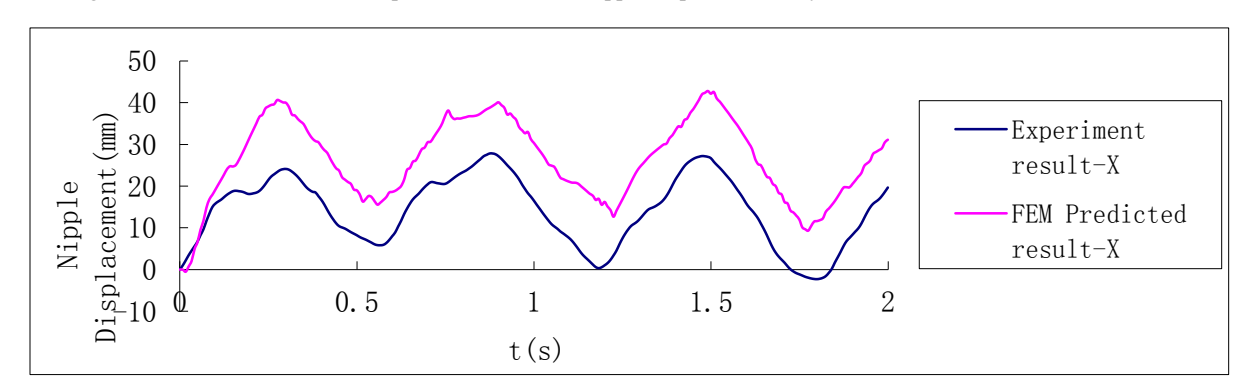


Figure 4c. Predicted result and experimental result of nipple displacement in x-direction

Table 3 Root mean square error percentages of the predicted breast displacements during running

Direction	X	y	Z
RMS %	3.83	0.59	0.65

The correspondent values of Young's moduli of the breasts and skin are shown as Table 4.

650

0.52

Dermis

**Epidermis** 

Elastic

Elastic

Con	nponents	Material model	Material Constants								
			Yong's Modulus (E/kPa)	Possion ratio (v)	C10	C01	C20	C11	C02	D1	D2
Т	horax	Elastic	489	0.3				null			
I	Breast	Hyper elastic		0.495	0.09	-0.06	0.04	-0.02	0.01	3.65	0
Skin	Hypodermis	Elastic	0.45	0.495				null	•		

0.495

0.495

null

null

Table 4 Material parameters of different body parts

Using the validated material parameters, an FE contact model was developed to simulate the contact pressure between a well-fitting bra and a female subject's breast region. As Figure 6 shows, in this good-fitting condition, the maximum contact pressure is 0.1kPa distributed along the neckline of cup, wire, and the left straps. The cups have not much pressure because it is a natural fit bra. The pressure generated from the center gore to the wire and the straps is due to the tension pulling from the centre back hooks and the back neck. As the left strap has one layer of elastic band while the right strap has two layers for the sliding adjustments, the contact pressure on the left is higher than that on the right.

The contact pressure (Figure 5a) and deformation (Figure 5b) are small in the cups, but bigger in the gore and the wire because they are under the highest tension during natural fit bra-wearing.

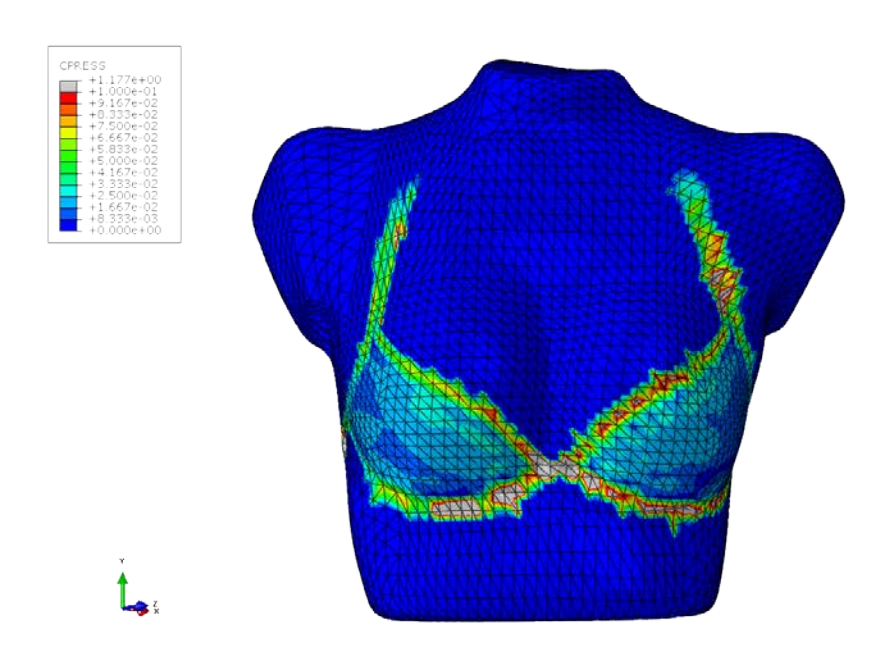


Figure 5a. Contact Pressure between bra and breast

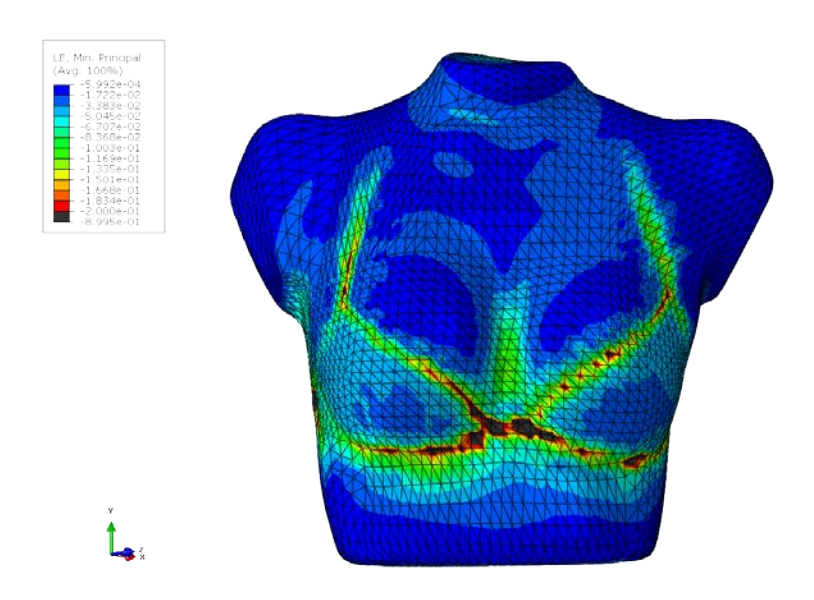


Figure 5b. Deformation between bra and breast

#### CONCLUSIONS

This paper presents a finite-element mechanical contact model of a simulated well-fitting bra being worn by a female torso. The body is in a standing condition and the pre-tension of bra is considered. This contact model is composed of a hyper-elastic breast sub-model with elastic skin and rigid thorax. The mechanical properties of breast sub-model are validated with experimental data of bare-breasted running. The bra cups are meshed as shell and the gore is regarded as a beam. The simulation results are: (1) The maximum contact pressure is distributed along the bra neckline, the wire, and the left straps in the well-fitting bra. (2) The contact pressure of single strap is higher than the double layers of straps. (3) The contact pressure and deformation in the gore and wire is the highest in a well-fitting bra. This FE contact model shows a promising approach for the calculation of force mechanics of body–garment interaction.

#### REFERENCES

Balaniuk R., Melo J., (2007). 3D Dynamic Simulation of the Breast, VII Workshop, de Informática Médica.

Chen, L. H., Ng, S. P., Yu, W., Zhou, J., & Wan, K. F. (2013). A study of breast motion using non-linear dynamic FE analysis. Ergonomics, 56(5), 868-878.

Fung YC, (1993). Biomechanics: mechanical properties of living tissues (2nd) Springer Verlag.

Gefen, A. Dilmoney, B., (2007). Mechanics of the normal woman's breast. Technology and Health Care, 15(4), 259-271.

Hibbitt, Karlsson and Sorensen, (2012). ABAQUS Theory Manual: 745-792.

Imaoka, H., & Atkinson, J. (1996). Three models for garment simulation. International Journal of Clothing Science and Technology, 8(3), 10-21

Jonathan P. Whiteley D.J., (2007). Non-linear modelling of breast tissue. Mathematical Medicine and Biology, 24: 327-345.

Kawabata, H., Tanaka, Y., Sakai, T., and Ishikawa, K., (1988). Measurement of Garment Pressure: I. Pressure Estimation from Local Strain of Fabric, Sen-i-Gakkaishi, 44, 142–148.

Krouskop, T. A., Wheeler, T. M., Kallel, F., Garra, B. S., & Hall, T., (1998). Elastic moduli of breast and prostate tissues under compression. Ultrasonic imaging, 20(4), 260-274.

Lee Y.A., Hyun K.J., Tokura H., (2000). The effects of skin pressure by clothing on circadian rhythms of core temperature and salivary melatonin. Chronobiology international, 17(6):783-793.

Li Y., Zhang X., Yeung K.W., (2003). A 3D bio-mechanical model for numerical simulation of dynamic mechanical interactions of bra and breast during wear. Sen-i Gakkaishi, 59(1):12-21.

Lu M. H., Yu W., Huang Q. H., Huang Y. P., Zheng Y. P., (2009). A Head-held Indentation System for the Assessment of the Mechanical Properties of Soft Tissues in vivo, IEEE Transactions on Instrumentation and Measurement, 58(9):3079-3085.

- Makabe, H., Momota, H., Mitsuno, T., and Ueta, K., (1993). Effect of Covered Area at the Waist on Clothing Pressure, Seni-Gakkaishi, 49,513–521.
- Maximilian E., Stefan R., Jalil J., et al., (2013). Comparison of Different Material Models to Simulate 3-D Breast Deformations Using Finite Element Analysis. Annals of Biomedical Engineering, 42(4): 843-857.
- Miyatsuji A., Matsumoto T, Mitarai S, Kotabe T, Takeshima T, Watanuki S, (2002). Effects of clothing pressure caused by different types of brassieres on autonomic nervous system activity evaluated by heart rate variability power spectral analysis. Journal of physiological anthropology and applied human science, 21(1):67-74.
- Nakahashi, M., Morooka, H., and Morooka, H., (2000). An Estimation of the Comfortable and Critical Clothing Pressure Values on Legs, and an Analysis of Factors Affecting Those Values, Jpn. Res. Assn. Text. End-Uses, 41, 45–51 [in Japanese].
- Perez del Palomar A., Calvo B., Herrero J., Lopez J., Doblare M, (2008). A Finite Element Model to Accurately Predict Real Deformations of the Breast, Medical Engineering & Physics, 30(9):1089-1097.
- Rajagopal R., Lee A., Chung J.H., Warren R., (2008). Creating individual-specific biomechanical models of the breast for medical image analysis. Academic Radiology, 15(11):1425-1436.
- Rajagopal V., Nielsen P.M., Nash M.P., (2010). Modeling breast biomechanics for multi-modal image analysis- successes and challenges, Wiley Interdisciplinary Reviews: Systems Biology and Medicine, 2(3):293-304.
- Samani A., (2001). Biomechanical 3-D finite element modeling of the human breast using MRI data, IEEE Transactions on Medical Imaging, 20(4):271-279.
- Sarvazyan A.P., Skovoroda A.R., Emelianov S.Y., (1995). Biophysical bases of elasticity imaging. EJ Jones (Ed.), Acoustical imaging, 21Plenum, New York, NY
- Sinkus R., Tanter M., Xydeas T., Catheline S., (2005). Viscoelastic shear properties of in vivo breast lesions measured by MR elastography, Magnetic Resonance Imaging, 23:159-165.
- Skovoroda A.R., Dawson K.A., Gusakyan D.A, 1995. Quantitative analysis of the mechanical characteristics of pathologically changed soft biological tissues. Biophysics 40:1359–1364.
- Tan X. (2007). FEM Contact Analysis and its Application on the Release Mechanism Connected to a Plane. Xidian University Dissertations 3:21-23.
- Wang, R., Liu, Y., Luo, X., Li, Y., & Ji, S. (2011). A finite-element mechanical contact model based on Mindlin–Reissner shell theory for a three-dimensional human body and garment. Journal of Computational and Applied Mathematics, 236(5), 867-877.
- You, F., Wang, J. M., Luo, X. N., Li, Y., and Zhang, X., (2002). Garment's Pressure Sensation (1): Subjective Assessment and Predictability for the Sensation, Int. J. Clothing Sci. Technol.14, 307–316.
- Yu J., Cheung J.T.M., Fan Y., Zhang Y., Leung A.K.L. and Zhang M., (2008). Development of a finite element model of female foot for high-heeled shoe design. Clinical Biomechanics, 23(Suppl. 1), S31-S38.